ARKIV FÖR MINERALOGI OCH GEOLOGI

UTGIVET AV

K. SVENSKA VETENSKAPS-AKADEMIEN

Band 2 · Häfte 3

ALMQVIST & WIKSELL / STOCKHOLM

1957

ARKIV FÖR MINERALOGI OCH GEOLOGI Band 2 nr 9

Communicated 1 June 1955 by ERIK STENSIÖ and FRANS E. WICKMAN

Stratigraphical studies on the Triassic vertebrate fossils from Wadi Raman, Israel

By F. BROTZEN

With 7 plates and 5 figures in the text

Contents

Abstract 191
Introduction 192
Review of the geology of the Wadi Raman 192
The stratigraphy of the Triassic 193
    The base 194
    The wood-bearing member "A" 195
    The *Beneckeia* beds "B" 196
    Section of the *Beneckeia* beds "B" 200
    The reef beds—Member "C" 200
    The *Ceratites* beds "D" 201
Stratigraphical conclusions 206
The stratigraphical importance of the vertebrate fauna 207
References 208
Appendix: *Preliminary notes on some lamellibranchs and vertebrates from the Triassic of the Wadi Raman.*
Myalina beneckei n.sp. 209
Myalina ramanensis n.sp. 209
Remarks on the genus *Psephosaurus* Fraas 209
Psephosaurus mosis n.sp. 210
Psephosaurus picardi n.sp. 215
Notes on the stratigraphical distribution of the genus *Psephosaurus* and related genera 215
References 216

Abstract

Numerous finds of vertebrate fossils are recorded from the Triassic of Southern Israel, selachians, nothosaurs and placodonts all occur. The stratigraphy of the vertebrate-bearing Triassic is discussed and the section is divided into the wood-bearing member "A"; *Beneckeia* beds "B"; reef beds member "C"; "*Ceratites*" beds "D"; the beds A–C are of continental character with marine intercalations. Beds "D" are throughout of marine origin. The rich invertebrate and vertebrate faunas allow a correlation of this section with other localities. It seems that the vertebrate-bearing beds in Israel begin with Scythian = Prohungaritan and reach into the Ladinian stage (see table 1 p. 199). In the paleontological appendix two new lamellibranchs are described: *Myalina beneckei* n.sp. and *Myalina ramanensis* n.sp. The taxonomy of the armoured placodont *Psephosaurus* Fraas is briefly discussed. Two new species are described: *Psephosaurus mosis* n.sp. and *Psephosaurus picardi* n.sp. A half armour and a large skull fragment of the first, and a nearly complete dorsal armour of the second were studied. The stratigraphical distribution of the placodonts is noted.

Introduction

The Wadi Raman is situated in the Negev desert in southern Israel. The road to Elat (Aquaba Bay) crosses this wadi about 90 km south of Beersheva. The geology of the Wadi Raman is recorded in the geological map of Shaw (1947), and he is the first to note the occurrence there of Trias and to describe a type section of this formation. The geological succession was based on fossil determinations by L. Picard.

In September 1953 the author visited this locality and found there some vertebrate fossils, which were later prepared in Stockholm. These include, *inter alia*, the armour of a *Psephosaurus*. In connection with a tour of duty in Israel during 1954–55, the author continued the studies on the Triassic vertebrate localities in the Wadi Raman.

During the winter of 1953/54 the geological exploration of the Wadi Raman was intensified with the cooperation of the United States Operation Mission (USOM) and the Geological Institute of the State of Israel. The exploration was directed by Mr. M. Friedman (USOM) and Dr. Y. K. Bentor (Geol. Inst.). Mr. Israel Zak, a co-worker in this expedition, mapped the Triassic, but his mapping which was based exclusively on petrographical observations was of no help in solving the stratigraphical problem of the bone-bearing strata. Mr. Zak's results, containing a detailed mapping of the Triassic localities and the tectonics of this system are at present under preparation for publication.

The author's collection of vertebrate fossils was presented to Prof. G. Haas, Zoological Institute of the Hebrew University, who will describe this material with the exception of *Psephosaurus* and related genera which are being studied by the author.

A large number of the amonites collected by the author from the different zones of the bone-bearing formation was transferred to Prof. M. Avnimelech, Geological Institute, Jerusalem.

The author is very much indebted to all his friends in Israel for the help they gave him in his work. He is particularly grateful to Dr. Y. K. Bentor, who introduced him to the geology of the Negev and to Mr. Israel Zak, who assisted at the work in the Wadi Raman. Sincere thanks are also due to all the colleagues and especially to Prof. L. Picard, Prof. M. Avnimelech and Prof. G. Haas for helpful discussions.

The following descriptions are presented as the stratigraphical basis for the investigations on the vertebrate fauna.

Review of the geology of the Wadi Raman

The geological map of Southern Palestine by Shaw includes the structure of the Wadi Raman area. This area is an anticline in the direction WSW–ENE, having a length of approximately 40 km and a breadth of up to 10 km. It is part of a system, called by Bentor "the anticlinorium of Raman", which extends over a distance of

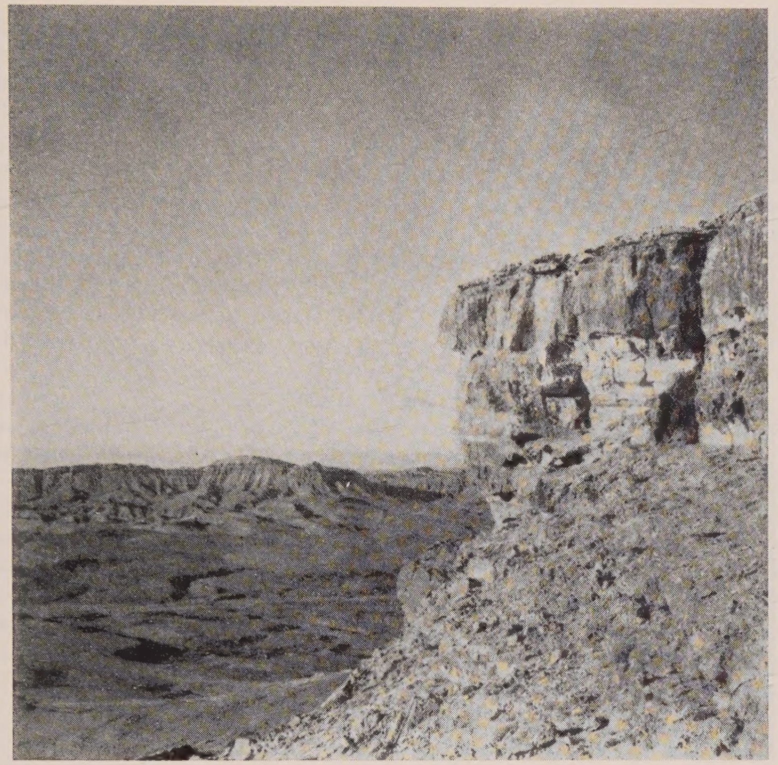

Textfig. 1. Wadi Raman, view to the South. Right: The northern side of the anticline, Upper Cretaceous limestones. Valley = Jurassic. Left: The hills of the Triassic and the southern Upper Cretaceous.

about 90 km. Its central part is deeply eroded, that is, it is morphologically an elongated erosion cirque. The walls of this cirque are built of Upper and Lower Cretaceous, the bottom of the wadi shows mainly Jurassic, and in the highest part of the anticline there is an outcrop of Triassic sediments on igneous rock. The building of the anticline is asymmetrical; in the north all the layers dip gently towards the north. Near the southern wall fault lines and dislocations occur irregularly (see sections by L. Picard, 1950).

As the Triassic is the deepest system of the Wadi Raman area, many details of its structure are of interest. The Trias forms a special anticline and generally its sediments lie conformably on an igneous rock, dipping towards the north (see textfigs. 1 and 2).

The stratigraphy of the Triassic

Shaw (1947) has not divided the section of the Triassic, he has only given a scheme of all beds from the base into the Jurassic. It is easy, however, to distinguish some larger units in his type section. Bentor gives a scheme for the Triassic divisions and it seems that Shaw's and Bentor's sections can be correlated as follows:

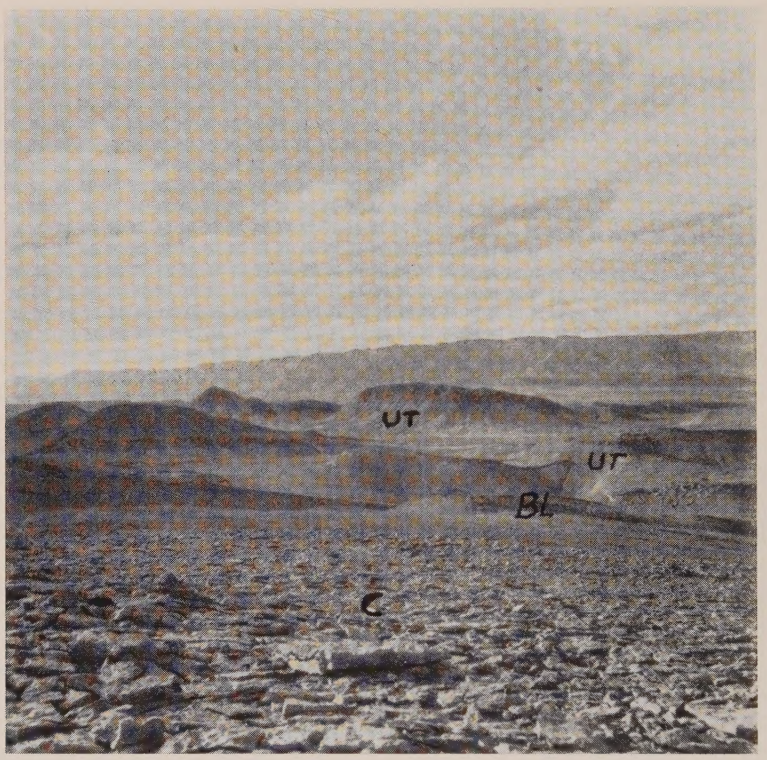

Textfig. 2. The Triassic of the Wadi Raman, view to the North. BL = bluish Limestone of the Member C; C = "Member C"; UT = Upper Triassic.

	SHAW	BENTOR
5.	*Gypsum* formation.	Marine Gypsum series—Keuper (?).
4.	Uppermost limestone formation without *Ceratites.*	Mainly limestone series—Muschelkalk.
3.	The lower limestone formation with *Ceratites.*	
2.	Shale & sandstone formation.	Bunter sandstone. Shale–sandstone series.
1.	Basal igneous rock.	

The vertebrate fossils are restricted to divisions 2 and 3, as already stated by Shaw. A single nothosaurian vertebra, described by Swinton (1952), was also found in one of these formations. According to Bentor, No. 2 corresponds to the Bunter or Lower Triassic (= Upper Eo trias according to Spath) and No. 3 to the Muschelkalk = Middle Triassic (= Meso trias Spath).

The base

Bentor (1952) discussed the igneous rocks at the base of the sediments and called them "the Triassic basal sills". He stated that the rock types are the same as intrusive rocks in the Jurassic formations of the Wadi Raman: "As the stock pierces Jurassic strata these related sheets found in the Lower Triassic must be intrusive, that is to say sills. If this is the case then they are the largest of all the sills in Wadi Raman."

If this view is correct, the "sills" must have intruded during the Triassic sedimentation. The type of rock is a porphyritic quartz syenite, with trachytic texture, characteristic of such types between intrusive and effusive rocks (according to Dr. W. Larsson, Geological Survey of Sweden, who kindly examined some of my thin sections). It could have been intruded in layers which were already eroded before the preserved Triassic was deposited, or it could have been intruded during a period after the Triassic deposition. Metamorphic contacts between the igneous and the sedimentary rocks are not evident; it appears, however, that the surface of the igneous rock was weathered before a new sedimentation took place. The sedimentary series starts with rocks which could have originated from eroded material of the basal "sill". But if the sill was intruded into the preserved sediments, the absence of a zone of contact would not be problematical, because it originated at a low temperature.

The possibility also exists that the basal rock is intrusive into the existing Triassic rocks. But the geological history of the basal beds appears to the author to be as follows: in Lower Triassic or Uppermost Permian sediments an intrusion of syenitic magma has built up a large sheet of rock; the thickness of this sheet could be only a few hundred meters at the most. After the intrusion of the magma, and possibly in connection with this activity, the sediments were exposed and eroded into the igneous rock. A new sedimentation cycle then began, partly on the continental shelf or near the shoreline, as demonstrated by plant remains and isolated marine fossils such as *Lingula*.

The wood-bearing member "A"

Concordant on the basal igneous rocks there are about 16 m of sandstones and shaly sandstones. The profile according to Shaw is as follows:

4) 2.5 m of sandstone.
3) 4.3 m of green-grey, also tan, laminated shale; *Lingula*.
2) 3.2 m of brown sandstone, interbedded with grey shales; *Lingula*, fish teeth, plant remains, bone fragments.
1) 6.4 m of grey laminated, medium hard shale, with badly preserved fossils.

It seems that a grey sandstone or loose sand, containing plant remains, generally wood, can be interbedded between layers 2 and 3. Such woody fragments are silicified and attain a length of up to 1.5 meters. According to Dr. B. Lundblad, Stockholm, the wood belongs to *Cetroxylum* or a related group. *Lingula* occurs rarely and this genus cannot be used for dating the rock. Bone fragments are also very infrequent and the presence of fish teeth, reported by Shaw, could not be confirmed, but according to Mr. Zak, "*Placodus*" teeth should occur in bed 3. Generally the vertebrate bones belong to reptiles.

The colour of the beds is intense, the brown sandstone is reddish or brick-red, and the green colour varies from grey to deep green and apple-green. In those cases where only layer No. 2 is exposed, it is conspicuous over long distances by its intense colour. These intense colours, the lack of invertebrate fossils and the relatively large pieces of wood, all indicate that much of this member has originated from a continental sediment.

The few *Lingula* specimens complete the picture of a littoral sedimentation with single, unimportant transgressions over the coast. The stratigraphical range of these layers is uncertain. Bentor added them to the next member of the section and correlated both with the Lower Trias. There is no lithological difference between this "wood-bearing" member and the next, "the *Beneckeia* formation". In the upper part of the member "A" there are the green shales and sandstones, and the same rocks occur also on the lower layer of member "B". The lithofacies makes it possible that the member "B" is a direct continuation of "A". Therefore the stratigraphical range of the beds "A" should be uppermost Lower Trias, or lower part of the lower Meso-trias.

The *Beneckeia* beds "B"

According to Shaw there follow on the member "A":

4) Tan and grey sandstone interbedded with green-grey shale—plant remains.
3) Greenish basalt, pillow weathering.
2) Green-grey laminated shale—pelecypods, *Lingula*.
1) Dark grey, hard, igneous rock, probably of felsitic affinities.

Bentor called the igneous rock at the base the "higher mass" of the "Triassic basal sills".

This "higher mass" does not occur in all exposed sections. The beds of the higher member often follow directly on the top of member "A" and the entire sequence of layers can be observed in sections with and without interruption by the "higher mass". This mass disappears for some hundreds of meters both to West and to East; it can also be established that its thickness decreases towards the North, and therefore, this "mass" seems to be a local magmatic intrusion into the Triassic.

A section of 28-meter thick beds, which is a little more than Shaw observed, will be grouped togehter here as the member "B" of the Trias in Israel. All these layers are characterized by the ammonites of the genus *Beneckeia* which in certain beds occurs abundantly.

It appears that a few different zones exist, each characterized by a certain type of *Beneckeia* species. The genus *Beneckeia* is known from the Central European lower Meso-Trias. Cox and Spath have already noted *Beneckeia* from Trans-Jordan. As observed by Spath, the *Beneckeia* specimens from Trans-Jordan do not resemble the Central European ones. The specimens from Wadi Raman are, with one exception, closely related to those from Trans-Jordan. The richly lobated sutures are described by Spath and this character distinguishes the group from the Central European species. The two specimens, collected in Trans-Jordan and studied by Cox and Spath, were too badly preserved to permit a definition or diagnosis of the species to be made. But the large number of specimens from Wadi Raman show that the majority of *Beneckeia* from zones 1–3 belong to the same types which are described from Trans-Jordan. It seems that the specimens from zone 1 have a smaller diameter than those from the higher zones. The *Beneckeia* in zone 2 belong to the same group as those in zone 1. The average diameter increases, but the pattern of the suture lines and the sections are apparently unchanged. Typical of these *Beneckeia* sp. 1 (with small diameter) and sp. 2 (with larger diameter) is that the suture lines follow closely on each other and the dwelling chamber is small, though seldom preserved.

The type with a large diameter occurs together with another type of *Beneckeia* in zone 3. *Beneckeia* sp. 1 and 2 are always fossilized in grey or blackish limestone or sandy limestone and if the specimens are not weathered, parts of their shells are preserved, covering the suture lines. The type species of zone 3 and 4 is preserved in clay iron-stone, of intense brownish colour. The suture lines are indistinct, visible only in broken specimens, the dwelling chamber is generally large, and the flanks of the ammonites seem to be more curved than in the *Beneckeia* sp. 1 and 2. Entire specimens were not found, but large fragments occur abundantly. In zone 3 the brown *Beneckeia* is not so frequent as the older one. In zone 4 the brown *Beneckeia* is dominant.

The stratigraphical distribution of the *Beneckeia* would be:

Zone 4 *Beneckeia* sp. 3 = brown with large dwelling chamber.
,, 3 ,, large Trans-Jordan type (sp. 2) + *Beneckeia* sp. 3.
,, 2 ,, large Trans-Jordan type (sp. 2).
,, 1 ,, small Trans-Jordan type (sp. 1).

All these characters of *Beneckeia* are given provisionally and research on their variation must be undertaken. It is not yet clear if these ammonites belong to the genus *Beneckeia* sens. strict. Only a few species of the genus are known and it seems that the new group from Israel and Trans-Jordan differs in many details from the Central European species of *Beneckeia*. The final determination will be made by Prof. M. Avnimelech of the Hebrew University, Jerusalem, who is preparing the general investigation of this group.

The *Beneckeia* beds are well exposed in many places. Hard sandstone or limestone layers limit the different zones and in the outcrops these hard layers form steps, covered with fossils.

Beneckeia occurs abundantly in different layers. Certain limestones are filled only with shells of *Beneckeia*. The first stratum to have numerous *Beneckeia* specimens occurs above the "higher mass", and this bed could be followed in all outcrops of the *Beneckeia* beds. The fauna of the *Beneckeia* beds is rich in specimens but the number of species is limited. Nautiloids occur rarely, and seem to belong to the genus *Germanonautilus*. They first occur in this section together with *Beneckeia* sp. 1.

Myophoria and *Myophoriopsis* are dominant fossils in this member, which also make their first appearance in its deepest layers. These fossils are especially numerous in some marl beds, in which their shells cover all the weathered outcrops of the small morphological steps.

In addition to abundant examples of *Myophoria*, other lamellibranchs occur throughout the member "B". In certain beds at least three species of *Myalina* are dominant. The few specimens I brought back with me do not allow a final generic determination to be made, but an assistant in the Hebrew University in Jerusalem intends to undertake such a determination on the very large number of specimens there. No one of these types is identical with the species hitherto described and it seems that the Israelian ones fit best into the genus *Myalina*. Three types occur, of which the one is higher than the others, and it is characterized by its elongated test and sharp crest. This species *Myalina beneckei* n.sp., is the ancestor of a younger one, which characterizes the next member of the section and differs mainly in its larger size. The earlier species attains a length of 7 cm, the younger one, *Myalina ramanensis* n.sp., has a length of 15 cm.[1] Gastropods are rare and badly preserved, but they already occur with the first Beneckeia and continue throughout the entire member.

---

[1] A short description of the lamellibranchiata is added in the paleontological appendix, p. 209.

Brachiopods occur sporadically, and some species of *Waldheimia* and *Coenothyris* are found in the deepest layers whilst they seem to become more rare in the higher zones of this member. All lamellibranchs, gastropods and brachiopods are more or less restricted to sandy, sandy-limy and limy shales. In the parts of the section, where the shales are less limy or free from calcareous matter, the only fossils are *Lingula* and vertebrate bones. *Lingula* can fill up large parts of the shales, but since the specimens are broken and imperfect, a determination is difficult. The member "B" of the Triassic is of the greatest interest because of its content of vertebrate fossils. They occur not only in the layer with rich invertebrate fauna, but also in the shales, where only *Lingula* is present. Generally the bones lie isolated and irregularly in the beds. Here and there has been post-mortem concentration, so that bones of different animals occur together at the same place. In some places bone elements of the same animal are deposited togehter. Vertebrae of various reptiles are dominant and vertebrae of *Nothosauria* are most common. Beside *Nothosaurus*, even *Placodontia* and other reptile vertebrae, e.g. two vertebrae possibly belonging to *Tanystrophaeus* or a related genus (determined by Prof. G. Haas), were found in these beds.

Isolated teeth are not rare and even here the majority belong to *Nothosauria*, but examples of placodonts and fish teeth (*Hybodus* types) were also collected.

Broken and incomplete ribs are not infrequent and parts of the pectoral and pelvic girdles occur as isolated examples. The most characteristic vertebrate fossils of the Triassic of Wadi Raman are turtle-like placodonts, and isolated plates of their dorsal armour are not uncommon. The best preserved specimens are: a half dorsal armour with its margins and parts of the ventral shield, and an incomplete skull with the entire occipital region, the posterior part of the palate region and parts of the upper side. Both specimens, the dorsal armour and the skull, belong to the genus *Psephosaurus* and were found in the lower part of the zone with *Beneckeia* sp. 3 and at a distance of about a hundred meters from each other. The two elements do not, apparently, belong to the same individual. The abundance of pieces from the armour of *Psephosaurus* in all beds of the section demonstrates that these animals were common in this region during the Triassic.

A preliminary study of *Psephosaurus* leads to the conclusion that different species occur in the different members of the section. The genus *Psephosaurus* is known only from the lower part of the Upper Triassic in Germany, but all that has been found of this reptile in Germany does not allow any reconstruction of the skeleton to be attempted. The author has tried in the appendix to give a definition of the *Psephosaurus* species from Israel and their differences from *Psephosaurus suevicus* from Germany.

The species from the *Beneckeia* zones is named *Psephosaurus mosis* n.sp. and this species has already shown all characters of the entire group. It seems certain that, at least in the lower Trias, two very specialized groups of *Placodontia* existed which were already completely separated from each other, namely the group of *Placodus* and the turtle-like group of which *Psephosaurus mosis* n.sp. is the oldest known representative.

To summarize, the following vertebrates have hitherto been found in the *Beneckeia* beds:

Hybodus or related genera (teeth).
Stegocephalia (isolated bone plates).

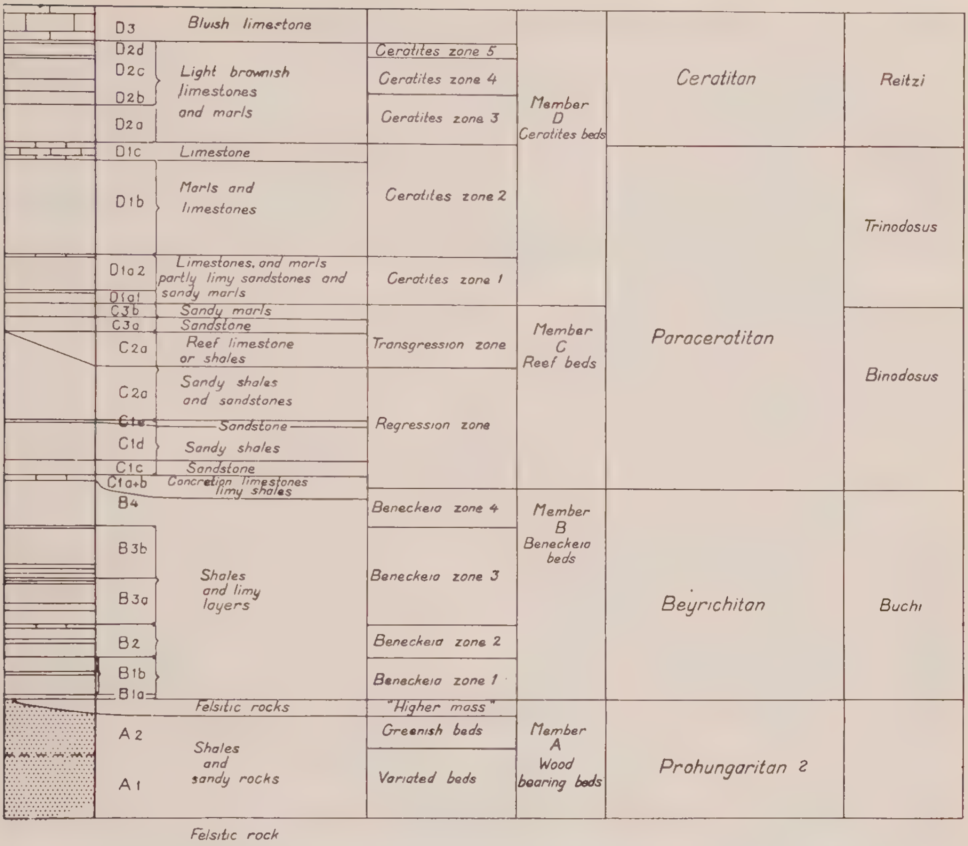

D3	Bluish limestone		Member D Ceratites beds	Ceratitan	Reitzi
D2d	Light brownish limestones and marls	Ceratites zone 5			
D2c		Ceratites zone 4			
D2b					
D2a		Ceratites zone 3			
D1c	Limestone	Ceratites zone 2		Paraceratitan	Trinodosus
D1b	Marls and limestones				
D1a2	Limestones, and marls partly limy sandstones and sandy marls	Ceratites zone 1			
D1a1					
C3b	Sandy marls	Transgression zone	Member C Reef beds		Binodosus
C3a	Sandstone				
C2a	Reef limestone or shales				
C2a	Sandy shales and sandstones	Regression zone			
~~C1e~~	Sandstone				
C1d	Sandy shales				
C1c	Sandstone				
C1a+b	Concretion limestones limy shales				
B4	Shales and limy layers	Beneckeia zone 4	Member B Beneckeia beds	Beyrichitan	Buchi
B3b		Beneckeia zone 3			
B3a					
B2		Beneckeia zone 2			
B1b		Beneckeia zone 1			
B1a					
	Felsitic rocks	"Higher mass"	Member A Wood bearing beds	Prohungaritan 2	
A2	Shales and sandy rocks	Greenish beds			
A1		Variated beds			

Felsitic rock

Table 1. Sections through the Lower and Middle Triassic of the Wadi Raman.

Nothosauria or related genera (parts of shoulder and pelvic girdle, bones of the extremities, vertebrae, teeth).

Psephosaurus mosis n. sp. (skull, parts of the dorsal and ventral armour).

Tanystrophaeus or related genera (two vertebrae).

Other reptilia not yet determined.

All bones were collected on the surface of the exposed beds, the skull and armour of *Psephosaurus* were only slightly exposed and were dug out from the beds. A systematic digging, especially in the middle part of the *Beneckeia* beds, would have very good prospects of finding more complete vertebrate fossils.

Plant remains are not very common and are very poorly preserved.

The stratigraphical range of the member "B" is given by the genus *Beneckeia* sens. lat. As already known, the genus occurs only in the uppermost Lower Triassic (Upper Eotrias) and in the Lower Mesotrias. It seems therefore that the *Beneckeia* bed in Israel belongs to the highest Lower Trias or to the lowermost Middle Trias.

Section of the *Benecheia* beds "B"

6 m	Marls, light yellow and brown. *Benecheia* 3, *Myalina* spp., bones.	ZONE 4
20–30 cm	Sandstone.	ZONE 3
ca. 5 m	Shales dark-green *Benecheia* sp. 3 and sp. 2. *Myalina* spp., bones.	
ca. 2.50 m	Shales with sandy layers containing *Benecheia* sp. 3 and sp. 2, *Myalina beneckei* & *Myalina* spp. bones.	
	Porphyritic sill (locally).	
ca. 30–40 cm	*Myalina* beds with bones.	
6 m	Shales, greenish *Psephosaurus* beds.	
20 cm	*Myalina* limestone.	ZONE 2
2 m	Marls with rich fauna *Benecheia* 2, *Myophoria* sp., brachiopods, bones.	
30–20 cm	Sandstones with trails.	ZONE 1
ca. 4 m	Shales with *Myalina*, *Myophoria*, bones.	
30 cm	Sandstone with *Benecheia* sp. 1.	
1.50 m	Brownish shales.	
	"The higher mass" locally limited (felsite)	

The reef beds = member "C"

The next group of beds is described by Shaw as follows:

4) 1.1 m. Sandstone.
3) 2.4 m. Tan, pink and blue shale with fish remains, bones, *Lingula*.
2) 1.2 m. Ash.
1) 16.6 m. Brown and grey laminated shale, sandy at the top; fish teeth, plant remains.

All beds seem to be of a sandy character and with the exception of *Lingula*, no marine invertebrates are found. New studies confirmed this succession, but the author found that the sections change horizontally.

Some sandy shales over the sandstone 4) belong to this member. The whole member reaches a thickness of 20–30 meters and begins with 30 cm of shaly or layered sandy, greenish grey limestone, above which follows 30 cm of concretion limestone. These two beds, which are very distinct in all outcrops, were named the guide banks of the member "C". On the guide banks lie 2 m of crossbedded sandstone with plant remains. This radical change of sedimentation can only indicate a regression of the sea. Sandy marls, partly variegated, partly yellow-brown, follow the sandstone layer with intercalations of various sandstones with crossbedding. It is easy to recognize these beds for a long distance in the sections. At two places, west of the main road, the upper part of these beds was replaced by black limestone, formed by large lamellibranchs. The maximum thickness of these masses can reach 4–5 meters. In all directions they diminish at some hundreds of meters from their centres. When the limestone on the sides of these "reefs" disappears, it is replaced by a half meter thick black or grey-blue layer.

Both "reefs" show the same characters and were formed during a short transgression. Generally the shells are closed, so that both valves are preserved together and they are packed one by one embedded in limestone.

The genus of this lamellibranch is uncertain, it is closely related to *Myalina* and has been given the preliminary name of *Myalina ramanensis* n. sp. (Appendix, p. 209).

In the lower part near their margins the massive limestone reefs can also include dark grey and bluish marls, which continue out from the reef facies and were described by Shaw as "Ash".

1.80 m below the "reef" the sandy shales and sandstones contain an abundance of bones, of which those of *Nothosaurus* are dominant; bones of *Psephosaurus* and other reptiles were also collected.

On the top of the "reef" occurs a crossbedded sandstone, the thickness of which is variable, but at certain places attains a thickness of 2 m. Badly preserved bones and plant remains were collected from this layer.

It is considered that 1–2 m of sandstone and shales, partly containing badly preserved lamellibranchs and bones constitute the marginal layers bordering on the next member of the section.

The conditions of sedimentation present few problems. The light and crossbedded sandstones indicate terrestrial origin while the reefs have been formed in a shallow sea. At the beginning of the sedimentation of the beds "C", the sea seems to have regressed from the Wadi Raman area. Generally the layers were deposited under terrestrial conditions, but near the end of this formation the sea transgressed for a short time, regressed again and at the beginning of the next period for the first time the sea took permanent control of the area.

It is impossible to determine the exact age of the reef beds. The lack of indicator fossils is the first difficulty and in addition the age of the base, the *Beneckeia* beds, is not definitely correlated with a certain Triassic zone. The following beds in the section are best fixed in their stratigraphical position as Lower Middle Trias and therefore the reef beds must belong to the Upper Lower Trias or more possibly they are to be correlated with Lower Middle Trias.

The *Ceratites* beds "D"

According to Shaw nearly 40 m of the section are characterized by ammonites of "*Ceratites*" types and by limestone beds with shales between. The abundance of lamellibranch shells in the limestone beds shows a resemblance to the Central European Muschelkalk. But the ammonite species and other fossils are different and the dominance of shales in the section gives the profile a very local character.

It must be emphasized, that the majority of ammonite species are not the same in the Israelian and German Triassic. During the field work it was easy to distinguish several ammonite types, lying in stratigraphical succession and it seems that at least five such ammonite zones exist. A large number of ammonites collected in the different zones was given to Prof. M. Avnimelech for detailed studies. Here it is only possible to give the main outlines to the stratigraphy.

Dr. G. el Din Hafez Awad published, in 1946, a very valuable paper entitled "The occurrence of Marine Triassic (Muschelkalk) Deposits in Sinai", in which he described ammonites which also occur in the Israelian Triassic. The distance between the Trias locality in Egypt-Sinai and Wadi Raman is only 30 km and the stratigraphy of both occurrences will be discussed later. Hafez Awad as early as 1938 recognized types of Sinai ammonites as belonging to some genus which showed *Ceratites binodosus* ornamentation and septal sutures, "yet differed from known *Ceratites* spp. in having a well developed keel on the ventre".

In connection with Hafez Awad's publication, L. F. Spath attempted an analysis of the "*Sinai Ceratites*". He stated:

1) The species are similar to those of the genus *Paraceratites* (but they are bituberculate, the suture-lines simpler).
2) The presence of a keel is against a comparison with *Prognoceratites*.
3) They are not similar to *Ceratites flexuosus*.
4) Possibly the Sinai group of *Ceratites* may claim a separate subgeneric name.
5) This "distinct, local group" comprises about half a dozen species.

Hafez Awad discussed the stratigraphical range and contradicted, to some extent, the views of Spath. He assumed that ammonites range throughout the *Paraceratites* zone and that the entire group is closely related by their ornamentation to the *Paraceratites binodosus* group.

Hafez-Awad gave the entire group a preliminary name: "*Sinai Ceratites*".

If the assumption is correct that the Trias of the Wadi Raman and of the Sinai (the dome of the Gebel Araif el Naga) belong to one unit, the different species figured and analysed by Hafez Awad and Spath occur in different zones of the "*Ceratites*" beds.

On the top of the reef beds follow some marly shales with a rich invertebrate and vertebrate fauna. Here occur, though rarely, small compressed ammonites of the "*Ceratites*" type figs. 19 and 20 of Hafez Awad and Spath. Higher in the same zone the compressed types continue to be present, but their diameter shows an increase. The zone has a thickness of about 6 m and is limited by the "*Terebratula*" layer, several centimeters thick. The ammonites give the impression of a very close relationship to such species as *Paraceratites elegans* Mojs.

This zone will be named zone 1 of the "*Ceratites* beds". In common with all other layers of the *Ceratites* beds, this zone is composed of marls and limestones, but it is distinguished by the presence of some limy sandstones characteristic only of this zone. Especially in the middle part of the zone these limy sandstones are bluish grey in their interior, but their weathered exterior is tan or yellow-brown.

Nearly all limestones and limy sandstones contain numerous coprolites, bone fragments and large bones such as to form, in places, real bone beds. Loose pieces of rock on the hill sides are easily recognized as coming from this zone because of their bone content.

The vertebrates from this zone are:

Hybodus or related genera (teeth).

Nothosaurus or related genera (a very typical skull fragment in which are preserved the upper side from the occipital to occular region and on its under side, the palatine region with the maxilla bearing teeth and roots. Parts of pectoral and pelvic girdles, bones of the extremities and numerous vertebrae and teeth).

Placodus or related genera (vertebrae, bones of the extremities, teeth).

Psephosaurus picardi n. sp. (more or less complete cast of a body armour, with large parts covered with bones, isolated bones and parts of the armour).

Psephosaurus spp. (various elements of the armour).

Dinosaurid (?) (parts of a skull, vertebrae, and isolated bones).

The rich fauna of lamellibranchs is variable and contains *Gervillia* and related genera, *Myophoria* and others, e.g. an extremely large *Pinna* or related genus, which reaches a length of about 40 or more centimeters. Gastropods occur sparcely, but large specimens of nautiloids are abundant. This zone and parts of the next one were described by Shaw as:

9.7 m Coloured shales interbedded with fossiliferous limestone, *Nautilus, Terebratula, Myophoria,* bone fragments, fish teeth, plant remains, *Lingula.*

Prof. L. Picard identified from this horizon (in Shaw p. 17):

Aff. *Homomya* (*Anoplophora*) *fossaensis.* Wiss. Muschelkalk.
Myophoria laevigata Gold. Trias.
Mysidia.
Lithophagoides Frech. Raibler
Coenothyris vulgaris Schloth. Muschelkalk.
Pleuromya elongata Schloth. Muschelkalk.
Nautilus sp. indet.

The boundary layer, filled with numerous "*Terebratula*",[1] is constantly observed in all sections of this zone and could be followed for a distance of 10–15 km. In outcrops, where parts of the section were obscured by scree, the guide horizon with "*Terebratula*" was easily recognized by numerous weathered terebratulas. In the Araif el Naga dome the *Terebratula* beds seem also to occur in the same stratigraphical position, i.e. below marls and limestones with numerous *Nautilus* and *Ceratites,* which belong to the next zone.

The age of this *Ceratites* zone 1 is given by the ammonite group of *Paraceratites elegans.* The beds must therefore be correlated with the *Paraceratites* age of Spath, and as the author will demonstrate later, belong to the middle or lower part of this stratigraphical unit.

Marly, shaly layers with many intercalations of lumachelle limestone are here grouped together as zone 2, which has a thickness of about 14 meters. It seems possible from more detailed study to distinguish, by its faunal elements, an upper and lower sub-zone. Zone 2 is extremely rich in ammonites both as regards the number of specimens and also the number of species and genera. Nautiloid species (*Germanonautilus* ?) occur abundantly and some of the specimens reach a diameter up to 40 cm. The main group of ammonites is closely related to *Paraceratites,* especially to some of the American species described by Smith 1914, e.g. *P. cricki* Smith and *Ceratites spinifer* Smith. Even types showing resemblance to the ornamentation of *Paraceratites trinodosus* and to the *Ceratites cimeganus* group, such as *Ceratites subnodosus* Mojs., occur abundantly. Another group of ammonites in zone 2 comprise involute, very compressed types, at first showing a typical *Trinodosus* ornamentation, but in the adult stage having plane sides and no ornamentation. Such types resemble *Ceratites semipartitus* Montf. in their general features, but they are not related to this species and they are distinguished by the presence of a keel in the initial stage.

Lamellibranchs in this zone resemble alpine ones and are also similar to those described from the Araif el Naga dome and from the lower parts of the Jordanian Triassic. Vertebrate bones are not infrequent, but do not occur as abundantly as in zone 1, bone beds are not observed.

---

[1] The very numerous "*Terebratula*" belong to different species and possibly to several genera.

The author has received the impression that a typical fauna of the *Trinodosus* zones of the Triassic of the Tethys is represented in zone 2 and that no objection can be raised from paleontological aspects, in regarding this zone as a *Trinodosus* zone, even if a typical *Paraceratites trinodosus* is lacking.

Two meters of hard limestone beds intercalated with some marls separate zone 2 from the next zone in the section.

The upper three zones (with ammonites) have altogether a thickness of about 16 meters. The lithological facies does not change, but the marls are somewhat lighter in colour than in the earlier stages.

The fauna of zone 3 is also very similar to that of zone 2. The ammonites change their characters and the compressed types without ornamentation in the adult stage disappear or occur but rarely. The *Trinodosus* types have the characters of *Paraceratites* in their initial stage, but in the adult stage their ribbing shows *Ceratites nodosus* characteristics or their external lateral tubercles developing in prominent, sharp spines.

New elements of the ammonite fauna of zone 3 are *Johannites, Arcestes* or related genera. These elements indicate that the age of zone 3 must be intermediate between the *Trinodosus* and beds, which are correlated with the *Protrachyceras reitzi* zone.

Zone 3 contains once again well preserved reptilian fossils. Vertebrae occur abundantly; a large part of a skull of *Nothosaurus* or a similar genus was found and teeth of *Placodus* and *Nothosaurus* were collected. The thickness of zone 3 is about 5 meters. Two marly and limy layers with a rich ammonite fauna form zones 4 and 5. These two zones are separated by limestone, half a meter thick. The ammonite fauna of zones 4 and 5 is poorer than in the two lower zones and a distinct tendency exists towards a diminishing diameter of the ammonites. Types with *Ceratites nodosus* and *spinulosus* ornamentation become dominant, but their initial part is always of *Trinodosus* = *Paraceratites* type, and distinctly keeled.

It is still too early to discuss phylogenetic questions and stratigraphical conditions without final taxonomic research on the ammonite fauna and any suggestions can only be very hypothetical. It appears, nevertheless, that there exists a trend in the "*Ceratites* bed" of the Wadi Raman towards an evolution of the *Paraceratites* having a certain convergence towards the lines of the *Ceratites* evolution in the German Muschelkalk. Thus, at the end of the evolution, the same ornamentation has been developed in Israel's *Paraceratites* as in Germany's *Ceratites*. The ultimate species are hence characterized by the "*nodosus*" and "*spinosus*" ornaments. The author therefore wishes to suggest that zones 4 and 5 are stratigraphically comparable with the upper part of the Ceratitian, and the higher part of the Muschelkalk. respectively.

Stratigraphically, the highest occurrence of the *Ceratites* in the section should limit the "*Ceratites* beds". The erosion of the Trias beds of Wadi Raman has cut out a distinct crest on the top of the "*Ceratites* beds" formed from a crystalline or semi-crystalline blue-black limestone about 3–4 meters thick. This limestone is an excellent stratigraphical marker and it is utilized in the mapping as showing the limit of the higher part of the Triassic. The author therefore concludes that the bone bearing part of the Triassic ends with the ammonites bed and that the blue-black limestone belongs to the "*Ceratites* beds".

The section measured by Mr. Zak and the author is about 11 meters thinner than that measured by the geologist of the Petroleum Development (Palestine) Ltd., as given in Shaw. An attempt to correlate the sections is suggested in the following scheme:

Shaw		Brotzen & Zak		
6.7 m	Steel-grey, very dense, very hard limestone, breaking in cubical blocks. *Myophoria blakei*, ?*Trigonodus*, *Encrinus*, *Gervillia*, *Terebratula* nov. sp.	3.20 m	Bluish limestone, very hard.	
4.2 m	Shale.	2.0 m	Limestone and marls with *Ceratites.*	ZONE 5
1.8 m	Tan and grey, medium bedded hard limestone. *Nautilus*, pelecypods, *Ceratites.*	5.8 m	Limestone and marls with *Ceratites.*	ZONE 4
5.0 m	Green-grey shales with limestone streaks, *Ammonites*, bones.	5.0 m	Light brown marls and limestones with *Ceratites*, *Arcestes*, *Johannites*, *Placodus.*	ZONE 3
6.7 m	Grey, crystalline, thick bedded, hard limestone, *Myophoria*, *Nautilus*, *Pseudoplacunopsis*, *Terebratula*, gastropods, bone fragments.			
3.1 m	Shale.			
1.1 m	Tan, marly hard limestone *Myophoria* pelecypods.	2.4 m	Hard limestone layers.	
6.1 m	Shale.			
6.7 m	Tan, thin bedded, hard limestone, big *Myophoria*, *Ceratites*, *Nautilus*, *Terebratula*, brachiopods, bone fragments, *Pseudoplacunopsis.*	ca. 13 m	Limestone and marls, *Paraceratites* spp.	ZONE 2
9.7 m	Coloured shales, interbedded with fossiliferous limestone, *Nautilus*, *Terebratula*, *Myophoria*, bone fragments, fish teeth, plant remains, *Lingula.*	0.10–0.40 m	*Terebratula* layer.	ZONE 1
		6.0 m	Sandy limestone (bluish) and shales with bone beds, *Paraceratites*, *Psephosaurus picardi*, n. sp. *Nothosaurus.*	
		1,8 m	Sandy and shaly layers.	
	Sandstone, crossbedded			MEMBER "C"

Stratigraphical conclusions

The stratigraphical results of the above description of the vertebrate bearing Triassic in Israel can be expressed in the following scheme: (see also Table 1)

Wadi Raman		Age (according to Spath)	Zone
Member D			
Ceratites Beds	Ceratites zone 5		
	,, ,, 4	Ceratitan	reitzi
	,, ,, 3		
	,, ,, 2		
	,, ,, 1		trinodosus
Member C	Transgression zone	Paraceratitan	
Reef Beds	Regression zone		binodosus
Member B	Beneckeia zone 4		
	,, ,, 3	Beyrichitan	Buchi Beds
Beneckeia Beds	,, ,, 2		
	,, ,, 1		
		?	
Member A	Greenish beds	Prohungaritan (?)	
Wood Bearing Beds	Variegated beds		

It seems that the *Ceratites Zones 3–5* could be correlated with the lower Ladinic in the Alps, especially with Alpinic facies in Hungary around the Bakonyer Wald (north-west of the Platten See). No exact determination of the *Ceratites* has hitherto been possible. The general succession of the ammonites in the section and the convergent evolution of them to *Ceratites nodosus*, indicates such a stratigraphical range.

The Ceratites zones 1–2 contain *Paraceratites* or very closely related genera, which seem to occur commonly in the *Paraceratites trinodosus* zones of North America and the Alps, and possibly the majority of the species is also common in the Platten See region in Hungary. The author therefore correlates zones 1 and 2 in the Raman section with the *Trinodosus* beds or with the upper Anisic in the Alpine Triassic.

The "Reef beds" or member *"C"* of the section contain no guide fossils. They are intermediate between the *Trinodosus* zone of the Anisic and the *Beneckeia* beds, the stratigraphical range of which will be discussed below. It seems possible, by its stratigraphical arrangement, that the "member C" could be correlated with the *Binodosus* zone or the lower part of the Alpine Anisic.

The Beneckeia beds do not contain any ammonite species hitherto known from other Triassic occurrences except those of Jordania and Sinai near to the Israelian outcrops. The genus *Beneckeia* is known from the uppermost Scythic to the deepest Anisic and it is possible that the *Beneckeia* beds and their base, the Wood-bearing beds, represent the entire development of the genus *Beneckeia*, from the Scythic to the lowermost Anisic, or in a stratigraphical scheme, according to Spath, they are to be correlated with the Prohungaritan and Beyrichitan.

The next occurrence of Triassic is situated about 30 km west of the Wadi Raman region on the other side of the Israelian and Egyptian border and is known as the

Araïf-el-Naga dome (Hafez Awad 1946). It seems that in the dome the deepest beds exposed are the *Beneckeia* beds, as in the Wadi Raman series. In the sections, noted by Hafez Awad, these beds are not observed, but isolated specimens of *Beneckeia* were found. The sandy layers below the lumachelles resemble the member "C" and lower "D" in the Wadi Raman, especially in that *Terebratula* concentrations are observed below such beds characterized by *Ceratites* and numerous Nautiloids. The higher beds cannot be correlated in detail with the Wadi Raman Triassic, but it appears that the same *Ceratites* beds are preserved and also the higher limestone without *Ceratites*.

The identification of the molluscs by Hafez Awad demonstrates that the stratigraphical position of the *Ceratites* beds must be Anisic or basal Ladinic.

The Araif-el-Naga dome is already indicated on Shaw's geological map of Palestine (1947). In 1952 Bentor and Vroman discovered an occurrence of Triassic at Mount Ariv, south-west of the Wadi Raman. There the *Ceratites* beds are similarly developed as in the Wadi Raman. Detailed observations are not available.

The oldest known Triassic in the region is reported by Cox in 1924 (discovered in 1923). He concluded that the fauna is sufficient to indicate a Carnic age. This corresponds with the Alpine Raibl Beds and with the German "Lettenkohle".

In 1932 Cox published a second paper on the Triassic of Trans-Jordan, in which he stated that in the Wadi Zerka-Main there occur Werfen Beds = Scythic. In this occurrence the entire section is formed of sandstones and shales and the stratigraphical range is very doubtful. It is a very important problem that the ammonites ("*Beneckeia* species") and the lamellibranchs indicate two different parts of the Triassic. Cox preferred to leave the question of the age quite open. The new results concerning the stratigraphy of the Wadi Raman make it fairly clear that a large part of the fauna of the Trias in Trans-Jordan belongs to upper Scythic and Lower Anisic.

It is too early to compare in detail the Sinai, Wadi Raman and Trans-Jordan Triassic with the Anatolian and Balkan occurrences. Such detailed comparisons provide scope for much fruitful work in the future, when exact determination of the rich fauna should allow a definition of the relation between the different parts of the sections in the different facies and localities in question.

The stratigraphical importance of the vertebrate fauna

Fishes occur rarely in the Raman Trias. The few remains of fishes all seem to belong to the *Elasmobranchii*. Scales of ganoid fishes were not discovered, although a great part of the author's short time in the Wadi Raman was taken up in searching for these fossils. The possibility exists that more fish remains will also be found in the Wadi Raman area, but it is already certain that they are not so common as, or possibly less well preserved than in certain localities in Germany, the Alps, Madagaskar or Greenland. The few *Elasmobranch* remains do not allow any conclusions to be drawn concerning the stratigraphy or relationships to other fish faunas.

The few fragments of *Stegocephalia* found in the Raman section confirm only the occurrence of this group in this region. *Stegocephalia* are wide-spread during the Middle Triassic in different parts of the Old World and their presence in the Negev demonstrates only one station between Europe, India and South Africa.

Nothosaurus sp. was already noted by Cox in 1924 from the Trans-Jordan Trias. The abundance of these reptiles in the Wadi Raman area is considered to be due to the fact that the environmental conditions were here the same as in the German Muschelkalk, where these reptiles were also fairly common. Isolated occurrences of nothosaurs outside the German Trias are rare, but the distribution from the Alpine facies to Palestine (Israel, Jordan, and northern part of Sinai) is not unexpected. If the remains are studied in detail, it will be possible to draw fined conclusions on the relationship between the Mediterranean (Palestine) nothosaurs and the German ones.

No *Placodus* or related genera were hitherto known outside Europe. The reason for its occurrence in Israel is the same as for the nothosaurs, i.e. identical environmental conditions here and in Central Europe at the times when these animals were living. Both *Placodus* and nothosaurs seem to have had a much wider distribution in space and time than has previously been observed.

The genus *Psephosaurus* was formerly known only from the lowest Upper Trias in Germany, where it occurs very infrequently and in only a few localities. In the Raman Trias it is common and distributed from the very beginning of the sections up to the highest layers containing vertebrate bones. As our knowledge of the distribution of the Triassic reptiles is very incomplete, it is difficult to theorize on the faunistic relation of the genus (see Appendix). The presence of *Psephosaurus* in the Lower part of the Muschelkalk or in the deepest Anisic makes it possible that the evolution of this genus is mostly confined to the Israelian region. All the other related genera are Upper Triassic: they are found in the upper part of the Keuper in the German Alps, in the Rhaetic of England and in the Rhaetic of Italy, in the German Lettenkohle and in the Keuper of the Balaton Lake region in Hungary. In all localities where these reptiles are found, the same facies conditions prevail: litoral margins or shallow sea.

The occurrence of *Tanystropheus* is hitherto known from the Anisic of the Alps. The finds of this fossil in Israel have the same stratigraphical position.

References

A list of works on Triassic stratigraphy up to 1948 will be found in Sherlock, R. L., The Permo-Triassic Formations, Hutchinson, London, 1948. In the references below publications of particular importance are listed.

Bentor, Y. K. (1952), Magmatic intrusions and lava sheets in the Raman area of the Negev (Southern Israel) Geol. Mag. Vol. 89.
Bentor, Y. & Vroman, A. (1952), A new occurrence of marine Triassic in Israel. Bull. of the Research Council of Israel. Vol. 1.
Brotzen, F. (1955), Occurrence of Vertebrates in the Triassic of Israel. Nature, Vol. 176.
Cox, L. R. (1924), Triassic fauna from the Jordan Valley. Ann. & Mag. Nat. Hist. Ser. 9, Vol. XIV.
—— (1932), Further notes on the Trans-Jordan Trias. Ann. & Mag. Nat. Hist. Ser. 10, Vol. X.
Eicher, D. B. (1947), Micropaleontology of the Triassic of North Sinai. Bull. Inst. d'Egypte, Tome XXVIII.
El-Din Hafez Awad, G. (1946), On the occurrence of marine Triassic (Muschelkalk) deposits in Sinai. Bull. Inst. d'Egypte, Tome XXVII.
Picard, L. (1947), See Shaw.
—— (1950), Geomorphogeny of Israel. Part I. The Negev. Geol. Survey of Israel. Publ. no 1.
Shaw, S. H. (1947), Southern Palestine. Geol. Map on a Scale of 1/250.000 with Explanatory Notes. Governm. of Palestine, Jerusalem.
Spath, L. F. (1934), Catalogue of the fossil Cephalopoda. Part IV. The Ammonidea of the Trias, London.
—— (1946), The Middle Triassic Cephalopoda from Sinai. Bull. Inst. d'Egypte, Vol. 27.
Swinton, W. F. (1952), A nothosaurian vertebra from Israel. The Ann. & Mag. Nat. Hist. Ser. 12, Vol. 5.

APPENDIX

Preliminary notes on some lamellibranchs and vertebrates from the Trias of Wadi Raman

In the previous discussion on the stratigraphy of the vertebrate-bearing beds of the Triassic in the Wadi Raman region, two new lamellibranchs and two new species of *Psephosaurus* have been reported. These fossils occur very abundantly, and from a stratigraphical point of view it is necessary to give short descriptions. More detailed studies are in progress and will be published in the near future.

Myalina beneckei n. sp.

Pl. 1, fig. 2 a, b, c.

Valve smooth, obliquely elongated, apical angle narrow, length: breadth about 2:1, height of each valve a little less than the maximal breadth. Characterized by its S-shaped crest. Length: about 7 cm.

This species differs from *M. tommasii* Salom. and *M. tommasii* Salom. var. *obtusa* Salom. by its elongated shape, the higher valves and the distinctly shaped crest. It seems that the hinge structure is typical and like that in other species of the genus. *Myalina blezingeri* Ph. is broader and not as high as this new species.

This species occurs very abundantly in the Member "B" of the Raman Triassic, often together with typical specimens of *Myalina tommasii* Salom. var. *obtusa* Salom. Most of the material collected in the sections has been given to the Geological Institute at Jerusalem and one specimen, the holotype, is in the collection of the Palaeozoological Department of the Natural History Museum in Stockholm.

Size of holotype: length approximately 7 cm, breadth approximately 5 cm.

Myalina ramanensis n. sp.

Pl. 1, fig. 1 c. Pl. 2, fig. 1 a, b.

Shell equivalvated, obliquely elongated, hinge margin long and straight, apical angle about 45, length : breadth about 5:3, length : height of each valve 5:2, average length 15 cm. Characterized by a sharp, S-shaped crest near the posterior margin. Surface more or less smooth, with concentric undulations. In nearly every detail this species resembles the previous *Myalina beneckei* n.sp. It differs in size, the stronger S-shaped crest of a more lateral position. In many aspects these reef building shells resemble some species of *Mytilus* from younger systems, but the hinge regions are very different. Related Triassic species are unknown. Numerous, well preserved, specimens were collected from the reefs of the Member C, and deposited at the collection of the Geological Institute in Jerusalem. The specimen described here, the holotype, is deposited in the collections of the Paleozoological Department of the Museum of Nat. Hist. in Stockholm.

Remarks on the genus *Psephosaurus* Fraas

Reptiles, characterized by a flat, turtle-like carapace were first described by von Meyer (1858) from the uppermost Triassic of the Alps. Since von Meyer's publication some new genera have been erected, which are all closely related. Several diverging views exist concerning their classification but all workers agree that this group of reptiles belongs to the *Placodontia*. The taxonomic rank of the *Placodontia* is not yet settled so far. Kuhn (1933) and v. Huene (1936 and 1952) regard them as an order whilst von Meyer, Jaekel, Camp, Welles and Morton Green (1953) consider them to be a suborder of the order *Sauropterygia*.

Huene (1936) divided the order *Placodontia* into two families: *Placodontidae* and *Cyamodontidae*, the latter comprising the subfamilies *Cyamodontinae* and *Henodontinae*, whilst Camp, Welles and Green (1953) distinguish four families in this suborder: *Cyamodontidae*, *Henodontidae*, *Placochelyidae* and *Placodontidae*.

The flat turtle-like genera belong to the *Placochelyidae* and the *Henodontidae*. Both "families" are characterized by the armour, which is composed of a great number of compact bony plates. This compact armour is lacking in all other "families" of the *Placodontia*, the short flattened rounded body distinguishes this group from all the other genera of the *Placodontidae* and *Cyamodontidae*.

The skulls of *Henodus* and *Placochelys* differ in many details from those of *Placodus* and *Cyamodus*, although the teeth of *Placochelys* demonstrate a relationship to the *Placodontidae*. The skull of *Henodus* is, however, too highly specialized, so that relationships with other *Placodontia* are difficult to prove. The author proposes therefore to classify the armoured turtle-like reptiles in a family of their own: *Placochelydidae*.

The known genera, which should be placed in this new family, are differentiated into two groups: one having a very heavy armour, a short, triangular skull with placodont teeth, the other having a lighter armour and a toothless rectangular skull. To the first group belong the genera *Psephosaurus*, *Psephoderma*, *Placochelys*, and to the second the genus *Henodus*.

V. Huene (1936) gave an account of the geological distribution of the Placodontia (including *Placodontia* sens. strict. and the *Placochelydidae*). The *Placochelydidae* as known at that time begin with *Psephosaurus* in the Lowermost Keuper (Lettenkohle) and came to an end on the boundary between the Triassic and the Lias. All placodonts have previously been found in Central Europe only, but the new fossils from Israel make a much larger distribution of the group in space and time evident.

***Psephosaurus mosis* n. sp.**

Pl. 3. 4, 5, 6. Text-figs. 3, 4, 5.

DIAGNOSIS. Skull short, triangular, squamosal large, provided with distinct and projecting tubercles.

Dorsal armour approximately as wide as long; almost flat, truncated or with a concave emargination for the neck and with distinct emarginations for the hind limbs. Lateral walls forming angle of 110–150 degrees with the dorsal surface. Dorsal armour composed of a great number of irregular, polygonal plates. All plates of the dorsal armour grow together into a complete unit. Ventral armour (as far as preserved) composed of plate-like gastral ribs, which are not fused.

REMARKS.—The occipital and middle part of the skull is preserved but as the complete preparation will require a considerable time, only the main characters will be discussed here.

The parietal side is not yet prepared and only the posterior edge of the squamosal. showing three prominent bony tubercles, similar to those of *Placochelys placodonta*, are visible. They are of the equal size, and do not decrease towards the orbits, as in *Placochelys*. This typical ornamentation of the squamosal is also present in *Henodus*.

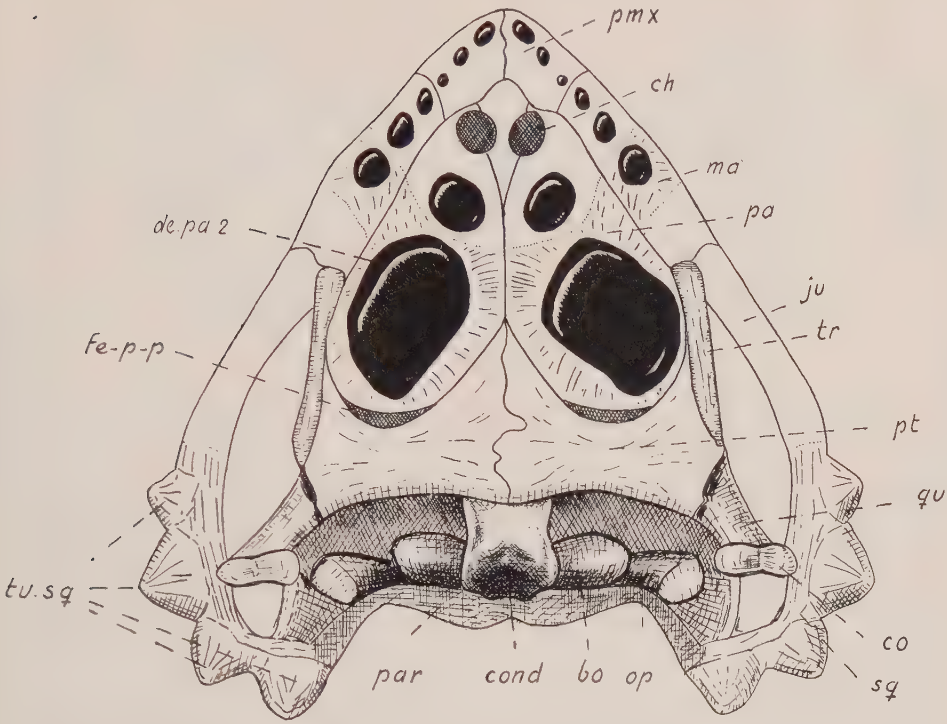

Textfig. 3. Skull of *Psephosaurus mosis* n. sp. Palatal view. Abbreviations as in plate 3.

The occipital region is fairly depressed and not as high as in *Placochelys*. The parietal roof has been crushed during fossilization and the preparation is not yet complete. The boundary between the parietals and the squamosal is not distinct and the junction between the quadrate and the squamosal is difficult to see, but the quadrate shows an intact condyle, which is saddle shaped. The quadrate meets the pterygoids, which form a distinct step towards the occipital region, resembling *Placochelys* in nearly all details. The bones around the foramen magnum differ strongly from those in *Placochelys*. There is probably a paired element and two seperate exoccipitals reaching far down around the foramen magnum.

The exoccipitals are transversely narrow and reach downwards only as far as the foramen in the jugulum. The basioccipital alone forms a well rounded condyle, whilst the lower part of the opisthotic has a long ridge from the occipital region downwards to the junction between the quadrate and the squamosal. This ridge together with the large basioccipital condyle give the occipital view of the skull a peculiar character, differing from *Placochelys*, *Henodus* and *Cyamodus*. The basioccipital condyle and also the ridge of the opisthotic resemble, principally, the corresponding parts of *Placodus*, but the pterygoid, squamosal and quadrate regions are very similar to both *Placochelys* and *Cyamodus*.

The palatal face shows the lower parts of the occipital region, the condyle of the quadrate, the pterygoids, the palatines with one large tooth on each side, and the remains of one maxilla bearing a tooth.

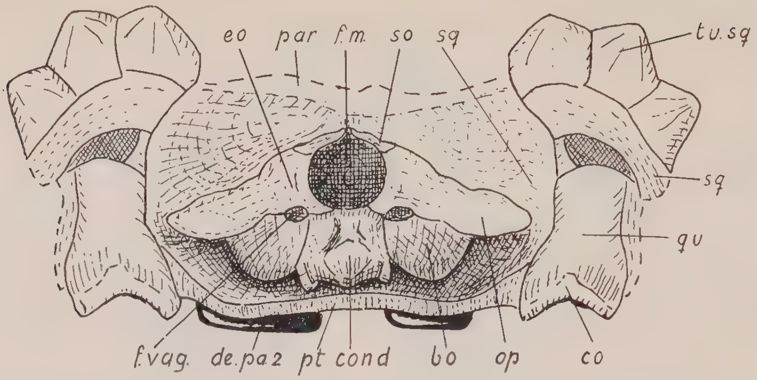

Textfig. 4. Skull of *Psephosaurus mosis* n. sp. Occipital view. Abbreviations as in plate 3.

The general arrangement of the quadrate, pterygoid, palatine and of the teeth does not differ substantially from *Placochelys*, but in details shows a greater similarity to *Cyamodus*. The anterior border of both pterygoids form an angle projecting between the palatines as in *Cyamodus*. Along the posterior border of the palatines, between the large teeth and the pterygoid, there are some foramina similar to those figured by Jaekel in *Cyamodus*. The shape of the teeth resembles closer those of *Cyamodus* than of *Placochelys*.

The bony tubercles on the squamosal indicate that the skull belongs to a member of the family *Placochelydidae* and is closely related to *Placochelys*, but having ancestral characters resembling *Cyamodus* and *Placodus*. In connection with the abundance of armour fragments of *Psephosaurus*, this skull seems to belong to the genus *Psephosaurus* since it was found in the same layer as the carapace. The author does not hesitate, therefore, to place the skull and the carapace to the same species. Both elements were found some 50–100 meters apart.

The whole carapace has been embedded completely, the missing half however has been eroded, parts of the broken section were visible on the surface of the rock. The entire block was transported to Stockholm for preparation, subsequently the original was returned as a gift to the Hebrew University in Jerusalem. The preserved fossil shows a part of the dorsal carapace, its margin and some elements of the plastron. The fossil is broken into three parts by fissures, which are of tectonic origin and filled with gypsum, and which cross both sutures and plates.

The dorsal armour has a flat dorsal side with a wide anterior emargination; the lateral margins are rounded, except in their posterior part, where the margin is incised for the hind limb. The caudal margin is not preserved. It is not possible to give the exact size of the complete dorsal armour. The length of the middle line from the incision for the head to the broken part of the caudal margin is about 53 cm, the greatest breadth (between the angles of the dorsal surface and the lateral walls) measures about 35–37 cm, the lateral walls have a maximum height of 6 cm, whilst the angle between the lateral wall and the dorsal plane is about 110–150 degrees. The dorsal armour is 14–16 mm thick and is composed of numerous plates, which are bordered on the outside by deep and distinct grooves and on the inside by more or less indistinct sutures; the shape and size of the plates is very variable. The edge between the lateral and dorsal wall is marked by a row of plates which are of two

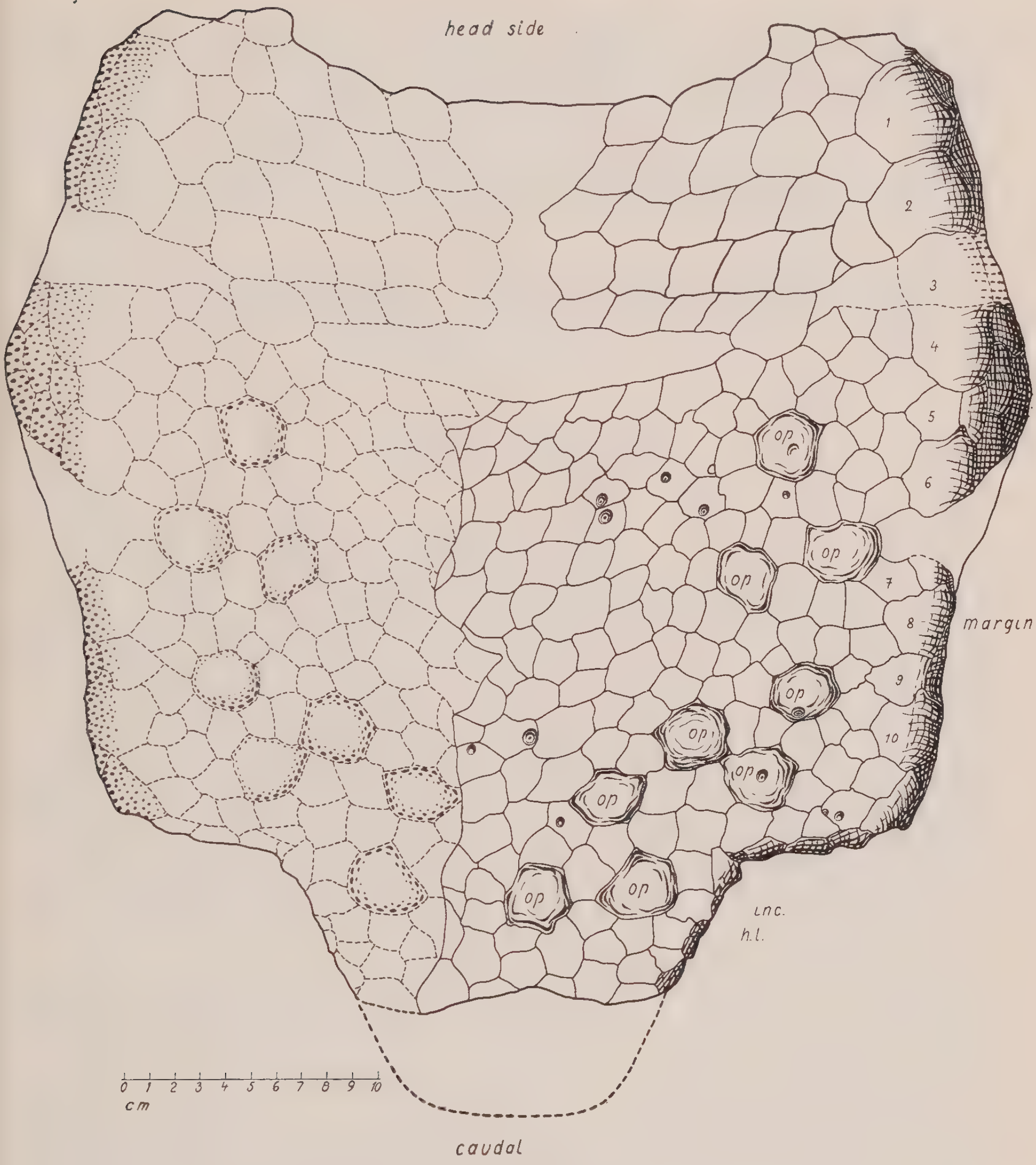

Textfig 5. *Psephosaurus mosis* n. sp. Reconstruction of the dorsal armour. *inc. h.l.* = emargination for the hind leg. *op* = ornamented plates. 1–10 = marginal plates.

types, one larger and more elevated than the other. The larger plates are angular polygonal and decrease in diameter caudally. There are eight large plates. The first four anterior plates follow each other without interruption, two small plates are situated behind plate number four, but the next is also a large one. The shape of the plates of the edge does not show any regularity. The first ones are more or less rounded, or hexagonal, with rounded angles and the third is partly indented into the second. These first three plates are only slightly elevated and not higher than the surrounding ones but the fourth and the succeeding large plates of the edge are elevated.

Only on the dorsal surface do the plates of the anterior part show some regularity. It is possible to trace four transverse rows of rhomboidal plates, whose sutures are slightly depressed. The medial and caudal part of the dorsal surface is composed of very irregular plates, with strongly depressed and very distinct sutures. Near the margin of the caudal part some single plates are larger than the others and somewhat elevated.

The lateral walls are depressed and appear to be built up of two or three rows of elements with indistinct sutures. Only under the anterior portion of the armour several gastralia are preserved; five rib-like plates are exposed, building up a closed ventral armour. These plates are 2–3 cm broad, about 5–6 mm thick, unfortunately very poorly preserved.

Between the heavy dorsal and ventral armour parts of the internal skeleton can be discerned; one element appears to be a coracoid.

RELATIONSHIP.—The number of described forms of armoured placodonts is very small. *Psephosaurus suevicus* Fraas 1896 from the lowermost Keuper of Germany most nearly resembles the new species. Even to the present time fragments only of the dorsal armour constitute our only knowledge of this genus. Huene described and figured in 1936 the largest fragment, which has approximately the same size as ours (38 × 22 cm), but unfortunately all the fragments of *Psephosaurus suevicus* belong to the central part of the dorsal armour and no marginal parts are preserved. The irregular pattern of the plates of *Psephosaurus* comprising a few scuttered large plates, resembles the new species. The plates of the German species are generally more rounded and not so irregularly angular or rhomboidal as in the new species. The larger plates of *Psephosaurus suevicus* are distinctly provided with a medial tubercle on each plate, which does not conform with the new find. It seems that *Psephosaurus suevicus* and the new fossil are closely related, but as long as both species are imperfectly known, it will be very difficult to decide whether one or two genera are represented. The author, therefore, describes the new fossil provisionally as a "*Psephosaurus*". There is no doubt that the fossil from Germany and that from Israel belong to two different species clearly distinguished by the shape of the plates and their sutures.

Psephosaurus mosis n.sp., *Psephoderma*, and *Placochelys* exhibit many common characters in the dorsal armour. *Placochelys placodonta* Jaekel has differently shaped plates, but the edges between the dorsal surface and the lateral walls are covered with a row of larger plates, as in *Psephosaurus mosis* und the angle and height of the lateral walls are very similar to the Israelian species.

In *Psephoderma alpinum* Meyer, again, the best known of all related genera, the plates are different in shape from those of our fossil; it seems, however, that the shape of the entire shield is very similar to that of *P. mosis*. These species have also another characteristic feature in common: in *Psephoderma alpinum* many plates have circular depressions, irregularly distributed on the armour, whose diameter varies from 3 to 7 mm and similar depressions are observed on the new species.

The name of the new species has been given in honour of Dr. Moshé Avnimelech, Hebrew University, Jerusalem, who for thirty years has been collecting and describing geological and paleontological material from Israel, Jordan and Syria.

SIZE.—The skull: Half the breadth of the occipital region; from the middle of the forâmen magnum to the highest point of the tubercles of the squamosal 5.2 cm or the maximum breadth 10.4 cm (*Placochelys placodonta* Jaek. 12.5 cm; *Cyamodus* sp. according to Jaekel 12.8 cm); height of the occipital region from the parietals to the pterygoid plane: 3.5 cm (parietals depressed), *Placochelys placodonta* 4.8 cm. Maximum breadth between the large palatine teeth: 6 cm (*Placochelys placodonta* head no. 2 acc. Jaekel 5.2 cm; *Cyamodus* acc. Jaekel 4.8 cm).

CARAPACE: Length of middle line from the emargination for the neck to the end of the preserved armour: 37 cm (reconstructed specimen: about 41 cm); length of the largest preserved carapace of *Psephoderma suevicus* according to Huene 1936, 38 cm.

Largest width of the preserved armour 19 cm, including the marginal plates 21 cm. Width of the reconstructed carapace about 40 cm. Height of the carapace 4 cm.

STRATUM.—*Beneckeia* beds zone 1–4 (Upper Scythic or Lowermost Anisic).

HOLOTYPE.—Dorsal armour, Hebrew University, Jerusalem.

Psephosaurus picardi n. sp.

Pl. 7.

MATERIAL.—An interior cast of a large carapace, partly covered with the bones. Many fragments of the armour from different layers.

CHARACTERS.—Carapace with high lateral walls nearly perpendicular to the dorsal plane. Outline of the carapace rounded and caudally elongated. Length unknown, possibly over 50 cm, maximum breadth about 50 cm, height of the lateral walls 7–8 cm. Elements of the carapace variable in shape and size. Sutures between single elements form an irregular zigzag.

REMARKS.—This species is distinguished from *P. mosis*, by its larger carapace, its steeper and higher lateral walls, and its generally smaller armour elements. Even the elements on the marginal border are extremely small in comparison with those of *P. mosis*, therefore the number of rows is larger. Another character which distinguishes this species from *P. mosis* consists in more irregular sutures of the single elements. This character shows a resemblance to the elements of *Psephosaurus suevicus* Fraas from the German Lettenkohle (Uppermost Ladinic) but their arrangement is different: tubercle-bearing plates do not exist in this new species.

The carapace with its high, steep lateral walls and small armour elements, permits to erect a new species of the well characterized genus *Psephosaurus*.

Further details of the species will be published later.

STRATIGRAPHICAL DISTRIBUTION.—*Ceratites* beds in the Triassic of the Wadi Raman.

HOLOTYPE.—The cast of a carapace. Paleozoological Department, Natur. History Museum, Stockholm.

This species is named in honour of Prof. L. Picard, Hebrew University, Jerusalem, founder of modern geology in Israel and the neighbouring regions.

Notes on the stratigraphical distribution of the genus *Psephosaurus* and related genera

According to von Huene (1936) and Kuhn (1933) the different genera of the order Placodontia are stratigraphically distributed as follows:

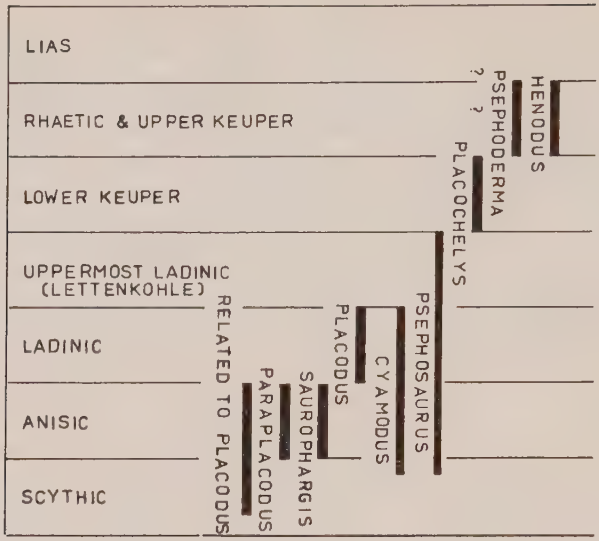

All these genera occur very rarely, and our knowledge of the stratigraphical distribution is very imperfect indeed. From the upper part of the Scythic only a few isolated teeth of *Placodus* (?) *impressus* Ag. are known. In the Anisic are found *Paraplacodus*, *Saurosphargis* and *Cyamodus*. The new specimens from Israel demonstrate that teeth of *Placodus* or related genera are present in the *Beneckeia* beds and typical species of *Psephosaurus* are already known from the same beds. The stratigraphical range of the *Beneckeia* beds is probably Uppermost Scythic or Lowermost Ladinic, which demonstrates that the two families, *Placodontidae*, comprising *Paraplacodus* and *Cyamodus*, and *Placochelydidae* represented by *Psephosaurus*, are already separated at least in the Lowermost Anisic.

Another hypothesis is possible, namely, that the very specialized order of *Placodontia* occurs in the Lower Triassic simultaneously with three highly specialized groups:

Placodontia with elongated skulls, three pairs of palatine teeth and without compact body armour.

Cyamodontidae. Placodontia with triangular skulls, two pairs of palatine teeth, without compact body armour.

Placochelydidae. Placodontia with triangular skulls, two pairs of palatine teeth, and with compact body armour.

This indicates the possibility that more genera of this group than hitherto known already existed in the Lower Triassic and the specialization of genera and species seems to have begun long before the Middle Triassic.

References

Fossilium Catalogus I. Pars 8: C. Diener (1915), Cephalopoda triadica. Pars 19: C. Diener (1923), Lamellibranchiata triadica. Pars 51: A. Kutassy (1831), Lamellibranchiata triadica. II. Pars 56: A. Kutassy (1933), Cephalopoda triadica. II. Pars 62: O. Kuhn (1934), Placodontia.

BONI, ALFR. (1937), Vertebrati Retici Italiani. R. Accademia Nazionale dei lincei. Ser. VI, Vol. VI.

BROTZEN, F. (1955), Occurrence of vertebrates in the Triassic of Israel. Nature. Vol. 176.

CAMP, C. L., WELLES S. P., and GREEN, M. (1949), Bibliography of Fossil Vertebrates 1939–1943. The Geological Society of America. Memoir 37.

—— (1953), Bibliography of Fossil Vertebrates 1944–1948. The Geological Society of America. Memoir 57.

COX, L. R. (1924), Triassic fauna from the Jordan Valley. The Ann. & Mag. Nat. Hist. Ser. 9, Vol. XIV.

—— (1932), Further notes on the Trans-Jordan Trias. Ann. & Mag. Nat. Hist. Ser. 10, Vol. X.

DREVERMANN, F. (1933), Das Skelett von Placodus gigas Ag. im Senkenberg Museum, Abh. Senkenberg Naturf. Ges. Bd. 38.

EL-DIN HAFEZ AWAD, G. (1946), On the occurrence of marine Triassic (Muschelkalk) deposits in Sinai. Bull. Inst. d'Egypte, Tome XXVII.

GREGORY, W. K. (1946), Pareiasaurs versus Placodonts as near ancestors to the turtles. Bull. Americ. Museum Nat. Hist. Vol. 86, New York.

HUENE, F. VON (1936), Henodus chelyops, ein neuer Placodontier. Paleontographica Bd. 84.

—— (1952), Die Saurierwelt und ihre geschichtlichen Zusammenhänge. Jena.

SPATH, L. F. (1934), Catalogue of the fossil Cephalopoda. Part IV, The Ammonoidea of the Trias. London.

—— (1946), The Middle Triassic Cephalopoda from Sinai. Bull. Inst. d'Egypte. Vol. 27.

SWINTON, W. F. (1952), A nothosaurian vertebra from Israel. The Ann. & Mag. Nat. Hist. Ser. 12, Vol. 5.

These works contain all older publications quoted in the text.

Tryckt den 5 december 1956

Uppsala 1956. Almqvist & Wiksells Boktryckeri AB

PLATES

Plate 1

Fig. 1 c. *Myalina ramanensis* n. sp. Apical view (see pl. 2, fig. 1 a, b). Wadi Raman. Member C. (Natural size.)

Fig. 2 a, b, c. *Myalina beneckei* n. sp. (a) Frontal view; (b) marginal view; (c) apical view. Wadi Raman. Member B. (Approximately natural size.)

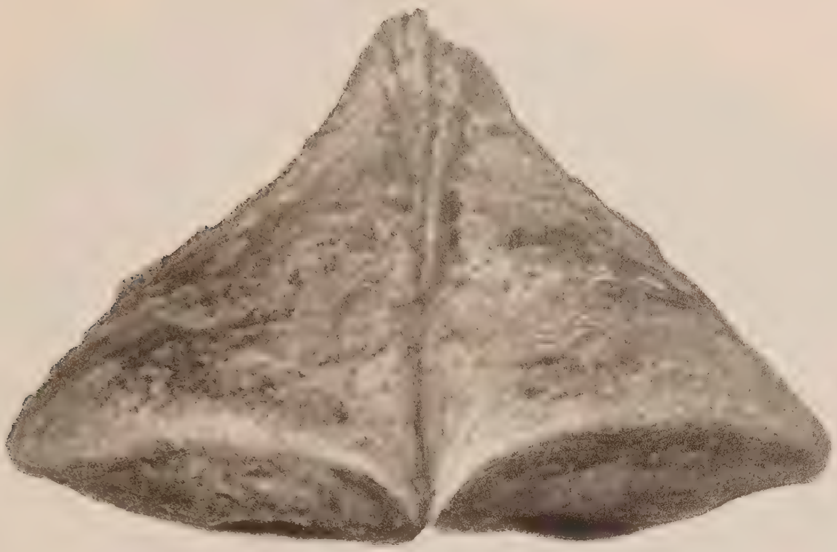

1c

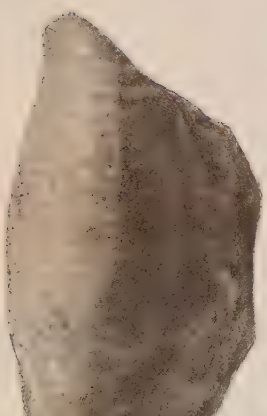

2a

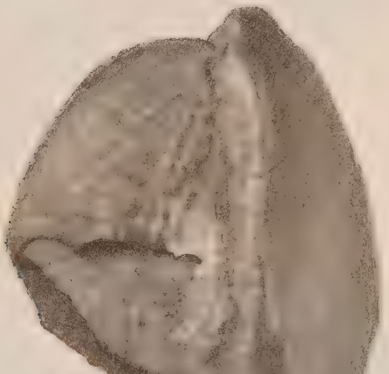

2b

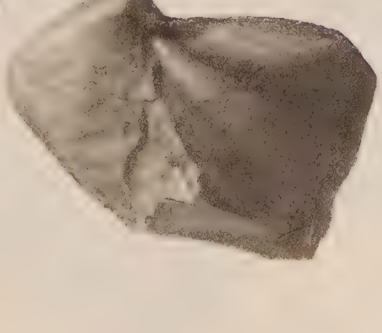

2c

Plate 2

Fig. 1 a, b. *Myalina ramanensis* n. sp. (a) Frontal view; (b) marginal view. Wadi Raman. Member C. (Approximately natural size.)

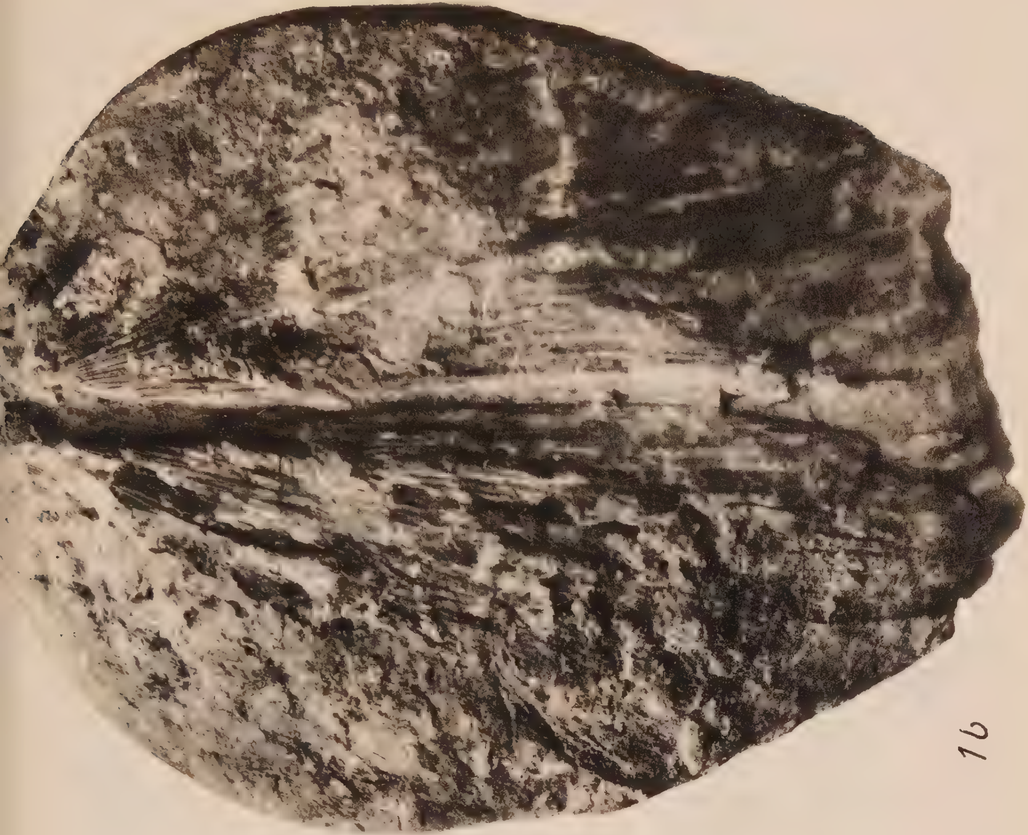

1b

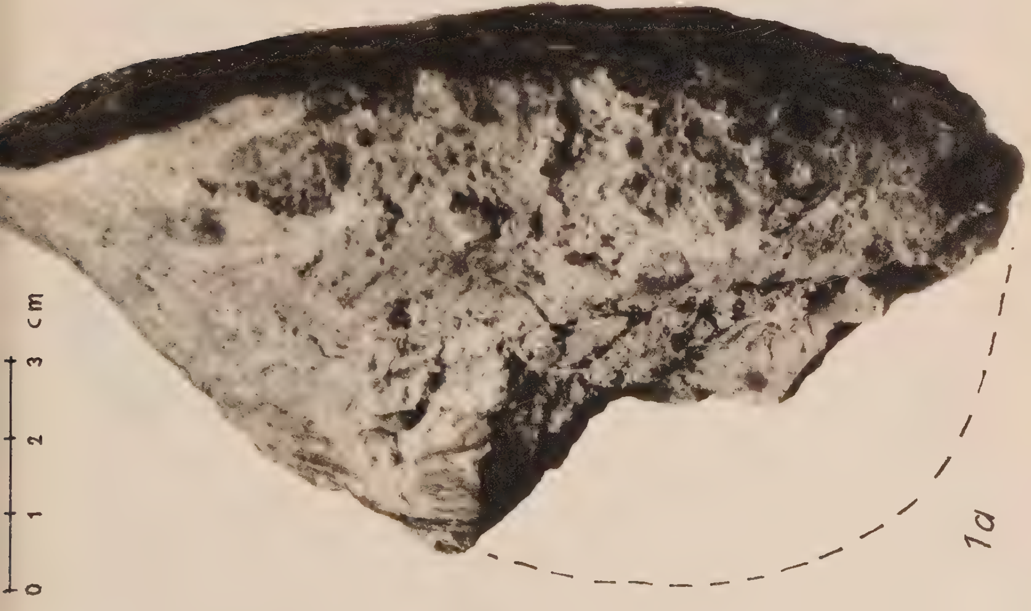

1a

Plate 3

Psephosaurus mosis n. sp.

(A) skull, palatal view; (B) skull, occipital view.

bo	basioccipital
co	condyle of quadrate
cond.	basioccipital condyle
de. pa$_2$	anterior tooth on the palatine
eo	exoccipital
f. m	foramen magnum
fe. p-p	palatine-pterygoid fenestra
f. vag	foramen for the nerves of the vagus group and the vena cerebralis posterior
ju	jugal
ma	maxillary
op	opisthotic
pa	palatine
par	parietal
pmx	premaxillary
pt	pterygoid
qu	quadrate
so	supra occipital
sq	squamosal
r	transverse
u. sq	tubercle on the squamosal

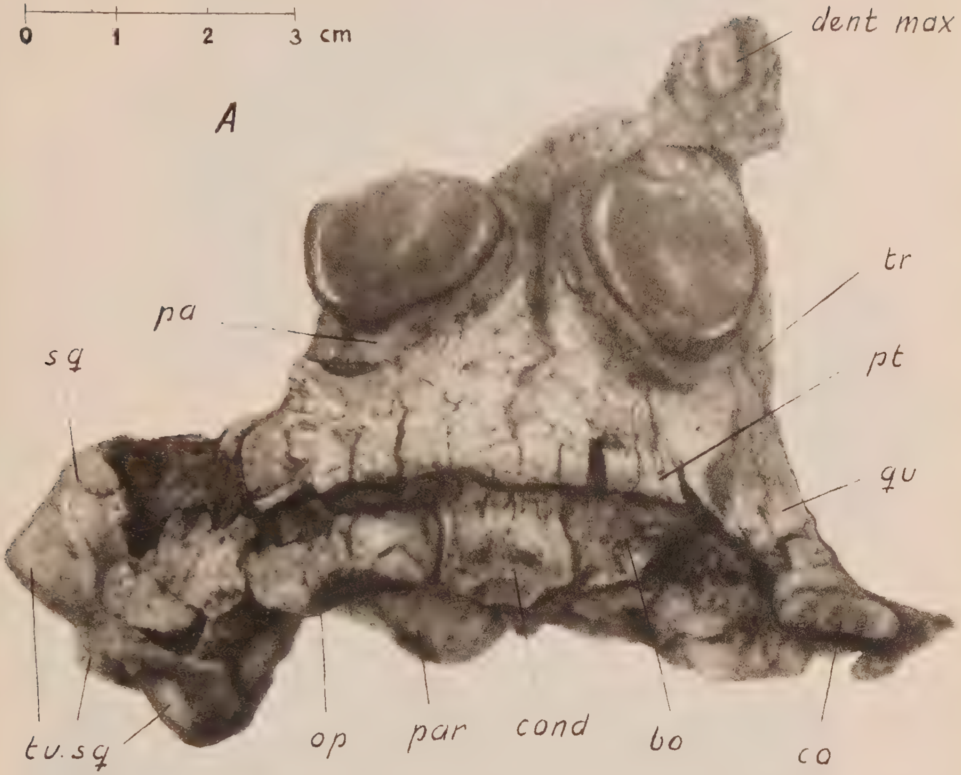
0
1
2
3 cm
dent max
A
tr
pa
sq
pt
qu
tu.sq
op
par
cond
bo
co

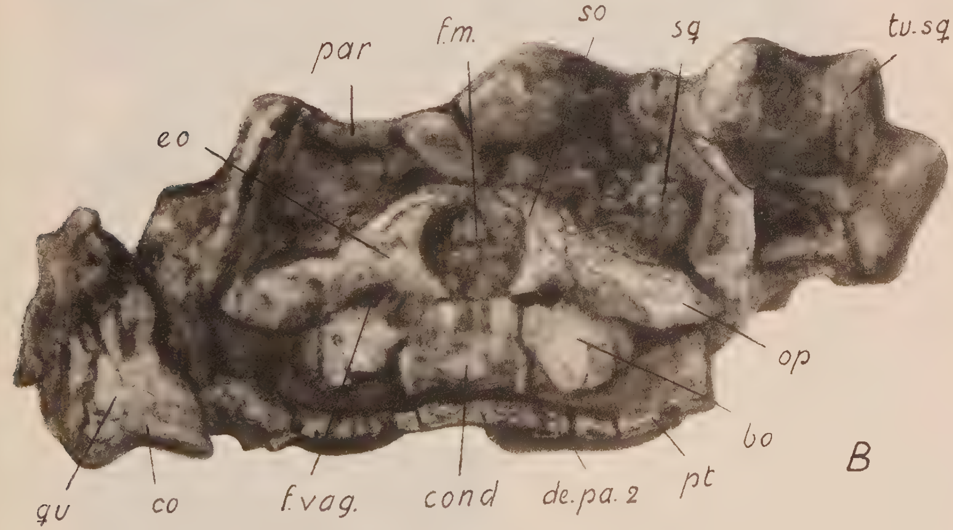
so
f.m.
sq
tu.sq
par
eo
op
bo
B
qu
co
f.vag.
cond
de.pa. 2
pt

Plate 4

Psephosaurus mosis n. sp. Dorsal armour.

e. an.	emargination for the anterior leg
e. po.	emargination for the hind leg
ma.	marginal part of the armour

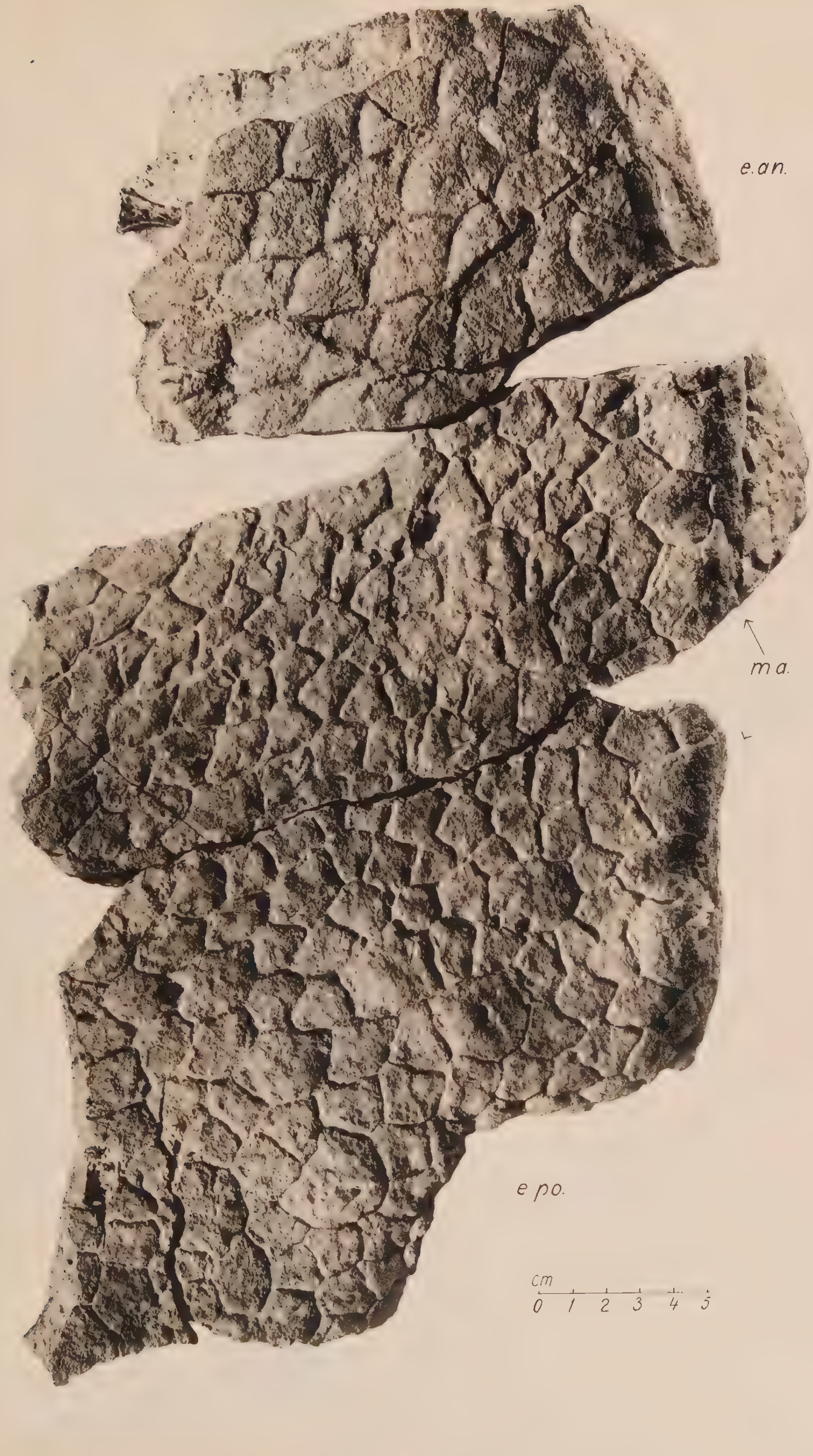
e.an.
ma.
e po.
cm
0 1 2 3 4 5

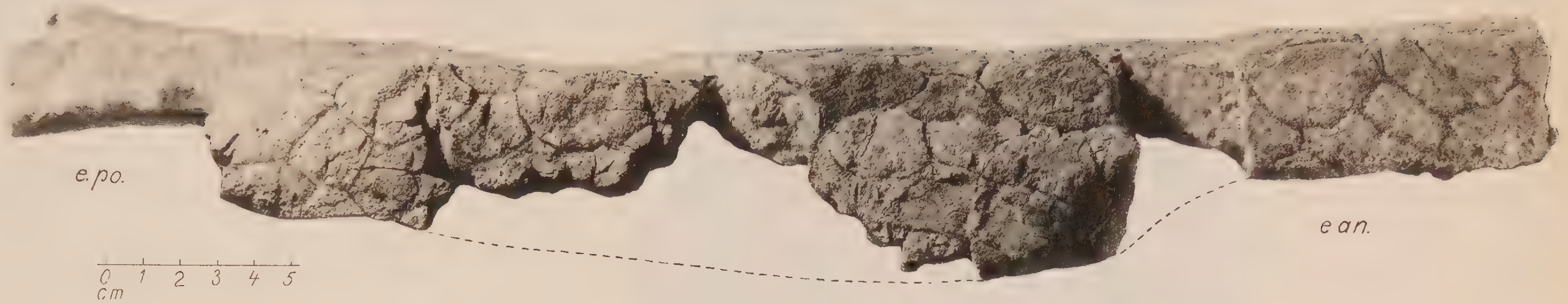

Plate 5

Psephosaurus n. sp. Side view of the dorsal armour.

e. an. emargination for the anterior leg
e. po. emargination for the hind leg

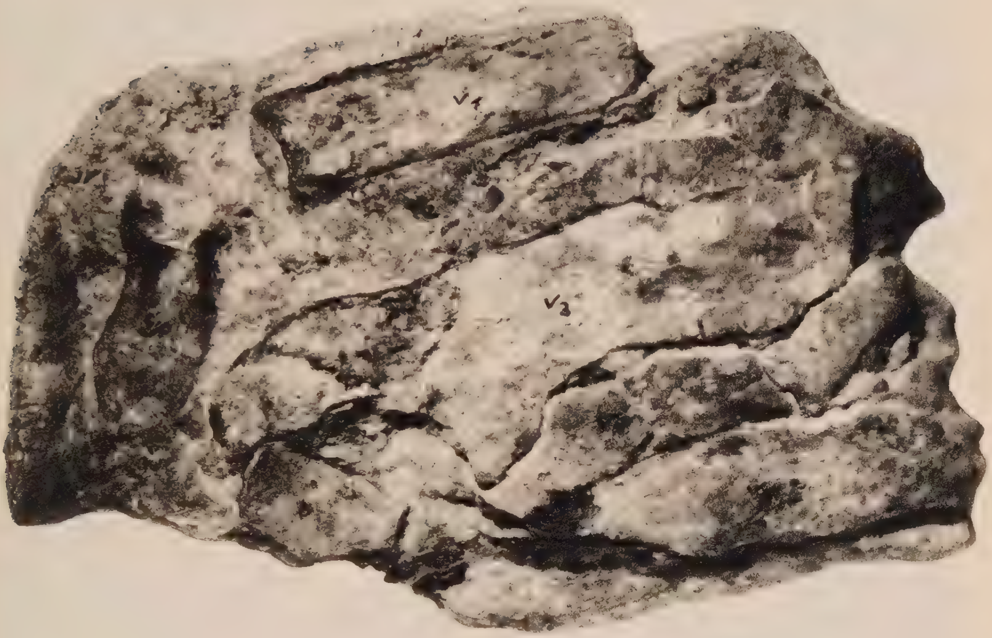

Plate 6

Psephosaurus mosis n. sp. Ventral side.

b Isolated bone; *Sc*? coracoid; *v* 1–5, gastral ribs.

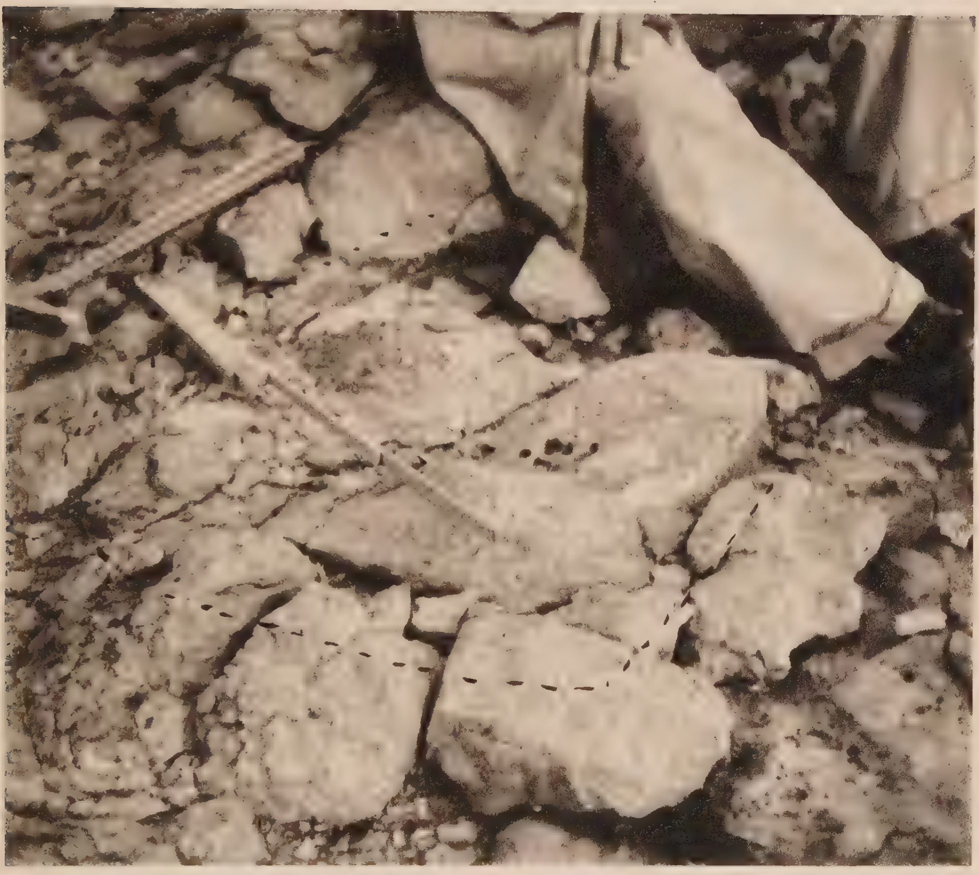

Plate 7

Psephosaurus picardi n. sp. Cast of the dorsal armour, partly covered with the bones. Original under preparation.

ARKIV FÖR MINERALOGI OCH GEOLOGI Band 2 nr 10

Communicated 9 November 1955 by ERIK STENSIÖ and KARL LANG

On the relations of the principal muscles to the shell in *Nautilus* and some fossil nautiloids

With a taxonomic appendix

By HARRY MUTVEI

With 20 plates and 24 figures in the text

Contents

Page
Introductory Remarks 219
Nautilus
1. Anatomic ground-plan and body orientation. 220
2. The shell and its relations to the soft parts 222
   a) Domiciliary division. 223
   b) Septate division. 226
Fossil nautiloids
1. Coiling of the shell 228
2. Annular elevation 228
Taxonomic appendix
Measurements 244
Uranoceras HYATT 244
U. (?) *longitudinale* (ANGELIN) 245
Lyecoceras n. gen.. 248
L. gotlandense n. sp. 248
L. longistriatum n. sp. 250
References 253

Introductory remarks

The present paper, which represents a part of the writer's studies on the shell structure and systematics of fossil nautiloids, deals with the functional areas of origin of the retractor muscles, longitudinal mantle-musculature and sub-epithelial musculature in the dorsal portion of the body proper in certain fossil nautiloids. In order to interpret these areas of origin in the fossil forms a general survey of the corresponding structures in recent *Nautilus* is also made. This survey is based on the literature, but since the statements in the literature often are rather obscure and incomplete the present writer has made some complementary investigations on *N. pompilius* L. (one specimen preserved in alcohol and several dried shells). The shell terminology in *Nautilus* has also been revised and several misleading and erroneous terms have been replaced by new and more suitable ones. This new terminology is, of course, wholly applicable to the shells of fossil nautiloids.

In addition to material in the possession of the Palaeozoological Department of the Swedish Museum of Natural History, Stockholm (below abbreviated to RM) I have also had at my disposal specimens belonging to the following institutes and museums: the Paleontological Institute, Uppsala (below abbreviated to UPI); the Geological Survey of Sweden, Stockholm; the Paleontological Institute, Lund; and the British Museum (Natural History), London. I would like to express my very sincere gratitude to the authorities of these institutes and museums for generously lending their material. I wish to record also my best thanks to Dr. V. Jaanusson, Uppsala, who suggested this paper, and to Dr. L. F. Spath, London, who assisted with the correct identification of several Mesozoic nautiloids.

The orientation of the nautiloid shells figured in the following text-figures and plates is in most cases the reverse of their anatomical orientation; on every plate and text-figure, therefore, the ventral and dorsal directions are given.

Nautilus

1. Anatomic ground-plan and body orientation

The main outlines in the anatomy of molluscs are, according to Hescheler (1900), Pelseneer (1906) and Naef (1926), briefly as follows. The anterior portion of the molluscan body is formed into a head (*h*, text-fig. 1 D, E, G, H) and the ventral portion of the body into a powerful, muscular foot (*f*, text-fig. 1 A–F). Around the periphery of the body there exists a downwardly hanging fold, the mantle fold (*mf*, text-fig. 1 C), which constitutes the external wall of a cavity, the mantle cavity (*mc*, text-fig. 1 C–H). The posterior portion of the mantle cavity, which is considerably dilated, houses the pallial organ-complex which includes the gills (*g*, text-fig. 1 D–H) and the anal (*a*, text-fig. 1 A–H), reproductive and excretory apertures. The dorsal portion of the body is enclosed by a shell which is secreted by the epithelium of the dorsal surface of the body and by the external and marginal epithelium of the mantle fold. The powerful foot contains, *inter alia*, a special retractor muscle which has its functional origin on the inside of the shell (see below). The nervous system is composed of (1) a circumoesophageal nerve-ring (*cr*, text-fig. 1 D–H) along which, in most cases, the nerve cells are localised in three pairs of ganglia (cerebral, pedal and pleural), and (2) two paired nerve cords, a ventral pedal cord (*pc*, text-fig. 1 D, E) and a dorsal pleuro-visceral cord (*pvc*, text-fig. 1 D–H), both of which issue from the circumoesophageal ring whence they run backwards. The pedal cord innervates the foot, whilst the pleuro-visceral cord innervates the dorsal integument, including the mantle fold, the viscera and gills.

Huxley (1853), Balfour (1880), Hescheler (loc. cit.), Pelseneer (loc. cit.), Plate (1922) and Naef (loc. cit.) have correctly pointed out that in cephalopods the mantle fold, the pallial organ-complex and the shell are developed in accordance with these principles of molluscan anatomy. In connection with the transition from a creeping to a largely drifting way of life the cephalopods acquired a high, conical shape (text-fig. 1 H). The head, together with the mouth, secondarily moved downwards to the ventral side of the body, whilst the foot was modified into the funnel (*fl*, text-fig. 1 G, H) and into the tentacles around the head (text-fig. 1 G, H). That the nautiloids have undergone such an evolution is proved by the following facts: (1) the nerves of the tentacles must be derived from the original pedal nerve cord (Thore 1939); (2) the tentacles originate embryologically between the mouth and the anus on the ventral side of the body, and it is fairly late, during ontogeny, that they take up a position around the head; and (3) the original retractor muscle of the molluscan foot persists and is inserted on the cartilages in the head and in the anterior portion of the funnel; in dibranchiates it is differentiated into both the retractor capitis and the depressor infundibuli.

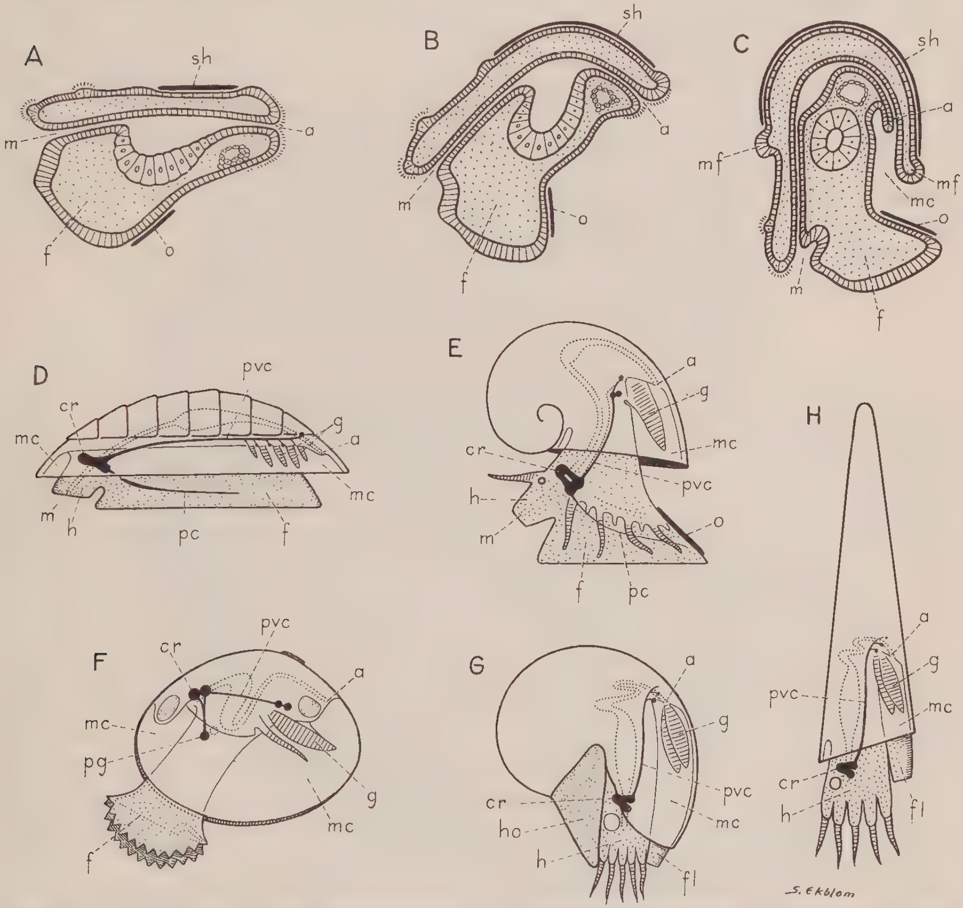

Text-fig. 1. Diagrams to show main features of molluscan anatomy and orientation of body. A, B, C, median-sagittal sections through an embryo of *Paludina* at three successive stages; these figures show retroflexion of rectum, development of mantle fold and of shell; D, prototype of chitonid; E, prototype of gastropod; F, prototype of lamellibranch; G, *Nautilus*; H, straight-shelled fossil nautiloid (figs. A–F after Naef 1926).

a, anus; *cr*, circumoesophageal nerve-ring; *g*, gills; *f*, foot; *fl*, funnel; *h*, head; *ho*, hood; *m*, mouth; *mc*, mantle cavity; *mf*, mantle fold; *o*, operculum; *pc*, pedal nerve-cord; *pvc*, pleuro-visceral nerve-cord.

The shell in dibranchiates is more or less secondarily reduced and lies embedded in the soft tissues, whilst the shell in tetrabranchiates, i.e. *Nautilus*, is unreduced and external. Since the shell in the latter form bends into a forwardly directed spiral the dorso-ventral axis of the shell also is twisted into a corresponding spiral (text-figs. 1 G, 2 A), The morphologically posterior side of the shell is the peripheral side of the whorl and the morphologically anterior side of the shell the central side of the whorl.

In relation to the orientation of the animal in the water the morphological dorso-ventral axis of the body in certain primitive, fossil nautiloids, with slightly coiled shells (e.g. *Orthoceros*, *Michelinoceras*, *Kionoceras*), was vertical, but in the majority of the fossil and recent cephalopods this axis has secondarily acquired a more or less horizontal position. This situation has arisen in connection with the adoption by the cephalopods of a more mobile manner of living either by the coiling of the shell, as in the many fossil nautiloids, ammonoids and in the living *Nautilus*, or by the reduction of the shell, as in dibranchiates. In both cases the body became streamlined and the funnel acquired a horizontal position which is more suited to its function. Due to the fact that the morphological dorso-ventral axis of the body of many cephalopods lies secondarily horizontally or approximately so many writers (e.g. Owen 1832, Keferstein 1860, Barrande 1877, Appellöf, 1893, Griffin 1900, Willey 1902) have considered it to be the antero-posterior axis of the body, but such an interpretation is based on a misunderstanding of the principles of molluscan anatomy.

2. The shell and its relations to the soft parts

From a descriptive point of view the *Nautilus*-shell may be regarded as composed of two divisions: (1) the *domiciliary division* (“dwelling chamber”, Owen; “grande chambre”, Barrande; “domicilium”, Holm; “body chamber”, Griffin, Flower, Miller; “living chamber”, Hyatt; “animal chamber”, Willey; “Wohnkammer”, Appellöf, Keferstein, Teichert; etc.) and (2) the *septate division* (“partie cloisonne”, Barrande; “phragmocone”, Teichert, Foerste; “phragmocone + protoconch”, Owen, Holm, Flower, Miller; etc.).[1]

---

[1] The term “phragmocone” was introduced by Owen (1832) for a certain division of the belemnoid shell, which, according to Owen (1844), is composed of three divisions: “1st. The terminal spathose body called the ‘guard’, sheath or rostrum. ... 2nd. The chambered or siphonated part of the shell which I have called the ‘phragmocone’, and which is lodged in the conical alveolus or cavity at the base of the ‘guard’. 3rd. The conical, thin, but dense, corneo-nacreous case, which immediately invests the phragmocone, and lines the alveolus of the guard; commencing at the bottom or apex of that cavity, and continued beyond the thin margins of the basal aperture of the alveolus, and beyond the last septum of the phragmocone, to form, as Dr. Buckland rightly describes, the large anterior chamber of the Belemnite containing the ink-bag and some other viscera.”

The “phragmocone” in this original sense represents the septa and the internal layer of the septate division in the nautiloid shell (cf. Naef 1922), whilst Owen’s third division, which was called the “conotheca” by Huxley (1864), corresponds to the external shell layer in nautiloids. Since the belemnoid shell was entirely embedded in soft parts its domiciliary division is strongly reduced and its septate division enclosed by the “guard” or the “rostrum”, which is a secondary formation, without any corresponding structure in nautiloids.

From these facts it is evident that the terms “phragmocone” and “conotheca” are misleading and superfluous and must therefore be rejected.

a) Domiciliary division

The domiciliary division which is the lowermost, youngest portion of the shell encloses a large continuous cavity, the *domiciliary cavity* (text-fig. 2 A; pl. 1). This cavity, which contains the head, the mantle fold and the greater portion of the body proper ("visceral hump"), is defined dorsally by the youngest septum and opens

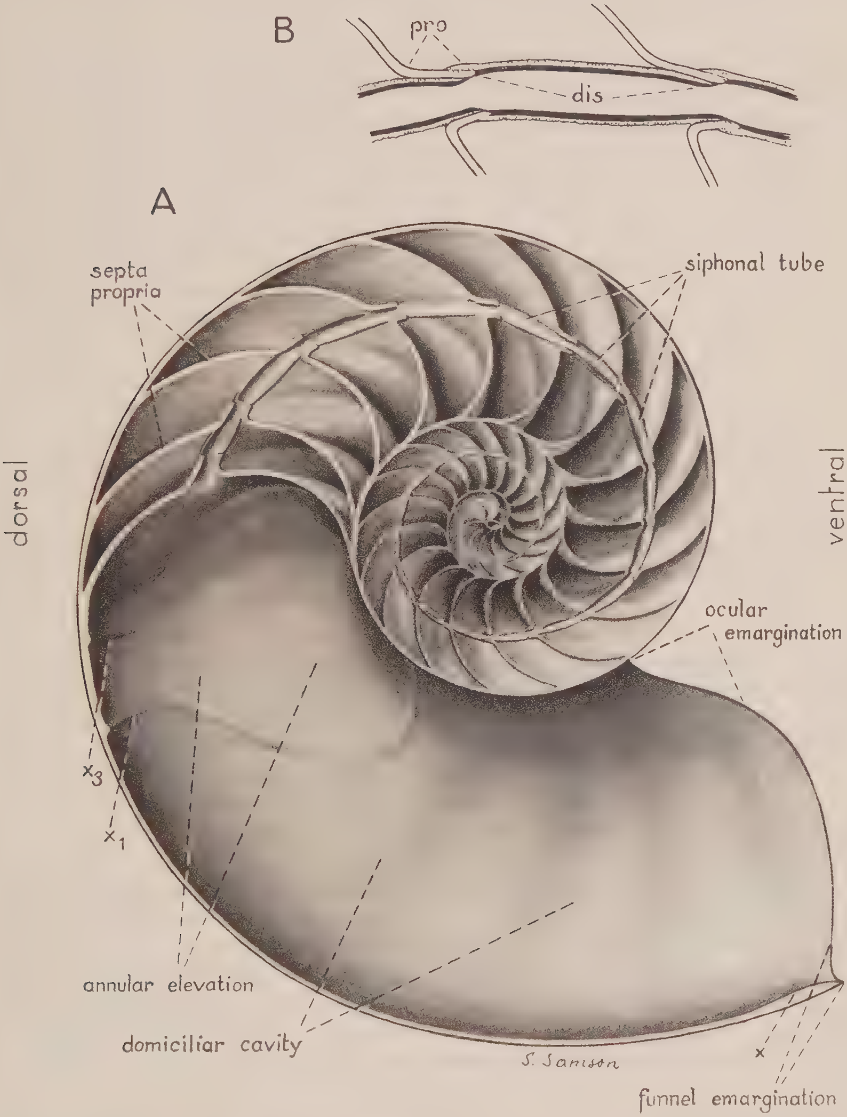

Text-fig. 2. *Nautilus pompilius* L. A, Left side of a full grown shell, sectioned median sagittally, $\times \frac{4}{5}$; B, diagram to show the structure of siphonal tube in median-sagittal section, × 3. *dis*, distal division of siphonal funnel; *pro*, proximal division of siphonal funnel; x, apertural ridge; x_1, ventral annular ridge; x_3, mural ridge.

downwards and outwards through the shell aperture. The margin of the shell aperture shows two emarginations: an antero-lateral paired *ocular emargination* and a posterior unpaired *funnel emargination* (text-fig. 2 A; "hyponomic sinus", Hyatt), separated from each other on either side by a downwardly projecting portion of the margin of the shell aperture.

The relations between the soft parts and the wall of the domiciliary division were first discussed by Owen (1832) who stated that the greater part of body proper lies free in the domiciliary cavity, but is attached by means of a horisontal, annular zone of epithelium on the inside of the shell somewhat below the youngest septum. For reasons which are more evident from the following description, this zone is here named the *epithelial zone I*, whilst for its corresponding zone of attachment on the shell wall the term *conchial zone I* is suggested (text-fig. 3). Owen stated, moreover, that the epitehlial zone I is composed of three portions: a narrow, unpaired posterior portion, a likewise narrow, unpaired anterior portion, and a broad, paired lateral portion, the latter being the area of origin for the retractor muscle of either side. The conchial zone I was described by Owen as a thin layer of "brown horny matter" which in fact is conchin.[1] Keferstein (1860) introduced the name "annulus" for the anterior and the posterior portions of the epithelial zone I. Waagen (1870) established that the thin conchin layer, which, according to Owen, was to be found only on the conchial zone I, actually extends upwards as far as to the youngest septum. From this fact Waagen, and later also Dewitz (1879a, b, c) and Schröder (1881), concluded that the entire conchin-covered surface ("Haftfläche", Waagen; "Verwachsungsband," Dewitz, Schröder) is an area of attachment for a continuous epithelial zone. It is, however, evident from the investigations of Appellöf (1893) that this interpretation is wrong. Appellöf found, rather, that the body proper is attached on the inside of the shell not only by means of the epithelial zone I but also by means of another, upper annular epithelial zone, here called the *epithelial zone II*, whose area of attachment, the *conchial zone II* (text-fig. 3), is situated immediately below the youngest septum. Griffin (1900) designated this epithelial zone the "posterior ventral aponeurotic band + dorsal aponeurotic band", whilst Willey (1902) named this the "septal aponeurosis". Both these terms are erroneous and misleading and must be discarded (the real aponeuroses are mesodermal structures). Rauther (1925) has investigated the histology of epithelial zones I and II, and the muscles lying just internal to these zones. From his investigations it is evident that the epithelial zone I is the area of origin for both the retractor muscles and the longitudinal mantle-musculature, whilst the epithelial zone II is the area of origin for the sub-epithelial musculature in the upper portion of the body proper.

The conchin-covered area described above, which extends from the lower margin of the conchial zone I upwards to the youngest septum, appears as a slight horizontal, ring-shaped elevation of the inside of the shell. This elevation, here named the *annular elevation* (text-figs. 2 A, 3), is of different widths in its different portions. The unpaired anterior and posterior portions are both narrow, especially the latter, whilst the paired lateral portion is, on the contrary, wide. This latter portion is so strongly produced dorso-ventrally that it forms an upper and a lower lobe. The annular elevation is composed of two thin layers: an external calcareous layer[1] which is attached on the internal shell wall, and an internal conchin layer.

---

[1] Conchin (Simroth 1897; "Epikutikula", "Konchyliolin", "Konchyolin") is a chitin-like, organic substance which generally occurs in the mollusc shell.

It is evident from the above description that the annular elevation topographically corresponds to the areas of origin of the retractor muscles, of the longitudinal mantle-musculature and of the sub-epithelial musculature in the dorsal portion of the body proper. These muscles do not, however, take their origin directly from the elevation under discussion, but from epithelial zones I and II which lie on the elevation and which secrete its calcareous and conchin layers. As in lamellibranchs and gastropods (Brück 1913, 1914; Röchling 1922), the epithelium at the origins of the muscles in *Nautilus* is probably crossed by special "epithelial" fibres, running in a basalo-superficial direction, which are directly continuous with the muscle fibres. These "epithelial" fibres in lamellibranchs and gastropods, and presumably in *Nautilus*, form together a sort of pseudo-tendon between the muscle fibres and the shell. The presence of this epithelium, called "Haftepithel" (Brück), accordingly, results in the muscles of molluscs reaching only indirectly the shell wall.

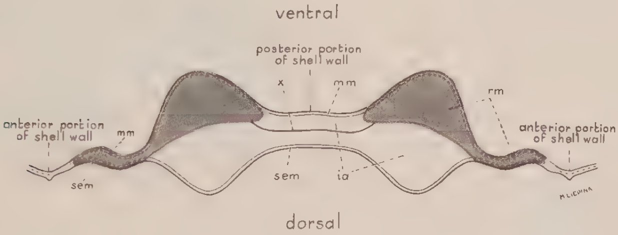
ventral
posterior portion of shell wall
x
mm
rm
anterior portion of shell wall
mm
anterior portion of shell wall
sem
ia
sem
M LIEPINA
dorsal

Text-fig. 3. *Nautilus pompilius* L. Diagram of annular elevation of shell projected in one plane × ½ (pl. 1).
ia, intermediate area; *mm*, functional area of origin of longitudinal mantle musculature (conchial zone I); *rm*, functional area of origin of retractor muscles (conchial zone I); *sem*, functional area of origin of sub-epithelial musculature of dorsal portion of body proper (conchial zone II); *x*, functional area of attachment of pallio-visceral ligament.

On the basis of the above one may say, therefore, that the retractor muscles, the longitudinal mantel-musculature and the sub-epithelial musculature in the dorsal portion of the body proper take their origin functionally on the annular elevation. More precisely, the functional origins of these muscles are situated as follows: (1) the area of origin for the retractor muscle of either side (*rm*, text-fig. 3; pl. 1) occupies the ventral lobe of the lateral portion of the annular elevation and, in addition, the adjacent half of the posterior portion of that elevation; (2) the area of origin of the longitudinal mantle-musculature (*mm*, text-fig. 3; pl. 1) is a narrow, ring-shaped zone along the lower margin of the elevation, whilst (3) the area of origin of the sub-epithelial musculature in the dorsal portion of the body proper (*sem*, text-fig. 3;

---

[1] This layer probably corresponds to the "helle Schicht", which Tullberg (1882) described in the lamellibranchiate-shell. According to Schmidt (1924) this "helle Schicht" differs only slightly from the nacreous layer of the shell.

pl. 1) is a, likewise, narrow, ring-shaped zone along the upper margin of the same elevation. Both these marginal zones lie far apart from each other posteriorly and laterally, but are close together antero-medially, where they merge with each other without any definite boundary. Moreover, the lower marginal zone merges both laterally and antero-laterally, without any boundary, with the area of origin of the retractor muscle, whilst the upper marginal zone is united antero-laterally only with it. The origins of the retractor muscles and the longitudinal mantle musculature on the one hand and the area of origin for the sub-epithelial musculature in the dorsal portion of the body proper on the other hand are separated laterally and posteriorly from each other by an *intermediate area* (*ia*, text-fig. 3; pl. 1) on which only the pallio-visceral ligament is attached.

It is well known that as the soft parts of the animal grow in size they shift downwards in the domiciliary cavity[1] causing a corresponding growth downwards of the shell at the margin of its aperture. *Pari passu* the annular elevation also grows slowly downwards by a gradual deposition of calcareous and conchin substance on its ventral side. Owing to the gradual shifting downwards of the soft parts, there arises in the upper portion of the domiciliary cavity a vacuity, which, in agreement with the shell chambers, is filled with gas. When this vacuity attains a certain size it is divided from the domiciliary cavity by a septum which is secreted by the epithelium on the dorsal surface of the body proper, and this process is repeated as long as the animal grows in size. The annular elevation is covered dorsally by the mural part of each new septum and is in this way gradually embedded in the shell wall. After the growth of the animal has ceased, the soft parts and the annular elevation also assume a fixed position in the domiciliary cavity. Simultaneously, of course, the formation of new septa ceases. The epithelium of the body immediately above the margin of the shell aperture, along the lower margin of the annular elevation and along the lower margin of the mural part of the youngest septum continues, however, in some cases to secrete shell substance for a period. Thereby horizontal, ridge-like thickenings are formed on the three corresponding places on the internal surface of the domiciliary division. These ridge-like thickenings are here called in succession from below upwards the *apertural ridge*, the *lower annular ridge*[2] and the *mural ridge* (x, x_1, x_2, text-fig. 2 A), respectively.

b) *Septate division*

The septate division of the shell will be more fully described in a forthcoming paper. Since, however, this division is important from the taxonomic point of view (e.g. the new terms, which are introduced for certain portions of the septum, are used in the taxonomic appendix to this paper) it is necessary here to discuss briefly this division.

The division of the shell in question here extends from the domiciliary division upwards to the apex of the shell and its cavity is divided by the septa into numerous chambers. In each septum two divisions may be distinguished: (1) the *septum proper*

---

[1] It is not quite clear at present how the "Haftepithel" during growth of the animal moves downwards on the inside of the domiciliary cavity. According to Keferstein (1861) and Appellöf (1893) the downward movement of the retractor muscle origin takes place in such a way that new muscle-substance is added to the ventral side of the muscle, whilst, simultaneously, the dorsal portion of the muscle is resorbed to a corresponding degree.

[2] In certain fossil nautiloids there occurs also an upper annular ridge (p. 231).

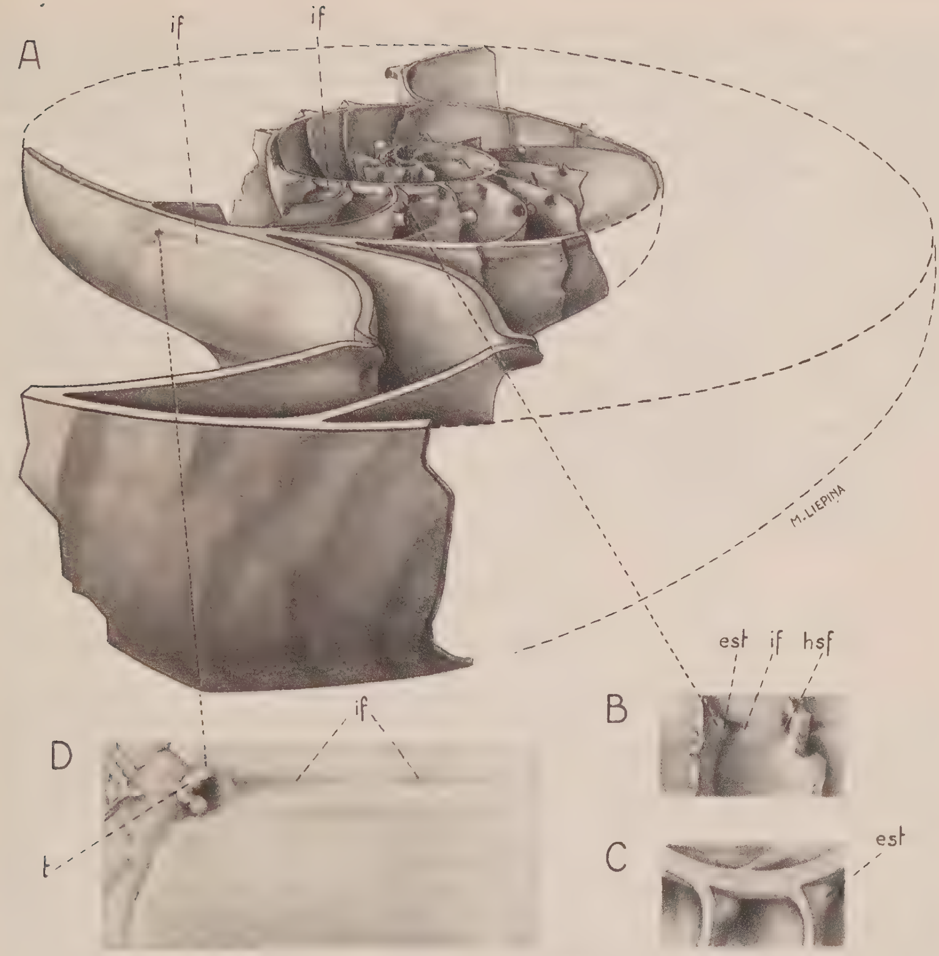

Text-fig. 4. *Nautilus pompilius* L. A, parts of right shell wall to show position of septal furrows and episeptal tubercles, $\times\frac{4}{5}$; B, details of septal furrows; hyposeptal fossae and episeptal tubercles in anterior view, $\times\frac{8}{5}$; C, details of episeptal tubercle from left side. $\times\frac{8}{5}$; D, details of septal furrow of the youngest septum, with a tubercle (*t*), $\times\frac{8}{5}$.
if, septal furrow; *est*, episeptal tubercle; *hsf*, hyposeptal fossa.

("free part of septum" Foerste & Teichert) and (2) the *siphonal funnel* ("siphonal segment"; text-fig. 2 B.).

The septum proper, which, corresponding to the internal shell layer, is composed of nacreous substance, is slightly arched with its convex face directed upwards. The individual septa have, on their ventral side close to the antero-medial margin, a little depression, the *hyposeptal fossa* (*hsf*, text-fig. 4 B; Appellöf 1893, pl. 10:3). On the dorsal side of the septum this depression is marked by an elevation, the *episeptal tubercle* ("dorsal lobe"; *est*, text-fig. 4 A, B, C; Appellöf loc. cit., pl. 10:2, 3). The hyposeptal fossa is distinct on the oldest septa, but becomes more and more shallow on the succeeding younger ones and is entirely lacking on the youngest septa. The septum proper is composed of several nacreous lamellae; the more dorsal of these lamellae are well defined periphericaly on the inside of the shell wall, whilst the ventral lamellae, on the contrary, continue downwards and merge with the shell wall without any distinct boundary (Appellöf, loc. cit.). In this way the lateral, mural parts of the latter lamellae ("mural part of septum") effects a fusion between each individual septum and the shell wall. The narrow zone, where every septum is thus fused on to the shell wall, is here called the *systegnosis* ("suture", "Lobenlinie").[1] The mural portion of each septum is very thin or absent entirely along the very antero-median line of the shell wall, where, accordingly, there arises a longitudinal septal furrow [Flower; "Normallinie", Sandberger (partim)] for each septum (*if*, text-fig. 4 A, B, D). In the older portion of the septate division this furrow extends from the hyposeptal fossa of each septum downwards to the episeptal tubercle of the septum next below. It should be noted that in certain full grown shells the septal furrow of the youngest septum ends ventrally in a little tubercle (*t*, text-fig. 4 D), which is not an episeptal tubercle.

The siphonal funnel and its terminology (text-fig. 2 B) has been already discussed by the present author (Mutvei 1956).

Fossil nautiloids

1. Coiling of the shell

It is well known that the posterior margin of the shell aperture in most fossil nautiloids is characterized by a distinct funnel emargination. In some shells there is, in addition, the septal furrow which is always situated on the anterior side of the shell (Flower 1939). With the guidance of the position of the funnel emargination Owen (1860) pointed out that the coiling of the shell in fossil nautiloids is of two kinds, forward and backward (according to Owen's terminology upward and downward), and that these types of coiling occur in different genera. By reference to the position of both the funnel emargination and the septal furrow the present writer was able to establish that so-called straight shells in paleozoic nautiloids are often also slightly coiled either along their entire height or only at the shell apex (text-fig. 5); this coiling is always backward.

Among the 9 genera discussed in the present paper 5 (*Uranoceras* (?), *Discoceras*, *Estonioceras*, *Eutrephoceras*, *Apheleceras*) have the shell coiled forwards and 4 (*Lyecoceras*, *Orthoceros*, *Geisonoceras*, *Baltoceras*) backwards.

2. Annular elevation

The annular elevation in fossil nautiloids has been described by many writers (Mojsisovics 1873; 1882; Dames 1879; Dewitz 1879a, b, c; 1880; Schröder 1881; 1882; Noetling 1882; Rüdiger 1889; Foord & Crick 1889, 1890; Remelé 1890; Hyatt 1894; Crick 1898b; 1904; 1905; Loesch 1914; Kessler 1923), who stated that the posterior, anterior or lateral portion of the elevation generally broadens downwards as a lobe, the *ventral lobe*. From this lobe, in spite of its position, the main portion of the retractor muscle took its functional origin, in a way similar to *Nautilus*. This muscle was probably paired in all nautiloids so far investigated (*rm*, text-fig. 6). The longitudinal mantle-musculature and the sub-epithelial musculature in the dorsal portion of the body proper certainly had, as in *Nautilus*, their functional origin on a narrow zone along the lower and the upper margin of the annular elevation, respectively (*mm*, *sem*, text-fig. 6).

---

[1] The term "suture" has been used with reference to vertebrates, arthropods, gastropods, cephalopods, and plants, but in each case with a different meaning. Its usage, referring to cephalopods, may therefore be misleading and an alternative term has been adopted in the present paper.

Owing to the varying position of its origin and to the varying curvature of the

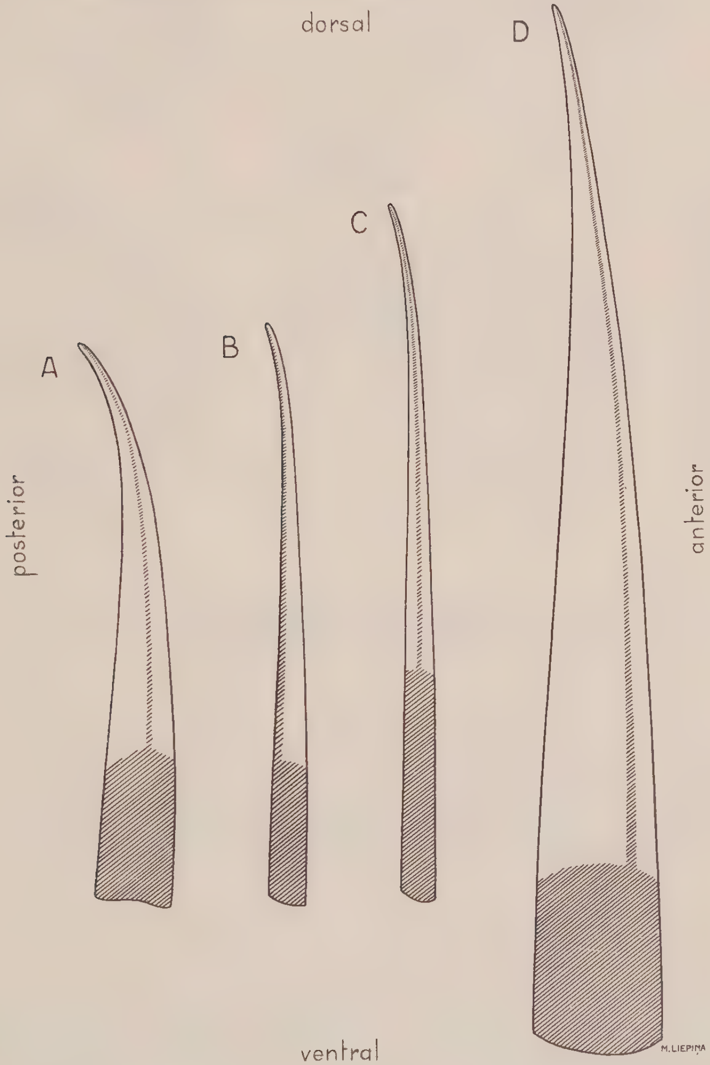

Text-fig. 5. Diagrammatic sketches of some backwarldy coiled shells of fossil nautiloids; A, *Lyecoceras gotlandense* n. sp.; B, *Baltoceras burchardi* (DEWITZ); C, "*Geisonoceras*" *scabridum* (ANGELIN); D, "*Orthoceras*" *angulatum* WAHL. All figures × ⅓.

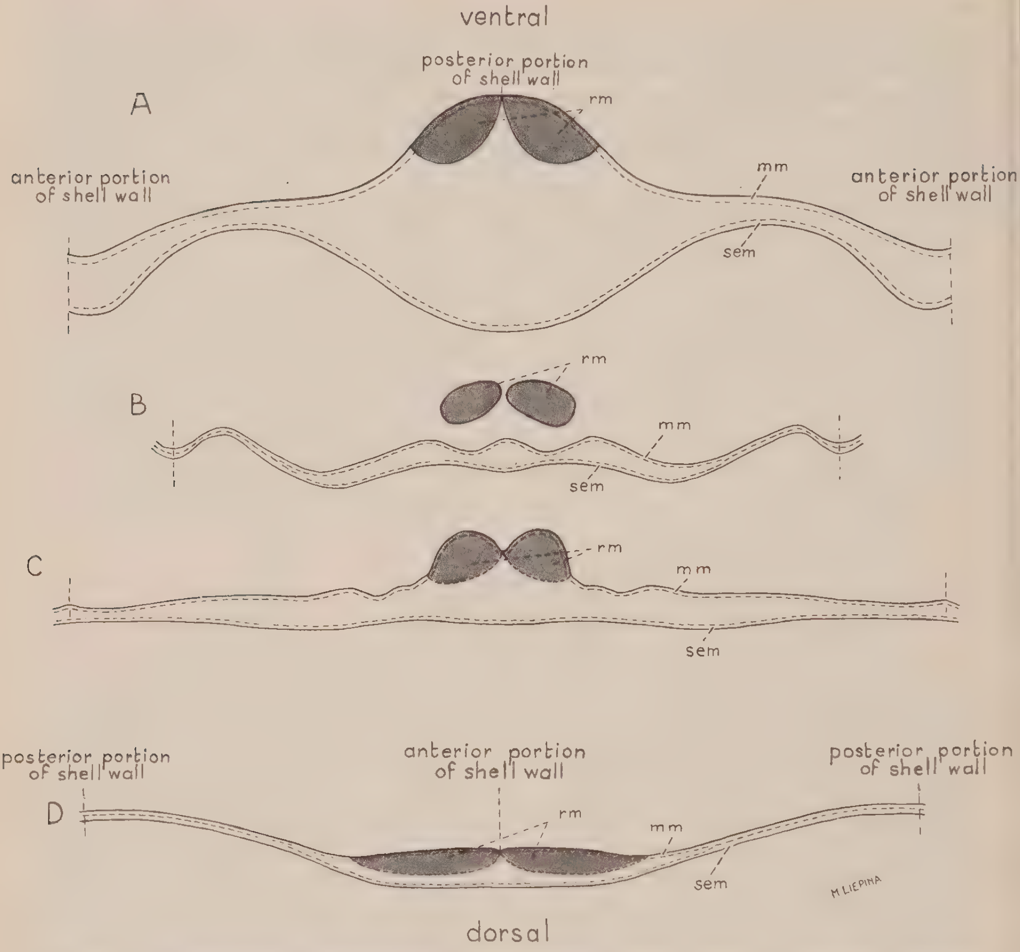
ventral
posterior portion of shell wall
A
rm
anterior portion of shell wall
mm
anterior portion of shell wall
sem
B
rm
mm
sem
C
rm
mm
sem
posterior portion of shell wall
anterior portion of shell wall
posterior portion of shell wall
D
rm
mm
sem
M LIEPINA
dorsal

Text-fig. 6. Diagrammatic reconstructions of functional areas of origin of muscles on annular elevation of shell in four fossil nautiloids; annular elevation projected in one plane, nat. size. A, *Estonioceras perforatum* (SCHRÖDER); B, *Discoceras angulatum* (SAEMANN); C, *Uranoceras* (?) *longitudinale* (ANGELIN); D, *Lyecoceras gotlandense* n. sp.
mm, functional area of origin of longitudinal mantle musculature; *rm*, functional area of origin of retractor muscles; *sem*, functional area of origin of sub-epithelial musculature of dorsal portion of body proper.

domiciliary division, the retractor muscle in fossil nautiloids had different positions in relation to the other soft parts (text-fig. 7).

With respect to the morphology of the annular elevation in fossil nautiloids the following features must be pointed out. The annular elevation is prominent over its whole area only in exceptional cases (text-figs. 12; 15 A, B, C; pl. 2:4, 5, 6), but in most full-grown fossil forms it is, as in *Nautilus*, very low and only along its inferior margin is it clearly marked by a ridge, the *lower annular ridge* (x_1, text-figs. 8 A, B, C, E; 9 A, B; 10; 13 A, B, C; 14 A, B, C, E; 16 A–E; 17 A, B, C; 18 A, B, C). Immedi-

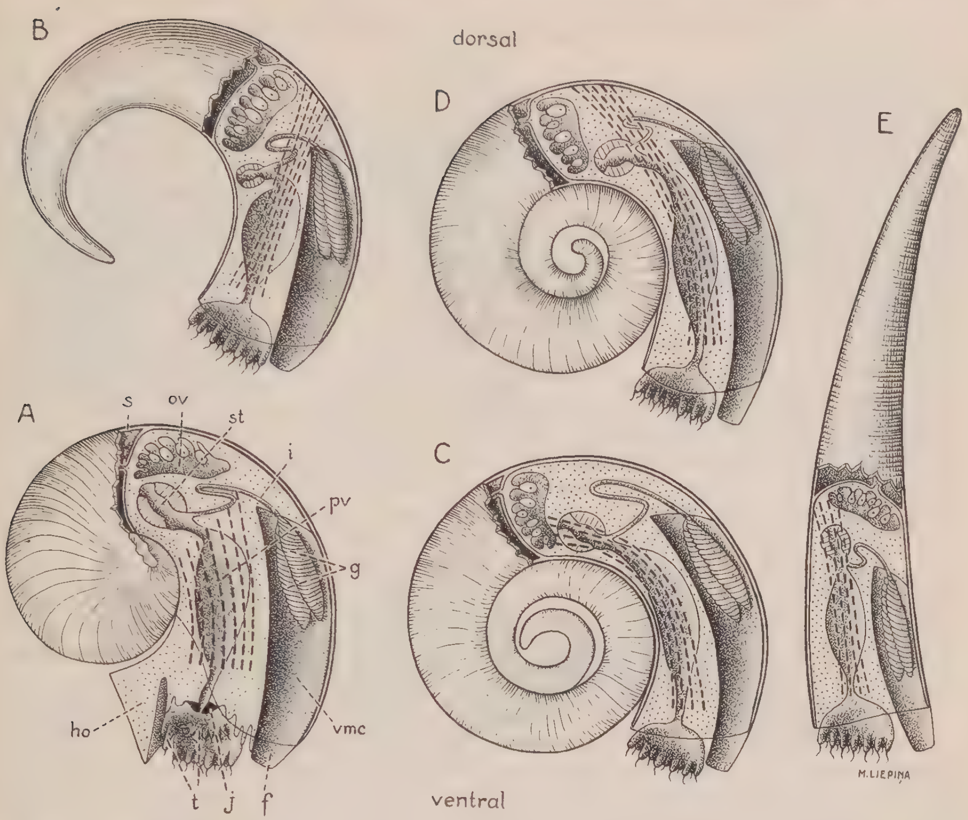

Text-fig. 7. Diagrams to show course of retractor muscles (broken lines) and their position in relation to other soft parts in *Nautilus* and in four fossil nautiloids. Soft parts in fossil forms, other than retractor muscles, reconstructed after *Nautilus*. A, *Nautilus pompilius* L.; B, *Uranoceras* (?) *longitudinale* (ANGELIN); C, *Apheleceras hibernicum* (FOORD & CRICK); D, *Estonioceras perforatum* (SCHRÖDER); E, *Lyecoceras longistriatum* n. sp.
f, funnel; *g*, gills; *ho*, hood; *i*, intestine; *j*, jaw; *ov*, ovarium; *pv*, proventriculus; *s*, siphonal cord; *st*, stomach; *t*, tentacles; *mc*, mantle cavity.

ately below the upper margin of the annular elevation there occurs also, in some forms, an *upper annular ridge* (x_2, text-figs. 8 A, B, C, E; 13 B, C; 16 A, B, C; 17 A, B, C) which has no corresponding structure in *Nautilus*. Apart from these two ridges, the surface of the annular elevation is mostly even and smooth. In certain cases, however, it shows more or less delicate vertical striae (text-figs. 8 A; 10 A; 13 A, C; 16 A, D; 17 A, B), or is divided into low tuberosities of varying form (text-figs. 10 D; 12 A, B, E; 15 A, B, C).

The functional area of origin of the paired retractor muscle, i.e. the ventral lobe of the annular elevation, is lateral in *Nautilus* and in Mesozoic nautiloids, but mainly anterior or posterior in Paleozoic nautiloids.[1] According to the position of the ventral lobe one may therefore distinguish in nautiloids three different types of annular elevation, here named (1) the *Nautilus* type, (2) the *Estonioceras* type, and (3) the *Lyecoceras* type.[1]

---

[1] In ammonites the area of origin for the retractor muscle is always situated dorsally (Waagen 1870; Mojsisovics 1873, 1882; Crick 1898a).

(1) The annular elevation of the *Nautilus* type, which is characterized by the laterally situated ventral lobe, is so far known only in the following 9 fossil genera: *Eutrephoceras* (text-fig. 18; pl. 15:4, 5, 6), *Apheleceras* (pl. 16:1, 2, 3; Foord 1900), *Vestinautilus* (Foord & Crick 1889), *Solenocheilus* (Foord & Crick 1890), *Cenoceras* (Foord & Crick 1890; Crick 1898 b), *Pleuronautilus* (Mojsisovics 1873), *Syringoceras* (Mojsisovics ibid.), *Germanonautilus* (Mojsisovics 1882), *Grypoceras* (Mojsisovics ibid.), and in some undetermined genera ["*Bisiphytes*" *polygonalis* (Sow.) Foord & Crick 1890; "*Nautilus*" *rogeri* LOESCH, Loesch 1914; "*Nautilus*" *rotundus* CRICK, Crick 1898 b].

(2) The annular elevation of the *Estonioceras* type, characterized by the posteriorly situated ventral lobe, is, at present, known in the following four genera: *Estonioceras* (text-figs. 6 A; 8; 9 A, B, C; pls. 2:1, 2, 3; 3; 4:1, 2; Hyatt 1894), *Planctoceras* (text-fig. 9 D, E; pl. 5; Dewitz 1879 b), *Uranoceras* (?) (text-figs. 6 C; 10; 11; pls. 4:3; 6; 7:4, 5), *Discoceras* (text-figs. 6 B; 12; 14; pls. 8; 9:1, 2, 3).

(3) The anteriorly situated ventral lobe is characteristic of the annular elevation of the *Lyecoceras* type which at the present time has been observed in the following four genera: *Lyecoceras* (text-figs. 6 D; 13; 16 A, B, C, G; pls. 9:4, 5; 10; 11; 12), *Orthoceros* (pl. 2:4, 5, 6; Dewitz 1879 a, b; 1880; Schröder 1881; Remelé 1890), *Baltoceras* (text-fig. 16 D–F; pl. 14:1–6; Dewitz 1879 c; 1880; Schröder 1881), *Lituites* (Schröder 1881; Noetling 1882), and in two undetermined genera ["*Geisonoceras*" *scabridum* (ANGELIN) text-fig. 15; pls. 13; 14:7, 8, 9; Rüdiger 1889; and "*Orthoceras*" *angulatum* WAHL., text-fig. 17; pl. 15:1, 2, 3].

Particular attention should be drawn to the fact that the annular elevation of the *Lyecoceras* type is to be found only in the backwardly coiled shells[2], whilst the annular elevations of the *Estonioceras* and the *Nautilus* types occur in the forwardly coiled shells. In spite of the fact that the annular elevation is so far known only in a small number of fossil nautiloids, it is already possible to foresee its great importance to nautiloid taxonomy.

---

[1] In the following review only those genera in which the annular elevation is reliably described are included [not *Endoceras* (Schröder 1881), *Clinoceras* (Mascke 1876; Dewitz 1880), *Rhynchorthoceras* (Schröder 1881), "*Meloceras*" (Crick 1905), Amphereopsis (Crick 1904)].

[2] In the genus *Lituites*, however, only the ventral portion of the shell is coiled backwards, whilst the dorsal portion forms a forwardly directed spiral.

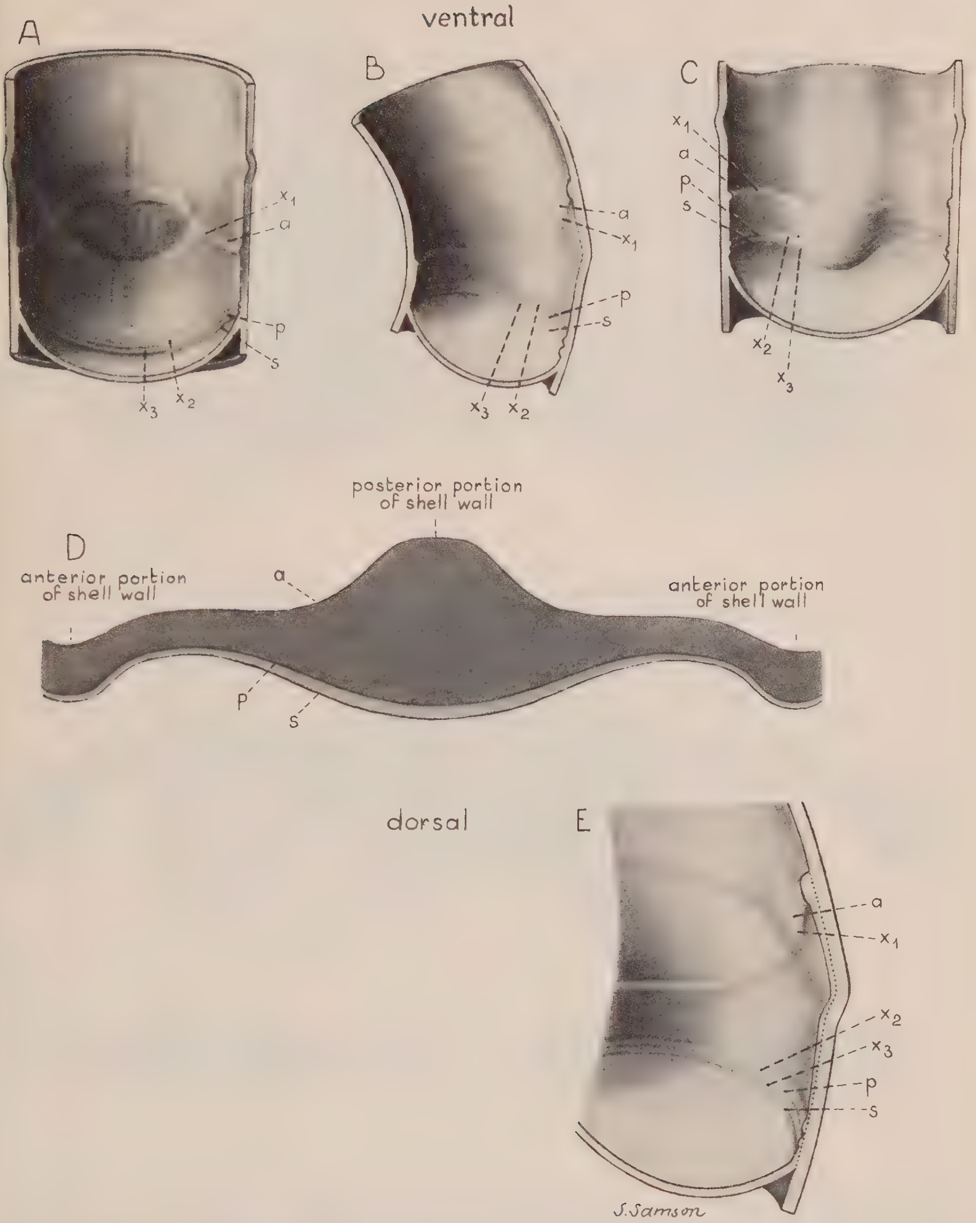
ventral
A
x1
a
p
s
x3
x2
B
a
x1
p
s
x3
x2
C
x1
a
p
s
x'2
x3
posterior portion of shell wall
D
anterior portion of shell wall
a
anterior portion of shell wall
p
s
dorsal
E
a
x1
x2
x3
p
s
S.Samson

Text-fig. 8. *Estonioceras impressum* (HYATT), same specimen as in pl. 2:1, 2, 3. A, B, C, reconstruction of annular elevation on posterior, lateral, and anterior portions of shell wall, respectively, $\times \frac{6}{5}$; D, annular elevation projected in one plane, $\times \frac{6}{5}$; E, details of fig. B, $\times \frac{12}{5}$.

a, ventral margin of annular elevation of shell; *p*, dorsal margin of annular elevation; *s*, angle between the youngest septum proper and its mural part; x_1, ventral annular ridge; x_2, dorsal annular ridge; x_3, mural ridge.

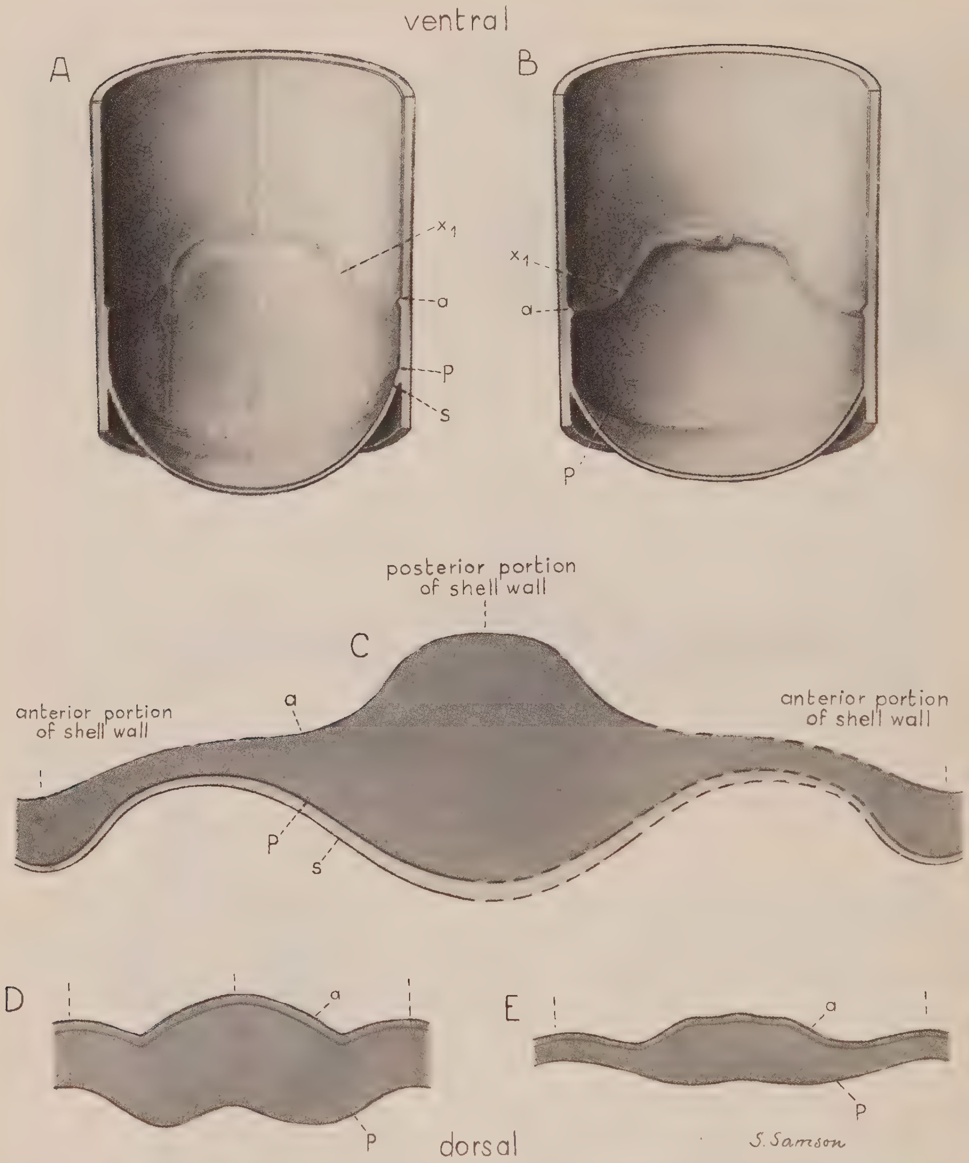
ventral
A
B
x1
a
p
s
x1
a
p
posterior portion of shell wall
C
a
anterior portion of shell wall
anterior portion of shell wall
p
s
D
a
p
E
a
p
dorsal
S. Samson

Text-fig. 9. A, C, *Estonioceras perforatum* Schröder, same specimen as in pl. 3:1, 2, 3; A, reconstruction of annular elevation on posterior portion of shell wall, ×$\frac{6}{5}$; C, diagram of annular elevation projected in one plane, ×$\frac{6}{5}$; B, *Estonioceras imperfectum* (Quenstedt), same specimen as in pl. 3: 4, 5; reconstruction of annular elevation on posterior portion of shell wall, ×$\frac{6}{5}$; D, E, *Planctoceras falcatum* (Schloth.), two diagrams of annular elevation projected in one plane, ×$\frac{6}{5}$; same specimens as in pl. 5:4, 5, 6, and pl. 5:1, 2, 3.

a, ventral margin of annular elevation of shell; *p*, dorsal margin of annular elevation; *s*, angle between the youngest septum proper and its mural part.

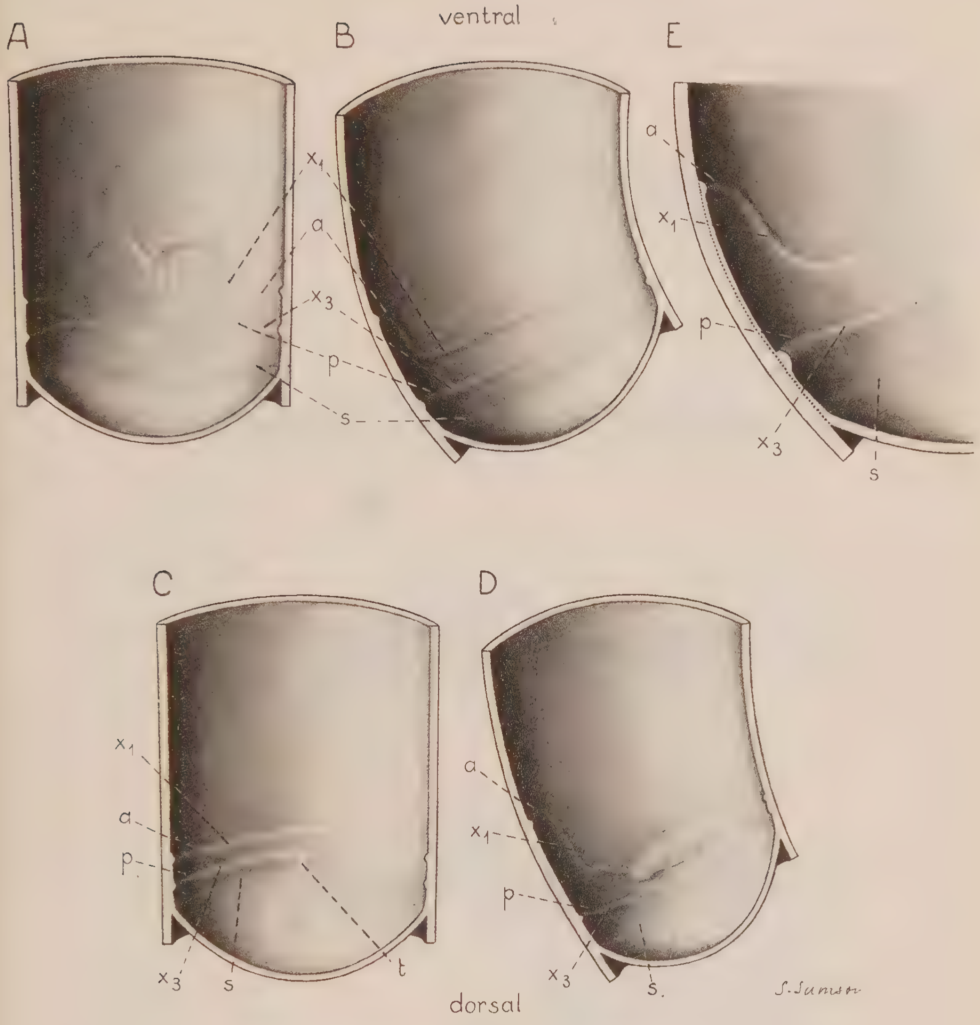

Text-fig. 10. *Uranoceras* (?) *longitudinale* (ANGELIN). A, B, C, reconstruction of annular elevation on posterior, lateral, and anterior portions of shell wall, respectively; same specimen as in pl. 6, $\times \frac{3}{4}$; E, details of fig. B, $\times \frac{3}{2}$; D, reconstruction of annular elevation on lateral portion of shell wall, same specimen as in pl. 4:3, $\times \frac{3}{4}$.
a, ventral margin of annular elevation of shell; p, dorsal margin of annular elevation; s, angle between the youngest septum proper and its mural part; t, tubercle of septal furrow of youngest septum; x_1, ventral annular ridge; x_2 mural ridge.

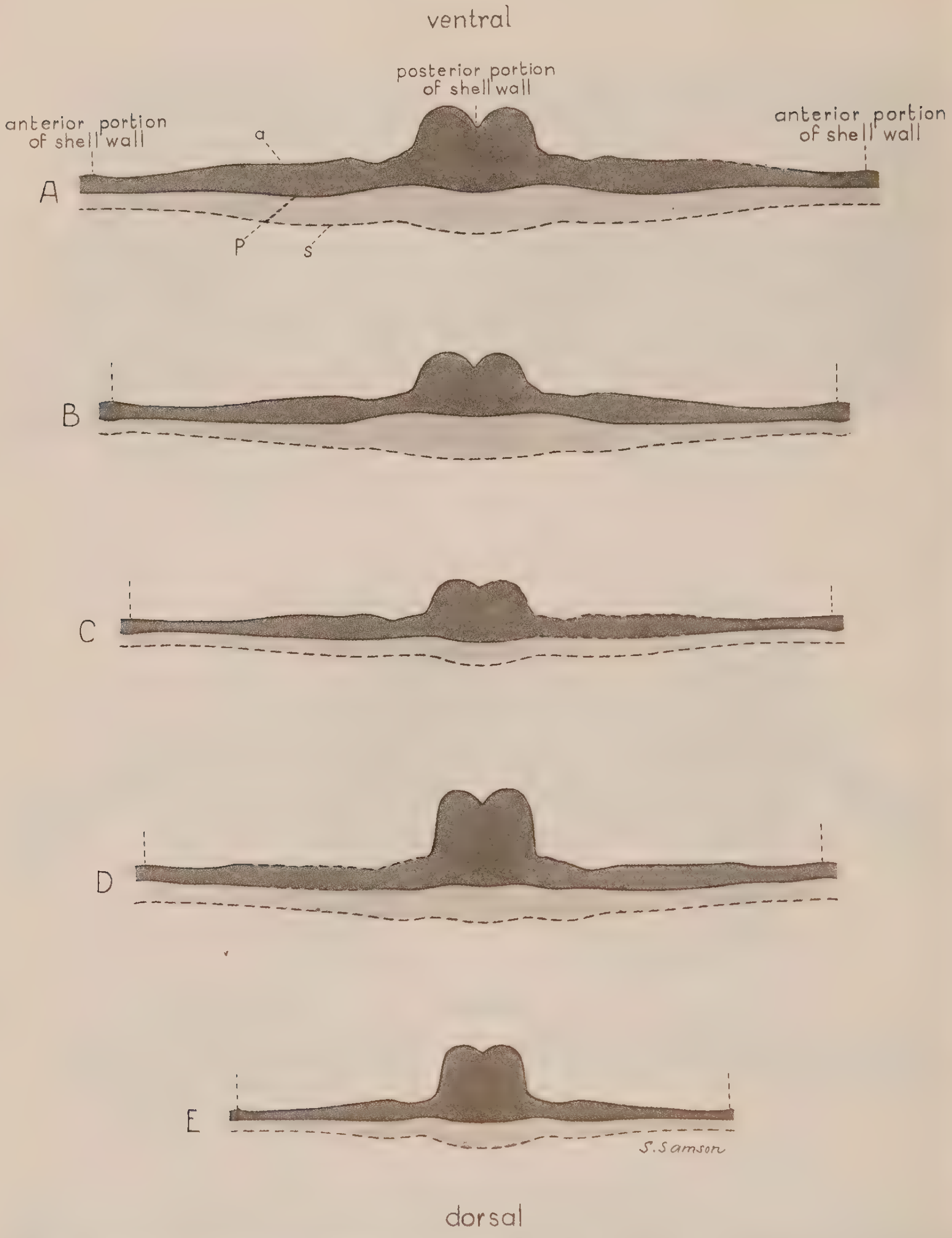
ventral
posterior portion of shell wall
anterior portion of shell wall
anterior portion of shell wall
a
A
P
s
B
C
D
E
S. Samson
dorsal

Text-fig. 11. *Uranoceras* (?) *longitudinale* (ANGELIN). Diagrams of annular elevation of shell in five specimens; annular elevations projected in one plane; $\times \frac{2}{3}$; A, same specimen as in pl. 6; B, specimen UPI, No. D 437; C, specimen UPI, No. D 436; D, same specimen as in pls. 4:3; 7:5; E, same specimen as in pl. 7:4.

a, ventral margin of annular elevation of shell ; p. dorsal margin of annular elevation; *s*, angle between the youngest septum proper and its mural part.

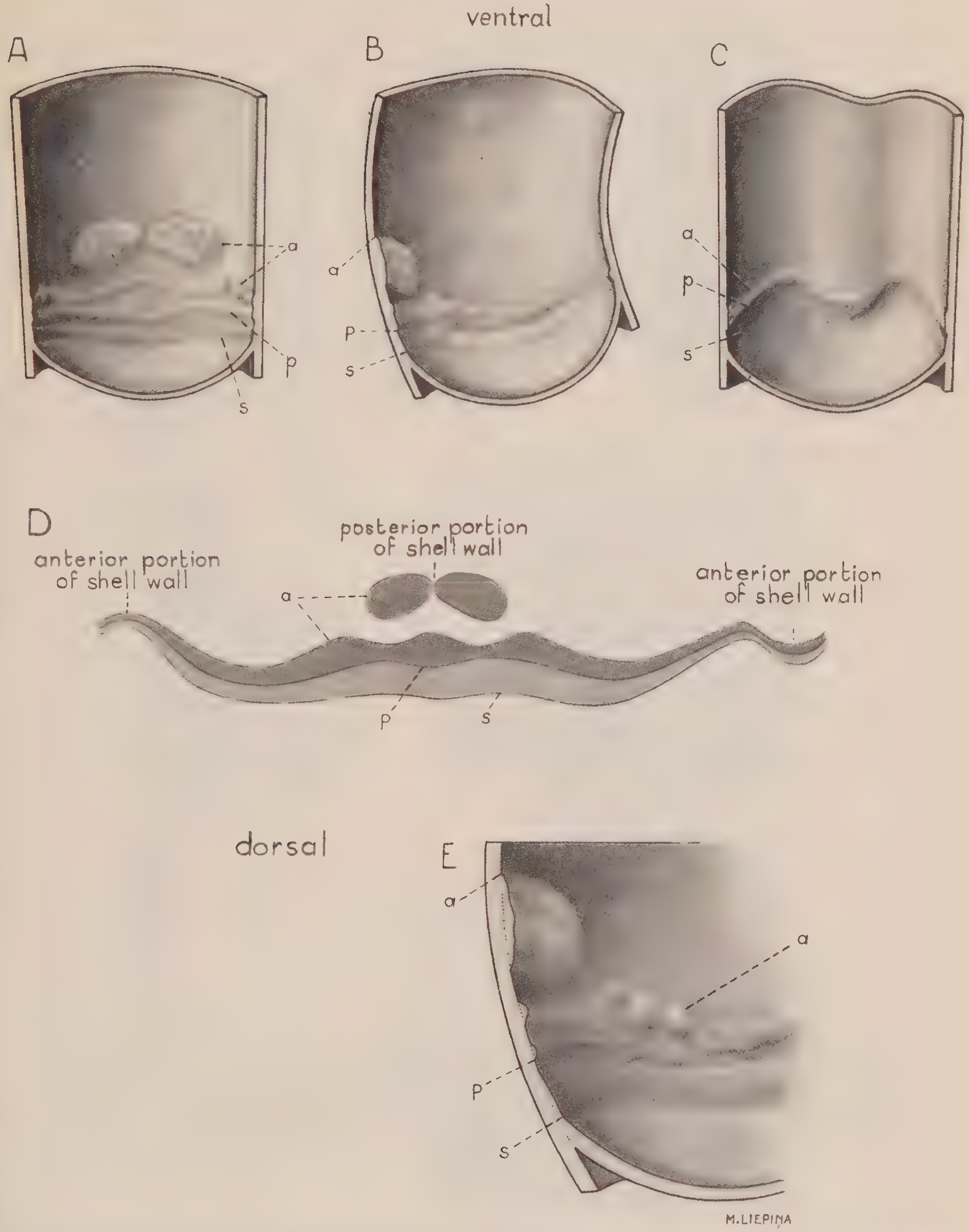
ventral
A
B
C
a
p
s
D
posterior portion of shell wall
anterior portion of shell wall
anterior portion of shell wall
dorsal
E
M.LIEPIŅA

Text-fig. 12. *Discoceras angulatum* (SAEMANN), same specimen as in pl. 8. A, B, C, reconstruction of annular elevation on posterior, lateral, and anterior portions of shell wall, respectively, ×$\frac{6}{5}$; D, diagram of annular elevation projected in one plane, ×$\frac{6}{5}$; E, details of fig. B, ×$\frac{12}{5}$. *a*, ventral margin of annular elevation of shell; *p*, dorsal margin of annular elevation; *s*, angle between the youngest septum proper and its mural part.

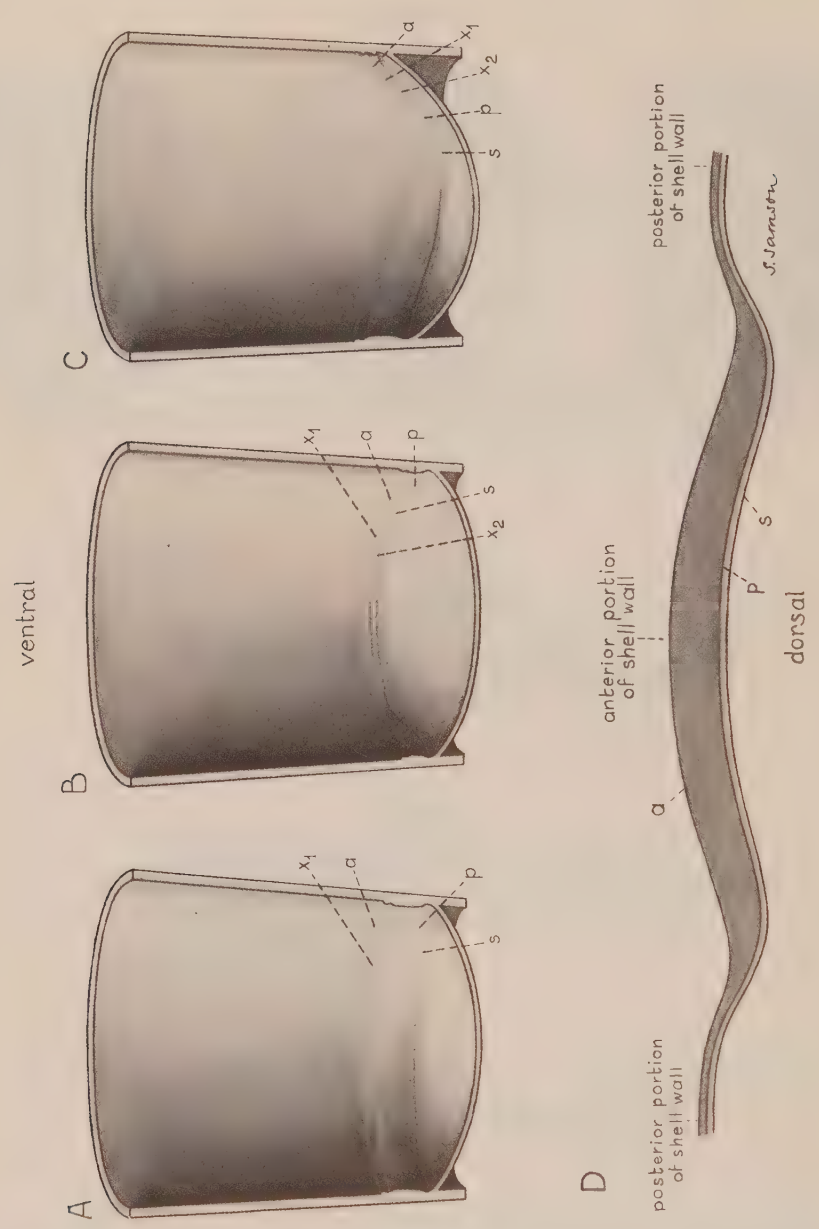
ventral
dorsal
A
B
C
D
x_1
x_2
a
p
s
anterior portion of shell wall
posterior portion of shell wall
posterior portion of shell wall
S. Samson

Text-fig. 13. *Lyecoceras* (?) sp., same specimen as in pl. 12. A, B, C, reconstruction of annular elevation on anterior, posterior, and lateral portions of shell wall, respectively, × 4/5; D, diagrams of annular elevation of shell projected in one plane, × 4/5.

a, ventral margin of annular elevation of shell; *p*, dorsal margin of annular elevation; *s*, angle between the youngest septum proper and its mural part; x_1, ventral annular ridge; x_2 dorsal annular ridge.

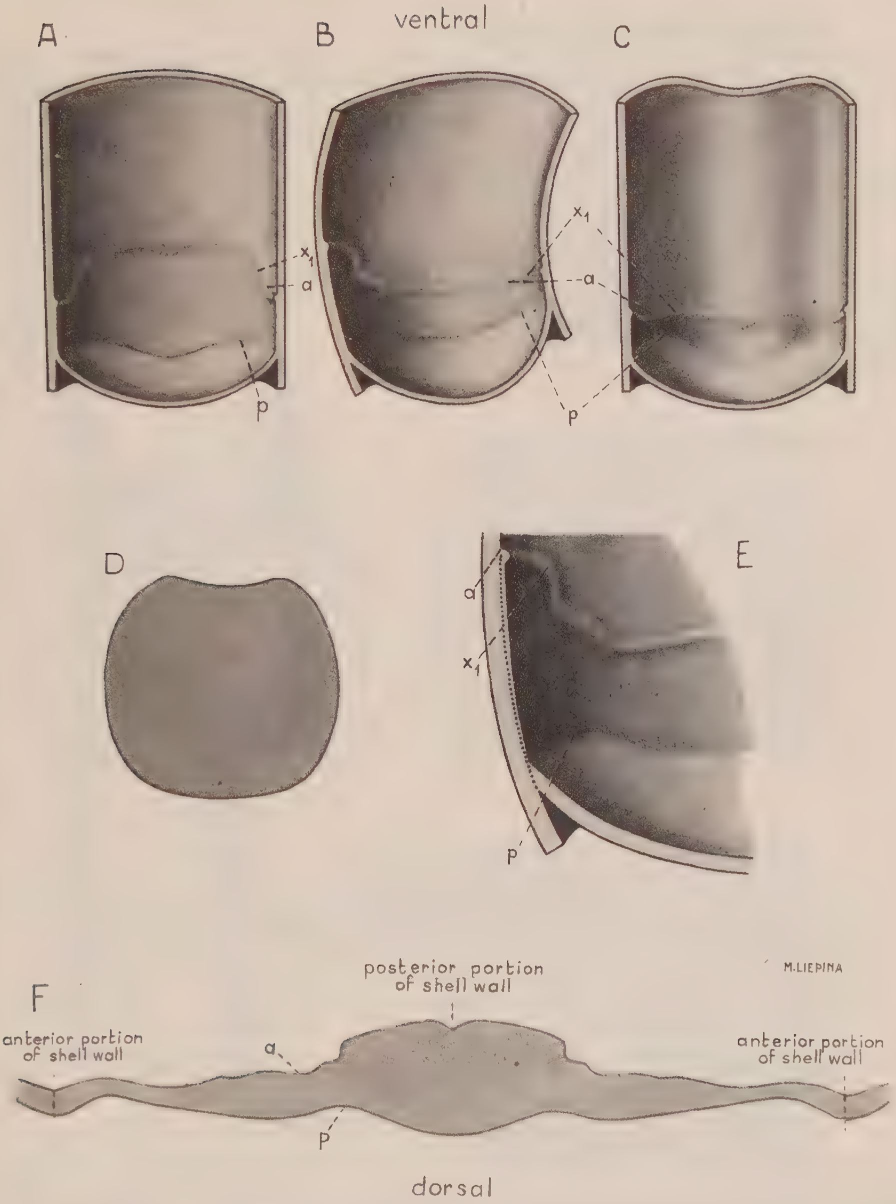
A
B
ventral
C
x_1
a
p
x_1
a
p
D
E
a
x_1
p
M.LIEPINA
F
posterior portion of shell wall
anterior portion of shell wall
a
anterior portion of shell wall
P
dorsal

Text-fig. 14. *Discoceras* sp., same specimen as in pl. 9:1, 2, 3. A, B, C, reconstruction of annular elevation on posterior, lateral, and anterior portions of shell wall, respectively, $\times \frac{6}{5}$; D, horizontal section of domiciliary division of shell, $\times \frac{6}{5}$. E, details of fig. B, $\times \frac{12}{5}$; F, diagram of annular elevation projected in one plane, $\times \frac{6}{5}$.

a, ventral margin of annular elevation of shell; *p*, dorsal margin of annular elevation; x_1, ventral annular ridge.

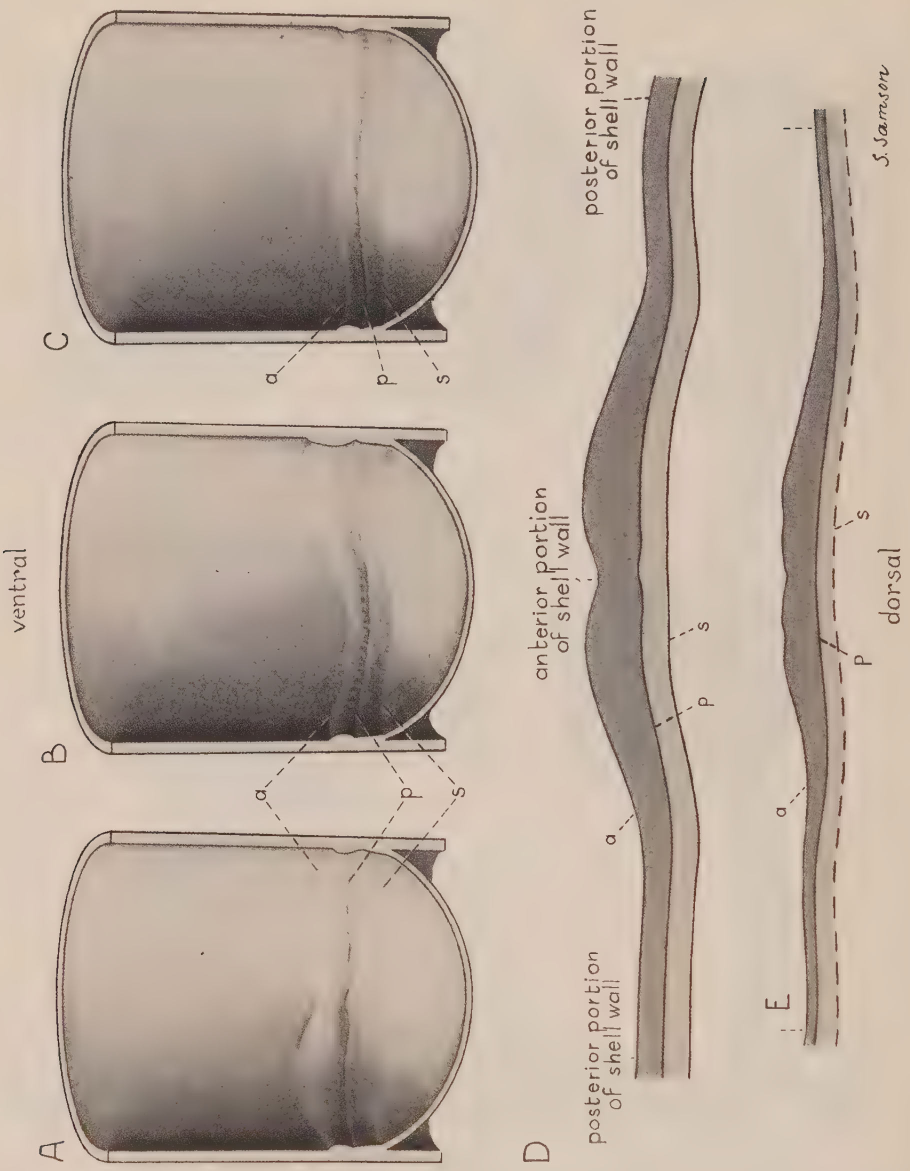
A
B
C
D
E
a
p
s
ventral
dorsal
posterior portion of shell wall
anterior portion of shell wall
posterior portion of shell wall
S. Samson

Text-fig. 15. "*Geisonoceras*" *scabridum* (ANGELIN). A, B, C, reconstruction of annular elevation on anterior, lateral, and posterior portions of shell wall, respectively, × 3, same specimen as in pl. 13:1–6; D, diagram of annular elevation of shell in same specimen projected in one plane, $\times \frac{12}{5}$; E, diagram of annular elevation of shell in same specimen as in pl. 14: 7, 8 projected in one plane, $\times \frac{12}{5}$.

a, ventral margin of annular elevation of shell; *p*, dorsal margin of annular elevation; *s*, angle between the youngest septum proper and its mural part; *t*, tubercle of septal furrow of the youngest septum.

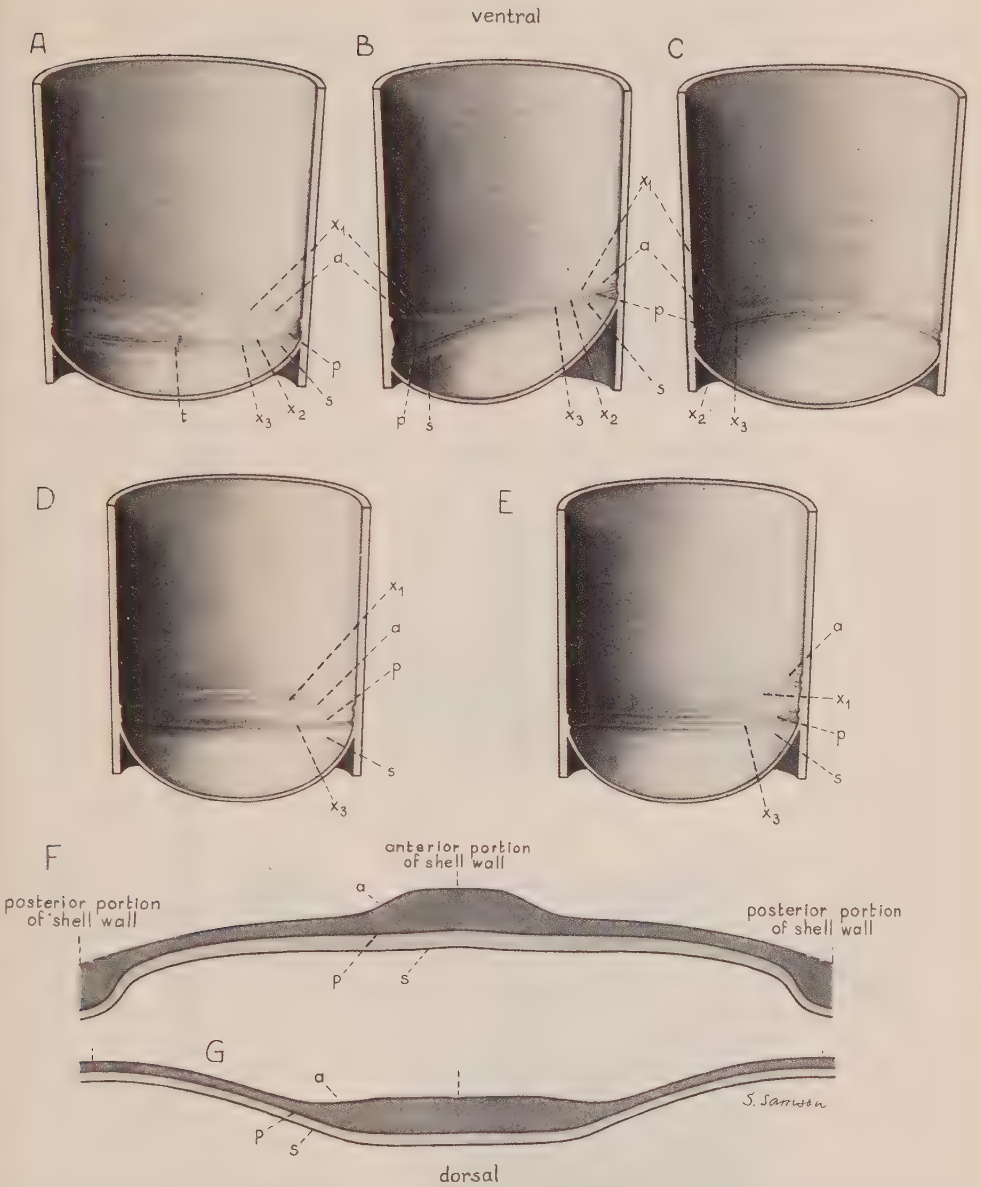
ventral
A
B
C
x_1
a
p
s
t
x_3
x_2
D
E
F
anterior portion of shell wall
posterior portion of shell wall
posterior portion of shell wall
G
S. Samson
dorsal

Text-fig. 16. *Lyecoceras gotlandense* n. sp., same specimen as in pl. 10. A, B, C, reconstruction of annular elevation on anterior, lateral, and posterior portions of shell wall, respectively, nat. size; G, diagram of annular elevation of shell projected in one plane, nat. size. D–F, *Baltoceras burchardi* (Dewitz), same specimen as in pl. 14:1–6. D, E, reconstruction of annular elevation on anterior and lateral portions of shell wall, respectively, × 2; F, diagram of annular elevation of shell projected in one plane, × 2.

a, ventral margin of annular elevation of shell; *p*, dorsal margin of annular elevation; *s*, angle between the youngest septum proper and its mural part; *t*, tubercle of septal furrow of youngest septum; x_1, ventral annular ridge; x_2, dorsal annular ridge; x_3, mural ridge.

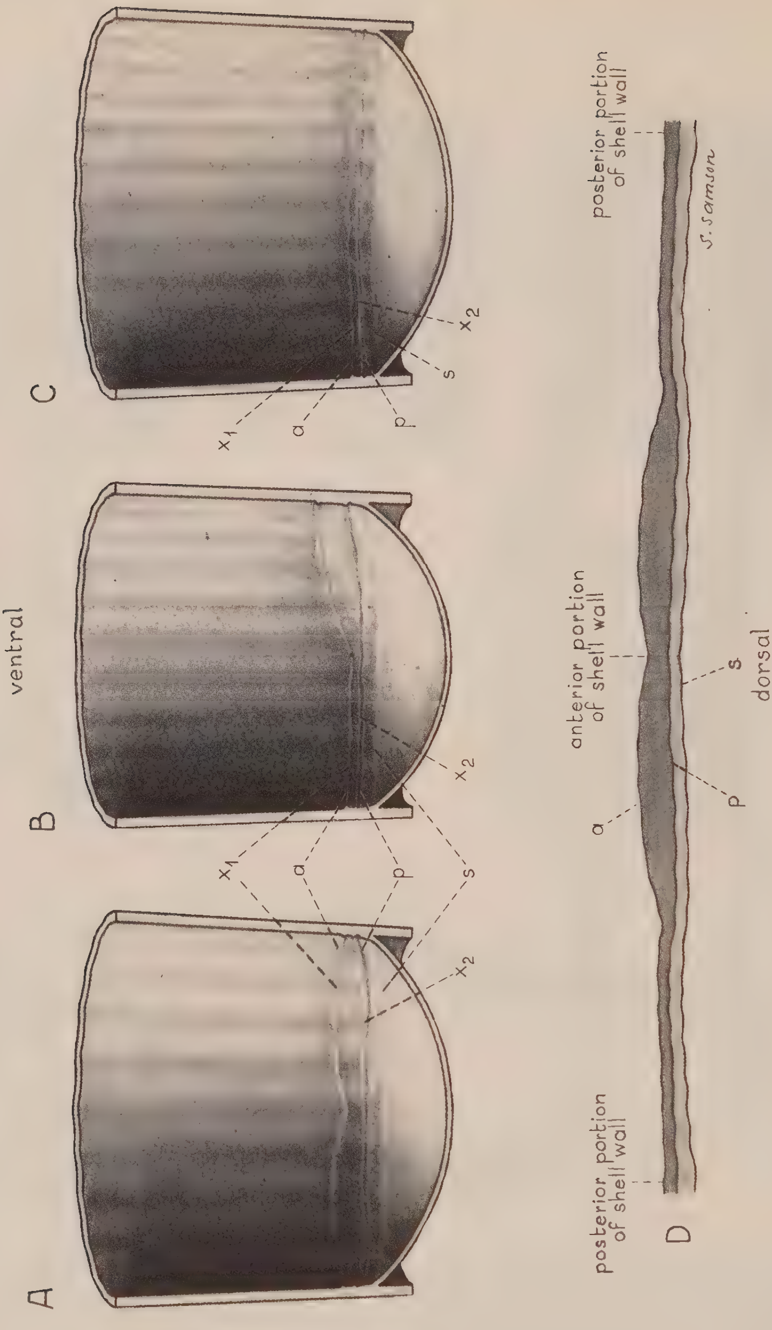
A
B
C
D
ventral
dorsal
x1
a
p
s
x2
anterior portion of shell wall
posterior portion of shell wall
posterior portion of shell wall
S. Samson

Text-fig. 17. "*Orthoceras*" *angulatum* WAHLENBERG, same specimen as in pl. 15:1, 2, 3. A, B, C, reconstruction of annular elevation on anterior, lateral, and posterior portions of shell wall, respectively, × $\frac{3}{4}$; D, diagram of annular elevation of shell projected in one plane, × $\frac{3}{4}$.
a, ventral margin of annular elevation of shell; *p*, dorsal margin of annular elevation; *s*, angle between the youngest septum proper and its mural part; x_1, ventral annular ridge; x_2 dorsal annular ridge.

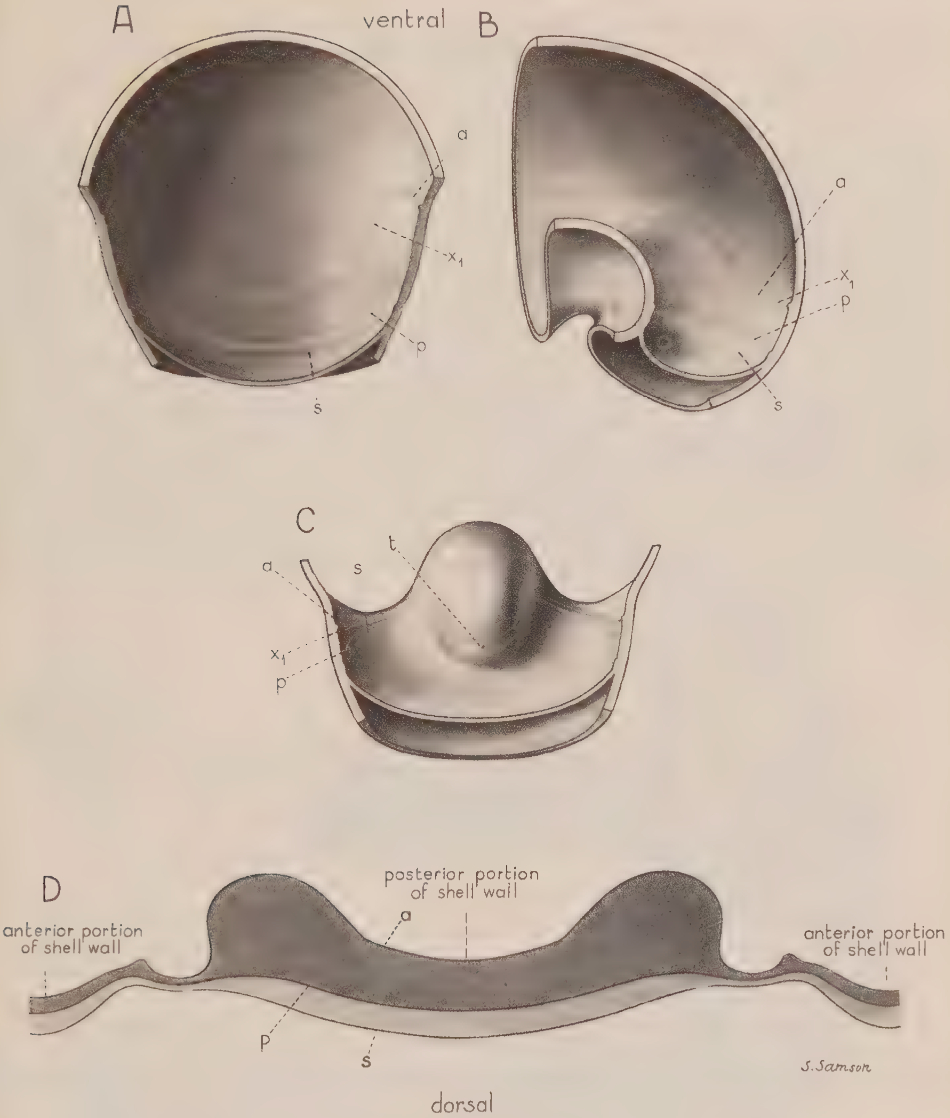
A
ventral
B
a
x_1
p
s
a
x_1
p
s
C
t
a
s
x_1
p
D
posterior portion of shell wall
a
anterior portion of shell wall
anterior portion of shell wall
p
s
S. Samson
dorsal

Text-fig. 18. *Eutrephoceras bellerophon* (LUNDEGREN), same specimen as in pl. 15:4, 5, 6. A, B, C reconstruction of annular elevation on posterior, lateral, and anterior portions of shell wall respectively, nat. size; D, diagram of annular elevation of shell projected in one plane, nat. size *a*, ventral margin of annular elevation of shell; *p*, dorsal margin of annular elevation of shell; *s* angle between the youngest septum proper and its mural part; *t*, tubercle of septal furrow of the youngest septum; x_1, ventral annular ridge.

Taxonomic appendix

Measurements

The dimensions used in measuring the shells of the fossil nautiloids dealt with below can be most easily explained by reference to a hypothetical, generalized, straight-shelled form (text-fig. 19 B). These dimensions are as follows: (1) the height, which is equal to the length of the dorso-ventral axis of the shell (*a-b*, text-fig. 19 B); (2) the length, which corresponds to the length of the antero-posterior axis of the shell (*c-d*, text-fig. 19 C); and (3) the breadth, which is equal to the length of the transverse axis of the shell (*e-f*, text-fig. 19 C). The structure of the septa and siphonal tube were suitably studied in a median-sagittal section of the shell (text-fig. 19 A), whilst the circumference of the shell was studied in horizontal sections (text-fig. 19 C) lying at right angles to the dorso-ventral axis of the shell. The distance between two succeeding septa is conveniently given in proportion to the morphological length of the shell, measured midway between the two septa.

The coiled shells were measured in the same manner as the straight ones having regard to their anatomical orientation. The height of the shell is thus equal to the length of the coiled dorso-ventral axis of the shell and the other dimensions are given in relation to this coiled axis.

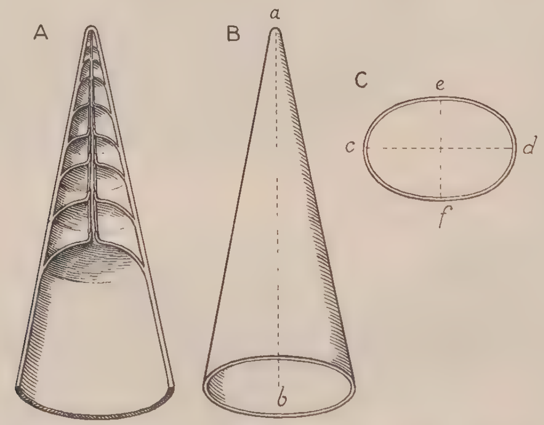

Text-fig. 19. Diagram of hypothetical, generalized straight-shelled nautiloid. A, median-sagittal section; B, external aspect; C, horizontal section.
a–b, height; *c–d*, length; *e–f*, breadth.

A. *Uranoceras* HYATT 1883

The genus *Uranoceras* was erected by Hyatt (1883) on a Bohemian species, "*Cyrtoceras*" *uranum* (Barrande 1866; 1867; 1877) and was later revised by Foerste (1925). On the basis of the descriptions of these three writers the following diagnosis may be given for this genus: shell coiled in an open whorl; morphological length of shell somewhat greater than breadth; circumference of shell elliptical, or somewhat quadrangular; shell ornamentation consisting of delicate, vertical ridges; systegnoses turn upwards in a paired curve on lateral portion of shell wall, but downwards in an unpaired curve on anterior and posterior portions of shell wall; siphonal tube situated slightly posterior to dorso-ventral axis of shell; proximal division of siphonal funnel short, distal division long; siphonal tube narrow in the former division, but widens in the latter; on the inside of siphonal tube slight annular ridges in some cases.

According to Foerste (loc. cit.) the genus *Uranoceras* includes the following three species: the genotype "*Cyrtoceras*" *uranum* (Barrande, loc. cit.) from the Silurian of Bohemia; *U. hercules* (WINCHELL & MARCY) and *U. dyeri* (HYATT), both from U.S.A., Racine dolomite, Middle Silurian. In addition, a fourth species, *U.* (?) *longitudinale* (ANGELIN) is here included in this genus.

Uranoceras (?) *longitudinale* (ANGELIN)

Text-figs. 6 C; 7 B; 10; 11; 20; 21; pls. 4:3; 6; 7; 17; 18.

1880 *Cyrtoceras longitudinale* n. sp. — Angelin, Fragm. Silurica, p. 11, pl. 16:5.

MATERIAL.—A great number of specimens which show the domiciliary division of the shell and the ventral portion of the septate division. Only few specimens are, however, sufficiently well preserved for description.

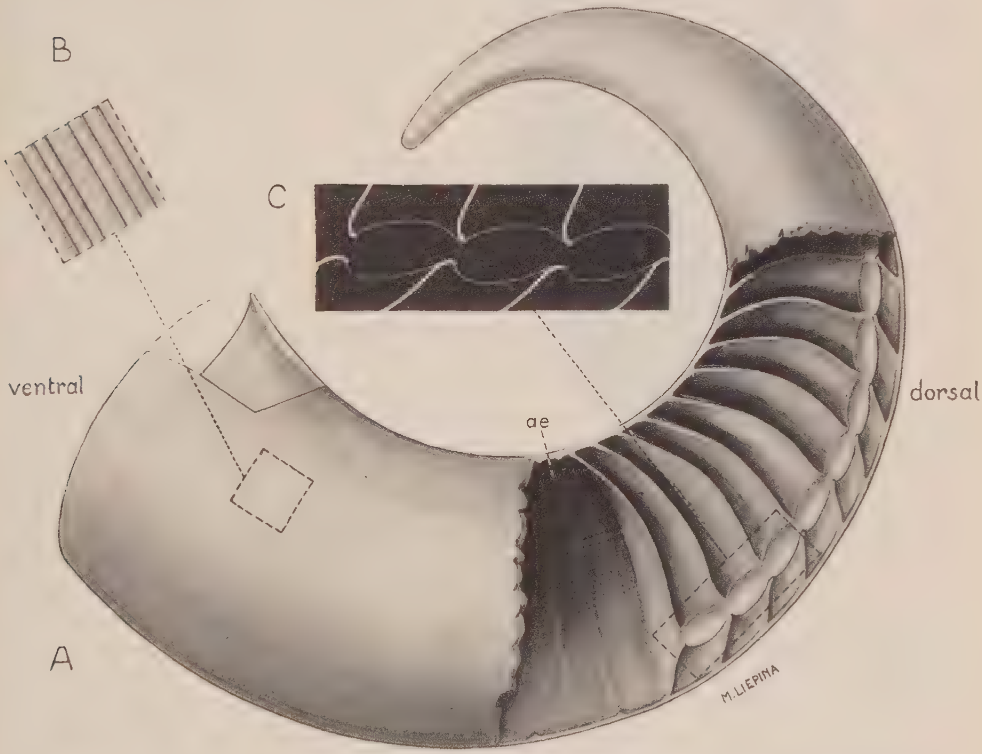

Text-fig. 20. *Uranoceras* (?) *longitudinale* (ANGELIN). A, reconstruction of shell in left lateral view, with shell wall and sections of septa removed at one place, × $\frac{4}{5}$; B, details of shell ornamentation, × $\frac{8}{5}$; C, part of siphonal tube in median-sagittal section, × $\frac{8}{5}$.
ae, annular elevation of shell.

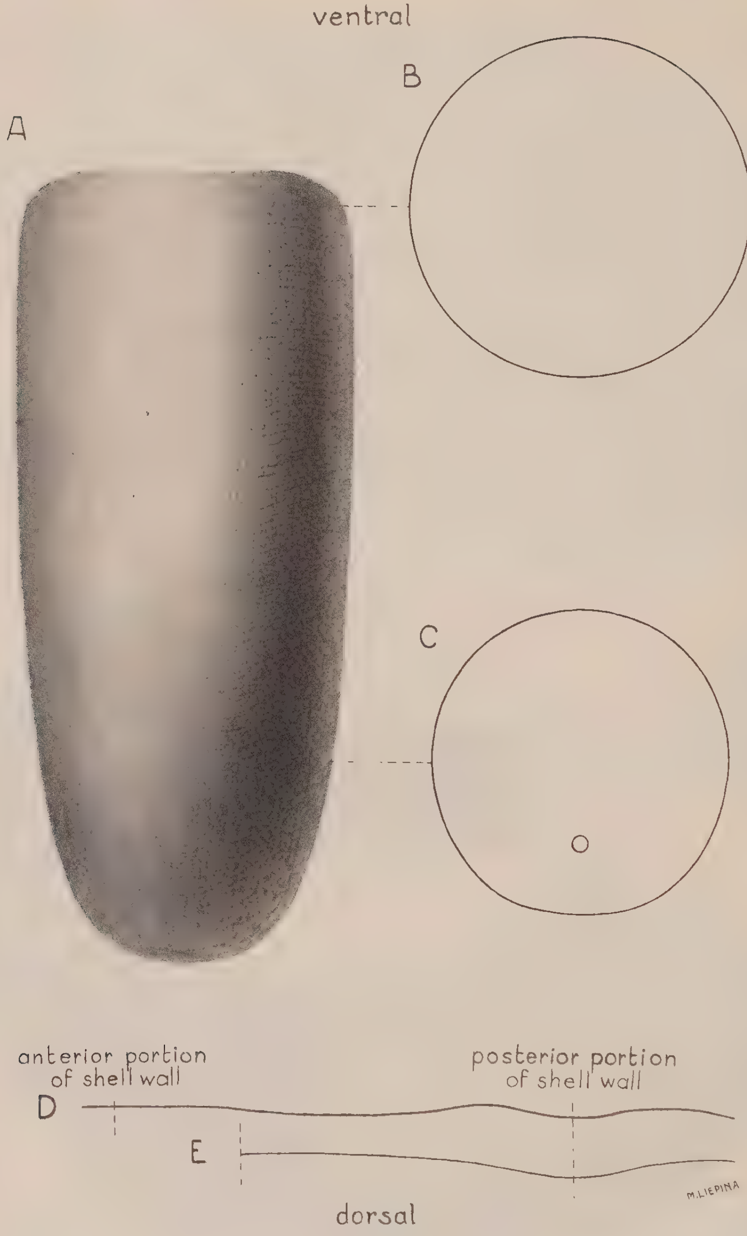

Text-fig. 21. *Uranoceras* (?) *longitudinale* (ANGELIN). A, reconstruction of shell in posterior view, × $\frac{4}{5}$; B, C, two horizontal sections of shell at the levels indicated; D, E, diagrams of two systegnoses projected in one plane, × $\frac{4}{5}$.

Lectotype: RM, No. Mo 149998 (pl. 17:2, 3; Angelin 1880, pl. 16:5).

Stratum and localities.—Boda Limestone, which belongs to the uppermost Ordovician; Dalecarlia: Kallholn, Osmundsberget and Solberga (?).

Diagnosis.—Morphological length of shell equal to breadth, or slightly greater; circumference of shell circular, or broadly elliptical; shell ornamentation consisting of delicate, vertical ridges separated by broad and smooth intervals; systegnoses practically horizontal on anterior portion of shell wall, but turn upwards in an unpaired curve on posterior portion of shell wall and in some cases in a slight, paired curve on lateral portion of shell wall; distance between septa in ventral portion of septate division equal to $\frac{1}{4}$–$\frac{1}{5}$ of the morphological length of shell; distance between siphonal tube and posterior portion of shell wall corresponds to $\frac{1}{5}$–$\frac{1}{6}$ of equal length.

Description.—A reconstruction based on several incomplete specimens shows that the shell must have formed a loose whorl (text-fig. 20 A), the coiling of which decreased slightly with the proceeding growth of the animal. The morphological length of the shell, which attains up to 60 mm at the shell aperture, is equal to the breadth, or slightly greater. Consequently, the circumference of the shell is circular, or broadly elliptical (text-fig. 21 B, C). The increase of the morphological length and breadth is, as a rule, greater in the dorsal portion of the shell than in the ventral portion, but in some specimens it is also quite considerable in the latter portion (pl. 4:3). The height of the domiciliary division in the full-grown shell is somewhat greater than $\frac{1}{3}$ of the whole morphological height of the shell. A slight antero-median tubercle (*t*, text-fig. 10 C) on the inside of the domiciliary cavity immediately below the youngest septum belongs, in all probability, to the septal furrow of the youngest septum.

The shell ornamentation is made up of delicate, vertical ridges separated by rather broad and smooth intervals (text-fig. 20 B; pl. 18). In certain places in the lectotype these ridges are replaced by furrows (pl. 18:1); the furrows, but not the ridges, are mentioned in Angelin's diagnosis.

The septa in the ventral portion of the septate division of the shell are practically horizontal (text-fig. 20 A; pls. 4:3; 6:2; 7:2). The distance between the septa in the ventral portion of the septate division corresponds to $\frac{1}{4}$–$\frac{1}{5}$ of the morphological length of the shell. The systegnoses are almost horizontal on the anterior portion of the shell wall (text-fig. 21 D, E; *s*, pls. 6:3; 7:3), but turn upwards in an unpaired curve of varying dimensions on the posterior portion of the shell wall (text-fig. 21 D, E; *s*, pls. 6:1; 7:1, 4, 5) and, in some cases, also in a slight paired curve on the lateral portion of the shell wall (text-fig. 21 D; *s*, pls. 4:3; 6:2). The distance between the siphonal tube and the posterior portion of the shell wall is equal to $\frac{1}{5}$–$\frac{1}{6}$ of the morphological length of the shell. The proximal division of the siphonal funnel is very short compared with the distal division (text-fig. 20 A, C; *pro*, *dis*, pl. 17:1); the siphonal tube narrows in the former division, but widens in the latter.

The annular elevation of *U.* (?) *longitudinale* has been discussed on pp. 230–232.

Remarks.—*U.* (?) *longitudinale* differs from the other species of the genus *Uranoceras* mainly in the fact that the systegnoses on the posterior portion of the shell wall turn upwards, and not downwards, in an unpaired curve. Owing to this difference it is not quite certain that this species belongs to the genus *Uranoceras*.

B. *Lyecoceras* n. gen.

Genotype: *Lyecoceras gotlandense* n. sp.

Diagnosis.—Shell slightly coiled in posterior direction; morphological breadth of shell equal to length, or rather greater; circumference of shell circular, or broadly elliptical; margin of shell aperture projects somewhat further down anteriorly than laterally and posteriorly; septa lie obliquely to morphological dorso-ventral axis of shell in such a way that posterior margin is more ventral than anterior; according to this position of septa systegnoses are almost horizontal on anterior portion of shell wall, but turn downwards in a broad, unpaired curve on lateral and posterior portions of shell wall; siphonal tube situated slightly anterior to morphological dorso-ventral axis of shell; proximal division of siphonal funnel short, distal division long; siphonal tube narrow in the former division, but widens slightly in the latter; septal furrow conspicuous; annular elevation forming an anteriorly situated ventral lobe.

In the genus *Lyecoceras* are included the following three species: *L. gotlandense* n. sp., *L. longistriatum* n. sp. and *Lyecoceras* (?) sp. The latter species, represented by only one incomplete specimen (text-fig. 13; pl. 12), differs from the other two species by a considerably larger size and at least by the fact also that the systegnoses on the anterior portion of the shell wall are not horizontal, but turn downwards in an unpaired curve.

At present the genus *Lyecoceras* is known only in the Hemse-Group of the Silurian, Isle of Gotland.

Lyecoceras gotlandense n. sp.

Text-figs. 5 A; 6 D; 16 A, B, C, G; 22; pls. 9:4,5; 10; 16:4,5,6; 19:2; 20.

Material: a large number of specimens (about 50).

Holotype: RM, No. Mo 149991 (pl. 10).

Stratum and localities: Hemse-Group, Lower Ludlow, Silurian; Isle of Gotland: Mannagårda, Lye; Sandarve kulle; Ethelhem and Linde klint.

Diagnosis.—Morphological breadth of shell slightly greater than length; circumference of shell broadly elliptical; external surface of shell ornamented only in dorsal portion of septate division with delicate, vertical striae; distance between siphonal tube and anterior portion of shell wall equal to $\frac{1}{3}$–$\frac{2}{5}$ of morphological length of shell.

Description.—The shell is very slightly coiled in its ventral portion, but its coiling lincreases a little towards the apex (text-fig. 22 B; pls. 16:5; 20:1, 2). The morphoogical breadth and length increase rather more in the septate division of the shell than in the domiciliary division (text-fig. 22 A, B). The circumference of the shell is broadly elliptical (text-fig. 22 F, G, H). The apertural margin of the shell projects somewhat further down anteriorly than laterally and posteriorly (text-fig. 22 A, B; pl. 10:2).

The external surface of the shell shows growth lines and also, in the dorsal portion of the septate division, delicate, vertical striae (text-fig. 22 D; pl. 19: 2). The internal surface of the shell has delicate, undulating, horizontal striae, similar to those in *L. longistriatum* (pl. 19:3).

The septa lie obliquely to the morphological dorso-ventral axis of the shell in such a way that the posterior margin is more ventral than the anterior. The younger

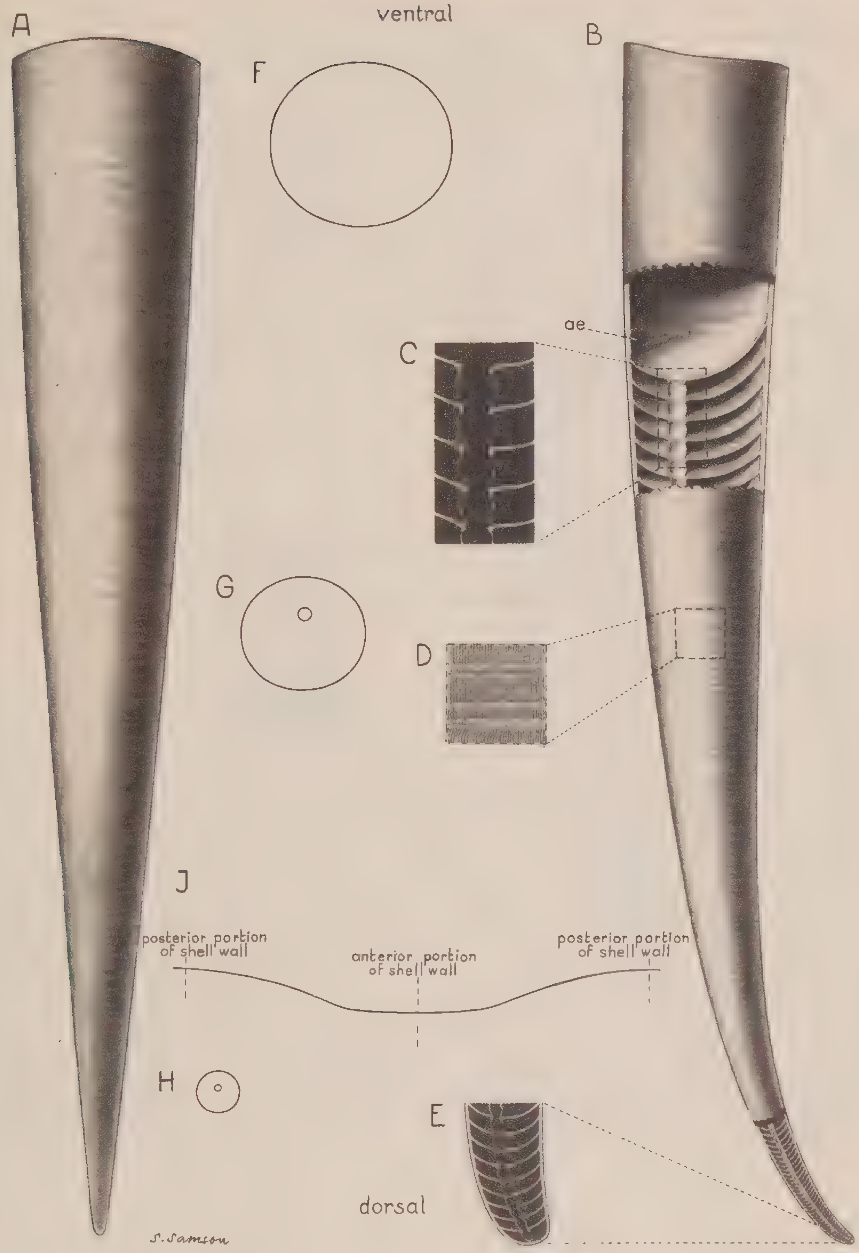
A
ventral
F
B
ae
C
G
D
J
posterior portion of shell wall
anterior portion of shell wall
posterior portion of shell wall
H
E
dorsal
S. Samson

Text-fig. 22. *Lyecoceras gotlandense* n. sp. A, reconstruction of shell in anterior view, ×$\frac{3}{5}$; B, reconstruction of shell in right lateral view, with shell wall and sections of septa removed at two places, ×$\frac{3}{5}$; C, part of siphonal tube in median-sagittal section, ×$\frac{6}{5}$; D, details of shell ornamentation, ×$\frac{6}{5}$; E, details of shell apex cut in a median-sagittal plane, ×$\frac{12}{5}$; F, G, H, three horizontal sections of shell; ×$\frac{3}{5}$; J, diagram of systegnosis of the youngest septum projected in one plane, ×$\frac{3}{5}$. *ae*, annular elevation of shell.

septa are more oblique than the older ones (text-fig. 22 B; pls. 10:2; 20). Moreover, the distance between the younger septa is greater than between the older ones, relative to the morphological length of the shell. More exactly, this distance corresponds to $\frac{1}{4}$–$\frac{1}{10}$ of the morphological length of the shell. The septal furrow is conspicuous (*if*, pl. 9:5). In the domiciliary cavity of the full-grown shell this furrow terminates ventrally in a little tubercle (*t*, text-fig. 16 A; pl. 10:1). The systegnoses are almost horizontal on the anterior portion of the shell wall (text-fig. 22 J; *s*, pls. 9:4, 5; 10:1), but turn downwards in a broad unpaired curve on the lateral and posterior portions of the shell wall (text-fig. 22 J; *s*, pl. 10:2, 3). The siphonal tube is situated a little anterior to the morphological dorso-ventral axis of the shell (text-fig. 22 B; pl. 20) and its distance from the anterior portion of the shell wall corresponds to $\frac{1}{3}$–$\frac{2}{5}$ of the morphological length of the shell. The dorsal end of the siphonal tube is hemispherical and probably lies in contact with the inside of the shell apex (text-fig. 22 E; pl. 20:2). The proximal division of the siphonal funnel is very short compared with the distal division (text-fig. 22 C, E; pl. 20), the siphonal tube is slightly narrower in the former division than in the latter.

The annular elevation in *L. gotlandense* has already been discussed (pp. 230–232).

Lyecoceras longistriatum n. sp.

Text-figs. 7 E; 23; 24; pls. 11; 19:1,3.

Material: 4 specimens.

Holotype: RM, No. Mo 149992 (pl. 11).

Stratum and localities: Hemse-Group, Lower Ludlow, Silurian; Isle of Gotland: Mannagårda, Lye; Tänglings hällar, Lye; Etlehem.

Diagnosis.—Morphological length of shell equal to breadth; circumference of shell circular; external surface of shell ornamented with horizontal ridges, irregular in spacing and size and with, in addition, delicate, vertical ridges.

Description.—This species can be easily distinguished from *L. gotlandense* by the following three characters: (1) a greater increase of the morphological length and breadth of the shell in relation to the height (cf. text-figs. 22 A and 23 A); (2) the circular circumference of the shell (text-fig. 24 B, C, D); and (3) the ornamentation of the external shell surface, consisting of horizontal ridges, irregular in spacing and size and also of delicate, vertical ridges (text-fig. 23 B; pls. 11; 19:1). The horizontal ridges are so distinct that they are even visible on the internal surface of the shell which, in addition, reveals delicate, undulating, horizontal striae (pl. 19:3). The distance between the septa is about the same as in *L. gotlandense*, and the siphonal tube has approximately the same position as in the latter species.

The annular elevation of *L. longistriatum* has been mentioned on pp. 230–232.

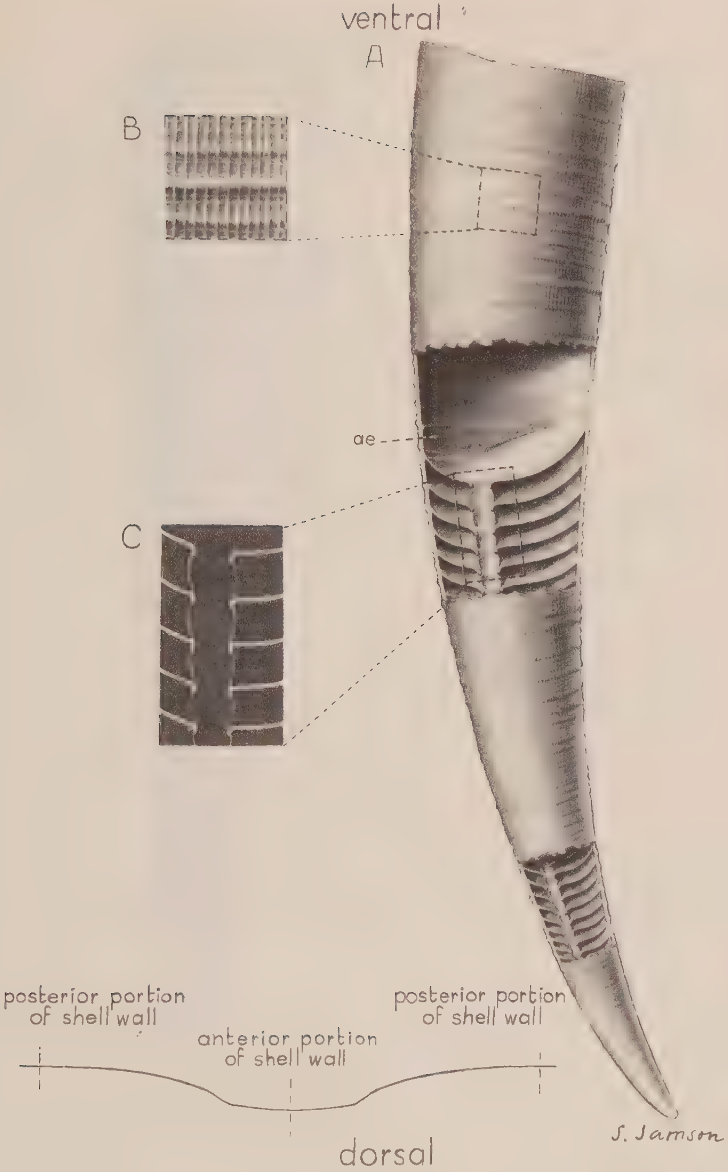
ventral
A
B
ae
C
posterior portion of shell wall
anterior portion of shell wall
posterior portion of shell wall
dorsal
S. Jamson

Text-fig. 23. *Lyecoceras longistriatum* n. sp. A, reconstruction of shell in right lateral view, with shell wall and sections of septa removed at two places, $\times \frac{4}{5}$; B, details of shell ornamentation, $\times \frac{8}{5}$; C, details of siphonal tube in median-sagittal section, $\times \frac{8}{5}$; D, diagram of systegnosis of the youngest septum projected in one plane, $\times \frac{4}{5}$.
ae, annular elevation of shell.

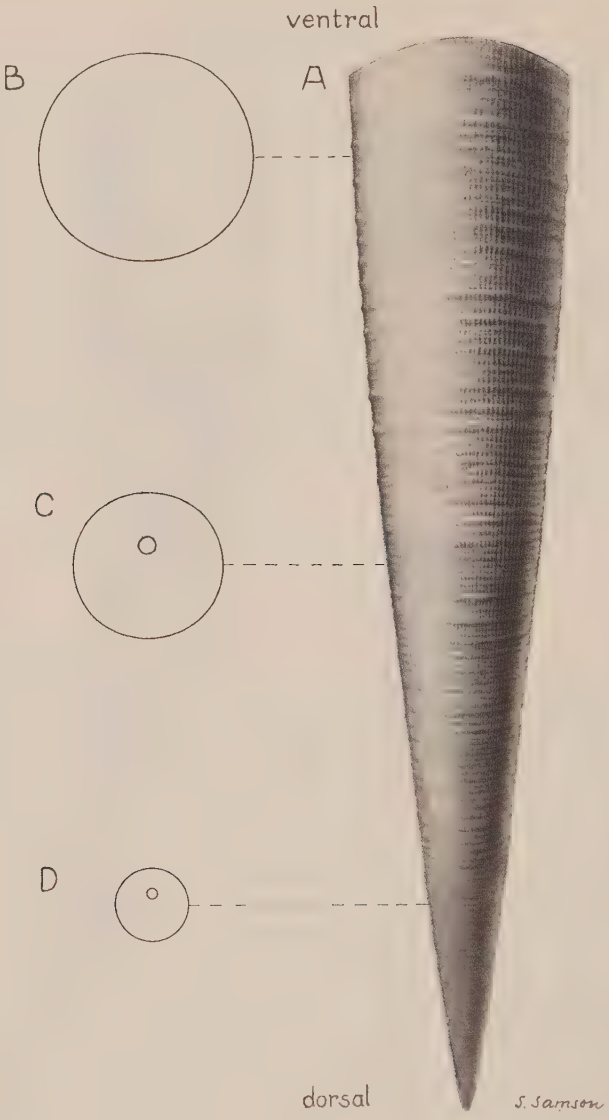

Text-fig. 24. *Lyecoceras longistriatum* n. sp. A, reconstruction of shell in anterior view, ×$\frac{4}{5}$; B, C, D, three horizontal sections of shell at the levels indicated, ×$\frac{4}{5}$.

REFERENCES

Angelin, N. P. and Lindström, G., 1880. Fragmenta silurica e dono Caroli Henrici Wegelin, Holmiae.

Appellöf, A., 1893. Die Schalen von Sepia, Spirula und Nautilus. Kgl. Svenska Vet. Akad. Handl. Bd. 25, No. 7, Stockholm.

Balfour, F. M., 1880. Handbuch der vergleichende Embryologie, Bd. 1, Jena.

Barrande, J., 1866. Système silurien du centre de la Bohême, Vol. 2, 2^{e} série, Planches.

—— 1867. Ibid., Texte, Part 1.

—— 1870. Ibid., 4^{e} série. Planches.

—— 1877. Ibid., Supplément, Texte.

Brück A., 1913. Über die Muskelstruktur und ihre Entstehung, sowie über die Verbindung der Muskeln mit der Schale bei den Muscheln. Zool. Anzeiger, Bd. 42, Leipzig u. Berlin.

—— 1914. Die Muskulatur von Anodonta cell. Schrot. Zeitschr. f. wiss. Zool., Bd. 110, Leipzig.

Crick, G. C., 1898 a. On the muscular attachment of the animals to its shell in some fossil Cephalopoda (Ammonoidea). Trans. Linnean Soc. London, Ser. 2, Vol. 7, Part 4.

—— 1898 b. Descriptions of new or imperfectly known species of Nautilus from the Inferior Oolite, preserved in the British Museum (Nat.Hist.). Proc. Malacolog. Soc., Vol. 3, Part 3, London.

—— 1904. On a new form of carboniferous Nautiloid (*Amphereopsis paucicamerata*) from the Isle of Man. Ibid., Vol. 6, Part 3, London.

—— 1905. On a specimen of *Cyrtoceras* (*Meloceras*) *apicale* from the Carboniferous Limestone, Kniveton, Derbyshire. Geol. Mag., Decade 5, Vol. 2, No. 488, London.

Dames, 1879. Annulus von *Lituites convolvens* aus der Untersilur von Reval. Sitzungsber. Ges. naturf. Freunde Berlin, No. 1.

Dewitz, H., 1879 a. Die Wohnkammer regulärer Orthoceratiten. Sitzungsber. Ges. naturf. Freunde Berlin, No. 3.

—— 1879 b. Der Verwachsungsband der Vaginaten. Ibid., Nr. 9.

—— 1879 c. Beiträge zur Kenntnis der in den Ostpreussischen Silurgeschieben vorkommenden Cephalopoden. Schr. Physik. Oek. Ges., Jahrg. 20, Königsberg.

—— 1880. Über einige ostpreussische Silurcephalopoden. Zeitschr. Deutsch. geol. Ges.

Flower, R. H., 1939. Study of the Pseudorthoceratidae. Paleontographica Americana, Vol. 2, No. 10, New York.

Foerste, A. F., 1925. Notes on Cephalopod genera, chiefly coiled Silurian forms. Denison Univ. Bull., Sci. Lab., Jour., Vol. 21, Granville, Ohio.

Foord, A. H., 1900. Monograph on the Carboniferous Cephalopoda of Ireland, part 3. Palaeont. Soc., London.

Foord, A. H. and Crick, G. C., 1889. On the muscular impressions of *Coelonautilus cariniferus* Sow., compared with those of the recent Nautilus. Geol. Mag. Decade 3, Vol. 6.

1890. On the muscular impressions of some species of Carboniferous and Jurassic Nautiloids compared with those of the recent Nautilus. Ann. Mag. Nat. Hist., March.

Griffin, L. E., 1900. The anatomy of *Nautilus pompilius*. Mem. Nat. Acad. Sci., Vol. 8, 5, Washington.

Hescheler, K., 1900. Mollusca. Lehrbuch der vergleichende Anatomie der wirbellosen Thiere von A. Lang, 1 Lief., Jena.

Huxley, T. H., 1853. On the morphology of the Cephalous mollusca, as illustrated of certain Heteropoda and Pteropoda collected during the voyage of H.M.S. "Rattlesnake" in 1846–50 Phil. Trans. Roy. Soc. Vol. 143, Part. 1, London.

—— 1864. On the Structure of the Belemnitidae; with a Description of a More Complete Specimen of Belemnites than any Hitherto Known, and an Account of a New Genus of Belemnitidae, *Xiphotheuthis*. Mem. Geol. Surv. United Kingd., Monogr. 2, London.

Hyatt, A., 1883. Genera of fossil Cephalopods. Boston Soc. Nat. Hist., Proc., Vol. 22.

—— 1894. Phylogeny of an acquired characteristic. Proc. Amer. Phil. Soc., vol. 32, No. 143.

Keferstein, W., 1861. Kopftragende Weichthiere (Malacozoa cephalophora). Bronns Klassen u. Ordn. d. Weichthiere, Bd. 3, Abt. 2, Leipzig u. Heidelberg.

Kessler, P., 1923. Beiträge zur Kenntniss der Organisation der fossilen Gehäusecephalopoden. Cbl. Miner. Geol. Paleont., 24, Stuttgart.

Loesch, H. C., 1914. Die Nautilen des weissen Jura. Erster Teil. Paleontographica, Bd. 61, 3. Stuttgart.

Mojsisovics, E. M., 1873. Das Gebirge um Hallstatt. Theil 1. Abh. k. k. geol. Reichsanst., Bd. 6 Wien.

—— 1882. Die Cephalopoden der mediterranen Triasprovinz. Ibid., Bd. 10.

MUTVEI, H., 1956. A preliminary report on the structure of the siphonal tube and on the precipitation of lime in the shells of fossil Nautiloids. Arkiv Mineral. Geol., Stockholm (in press).

NAEF, A., 1922. Die fossilen Tintenfische. Jena.

—— 1926. Studien zur generellen Morphologie der Mollusca. Teil 3. Ergeb. Fortschr. Zool., Bd. 6, Jena.

NOETLING, F., 1882. Über *Lituites lituus* MONTFORT. Zeitschr. Deutsch. geol. Ges.

OWEN, R., 1832, Memoir on the Pearly Nautilus. London.

—— 1843. Lectures on the Comparative Anatomy and Physiology of Invertebrate Animals. London.

—— 1844. A description of certain Belemnites, preserved, with a great proportion of their soft parts, in the Oxford Clay, at Christian-Malford, Wilts. Phil. Trans. Royal Soc., Parts 1, 6.

—— 1860. Paleontology. Edinburgh.

PELSENEER, P., 1906. Mollusca. In: A Treatise on Zoology, Part V. Edit. E. R. LANKESTER.

PLATE, L., 1922. Allgemeine Zoologie und Abstammungslehre. Teil 1, Jena.

RAUTHER, M., 1925. in SCHMIDT, M: Ammonitenstudien. Fortschr. d. Geol. u Paleont., H. 10, Berlin.

REMELÉ, A., 1890. Untersuchungen über die versteinerungsführenden Diluvialgeschiebe der norddeutschen Flachlandes. 1. Stück, Theil 2, Berlin.

RÖCHLING, E., 1922. Der Kolumellarmuskel von *Helix pom.* und seine Beziehung zur Schale. Zeitschr. wiss. Zool., Bd. 119, H. 3, Leipzig.

RÜDIGER, H., 1889. Über die Silur-Cephalopoden aus den mecklenburgischen Diluvialgeschieben. Arch. d. Freunde d. Naturg. Meckl., Güstrow.

SCHMIDT, W. J., 1924. Die Bausteine des Tierkörpers in polarisiertem Lichte. Bonn.

SCHRÖDER, H., 1881. Beiträge zur Kenntniss der in ost- und westpresussischen Diluvialgeschieben gefundenen Silurcephalopoden. Schr. d. Physic. Oek. Gesellsch. zu Königsberg, Jahrg. 22.

—— 1882. Ibid. (Fortsetzung), Jahrg. 23.

TULLBERG, F., 1882. Studien über den Bau und das Wachstum des Hummerpanzers und der Molluskenschalen. Kgl. Svenska Vetensk. Akad. Handl. 19, Stockholm.

WAAGEN, W., 1870. Über die Ansatzstellen der Haftmuskeln beim *Nautilus* und Ammoniden. Palaeontographica, Bd. 17, 5. Cassel.

WILLEY, A., 1902. Zoological Results based on material from New Britain, New Guinea, Loyalty Islands and elsewhere, collected during the years 1895–1897. Part 6, Cambridge.

Tryckt den 22 mars 1957

Uppsala 1957. Almqvist & Wiksells Boktryckeri AB

PLATES

Plate 1

Nautilus pompilius L.

Ventral view of shell, preserved in alcohol, to show domiciliary cavity, with functional area of origin of muscles on lateral and posterior portions of annular elevation (text-figs. 2 A, 3), nat. size.

ia, intermediate area; *mm*, functional area of origin of longitudinal mantle-musculature; *rm*, functional area of origin of retractor muscles; *s*, youngest septum; *sem*, functional area of origin of sub-epithelial musculature of dorsal portion of body proper; *x*, functional area of attachment of pallio-visceral ligament.

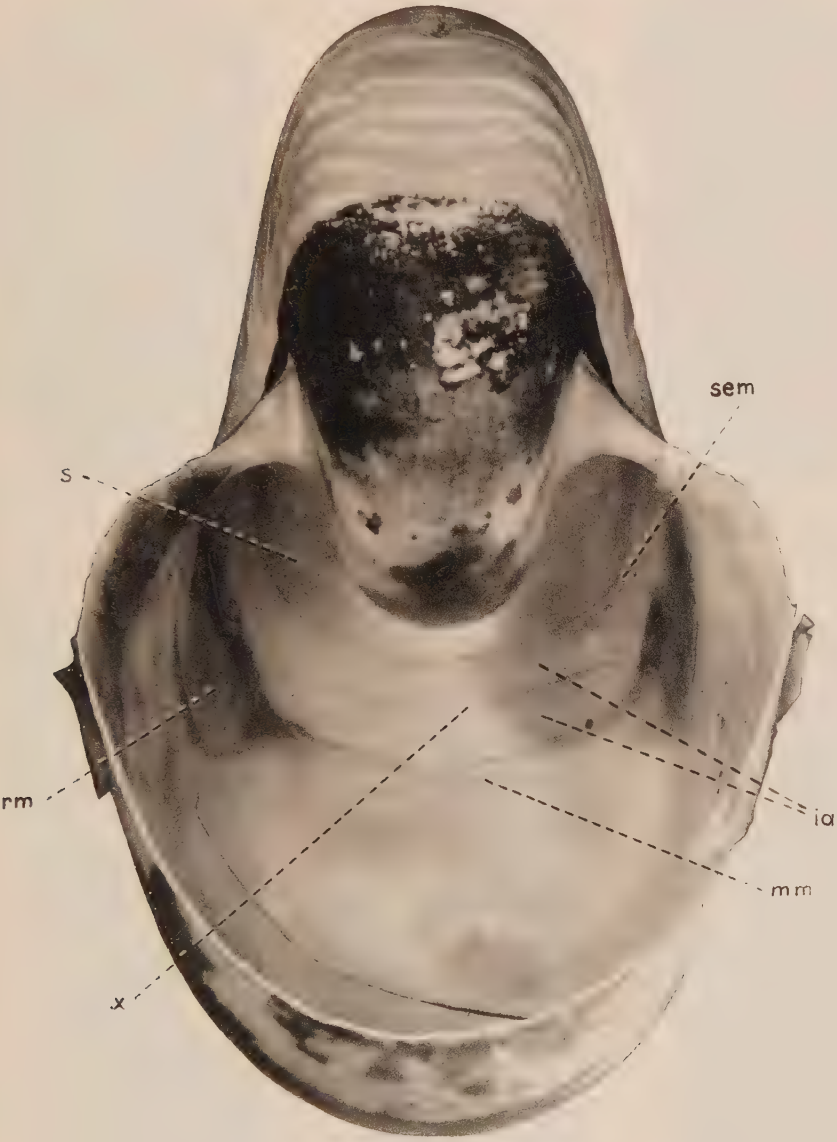
sem
s
rm
ia
mm
x

Plate 2

Estonioceras impressum (Hyatt).

Figs. 1, 2, 3. Cast of domiciliary cavity of shell in posterior, lateral, and anterior views, respectively (text-fig. 8), × $\frac{4}{3}$; Möthlitz, Germany, B III, from a Diluvial boulder of Lower Ordovician.

Orthoceros regulare (Schlotheim).

Figs. 4, 5, 6. Cast of domiciliary cavity of shell in anterior, lateral, and posterior views, respectively; × $\frac{4}{3}$; specimen RM, No. Mo 149996, Sjönhem, Kellinge, Isle of Gotland, from a Diluvial boulder of Middle Ordovician.

a, impression of ventral margin of annular elevation of shell; *p*, impression of dorsal margin of annular elevation; *s*, impression of angle between the youngest septum proper and its mural part.

ventral

1

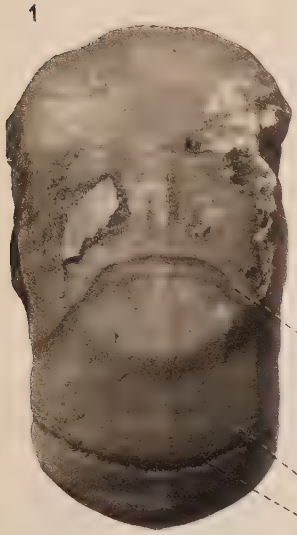

2

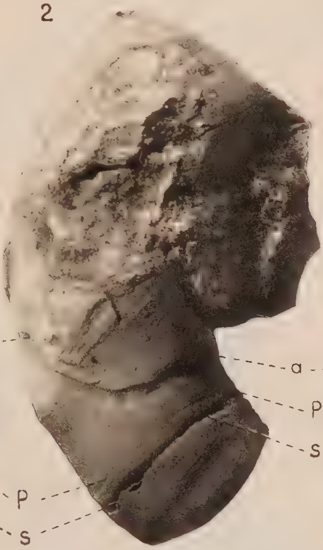

3

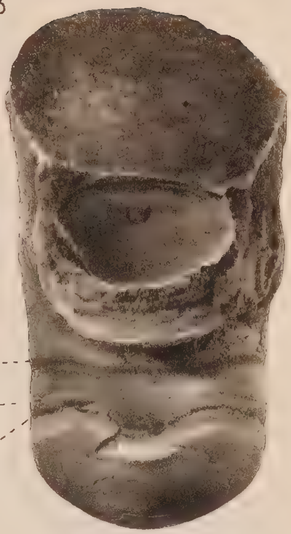

4

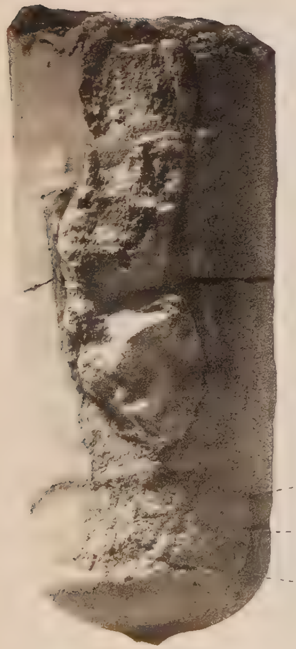

5

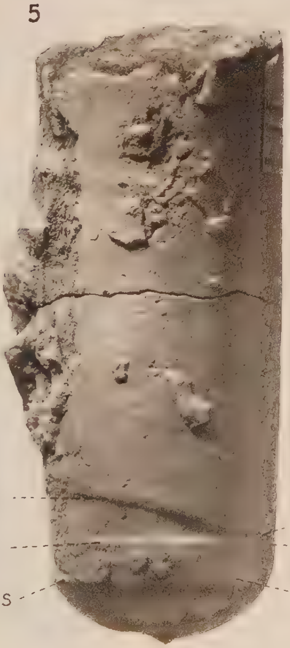

6

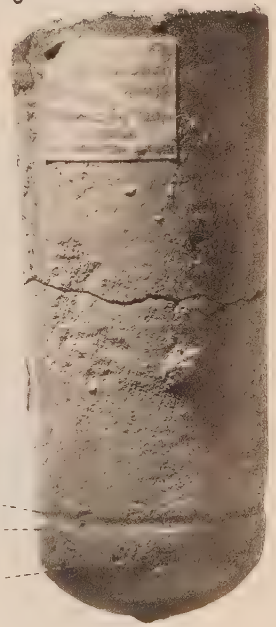

dorsal

Plate 3

Estonioceras perforatum SCHRÖDER.

Figs. 1, 2, 3. Cast of domiciliary cavity of shell in anterior, lateral, and posterior views, respectively (text-fig. 9 A, C,), × $\frac{9}{10}$; specimen RM, No. Mo 149983, Tallinn, Estonia, B III γ, Lower Ordovician.

Estonioceras imperfectum (QUENSTEDT).

Figs. 4, 5. Cast of domiciliary cavity of shell and shell chambers in lateral and posterior views, respectively (text-fig. 9 B), × $\frac{9}{10}$; specimen RM, No. Mo 149982, Tallinn, Estonia, B III γ, Lower Ordovician.

a, impression of ventral margin of annular elevation of shell; *p*, impression of dorsal margin of annular elevation; *s*, impression of angle between the youngest septum proper and its mural part; *si*, siphonal tube.

ventral

1

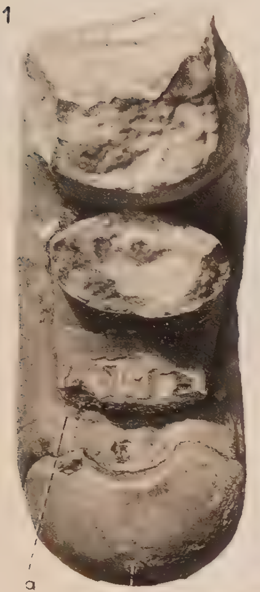

2

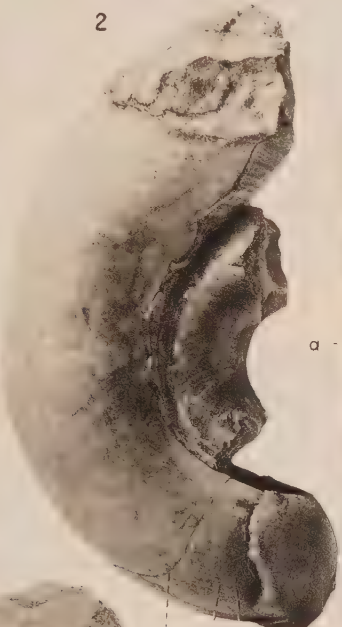

3

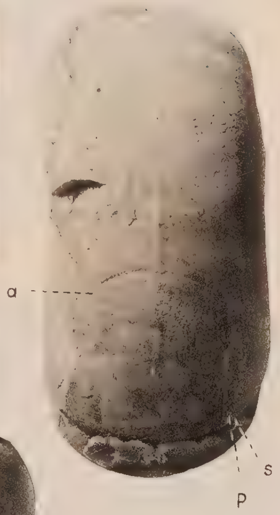

4

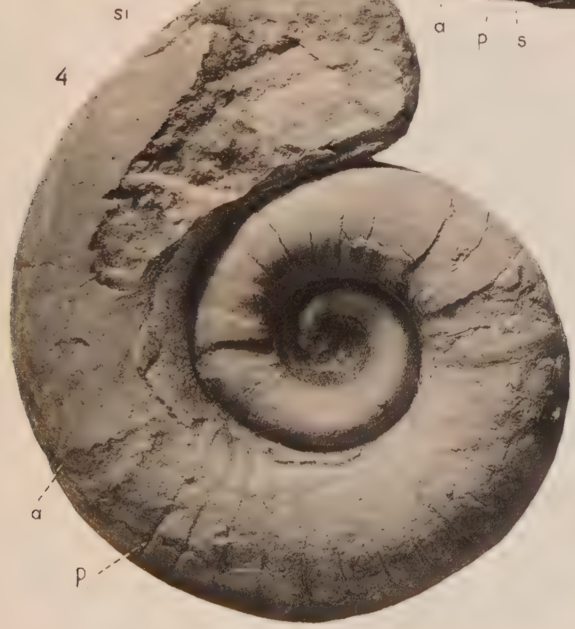

5

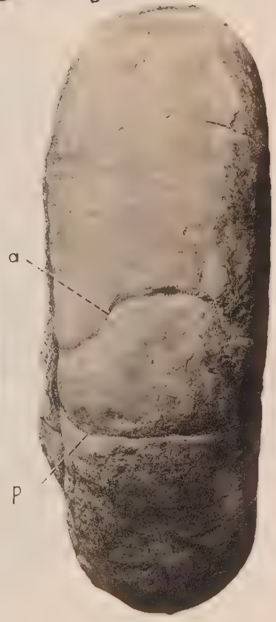

dorsal

Plate 4

Estonioceras perforatum SCHRÖDER.

Figs. 1, 2. Cast of domiciliary cavity of shell, and septate division of shell in lateral and posterior views, respectively, nat. size; specimen No. C. 15223, British Museum (Nat. Hist.), Tallinn, Estonia, B III γ, Lower Ordovician.

Uranoceras (?) *longitudinale* (ANGELIN).

Fig. 3. Cast of domiciliary cavity of shell in lateral view (text-fig. 10 D), nat. size; uncatalogued specimen, Geological Survey of Sweden, Kallholn, Dalecarlia, Boda Limestone.

a, impression of ventral margin of annular elevation of shell; *p*, impression of dorsal margin of annular elevation; *s*, impression of angle between the youngest septum proper and its mural part.

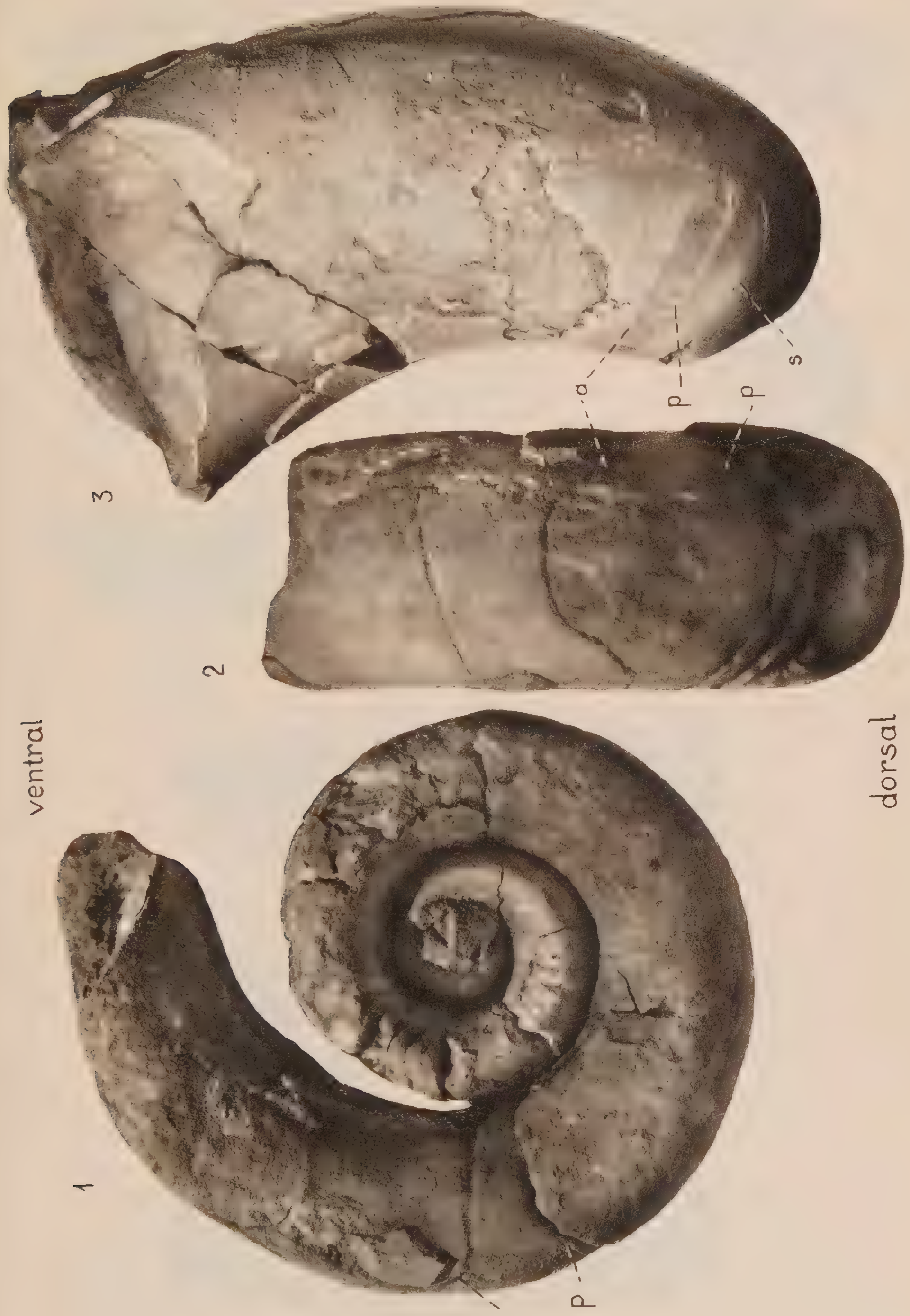
3
a
p
p
s
2
ventral
dorsal
1
a
p

Plate 5

Planctoceras falcatum (SCHLOTHEIM).

Two casts of domiciliary cavity of shell and of some shell chambers in posterior, lateral, and anterior views, respectively, nat. size; specimen No. C. 4074, British Museum (Nat. Hist,) (text-fig. 9 E) and specimen RM, No. Mo 149984 (text-fig. 9 D); both specimens from Tallinn, Estonia, B III γ, Lower Ordovician.

a, impression of ventral margin of annular elevation of shell; *p*, impression of dorsal margin of annular elevation.

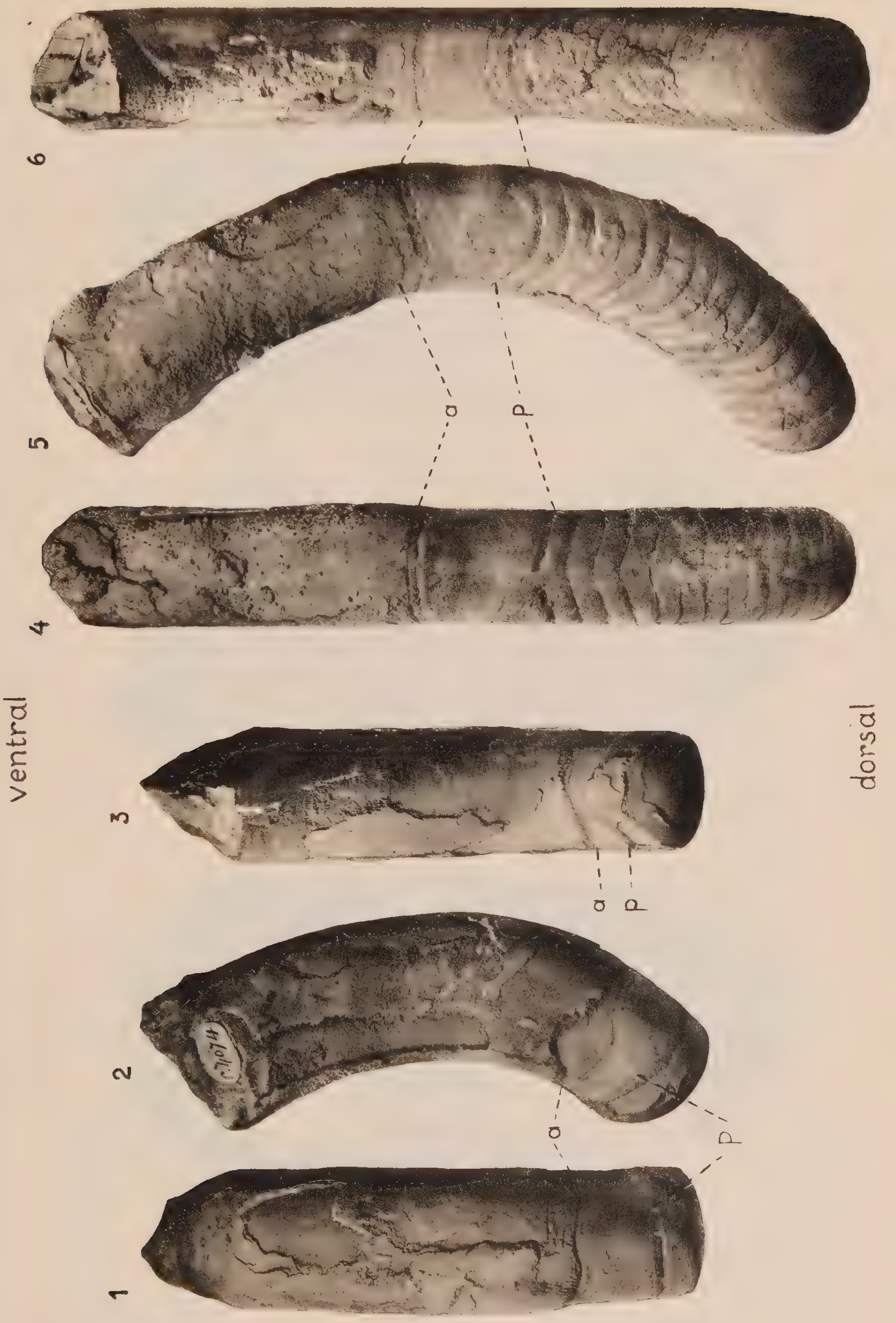
6
5
4
3
2
1
a
p
a
p
a
p
ventral
dorsal
c.4074

Plate 6

Uranoceras (?) *longitudinale* (ANGELIN).

Figs. 1, 2, 3. Cast of domiciliary cavity of shell in posterior, lateral, and anterior views, respectively (text-figs. 10 A, B, C, E; 11 A), $\times\frac{4}{5}$; specimen UPI, No. D 435, Osmundsberget, Dalecarlia, Boda Limestone.

a, impression of ventral margin of annular elevation of shell; *p*, impression of dorsal margin of annular elevation; *s*, impression of angle between the youngest septum proper and its mural part; *t*, impression of tubercle of septal furrow of the youngest septum.

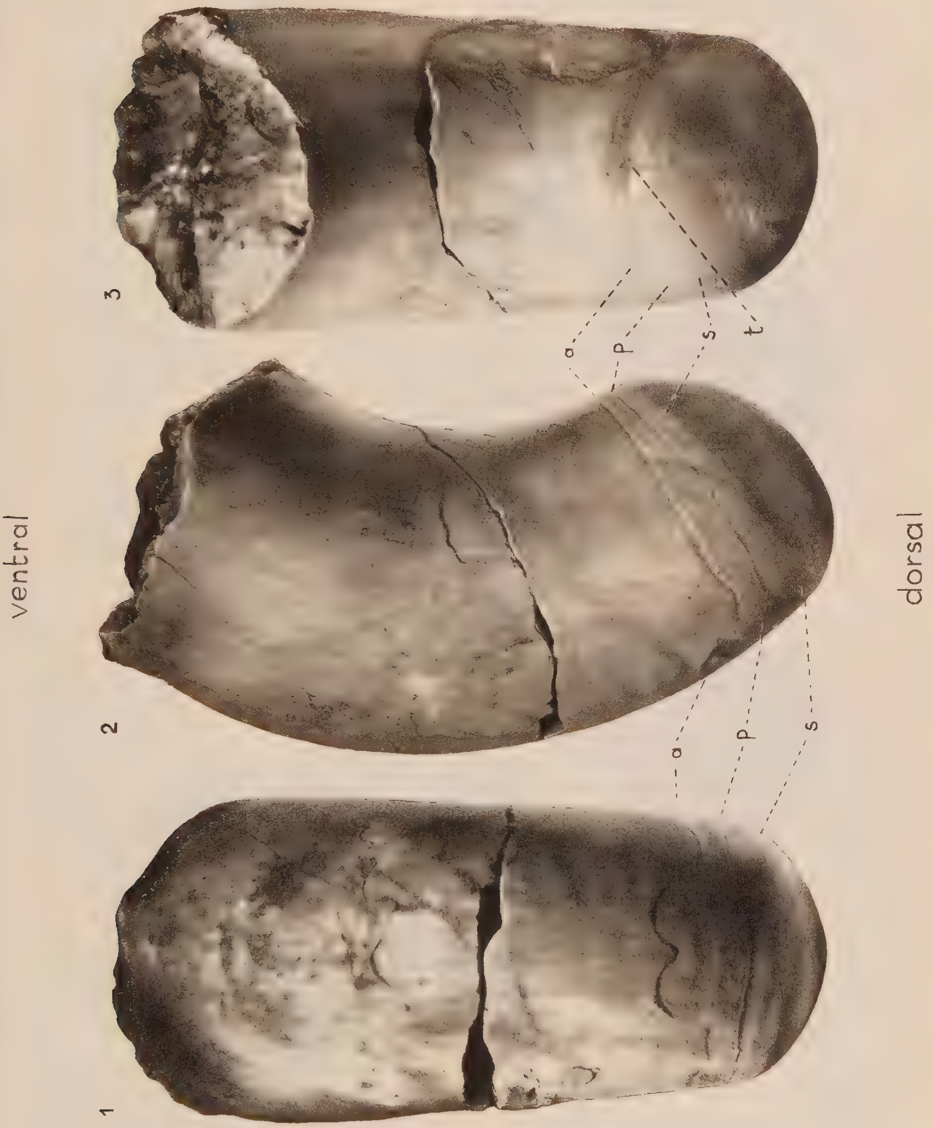
3
a
p
s
t
2
a
p
s
1
ventral
dorsal

Plate 7

Uranoceras (?) *longitudinale* (ANGELIN).

Figs. 1, 2, 3. Ventral portion of septate division of shell in posterior, lateral, and anterior views, respectively, × $\frac{4}{5}$; specimen UPI, No. D 434, Kallholn, Dalecarlia, Boda Limestone.

Figs. 4, 5. Two casts of domiciliary cavity of shell in posterior view (text-fig. 11 D, E), × $\frac{4}{5}$; specimen RM, No. Mo 149997, Solberga (?), Dalecarlia, and same specimen as in pl. 4:3.

a, impression of ventral margin of annular elevation of shell; *p*, impression of dorsal margin of annular elevation; *s*, impression of angle between the youngest septum proper and its mural part; *sep*, peripheral portion of septum proper; *si*, siphonal tube.

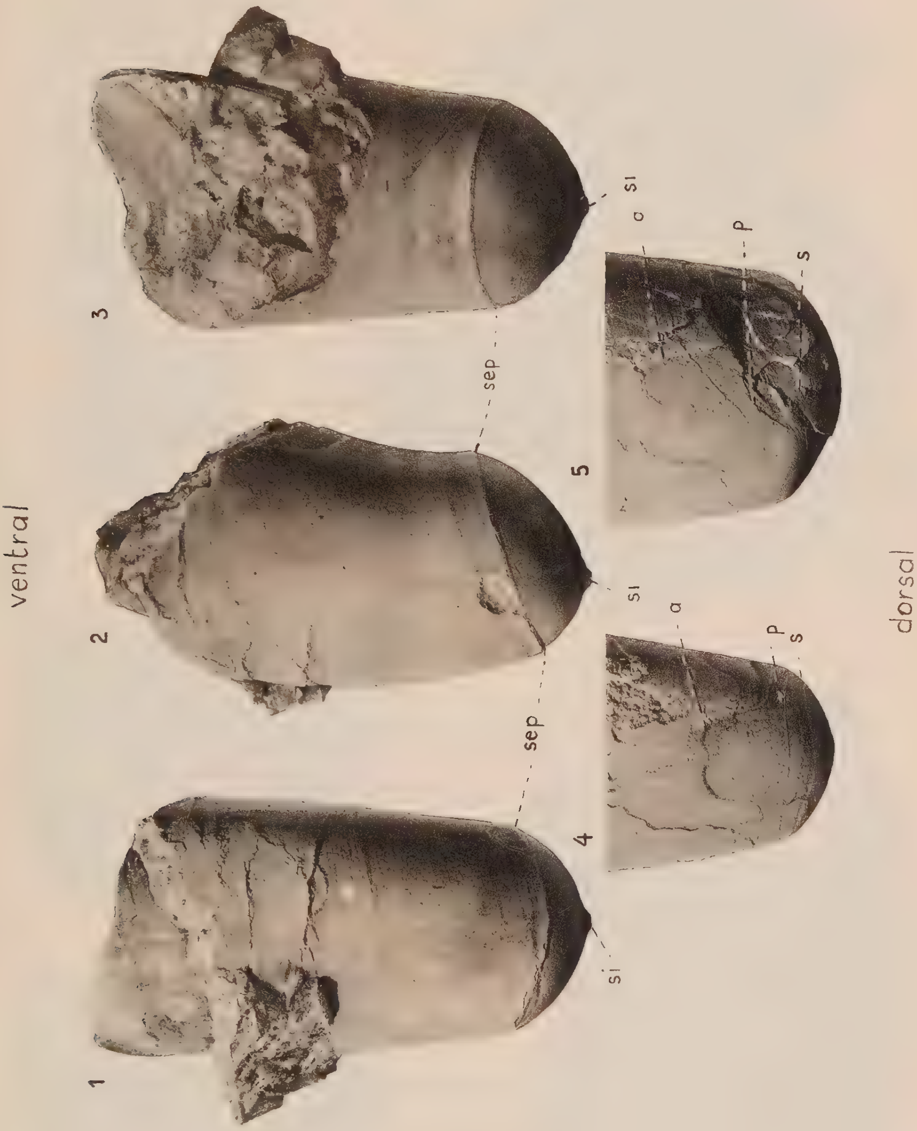
ventral
1
2
3
sep
sep
si
si
si
4
5
a
a
p
p
s
s
dorsal

Plate 8

Discoceras angulatum (SAEMANN).

Figs. 1, 2. Shell in posterior and lateral views, respectively, nat. size; specimen UPI, No. D 432, Osmundsberget, Dalecarlia, Boda Limestone.

Figs. 3, 4, 5. Details of same specimen to show cast of domiciliary cavity of shell in posterior, lateral, and anterior views, respectively (text-fig. 12), × 2.

a, impression of ventral margin of annular elevation of shell; *p*, impression of dorsal margin of annular elevation; *s*, impression of angle between the youngest septum proper and its mural part.

1

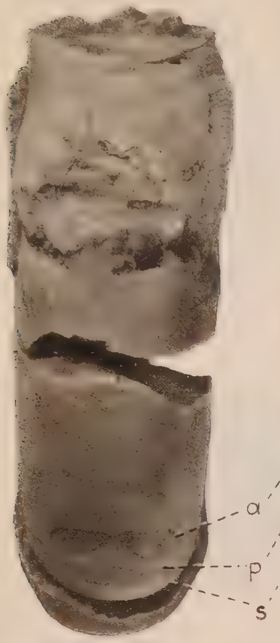

2

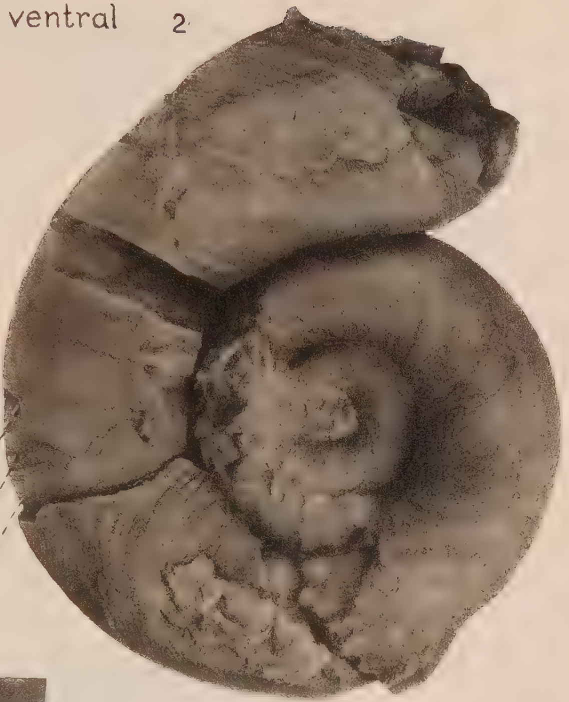

3

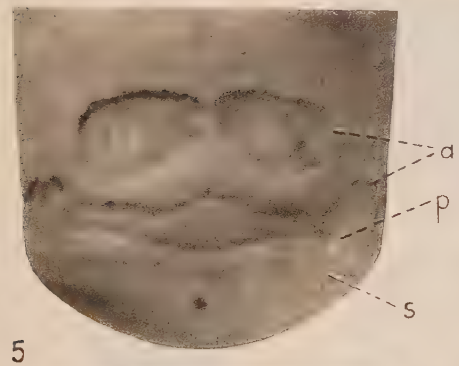

4

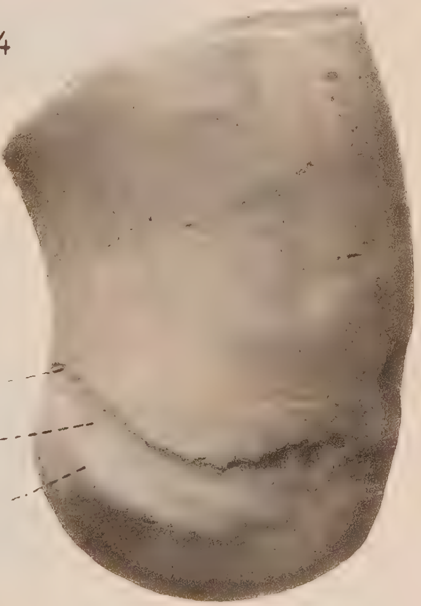

5

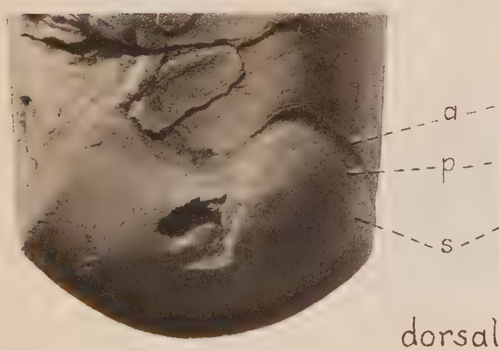

Plate 9

Discoceras sp.

Figs. 1, 2, 3. Cast of domiciliary cavity of shell and of several shell chambers in posterior, lateral, and anterior views, respectively (text-fig. 14), nat. size; specimen RM, No. Mo 149985, Idavere, Estonia, Idavere stage, Middle Ordovician.

Lyecoceras gotlandense n. sp.

Figs. 4, 5. Two casts of domiciliary cavity of shell in anterior view, $\times\frac{4}{3}$; specimen RM, No. Mo 44442 and RM, No. Mo 149990, both from Mannagårda, Lye, Isle of Gotland, Hemse-Group, Silurian.

a, impression of ventral margin of annular elevation of shell; *if*, impressions of septal furrows; *p*, impression of dorsal margin of annular elevation; *s*, impression of angle between the youngest septum proper and its mural part; *si*, siphonal tube.

ventral

dorsal

1

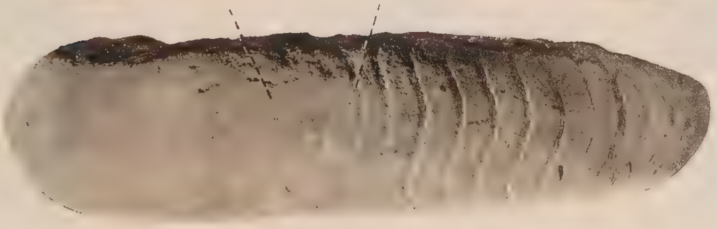

2

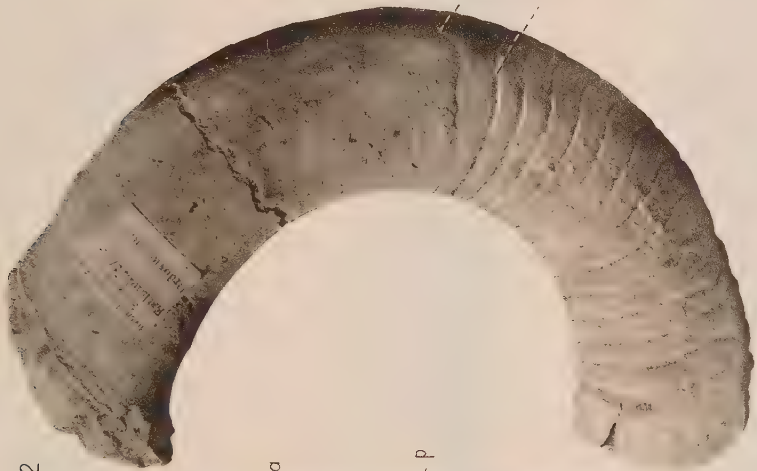

3

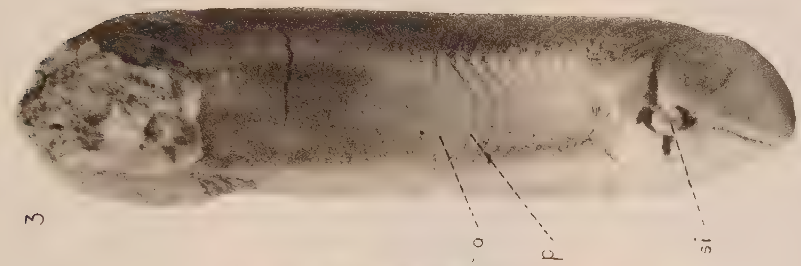

4

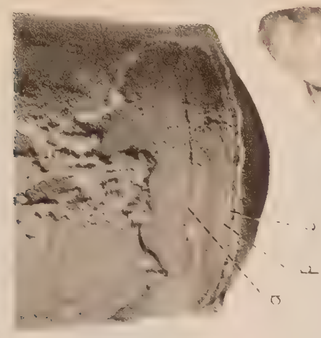

5

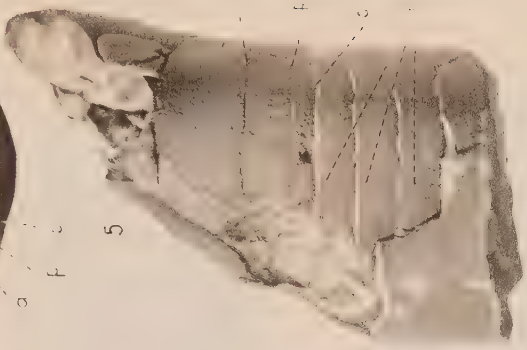

Plate 10

Lyecoceras gotlandense n. sp.

Figs. 1, 2, 3. Shell in anterior, lateral, and posterior views, respectively (text-fig. 16 A, B, C, G), × $\frac{4}{5}$; specimen RM, No. Mo 149991 (holotype), Mannagårda, Lye, Isle of Gotland, Hemse-Group, Silurian.

a, impression of ventral margin of annular elevation of shell; *p*, impression of dorsal margin of annular elevation; *s*, impression of angle between the youngest septum proper and its mural part; *t*, impression of tubercle of septal furrow of the youngest septum.

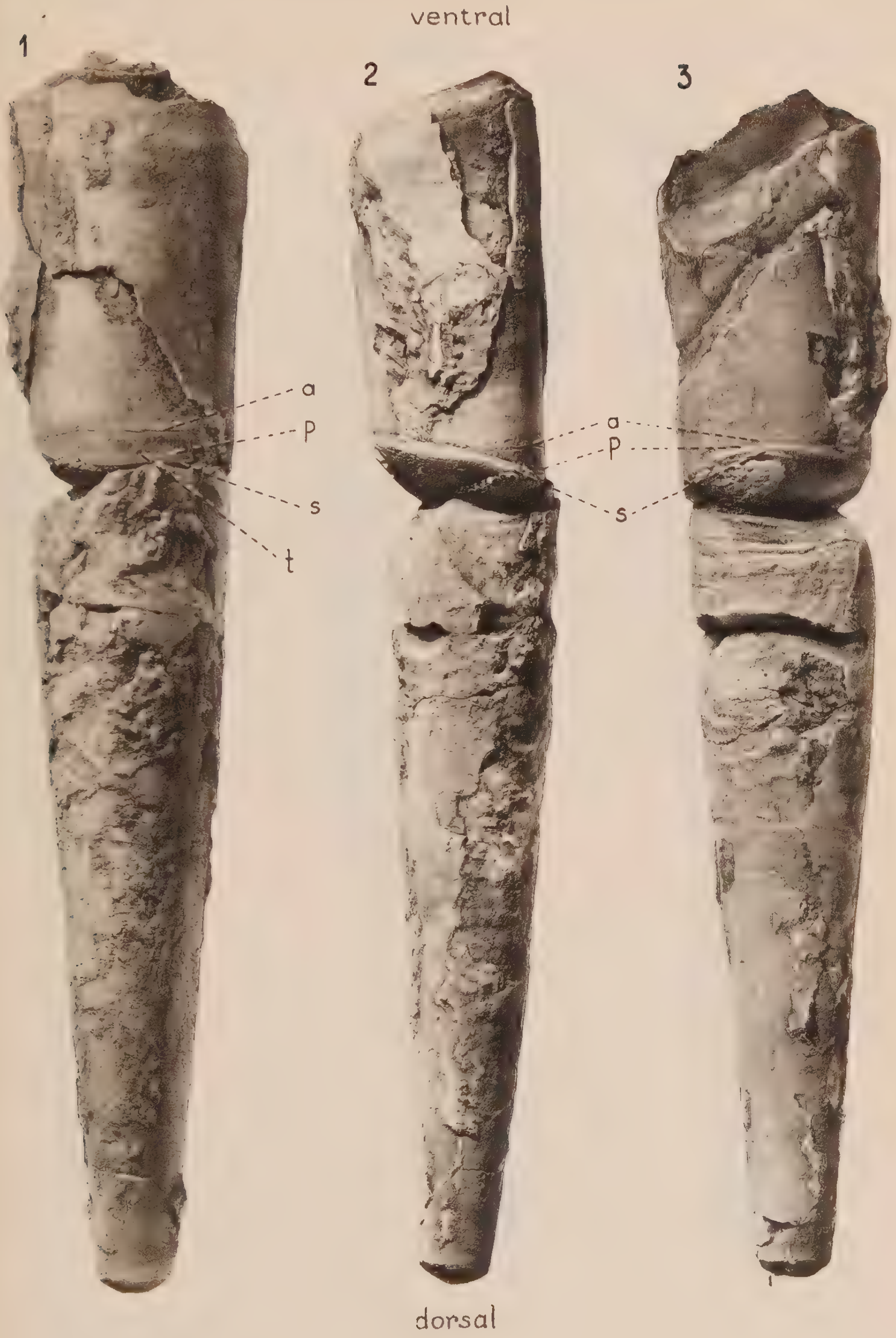
ventral
1
2
3
a
p
s
t
a
p
s
dorsal

Plate 11

Lyecoceras longistriatum n. sp.

Figs. 1, 2, 3. Shell in anterior, lateral, and posterior views, respectively, nat. size; specimen RM, No. Mo 149992 (holotype); Tänglings hällar, Etelhem, Isle of Gotland; Hemse-Group, Silurian.

a, impression of ventral margin of annular elevation of shell; *p*, impression of dorsal margin of annular elevation; *s*, impression of angle between the youngest septum proper and its mural part.

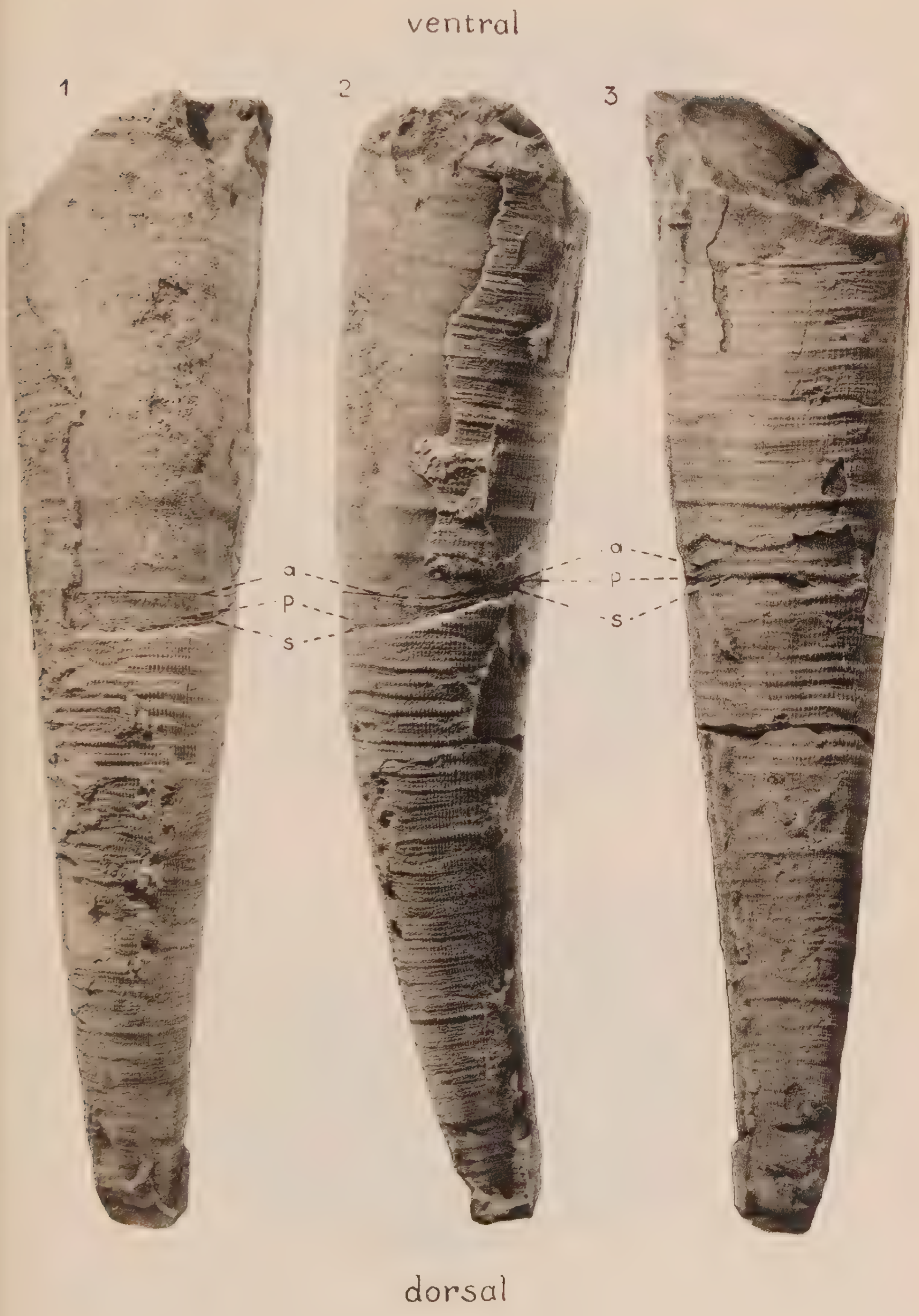
ventral
1
2
3
a
p
s
a
p
s
dorsal

Plate 12

Lyecoceras (?) sp.

Figs. 1, 2, 3. Cast of domiciliary cavity of shell in anterior, lateral, and posterior views, respectively (text-fig. 13), $\times \frac{6}{4}$; specimen RM, No. Mo 47702, Isle of Gotland, Silurian.

a, impression of ventral margin of annular elevation of shell; *if*, impressions of septal furrows; *p*, impression of dorsal margin of annular elevation; *s*, impression of angle between the youngest septum proper and its mural part.

1

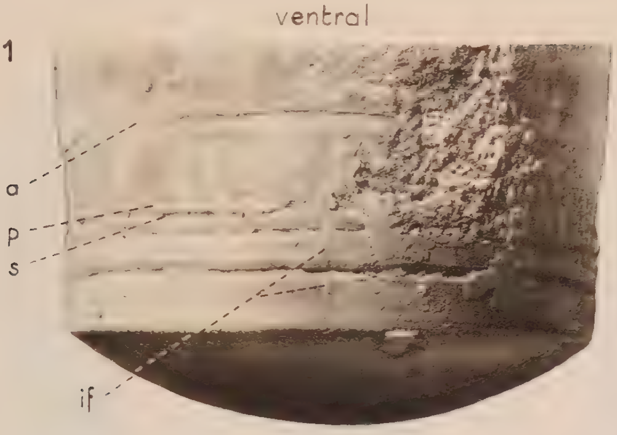

2

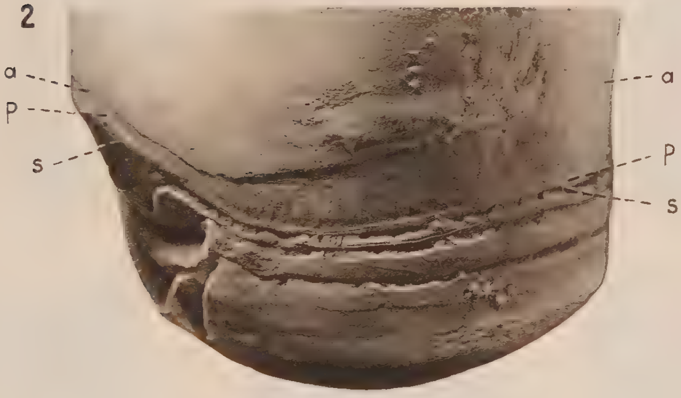

3

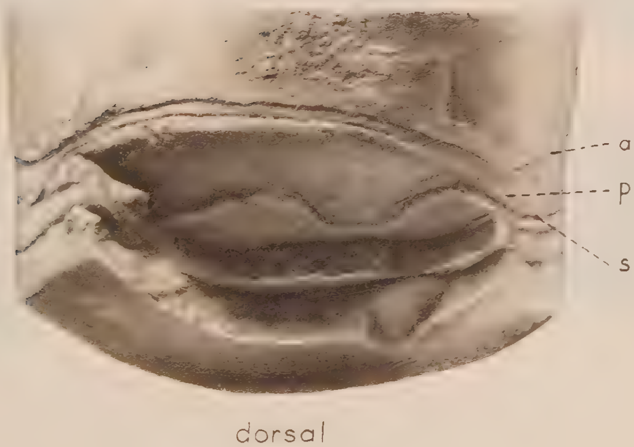

Plate 13

"*Geisonoceras*" *scabridum* (ANGELIN).

Figs. 1, 2, 3. Cast of domiciliary cavity of shell in anterior, lateral, and posterior views, respectively (text-fig. 15 A–D), nat. size; specimen RM, No. Mo 149986, Isle of Öland, Schroeteri limestone, Middle Ordovician.

Figs. 4, 5, 6. Details of same specimen, × 2.

Figs. 7, 8, 9. Cast of domiciliary cavity of shell in anterior, lateral, and posterior views, respectively, × 2; specimen RM, No. Mo 149987, Isle of Öland, Schroeteri limestone, Middle Ordovician.

a, impression of ventral margin of annular elevation of shell; *p*, impression of dorsal margin of annular elevation; *s*, impression of angle between the youngest septum proper and its mural part; *si*, siphonal tube; *t*, impression of tubercle of septal furrow of the youngest septum.

ventral

1

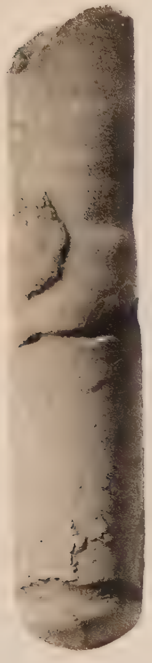

2

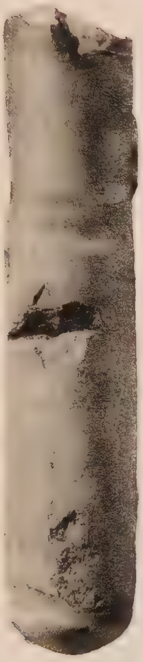

3

4

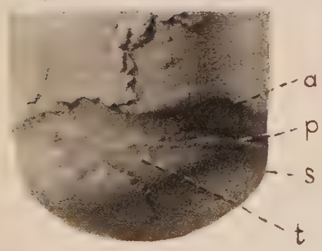

5

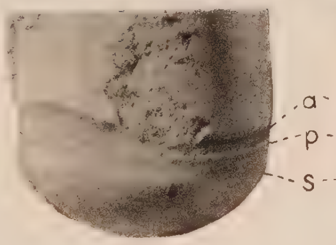

6

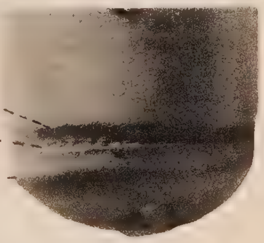

7

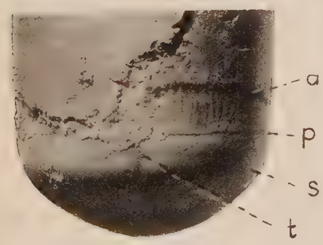

8

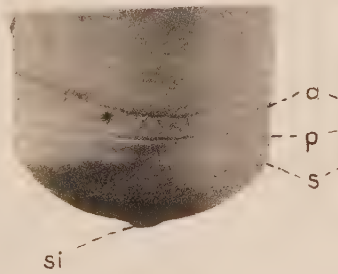

9

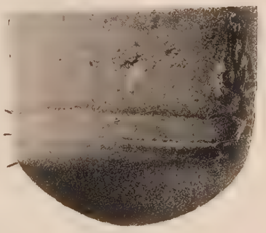

dorsal

Plate 14

Baltoceras burchardi (DEWITZ).

Figs. 1, 2, 3. Cast of domiciliary cavity of shell in anterior, lateral, and posterior views, respectively (text-fig. 16 D, E, F), nat. size; specimen RM, No. Mo 149999, Isle of Öland, Lower Ordovician.

Figs. 4, 5, 6. Details of same specimen, × 2.

"*Geisonoceras*" *scabridum* (ANGELIN).

Figs. 7, 8. Cast of domiciliary cavity of shell in anterior and lateral views, respectively (text-fig. 15 E), × 2; specimen RM, No. Mo 149988, Isle of Öland, Schroeteri limestone, Middle Ordovician.

Fig. 9. Cast of domiciliary cavity of shell in anterior view, × 2; specimen RM, No. Mo 149989, Isle of Öland, Schroeteri limestone, Middle Ordovician.

a, impression of ventral margin of annular elevation of shell; *p*, impression of dorsal margin of annular elevation; *s*, impression of angle between the youngest septum proper and its mural part; *t*, impression of tubercle of septal furrow of the youngest septum.

ventral

1

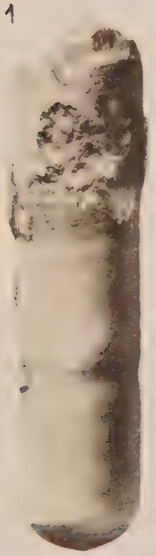

2

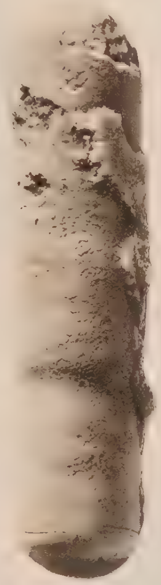

3

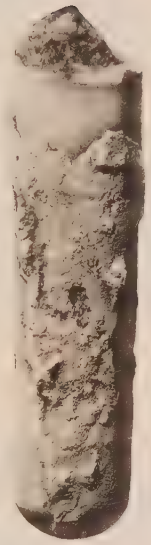

4

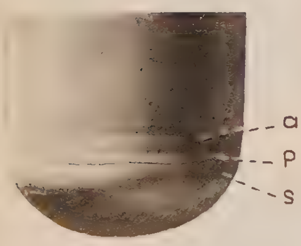

5

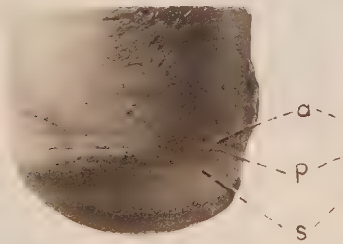

6

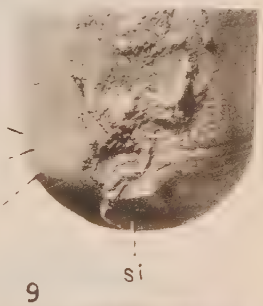

7

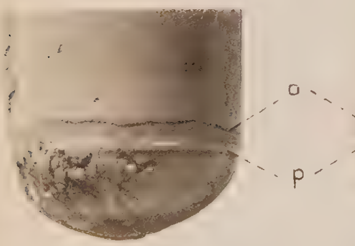

8

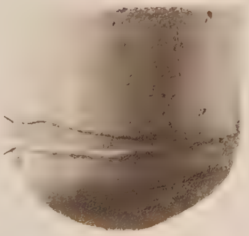

9

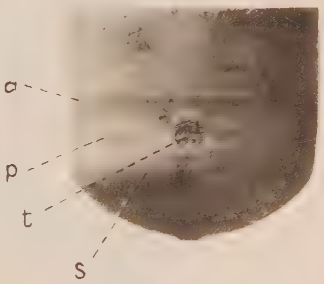

dorsal

Plate 15

"Orthoceras" angulatum WAHLENBERG.

Figs. 1, 2, 3. Cast of domiciliary cavity of shell in anterior, posterior, and lateral views, respectively (text-fig. 17), nat. size; specimen RM, No. Mo 149995, Isle of Gotland, Silurian.

Eutrephoceras bellerophon (LUNDGREN).

Figs. 4, 5, 6. Cast of domiciliary cavity of shell in posterior, anterior, and lateral views, respectively (text-fig. 18), nat. size; uncatalogued specimen, Paleontological Inst., Lund, Annetorp, Scania, Cretaceous.

a, impression of ventral margin of annular elevation of shell; *p*, impression of dorsal margin of annular elevation; *s*, impression of angle between the youngest septum proper and its mural part; *si*, siphonal tube; *t*, impression of tubercle of septal furrow of the youngest septum.

Plate 15

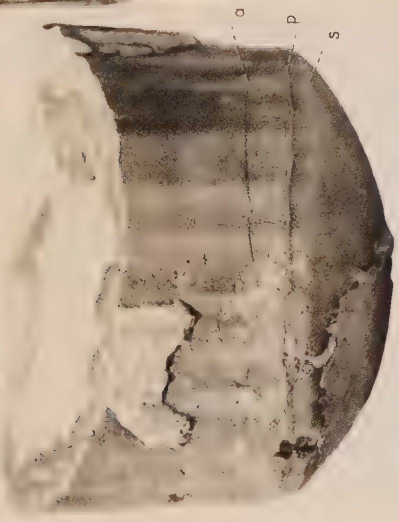

1

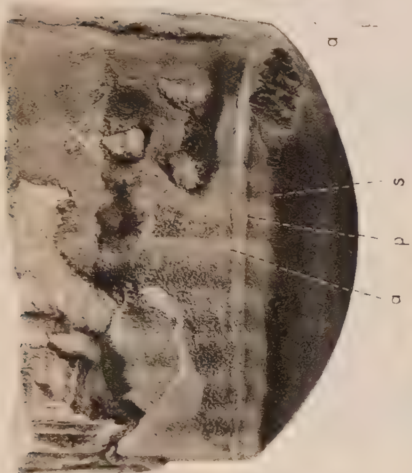

2

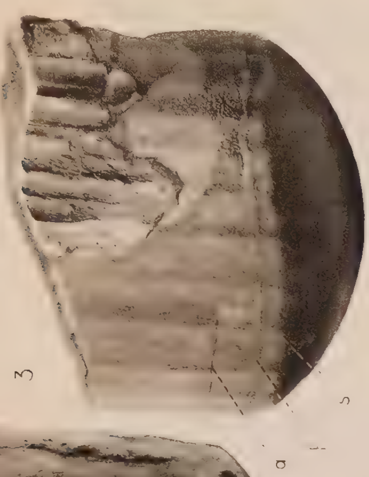

3

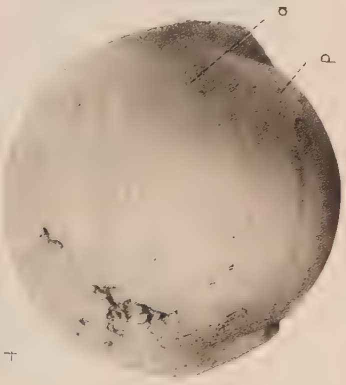

4

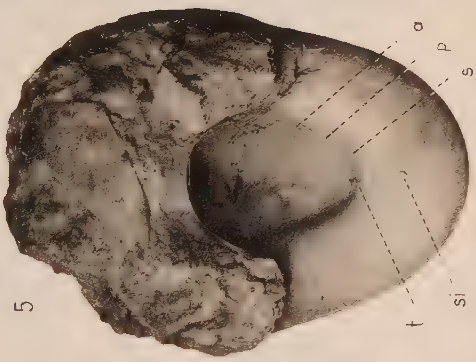

5

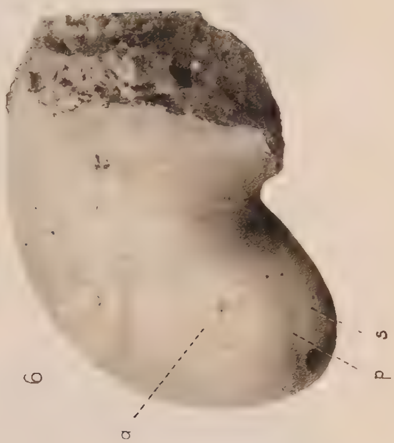

6

Plate 16

Apheleceras hibernicum (Foord & Crick).

Figs. 1, 2, 3. Cast of domiciliary cavity of shell in posterior, lateral and anterior views, respectively, nat. size; specimen No. C 7355, British Museum (Nat. Hist.), St. Doulaghs, Dublin, Ireland, Carbon.

Lyecoceras gotlandense n. sp.

Figs. 4, 6. Apical region of shell in posterior and lateral views, respectively, × 6; specimen RM, No. Mo 149993, Isle of Gotland, Hemse-Group, Silurian.

Fig. 5. Dorsal portion of septate division of shell in lateral view, nat. size; specimen RM, No. Mo 53015, Tänglings hällar, Etelhem, Isle of Gotland, Hemse-Group, Silurian.

a, impression of ventral margin of annular elevation of shell; *p*, impression of dorsal margin of annular elevation; *s*, impression of angle between the youngest septum proper and its mural part.

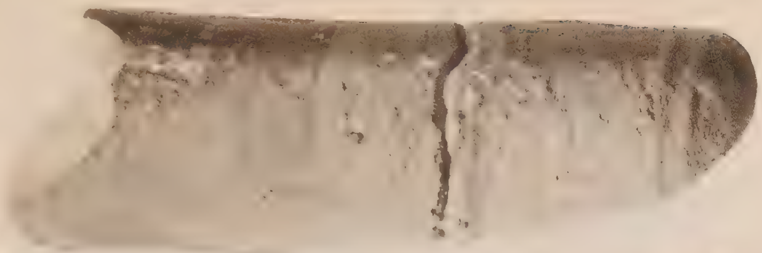
6

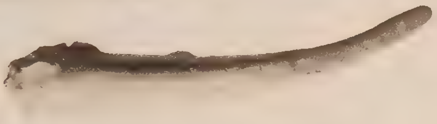
5

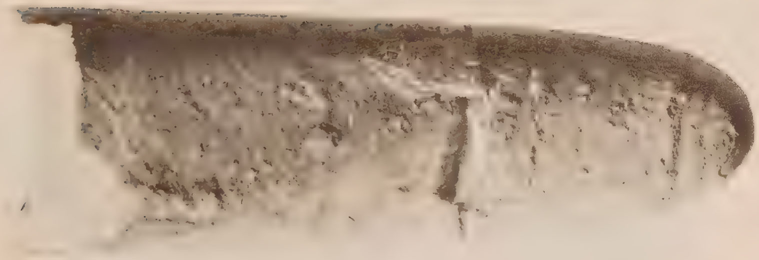
4

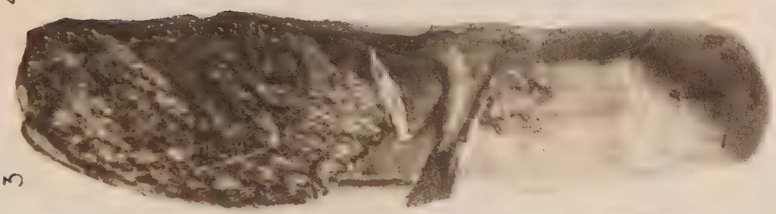
3

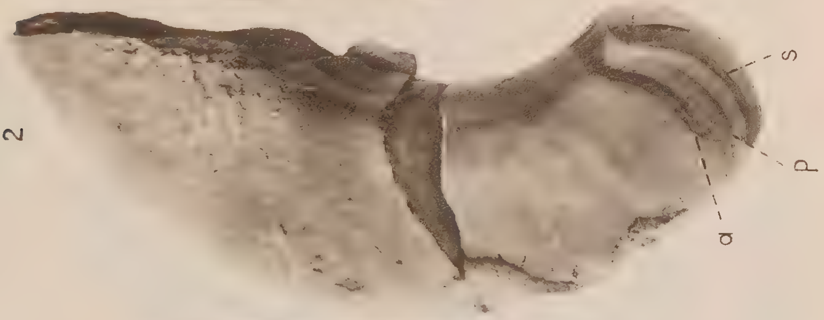
2

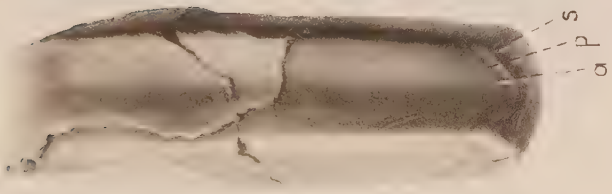
1

Plate 17

Uranoceras (?) *longitudinale* (ANGELIN).

Fig. 1. Median-sagittal section of ventral portion of septate division of shell, × $\frac{1}{6}$; specimen UPI, No. D 433, Kallholn, Dalecarlia, Boda Limestone.

Figs. 2, 3. Lectotype in anterior and lateral views, respectively, nat. size; specimen RM, No. Mo 149998 (pl. 18:1), Osmundsberget, Dalecarlia, Boda Limestone.

dis, distal division of siphonal funnel; *pro*, proximal division of siphonal funnel.

1

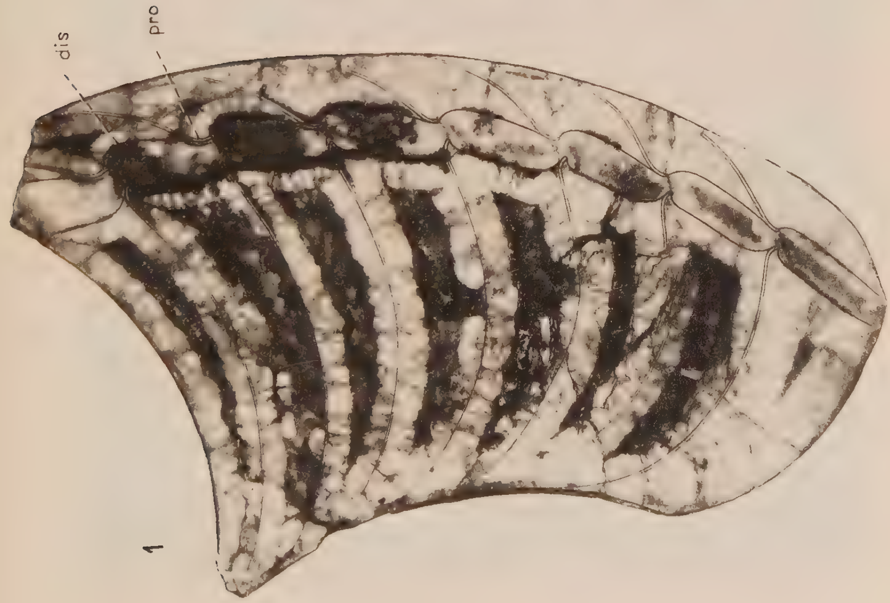

2

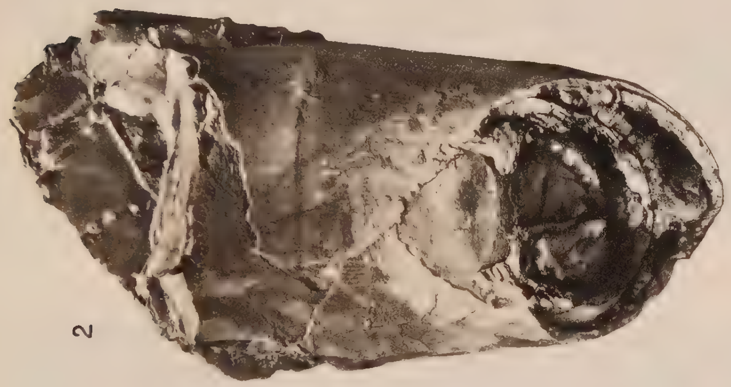

3

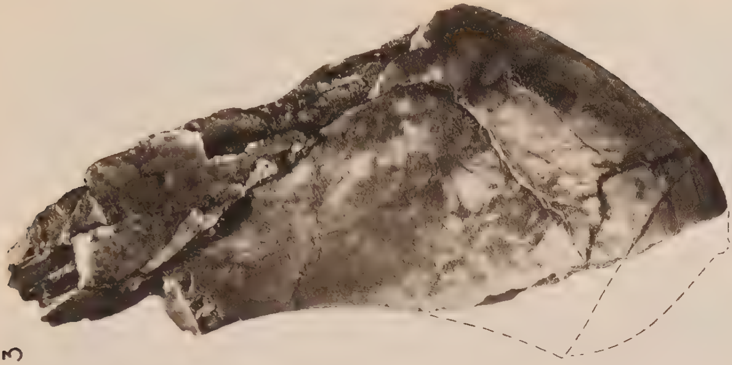

Plate 18

Uranoceras (?) *longitudinale* (Angelin).

Details of ornamentation of external shell surface, × 6.
Fig. 1. Same specimen as in pl. 17:2, 3.
Fig. 2. Same specimen as in pl. 6.

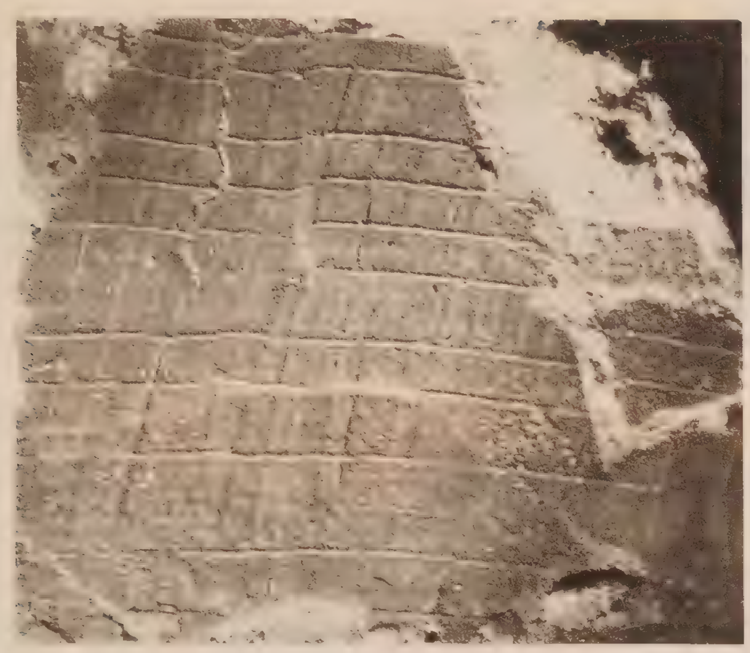

2

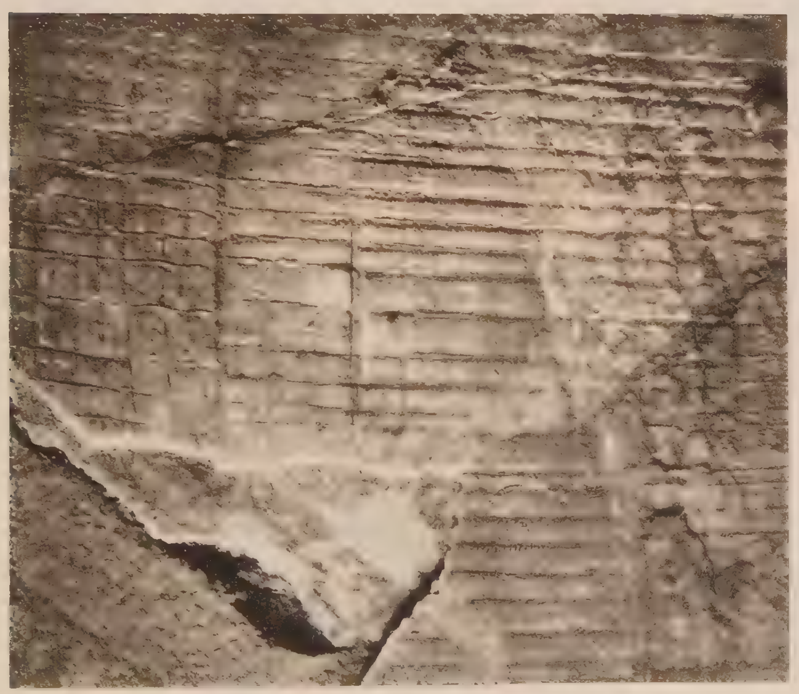

1

Plate 19

Lyecoceras longistriatum n. sp.

Figs. 1, 3. Details of ornamentation on external and internal surfaces of domiciliary division of shell, × 6; same specimen as in pl. 11.

Lyecoceras gotlandense n. sp.

Fig. 2. Details of ornamentation of external surface of shell, × 6; specimen RM, No. 51737, Sandarve kulle, Isle of Gotland, Hemse-Group, Silurian.

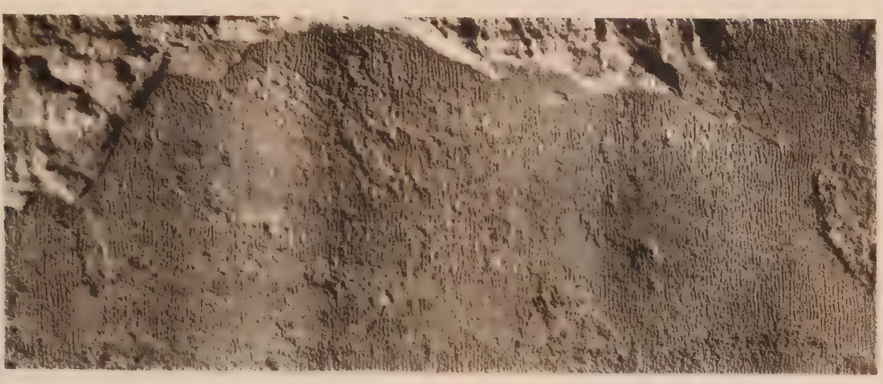

3

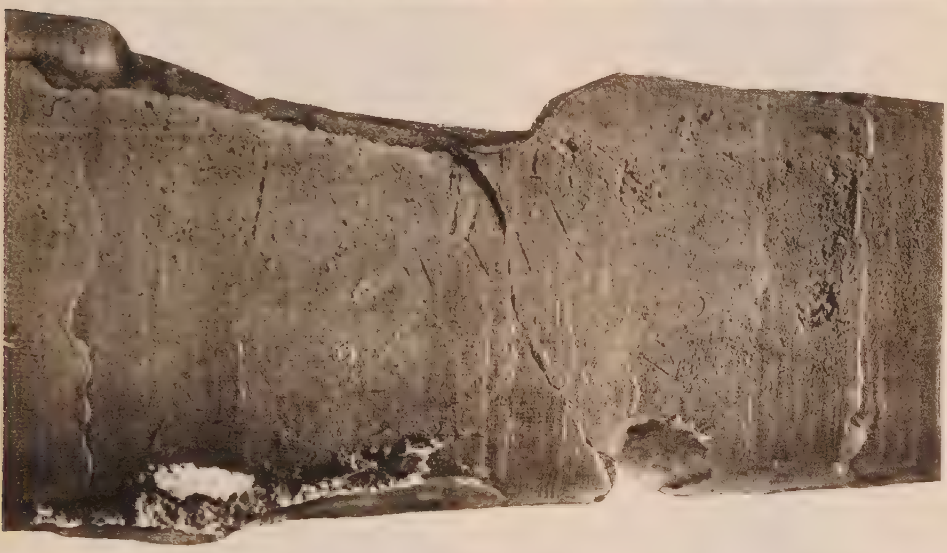

2

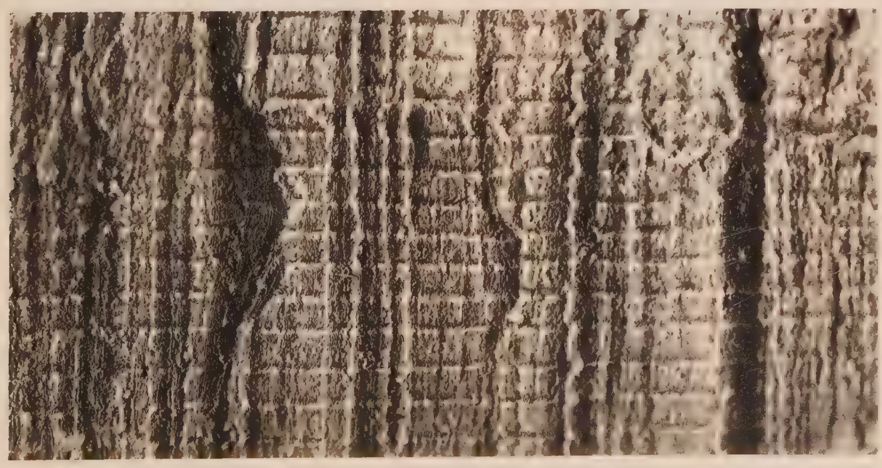

1

Plate 20

Lyecoceras gotlandense n. sp.

Median-sagittal section of septate division of shell.

Fig. 1. Specimen RM, No. Mo 149994, × 2, Tänglings hällar, Etelhem, Isle of Gotland.

Fig. 2. Specimen RM, No. Mo 51535, × 5, Sandarve kulle, Isle of Gotland; both specimens are from Hemse-Group, Silurian.

1

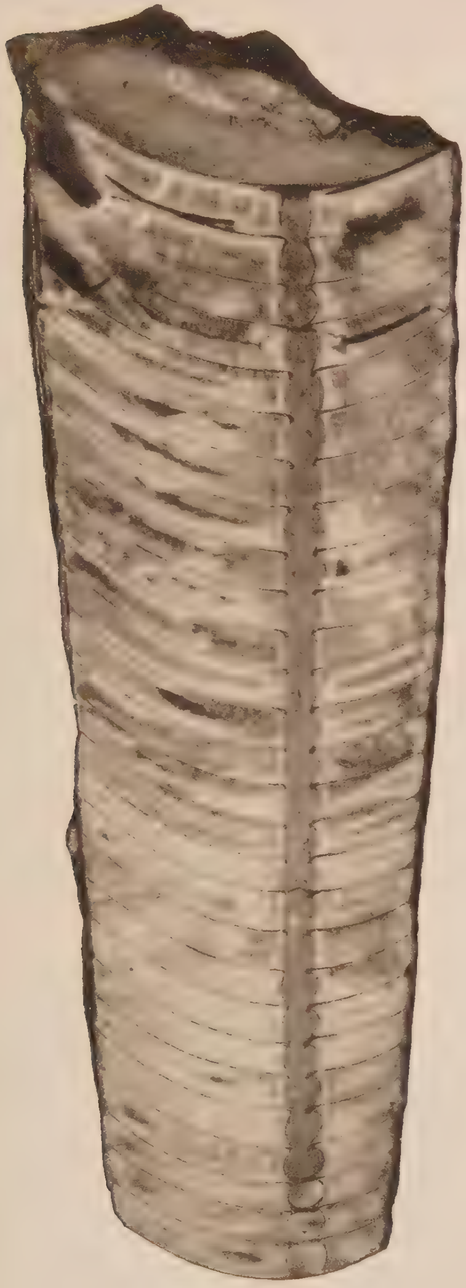

2

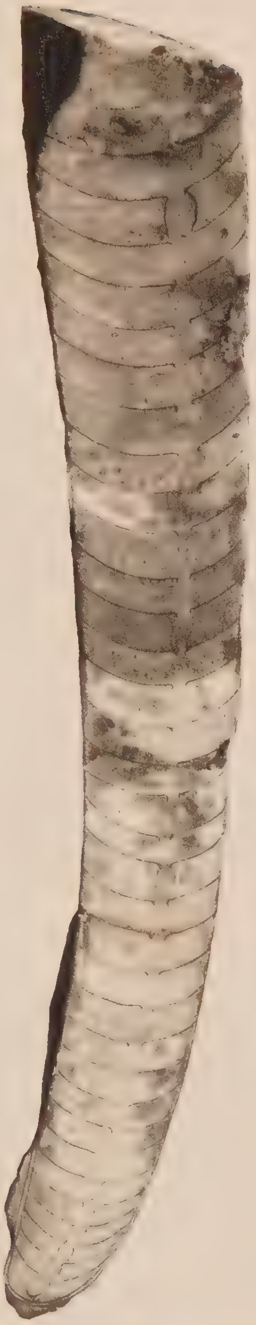

ARKIV FÖR MINERALOGI OCH GEOLOGI Band 2 nr 11

Communicated 25 April 1956 by PERCY QUENSEL and FRANS E. WICKMAN

Optical and physical properties of knebelite

By ÅKE HENRIQUES

With 8 figures in the text

Historical notes

Knebelite was named after its discoverer Major von Knebel and was found as early as 1818. It has not been possible to state the original locality of the mineral but according to Suckow (1855) it seems very likely that it could be located in a granite massive in the surroundings of Ilmenau. The description of the mineral given by Döbereiner (1818) does not, however, correspond altogether with the characteristics that are attributed to the minerals now known as knebelites. For example, cleavage is not pointed out in the original description of the mineral, in spite of the knebelite having marked cleavages in several directions. It is therefore not altogether certain that the mineral from Ilmenau is identical with the minerals now described as knebelites (Hintze, 1897).

In Sweden knebelite was found for the first time in the Dannemora mines. The mineral was described by Erdman (1851), and later Weibull (1882) has given a detailed description of the Dannemora knebelite. A more iron-rich knebelite was found in Vester-Silfberg, which Weibull (1883) gave the name igelströmit. However, when the identity of igelströmit was established Weibull changed the name to ironknebelite (1884a). In the mines at Hilläng, too, knebelite was found fairly early by Weibull (1884b). In the course of time knebelite has been found in a great number of manganese-rich iron ore deposits of Central Sweden.

Introduction

Knebelite forms an isomorphous series with fayalite Fe_2SiO_4 and tephroite Mn_2SiO_4, which also contains a varying quantity of forsterite Mg_2SiO_4. Whilst the isomorphous series fayalite–forsterite has earlier been the subject of exhaustive surveys, principally by Backlund (1909) and Bowen & Schairer (1935), interest in the optical and chemical characteristics of the knebelite has been comparatively small. However, Magnusson (1918) has given an important contribution towards the knowledge of the chemical and optical characteristics of the mineral group. Since the material on which Magnusson's examination was founded was not very comprehensive, it seems now, nearly 40 years later, advisable to deal with this mineral group again. As far as the Swedish manganese-rich iron ores are concerned, by far the greatest part of the manganese content of the iron ore seems to enter into a part of the silicate and carbonate minerals. The former consist mainly of knebelite, dannemorite and garnet. In connection with modern methods of enrichment it has been found necessary to be able to state in what or which minerals the main part of manganese is found, in order to utilize it conveniently. The principal purpose of this investigation has been to make it possible to make a quick estimation of the concentration of manganese in the knebelite minerals. Subsquent papers will describe the other manganese minerals and report an investigation of the distribution of manganese in a few mines in the centre of Sweden.

Investigation and treatment of the material

The material for this investigation has mainly been chosen from the collections of the Institute of Technology in Stockholm. Preliminary investigations soon showed that the knebelite minerals as a rule were not built up homogeneously. Careful control of the specimens was therefore necessary. This has been done in the following manner. From the specimen a cube with a side of 3 cm has been cut out. At the same time three thin sections have been made from parts orientated parallel to different surfaces of the cube. From each of these thin sections at least 2 determinations of the optical angle of knebelite have been carried out. If these did not fall within the limits of error the samples were discarded. If, however, the samples were homogeneously built up (same optical angles) the cube was crushed and the material sieved. The grain class + 100 mesh (Tyler standard) were chosen for all tests (chemical analyses, optical determinations etc.). The sieved material was then purified, first with an ordinary hand magnet, so that magnetite and grains rich in magnetite were extracted. Thereafter a separation with heavy liquids in a specially constructed separation funnel with double chambers was carried out. For a heavy liquid Clerici solution was used. Finally half grains and greatly altered knebelite grains were removed. Attempts to use an isodynamical magnetic separator failed, as almost all the grains (knebelite and impurities) were found to contain magnetite interpositions.

The homogeneity of the knebelite minerals

As mentioned previously, knebelite—like most skarn minerals—is often of a greatly varying chemical composition. This is also the case locally within the same deposit and especially for the more finely grained types, which are found together with magnetite and carbonates. The knebelite minerals that are usually formed in broad-stemmed aggregates, however, are chemically more similar in character. As an example of the heterogeneity of the knebelite minerals, for one thing within the same deposit and for another thing within one and the same specimen, optical angle determinations on specimens from Ställbergs mines are given in Fig. 1. From the variation of the optical angle it will be clear that the chemical composition varies considerably (see below).

Nomenclature

Besides the name knebelite other mineral names have been used in order to point out divergencies from the more normal composition. The iron-rich knebelites have alternatively been called igelströmit, ironknebelite (Weibull, 1883 and 1884) and

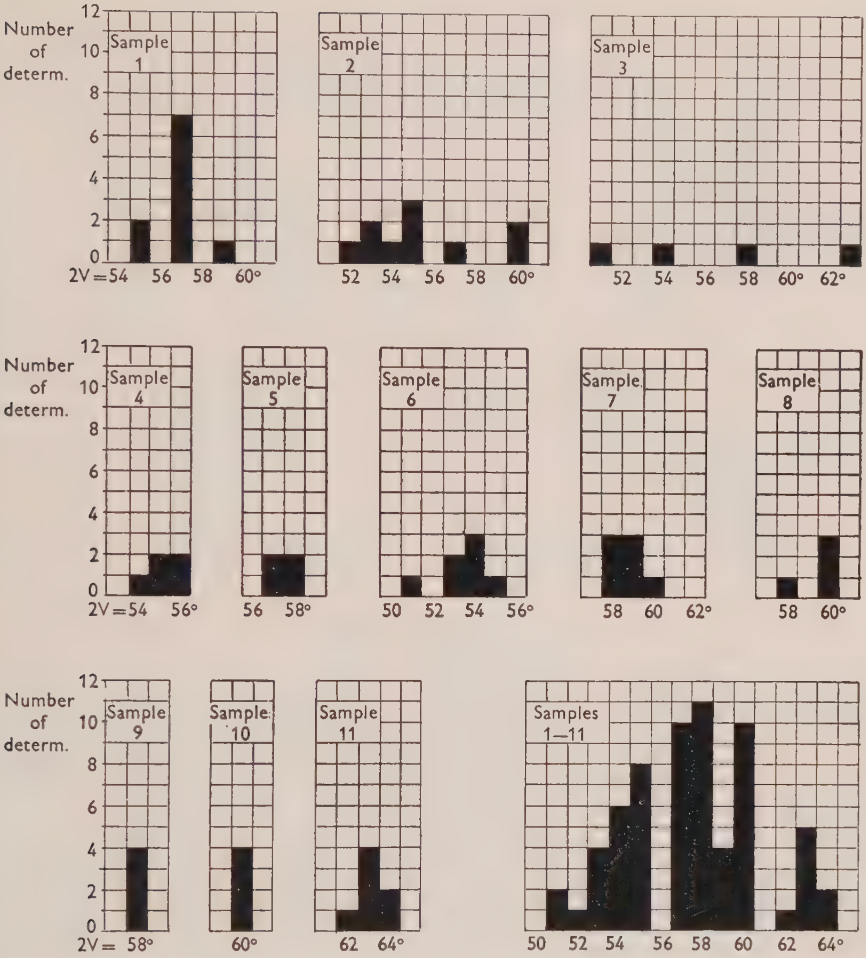

Fig. 1. Optical angle determinations carried out on material from the Ställberg mines.

manganfayalite. The knebelites rich in magnesium have been called talkknebelite (Igelström, 1890). However, no recognised nomenclature was used until Yosimura (1939) divided the fayalite–tephroite series into the following groups (see Table 1).

If the ten knebelites now analysed are put into this scheme, the knebelites from Bastkärn would be called manganfayalites, those from Smedjebacken and Skinnarängs mine ironknebelites and the rest knebelites. From several points of view, however, it seems convenient to reduce the number of variants in Yosimura's classification, and consequently the seven types can be conveniently reduced to five (see Table 2).

According to this classification the knebelites from Bastkärn should be grouped under ironknebelites, while the rest would belong to the knebelite class.

Table 1.

Mineral	Fe_2SiO_4, mol-%
Fayalite	100–95
Manganfayalite	95–80
Ironknebelite	80–60
Knebelite	60–40
Manganknebelite	40–20
Irontephroite	20– 5
Tephroite	5– 0

Table 2.

Mineral	Fe_2SiO_4, mol-%
Fayalite	100–90
Ironknebelite	90–70
Knebelite	70–30
Manganknebelite	30–10
Tephroite	10– 0

Chemical properties

The chemical composition of the analysed knebelite minerals is shown in Table 3. In addition to FeO, MnO, MgO and SiO_2 there are minor amounts of Fe_2O_3, Al_2O_3, CaO, K_2O, Na_2O, H_2O and CO_2 in the knebelites. A microscopical examination of the analysed material shows that the mineral grains are not completely homogeneous but often have several interpositions and that they are frequently altered. The interpositions as well as the alteration products can in many cases be easily identified; in other cases, however, it is impossible to determine them. Trivalent iron will mainly be found in the analysis material in the form of magnetite; a minor part can be found in different secondary minerals, as xylotile etc. In connection with the preparation of the material for the chemical analyses some of the divalent iron may have been oxidised. Aluminium may possibly be a structural constituent of the knebelite and substitute silicon. However, there is no proof of this, and earlier examinations have shown nothing to prove clearly that such a substitution can take place within the olivine group. The observed aluminium content will therefore be found completely or to a large extent, similar to H_2O, in different alteration products, such as antigorite, bowlingite, xylotile, etc. Calcium has been found in all samples, in amounts varying from 0.02 % to 0.80 %. Although no direct connection has been observed between the contents of calcium and CO_2 it nevertheless seems likely that calcium is mainly found in combination with carbonates, and also in the form of various alteration products. Yosimura (1939), for example has certainly established that considerable quantities of calcium (max. 4.5 mol- % Ca_2SiO_4) are contained in the knebelite minerals, but in all these cases the calcium content will possibly be entirely derived from admixtures in the analysed material, mainly in the form of carbonates. Concerning the observed alkali contents, these are of such minute quantities that their presence does not need to be further discussed.

Table 3. (Analyst A. Aaremäe.)

	Bastkärn 1	Bastkärn 2	Haggruvan	Smedjebacken	Skinnarängsgruvan	V. Silvberg	Hilläng	Tuna Hästberg	Dannemora 1	Dannemora 2
SiO_2	28.24	29.14	31.58	29.99	29.40	30.80	30.07	29.28	28.70	28.90
Al_2O_3	0.92	0.92	0.97	0.88	0.58	0.58	0.86	0.78	0.48	0.28
Fe_2O_3	0.87	1.20	0.69	0.78	0.72	0.66	1.73	0.67	2.02	1.73
FeO	60.65	56.90	38.58	47.87	44.92	41.45	39.49	38.28	36.90	31.87
MnO	5.75	9.74	14.62	17.25	19.59	21.40	23.53	27.88	29.85	34.63
MgO	2.32	1.12	12.46	1.82	3.89	4.51	2.68	2.14	0.97	1.42
CaO	0.29	0.34	0.24	0.56	0.07	0.02	0.80	0.26	0.09	0.18
$Na_2O + K_2O$					0.04					0.02
H_2O^+					0.59		0.58		0.80	0.83
H_2O^-					0.06		0.07		0.05	0.07
CO_2					0.16		0.15		0.08	0.05
Total	99.04	99.36	99.14	99.15	100.02	99.42	99.96	99.29	99.94	99.98

Table 4. Recalculated analyses, molecular proportions and molecular per cent.

	Bastkärn 1	Bastkärn 2	Haggruvan	Smedjebacken	Skinnarängsgruvan	V. Silvberg	Hilläng	Tuna Hästberg	Dannemora 1	Dannemora 2
$_2$ . . .	29.24	30.24	32.58	31.05	30.16	31.48	31.66	30.10	30.05	30.09
O . . .	62.40	58.49	39.49	49.21	45.75	42.05	40.75	39.04	37.68	32.37
O . . .	5.96	10.11	15.08	17.86	20.10	21.87	24.77	28.66	31.25	36.06
O . . .	2.40	1.16	12.85	1.88	3.99	4.60	2.82	2.20	1.02	1.48
					Molecular proportions					
$_2$ . . .	1.00	1.00	1.00	1.00	1.00	1.00	1.00	1.00	1.00	1.00
O . . .	0.89	0.81	0.51	0.66	0.64	0.56	0.54	0.55	0.52	0.45
O . . .	0.09 } 1.04	0.14 } 0.98	0.20 } 1.00	0.24 } 0.95	0.28 } 1.02	0.29 } 0.96	0.33 } 0.94	0.40 } 1.00	0.44 } 0.99	0.50 } 0.99
O . . .	0.06	0.03	0.29	0.05	0.10	0.11	0.07	0.05	0.03	0.04
					Molecular per cent					
SiO_4	85.82	82.61	50.84	69.65	62.48	58.07	57.50	54.22	52.95	45.26
$_2SiO_4$	8.30	14.46	19.67	25.60	27.80	30.60	35.40	40.33	44.49	51.06
$_2SiO_4$	5.89	2.92	29.49	4.74	9.72	11.33	7.10	5.45	2.56	3.68
SiO_4	91.18	85.10	72.10	73.12	69.21	65.49	61.89	57.35	54.34	46.99
$_2SiO_4$	8.92	14.90	27.90	26.88	30.79	34.51	38.11	42.65	45.66	53.01

The author consequently thinks that the constituents found in the analyses, with exception of the FeO, MnO, MgO and SiO_2, appear in the form of different impurities. In Table 4, therefore, a recalculation of the analyses has been carried out with consideration to this fact. (Small quantities of FeO, MnO, MgO and SiO_2 are also present in the impurities, but these have not been calculated with the exception of the amount of FeO present in the magnetite.)

Crystallography

Knebelite occurs mainly in grains of about 0.1–2 mm, which usually have no crystal borders. These grains occur in close correlation primarily with magnetite, carbonates and different silicates in manganese-rich iron ores. Knebelite is also found in broad-stemmed aggregates, consisting of individual crystals extending along the *c*-axis; sometimes the forms {110} and {001} and even {010} can be observed on these crystals.

Cleavages

The examined knebelite minerals all show well developed cleavage. As a rule these have been easily established with the help of the Universal Stage but in some cases an intensive fissuring has made this difficult or impossible. The cleavages have low indices, as in other minerals of the olivine-norbergite group. No connection has been observed between the indices, development and frequencies of the cleavages and chemical composition. Four different directions of cleavage can be observed; of these two, {010} and {001}, are perfect, one, {110}, distinct and one, {100}, which is probably due to parting, is imperfect. For comparison the cleavage directions stated in the literature are shown in Table 5.

Table 5.

	Cleavages		Remarks
	Excellent–perfect	Distinct–imperfect	
Analyses 1–10	{010} & {001}	{110} & {100}	
Dannemora (Weibull)	{110} & {010}	{100} & {001}	
W. Silvberg (Weibull)	{110}	{100} & {001}	ironknebelite
Kaso mine (Yosimura)	{010} & {001}	{100}	
Kaso mine (Yosimura)	{110}	{001} & {100}	ironknebelite
Bluebell mine (Gunning)	{110}	{001} ?	

Specific gravity

The specific gravity of the knebelite has been calculated and determined (Table 6). The calculated values are based upon the size of the cell volume and the chemical composition of the mineral on the basis that knebelite is an iron-manganese-magnesium-silicate $(Mn,Fe,Mg)_2SiO_4$. In six cases the specific gravity has been determined by a quartz pycnometer with ground-in thermometer and side capillary. The tests have been carried out at 20°C. The pycnometer-determined values show the specific gravity of the material; consequently in these cases interpositions and different alteration products will affect the values. Therefore a direct comparison between the calculated and the determined values is impossible. Further, it seems impossible to correct the pycnometer-determined values in a satisfactory way through a calculation of the actual mineralogical composition of the analysed material.

Table 6.

	Cell volume Å³	Calculated molecular weight	Specific gravity		Difference
			calculated	determined	
Bastkärn 1	309.17	199.9	4.294	4.245	0.049
Bastkärn 2	310.71	201.7	4.310		
Haggruvan	307.17	184.8	3.995		
Skinnarängsgruvan . .	311.79	197.2	4.199	4.166	0.033
V. Silvberg	312.14	196.1	4.170	4.159	0.011
Hilläng	313.54	198.7	4.208		
Tuna Hästberg	314.59	199.6	4.213	4.180	0.033
Dannemora 1	316.29	201.4	4.227	4.219	0.008
Dannemora 2	317.11	200.5	4.199	4.183	0.016

Colour

The colour of the knebelite is brown-black to grey-black, sometimes having a tendency towards black-green. The colour of the mineral has been observed on the uncrushed as well as on the material crushed to a 100 mesh. It has not been possible to show any connection between colour and chemical composition. Definite brown colour nuances were seen in Bastkärn 2 and V. Silvberg, in spite of considerable chemical differences. The colour of the mineral will therefore be determined to a great extent by the colours of the alteration products and the interpositions. The finely crushed mineral powder is of an ash-grey colour, at times tending towards brown.

Pleochroism and absorption

The knebelite minerals are weakly pleochroic. The pleochroism is directly proportional to the iron content and inversely proportional to the content of manganese and magnesium. Thus the knebelites from Bastkärn are clearly pleochroic while those from Dannemora are slightly pleochroic. In the latter case no change of colours can be observed if the position of the section is changed when thin sections of standard thickness (about 0.025 mm) are used. A microscopic determination of colours as a rule gives a strongly subjective result. This is particularly the case when determinations are made of faint colour intensities. Therefore, in Table 7 below, observations carried out by Weibull on the material from Dannemora have also been entered. The absorption is weak with $X > Y > Z$.

Table 7.

	X	Y	Z	Thickness of section, in mm
Dannemora (Weibull) . . .	Light grey with tendency towards yellow	light yellow-grey	greyish-white	?
Dannemora 2 .	very pale yellow-brown	very pale yellow-brown	colourless	0.1
Dannemora 2 .	colourless	colourless	colourless	0.025
Bastkärn 1 . . .	pale yellow-brown	pale yellow-brown	colourless	0.1
Bastkärn 1 . . .	very pale yellow-brown	very pale yellow-brown	colourless	0.025

Indices of refraction

The indices γ and β have been determined by the immersion method, whilst the index α has been calculated. Thanks to the cleavage of the mineral along $\{010\}$, several cleavage flakes were available from which γ and β were determined. In some cases however β was determined from grains so orientated that the emergent of one optical axis was parallel with the axis of the microscope. Standardized liquids varying by intervals of about 0.005 have been used. When the approx. index of refraction was determined, the liquids were mixed directly on the slide, a small sample was taken out and the index of refraction of the liquid was estimated with a Leitz-Jelly microrefractometer. A calculation of the determination errors—measuring and orientation errors—can scarcely be determined with regard to the spread of the refraction that is caused by the heterogeneity of the grains. However, the errors of the refraction determinations were approximately estimated to max. ∓ 0.002. In the determinations sodium-light was used at a temperature of 20°C.

Table 8. Indices of refraction, birefringences and optic axial angle of knebelite.

	1	2	3	4	5	6	7	8	9	1
	Bast-kärn 1	Bast-kärn 2	Hag-gruvan	Smedje-backen	Skinnar-ängsgru-van	V. Silv-berg	Hilläng	Tuna Hästberg	Danne-mora 1	Dan mor
α calc.	1.802	1.803	1.750	1.792	1.785	1.777	1.782	1.782	1.784	1.7
β	1.843	1.843	1.784	1.833	1.824	1.818	1.822	1.822	1.823	1.8
γ	1.853	1.851	1.796	1.842	1.834	1.828	1.831	1.830	1.830	1.8
$\gamma-\alpha$ calc. ...	0.051	0.048	0.046	0.050	0.049	0.051	0.049	0.048	0.046	0.0
$\gamma-\beta$	0.010	0.008	0.012	0.009	0.010	0.010	0.009	0.008	0.007	0.0
$\beta-\alpha$ calc....	0.041	0.040	0.034	0.041	0.039	0.041	0.040	0.040	0.039	0.0
$2V_\gamma$	50°7 ∓ .4	48°1 ∓ .5	61°2 ∓ .9	48°5 ∓ .3	51°5 ∓ .5	52°1 ∓ .5	49°6 ∓ .3	47°6 ∓ .3	45°6 ∓ .4	47°4

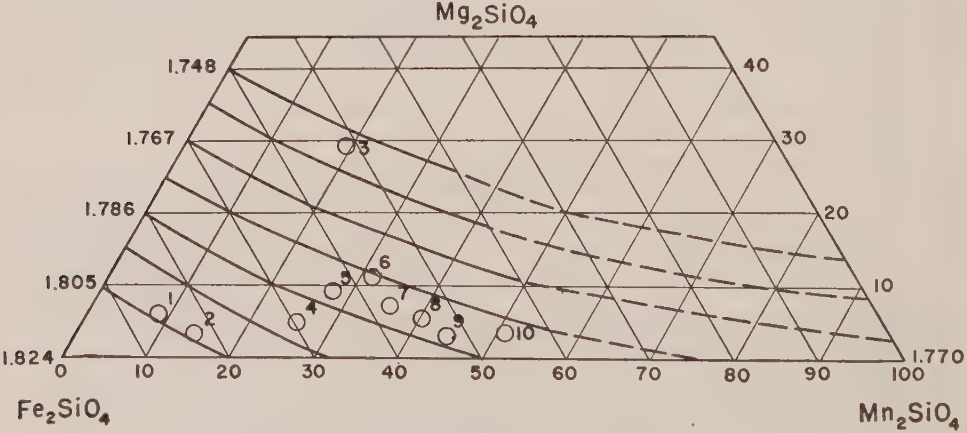

Fig. 2. Refractive indices of knebelite, α.

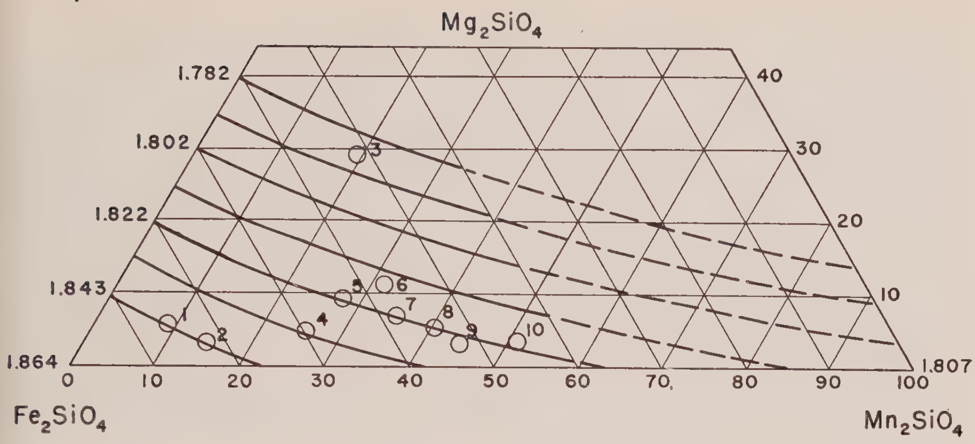

Fig. 3. Refractive indices of knebelite, β.

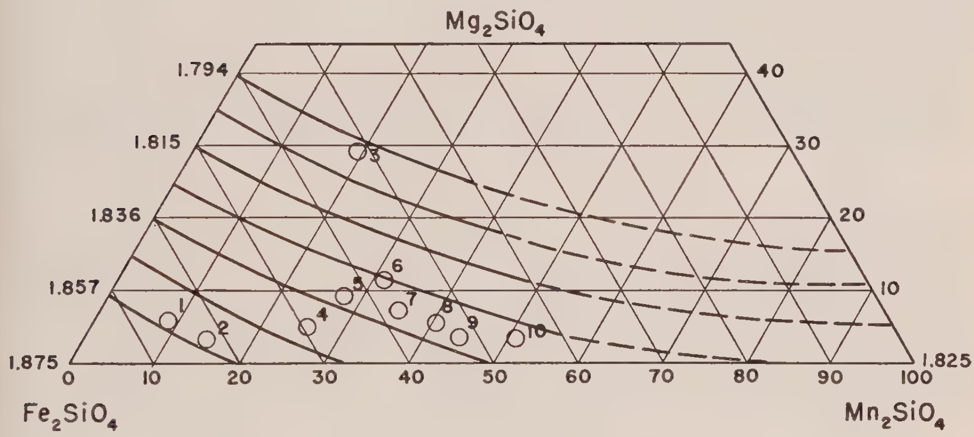

Fig. 4. Refractive indices of knebelite, γ.

The indices of refraction are found in Table 8 and Fig. 2, 3 and 4. The different values of the refraction have been marked off by circles, the radii of which correspond to the estimated errors in determination. It can be seen from the figures that the refraction of the knebelite is a function of its chemical composition. The refraction increases with an increased iron content, whilst increased contents of manganese and magnesium decrease the refraction. The three curves for γ, β and α do not run parallel: this is reflected in the changes of the optical angles, especially within the limits 45–55 mol-% Fe_2SiO_4 (see below).

Birefringence

The birefringence of the knebelites $\gamma - \beta$ have been measured whilst $\gamma - \alpha$ and $\beta - \alpha$ have been calculated. All these values are found in Table 8. The determinations have been carried out with the Universal Stage according to the method described by Berek (1924) and improved by Hess (1948). According to this method, the mineral powder is mixed with quartz and plastic powder, after which a thin section as far as possible plane parallel is made, after the material has been compressed in a bakelite press (150°C and 4000 lbs./sq. in.). The thickness of the thin section is estimated within the limits used by determination of the optical orientation of the quartz grains, and their retardation. By orientating the knebelite grains in desired positions the birefringence can easily be determined, by means of the Berek compensator, by measurement of the retardation.

Table 8 illustrates that the maximal birefringence $\gamma - \alpha$ varies within the limits 0.046 and 0.051. With regard to errors the determinations, which have been estimated to about ∓ 0.002, it is not possible to observe a clear connection between the maximal birefringence and the chemical composition.

Optic axial angle

The optical angle $2\,V_\gamma$ has been determined with the Universal Stage. For the determinations those mineral grains have been chosen which have been orientated in

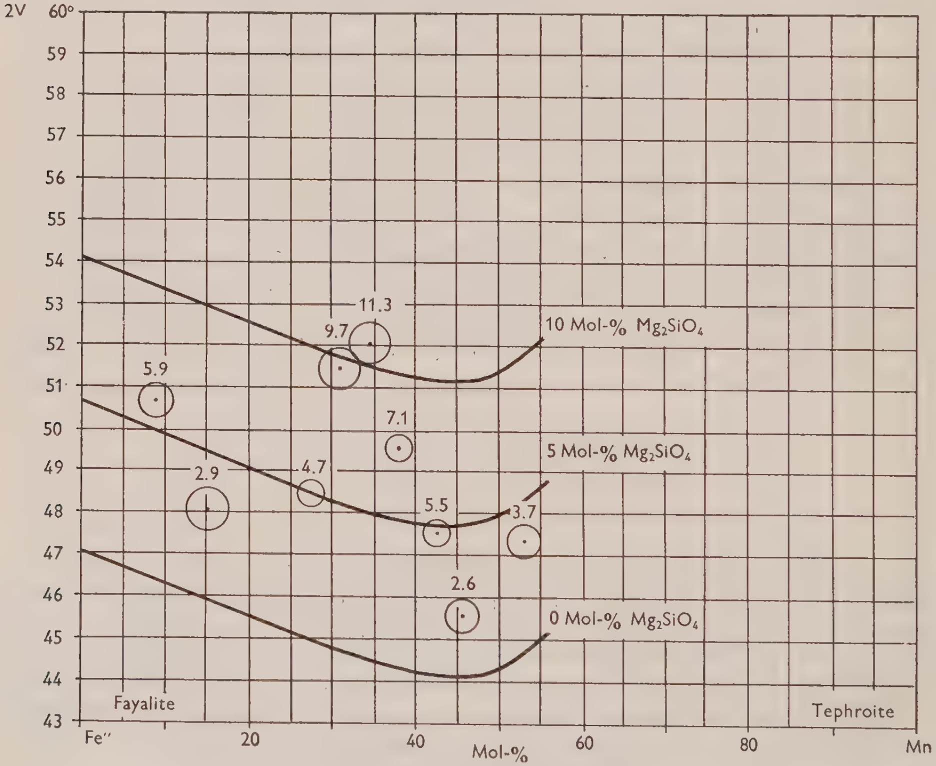

Fig. 5. Optic axial angle of knebelite.

such a way that it was possible to observe both emergents of the axes by direct rotation from one optic axis to the other. The optical angle has been determined for at least eight different grains within each sample. In the determinations the angle readings were repeated ten times. Adjustments for differences in refraction between mineral and segment have been made. The values obtained varied within certain limits (max. 2°). These divergencies are largely due to differences in the chemical composition (see below). Minor determination errors also influence the readings, the main reason for this being the difficulty in determining the exact position of the emergents of the axes. The knebelite often shows an undulating extinction. During the determinations sodium-light has been used. The values of the optical angles are found in Table 8. In Fig. 5 the optical angles have been marked off along the vertical axis and the chemical composition along the horizontal axis. A conversion of the analyses has been carried out in such a way that the content of Fe_2SiO_4 and Mn_2SiO_4 has been converted to 100 mol-% (Table 4). The observed optical angles have been put into their respective places in the diagram marked by circles, the radii of which correspond to the estimated errors in the determination (errors of measurement and spread). The course of the optical angle has been marked by three curves which represent different contents of Mg_2SiO_4 (0, 5 and 10 mol-%). The curves show that the optical angle has a minimum of about 44° at an Fe_2SiO_4 content of about 55 mol-% (0 % Mg_2SiO_4). With increased Mg_2SiO_4 content the optical angle increases considerably. Within the closely observed parts of the isomorphous series it will be seen that an increase of Mg_2SiO_4 content from 0 to 10 mol-% leads to an increase of the optical angle of about 7°. Similar changes in the optical angle (curves with maxima or minima when the mol relation is about 1:1 of the two components) have been observed in other isomorphous series, for example cordierite-ironcordierite and enstatite–orthoferrosilite. Changes in the cell dimensions that have any connextion with the course of the angle curve cannot be found by X-ray examinations.

The estimation of the average divergencies in the determinations for respective tests has been carried out by a simple analysis of variance. It is seen from this that the spread between the sizes of the optical angles is the greatest cause of variations, while the measuring errors are considerably smaller. Thus, between 65–85 % of the total spread is caused by differences of the optical angle, while 15–35 % is caused by the measuring methods (mainly depending on difficulties in finding the exact position of the emergents of axes). The average values of the optical angles and the mean average errors have been entered into Table 8.

Optical orientation

The optical orientation of knebelites have in all cases been:

$$X = b$$
$$Y = c$$
$$Z = a.$$

The optic plane is parallel to 001.

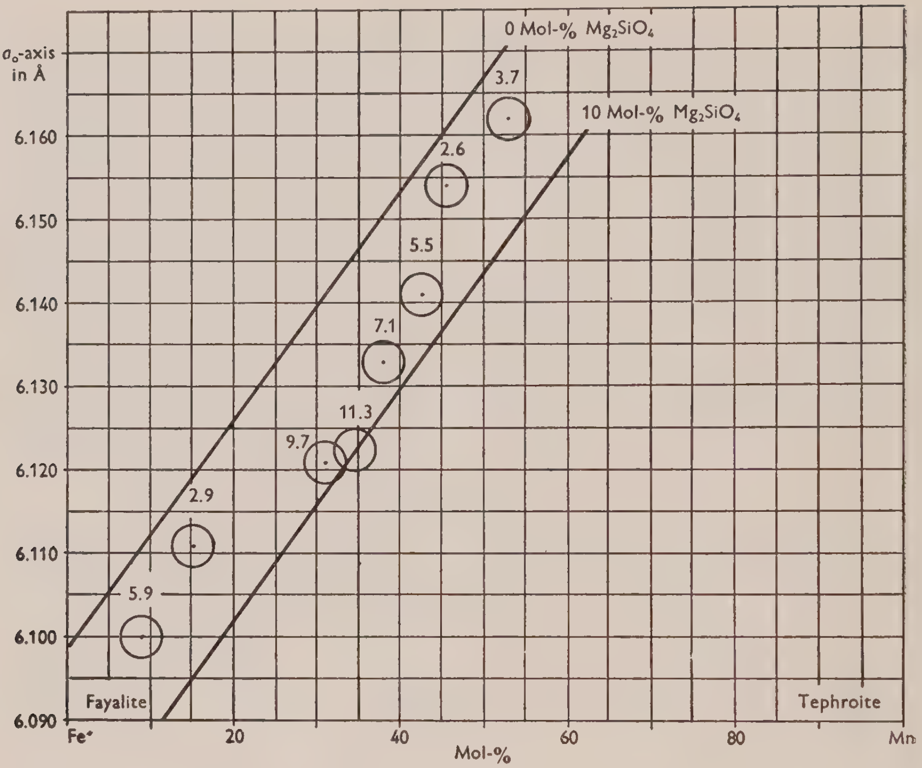

Fig. 6. Unit cell dimensions of knebelite (a_0).

X-ray data

Powder photograms were taken with a Guinier camera. Cu K_α-radiation (1.5418 Å) and a Ni-filter were used. KCl was used as internal standard with a calculated unit cell of 6.2930 Å. The cell dimensions a_0, b_0 and c_0 as well as the cell volume have been calculated. The results are found in Table 9 and Figs. 6, 7 and 8. These show that the cell dimensions are linear functions of the chemical composition of the mineral. The cell dimensions increase with increasing iron content and decrease with increasing manganese and magnesium contents.

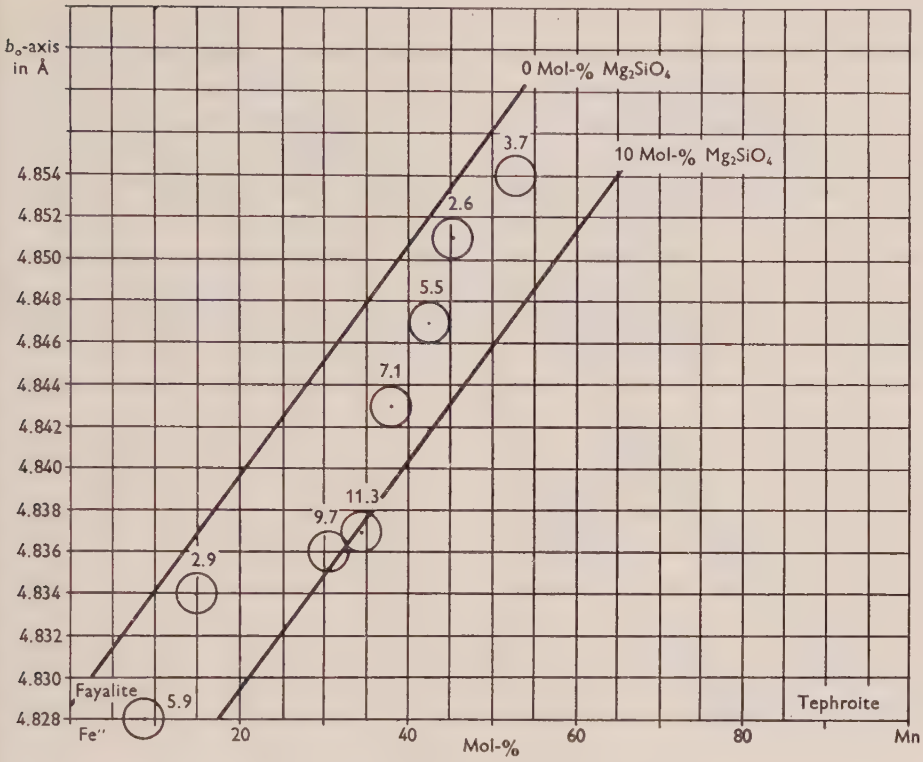

Fig. 7. Unit cell dimensions of knebelite (b_0).

Table 9. X-ray powder data for knebelite.

	a_0 in Å	b_0 in Å	c_0 in Å	Cell volume
Bastkärn 1	6.100	4.828	10.498	309.17
Bastkärn 2	6.111	4.834	10.518	310.71
Haggruvan	6.091	4.824	10.454	307.17
Skinnarängsgruvan	6.121	4.836	10.533	311.79
V. Silvberg	6.122	4.837	10.541	312.14
Hilläng	6.133	4.843	10.556	313.54
Tuna Hästberg	6.141	4.847	10.569	314.59
Dannemora 1	6.154	4.851	10.595	316.29
Dannemora 2	6.162	4.854	10.602	317.11

The errors in the determination are for $a_0 \mp 0.003$, $b_0 \mp 0.001$ and $c_0 \mp 0.002$ Å.

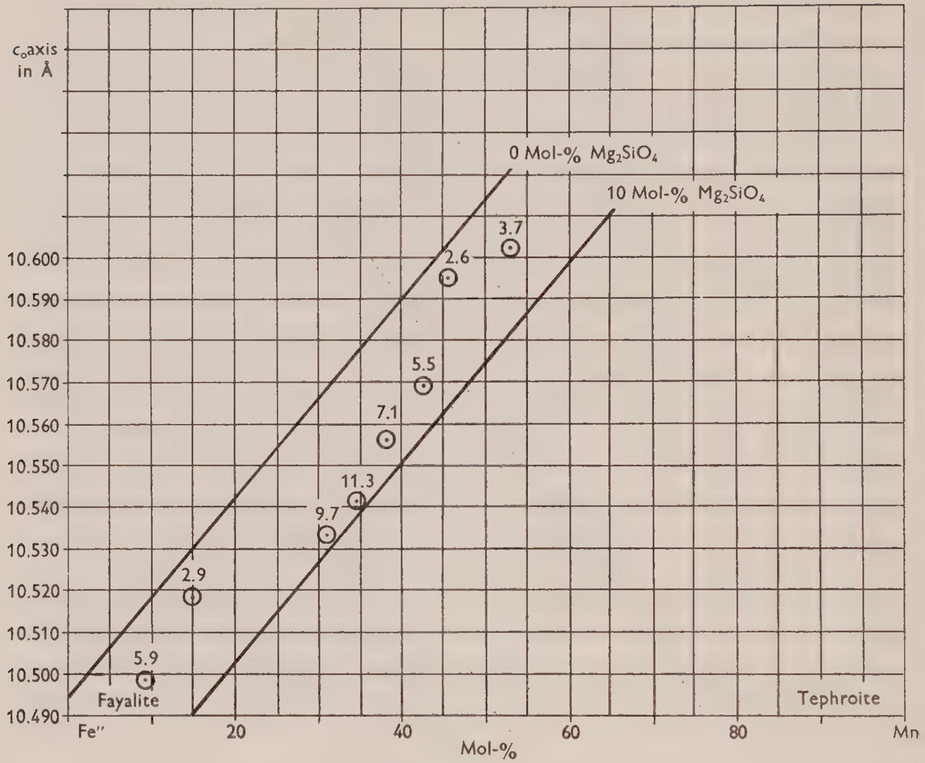

Fig. 8. Unit cell dimensions of knebelite (c_0).

ACKNOWLEDGEMENTS

The author wishes to convey his thanks to Prof. F. E. Wickman, Riksmuseet, and to Dr. N. Sundius for their critical reading of the manuscript, to Mr. A. Aaremäe for carrying out the chemical analyses, to Mr. L. Jansson for carrying out the mineral separations and parts of the X-ray work, to Mrs. I. Jansson and Mr. B. Honeth who constructed the diagrams, and to Mr. N. Sundberg for preparing about one hundred thin sections.

For financial support I am indebted to the Swedish Natural Sience Research Council.

REFERENCES

Backlund, H. (1909), Über die Olivingruppe. Ac. sc. St. Pétersbourg, Trav. Mus. géol. *III*, 77.

Berek, M. (1924), Mikroskopische Mineralbestimmung mit Hilfe der Universaldrehtischmethoden. Berlin.

Bowen, N. L. and Schairer, J. F. (1935), Olivines. Am. J. Sc. Ser. V, *XXIX*, 195–197.

Döbereiner, K. (1818), Schweiggers J. *21*, 49. Ref. Hintze (1897) *2*, 29.

Erdmann, A. (1851), Dannemora Jernmalmsfält i Upsala län. Stockholm.

Gunning, H. C. (1936), Knebelite from Bluebell mine, Kootenay Lake, B.C. Roy. Soc. Canada, Trans., *30*^{4}, 19–22.

Hess, H. H. (1949), Chemical composition and optical properties of common clinopyroxenes, part I. Am. Min. *34*, 621–666.

Igelström, L. J. (1890), Jb. Min I, 289. Ref. Doelter (1931) *4*^{3}, 1053–1054.

Magnusson, N. H. (1918), Beiträge zur Kenntnis der optischen Eigenschaften der Olivingruppe. Geol. För. Förh., *40*, 601–626.

Weibull, M. (1882), Untersuchung schwedischer Minerale. Tschermak, N. F. *7*, 119–121.

—— (1883), Några Manganmineral från Vester-Silfberget i Dalarne. Geol. För. Förh. *VI*, 500–503.

—— (1884 a), Ak. Stockholm, Handl. *9*, 11. Ref. Hintze (1897) *2*, 29.

—— (1884 b), Mineralogiska notiser, Igelströmit från Hillängs grufvor i Dalarne. Geol. För. Förh., *VII*, 263–265.

Suckow, G. (1855), Kenng. ueb. Min., *93*. Ref. Hintze (1897), *2*, 29.

Yosimura, T. (1939), Studies on the minerals from the manganese deposit of Kaso Mine, Japan. Hokkaido Univ., J. Fac. Sc. Ser. 4, 313–452.

Tryckt den 14 december 1956

Uppsala 1956. Almqvist & Wiksells Boktryckeri AB

ARKIV FÖR MINERALOGI OCH GEOLOGI Band 2 nr 12

Communicated 25 January 1956 by PERCY QUENSEL and FRANS E. WICKMAN

The alkali content of kyanite

By ÅKE HENRIQUES

ABSTRACT

Spectrochemical determinations of sodium and potassium have been carried out on kyanite from Hållsjöberget in Värmland (Sweden), and from a number of localities in Tessing and St. Gotthard (Switzerland). The investigations show that the alkali content never exceeds 0.06 % ($Na_2O + K_2O$), (assuming pure analytical material to have been employed). The chemical formulae of kyanite proposed by J. Jakob (1937 and 1941) are criticized. Accounts of new chemical analyses of kyanite from Hållsjöberget are given. Optical determinations have been made and the value of the specific gravity ascertained in the latter material.

Introduction

In connection with a petrographic examination of the kyanite-quartzite at Hållsjöberget a number of samples were taken from various parts of the deposit for analyses of the kyanite. Spectrochemical determinations made on pure kyanite prepared from the samples showed that only small amounts of alkalis are present in the kyanite. Jakob (1937, 1941) demonstrated, however, by means of analyses, that kyanite contains not inconsiderable amounts of alkalis and water, which caused him to devise new chemical formulae for kyanite (see below). Fairbain (1943) considers, with reference to the close-packed lattice of kyanite, that it is not very likely that the large Na ions could fit into the mineral's lattice. From both the theoretical and practical point of view it has been desirable to establish to what extent various kyanite modifications occur with and without alkalis. Since it is open to suspicion that the analytical material used by Jakob could have been more or less impure, specially as regards such micaceous minerals as paragonite and muscovite, new determinations of Na_2O and K_2O have been made on material from the same deposits in Tessin from which Jakob's samples were derived. Two further specimens of kyanite from St. Gotthard have been studied.

Investigation and treatment of the material

The material for the chemical analyses as well as the other determinations was, in the case of the Hållsjöberget kyanite, obtained from small, kyanite-rich specimens (not exceeding 150 gm in weight). The material was crushed and sieved (+ 100 mesh, Tyler standard) after which separation by means of heavy liquids was carried out. The material for analyses from Tessin and St. Gotthard was selected from colourless or faintly blue crystals of the transparency of the glass. Any impurities present (particularly micaceous minerals) were removed.

Table 1. (Analyst V. Muld.)

No.	% Na_2O	% K_2O	% H_2O	Remarks
1	< 0.03	< 0.01	0.05	
2	< 0.03	< 0.01	0.04	
3	< 0.03	< 0.01	0.05	
4	< 0.03	< 0.01	0.06	
5	≤ 0.03	< 0.01	0.08	
6	0.05	0.01		
7	0.03	0.01		
8	0.20	0.05		Impure material
9	0.04	0.02		
10	0.15	0.04		Impure material
11	0.05	0.01		
12	< 0.03	< 0.01		
13	0.02	0.01		

No. 1 Kyanite from Hållsjöberget, K.T.H. H 1.
2 ,, ,, Hållsjöberget, K.T.H. H 2.
3 ,, ,, Hållsjöberget, K.T.H. H 3.
4 ,, ,, Hållsjöberget, K.T.H. H 4.
5 ,, ,, Hållsjöberget, K.T.H. H 5.
6 ,, ,, Alpe Sponda, Tessin, M.R.A. g 17579.
7 ,, ,, Tessin, K.T.H. 518.
8 ,, ,, Tessin, K.T.H. 4404.
9 ,, ,, Pizzo Forno, Tessin, K.T.H. 4393.
10 ,, ,, Tessin, S.H. M53024.
11 ,, ,, Campolungo, Tessin, S.H. M3626.
12 ,, ,, St. Gotthard, K.T.H. 4376.
13 ,, ,, St. Gotthard, K.T.H. 4386.

K.T.H.: Collection of the Institute of Technology in Stockholm.
R.M.A.: Collection of the Swedish Museum of Natural History
S.H.: Collection of the University of Stockholm.

The refractive indices of the minerals were determined by the immersion method. The other optical investigations were carried out with the universal stage. All determinations were made in Na light. Finally, the specific gravity was evaluated by the suspension method, in which homogeneous kyanite were used (+ 50 mesh, temp. 20° C).

The alkali content of the kyanite

As indicated in Table 1, alkali contents greater than 0.06 % ($Na_2O + K_2O$) have not been observed in the analysed kyanites apart from two exceptions. In these a maximum alkali content of 0.25 % has been shown. Closer inspection discloses, however, that these samples consist of kyanite with a diffuse "skin of alteration", which probably consists of very small scales of mica. Owing to the small amounts present of this "skin" it has not been possible to ascertain its mineralogical nature. Concerning the other examples of kyanite with low content of alkali, the sodium and potassium probably are derived from micaceous minerals, the presence of which is not possible to demonstrate. A further possibility is that small additions of alkalis have taken place in connection with the preparation and analysis of the material.

The present investigation thus indicates that kyanite with considerable amounts of alkali has in no case been proved—since pure analytical material was used. Although Jakob's investigations suggest the opposite to be the case, it seems likely that his material was not "analytically pure", since several of the analysed specimens of kyanite recorded in the present paper come from the same deposits in Tessin.

The chemical formulae proposed by Jakob for kyanite,

$$40\ SiO_2\ 40\ Al_2O_3\ a\ Na_2O\ b\ H_2O,$$

where $a = 1,\ 2$

$$b = 1,\ 2,\ 3,\ (4),\ (5),\ 6$$

seem to lack agreement with the true composition of kyanite.

The kyanite from Hållsjöberget

Perusal of the five analyses (Table 2) shows that the kyanite from Hållsjöberget is subject to only slight variation in composition throughout the deposit. This is reflected above all by the insignificant variation in the iron content of the kyanite (min. 0.71 %; max. 0.80 % Fe_2O_3). The iron probably replaces aluminium in the kyanite's crystal lattice to a considerable degree. Only slight quantities should have been derived from slight accompanying impurities. These consist principally of phosphatic minerals with the bivalent metals Ca, Mg and Mn and of rutile. Concerning the sodium and potassium content, see the previous section.

Demonstrable differences in the refractive indices, the optical angle, and the specific gravity have not been observed for the five specimens of kyanite from Hållsjöberget. The various determinations are accounted for in Table 3.

Table 2. (Analysts A. Aaremäe and V. Muld*.)

	1	Mol. prop.		2	Mol. prop.		3	Mol. prop.		4	Mol. 'prop.		5	Mol. Prop.	
O_2	36.46	0.6071	0.98	37.14	0.6184	1.01	37.46	0.6237	1.03	36.31	0.6046	0.97	36.45	0.6069	0.98
$_2O_3$	62.40	0.6120	1.00	61.72	0.6055	1.00	61.52	0.6035	1.00	62.72	0.6153	1.00	62.58	0.6139	1.00
$_2O_3$	0.72	0.0045		0.80	0.0050		0.71	0.0044		0.78	0.0049		0.74	0.0046	
$_2O_3$*	0.01	0.0001		—			—			—			—		
$_2O$*	0.03	0.0005		0.03	0.0005		0.03	0.0005		0.03	0.0005		0.03	0.0005	
O*	0.01	0.0001		0.01	0.0001		0.01	0.0001		0.01	0.0001		0.01	0.0001	
O	0.06	0.0011		0.06	0.0011		0.02	0.0004		—			—		
gO	0.05	0.0012		0.02	0.0005		0.03	0.0007		—			—		
nO	0.005	0.0001		0.012	0.0002		0.006	0.0001		—			—		
O_2	0.06	0.0008		0.10	0.0013		0.03	0.0004		0.04	0.0005		0.05	0.0006	
O_5	0.06	0.0006		—			—			—			—		
O	0.05	0.0028		0.04	0.0022		0.05	0.0028		0.06	0.0033		0.08	0.0044	
	99.92			99.93			99.86			99.95			99.94		

os. 1—5, kyanite specimens from Hållsjöberget.

Table 3. The physical properties of kyanite from Hållsjöberget.

Cleavage	Perfect along {100}, good along {010} and {001}.
Twinning	Common, twinning plane {100} etc.
Extinction angles	On (100) $\gamma': c = 30^\circ \mp 1^\circ$ On (010) $\gamma': c = 7^\circ \mp 1^\circ$ On (001) $\alpha': a = 2^\circ \mp 1^\circ$
Colour	Light blue. Colorless in thin section.
Index of refraction	$\alpha = 1.713 \mp 0.002$ $\beta = 1.720 \mp 0.001$ $\gamma = 1.728 \mp 0.002$
Optical angle	$83^\circ (-) \mp 1^\circ$ (10 det.)
Specific gravity	3.63 ∓ 0.01 20° C (5 det.)

ACKNOWLEDGEMENTS

The author wishes to convey his thanks to Prof. F. E. Wickman, Riksmuseet, for valuable discussions and for his critical reading of the manuscript, to Persbergs Grufve A.B., Persberg, for defraying the cost of the analyses, and to Mr. L. Jansson for carrying out the mineral separations.

REFERENCES

FAIRBAIN, H. V. (1943), Packing in ionic minerals. Geol. Soc. Am. Bull. *54*^{2} 2, 1305–1374.

JAKOB, J. (1937), Über den Alkaligehalt der Disthene. Schweizer. Min. u. Petr. Mitt. *XVII*, 214–219.

—— (1941), Chemische und strukturelle Untersuchungen an Disthen. Schweizer. Min. u. Petr. Mitt. *XXI*, 131–135.

Tryckt den 14 december 1956

Uppsala 1956. Almqvist & Wiksells Boktryckeri AB

ARKIV FÖR MINERALOGI OCH GEOLOGI Band 2 nr 13

Communicated 14 November 1956 by Percy Quensel and Frans E. Wickman

Cell dimensions of sphalerite

By Åke Henriques

With 1 figure in the text

ABSTRACT

The length of the unit cell for 5 specimens of sphalerite with varying iron content has been determined (min. 0.009 and max. 20.31 wt. % FeS). Comparisons with earlier investigations of the same type are made.

Influence of iron content on the size of the unit cell

During the last 25 years a number of investigations have been carried out in order to ascertain to what extent the size of the elementary cell of sphalerite is governed by the iron content. Braekken (1934) has examined some ten samples of sphalerite with a maximum iron content of 24.2 wt. % FeS. He has found that the length of the cell (a_0) does not depend on the iron content but is constant, viz. 5.403 ± 0.005 Å. Chudoba and Mackowsky (1939) and Kullerud (1953) have, however, demonstrated that the length increases with increasing iron content. The values for a_0 obtained by them (for a definite iron content) do not agree (for 0.75 wt. % FeS Chudoba and Mackowsky found a_0 to be 5.412 ± 0.006 Å, while Kullerud determined a_0 as 5.3985 ± 0.0001 Å for sphalerite with almost the same composition as that investigated by Chudoba and Mackowsky, (see Table 1). Closer examination of Kullerud's calculations of the unit cell dimensions of sphalerite discloses that these must first be corrected before they can be compared with values obtained by other workers. Kullerud employed NaCl as internal standard using the value for a_0 determined by van Bergen of 5.62869. This value of van Bergen refers, however, to *kX* units, a point not taken into account by Kullerud (nor by Wyckoff). These authors have incorrectly given the length of the unit cell of NaCl in ångström units (5.62869 Å). Consequently all determinations of cell dimensions in Kullerud's paper are wrong. Thus, in the tables and diagrams below Kullerud's determinations have been corrected with reference to his mistake with the ångström and *kX* units. Moreover, Kullerud has throughout, in the tables and diagrams, made use of values in giving both wt. % and mol. % that do not agree with each other. These errors have also been corrected in the following (in the latter case it was assumed that the figures expressed as wt. % are correct). In spite of this, however, Chudoba and Mackowsky's and Kullerud's values for the unit cell length of sphalerite do not agree (within a given margin of error) for iron-rich sphalerite. An explanation of why the unit cell lengths for more iron-rich sphalerite do not agree (i.e. Chudoba and Mackowsky's on the one hand and Kullerud's on the other) may

Table 1.

FeS content of mix-crystals		Unit cell length a_0 in Å	Calculated spec. grav.	Determined spec. grav.	
wt. %	mol. %				
0.25	0.28	5.412 ∓ 6			1)
16.23	17.70	5.4213 ∓ 60			2) Chudoba and
28.73	30.00	5.431 ∓ 6			3) Mackowsky
41.24	43.75	5.439 ∓ 6			4)
0	0	5.4095 ∓ 1	4.0900	4.110 ± 0.003	Kullerud*
5	5.51	5.4111 ∓ 2			
10	10.98	5.4128 ∓ 2			
15	16.36	5.4153 ∓ 2			
20	21.70	5.4176 ∓ 2			
30	32.20	5.4219 ∓ 2			
36.5	38.92	5.4244 ∓ 2	3.9120	3.935 ± 0.003	
0.008	0.009	5.410 ∓ 2	4.087		Henriques (see Table 2)
0.121	0.135	5.409 ∓ 2	4.086	4.085 ± 0.002	
0.310	0.344	5.411 ∓ 2	4.086	4.085 ± 0.002	
9.57	10.51	5.413 ∓ 2	4.038	4.038 ± 0.002	
20.31	22.03	5.416 ∓ 2	3.985	3.990 ± 0.002	

* Corrected values.

1) Santander, Spain.
2) Alston, Cumberland, England.
3) Breitenbrunn, Saxony, Germany.
4) St. Agnes, Cornwall, England.

Table 2. Chemical analyses of sphalerites. (Analysts V. Muld and A. Parvel.)

Analysis No.	% Zn	% Cd	% Ga	% In	% Ge	% Mn	% Fe	% Co	% Ni	% Cu	% Ag	% Sn	% Pb	% Mg	% Al	% Si
1		0.05	0.003	0.003	0.001	0.009	0.005	0.001	—	—	0.0003	0.002	0.003	0.1	0.1	0.5
2		0.1	0.003	0.003	0.001	0.005	0.077	0.001	—	—	0.0003	0.001	0.003	0.1	0.1	0.5
3		0.25	0.003	0.003	0.001	0.005	0.197	0.001	—	—	0.0003	0.001	0.003	0.1	0.1	0.05
4		0.04	0.003	0.01	0.001	0.4	6.08	0.001	—	—	0.0003	0.001	0.003	0.1	0.1	0.07
5	49	0.13	—	0.003	—	1.43	12.9	0.001	0.001	1	—	—	—	0.3	—	2

1) Franklin, New Jersey, U.S.A. Glass-clear, very faintly yellow, crystal.
2) Picos de Europa, Santander, Spain. Yellow-brown, transparent crystals.
3) Chivera, Cananea, Sonora, Mexico. Feebly olive-green, transparent crystal.
4) Nordmarks gruva, Nordmark s:n, Sweden. Dark-brown crystals.
5) Storfallsgruvan, Grangärde s:n, Sweden. Black, coarse zincblende.

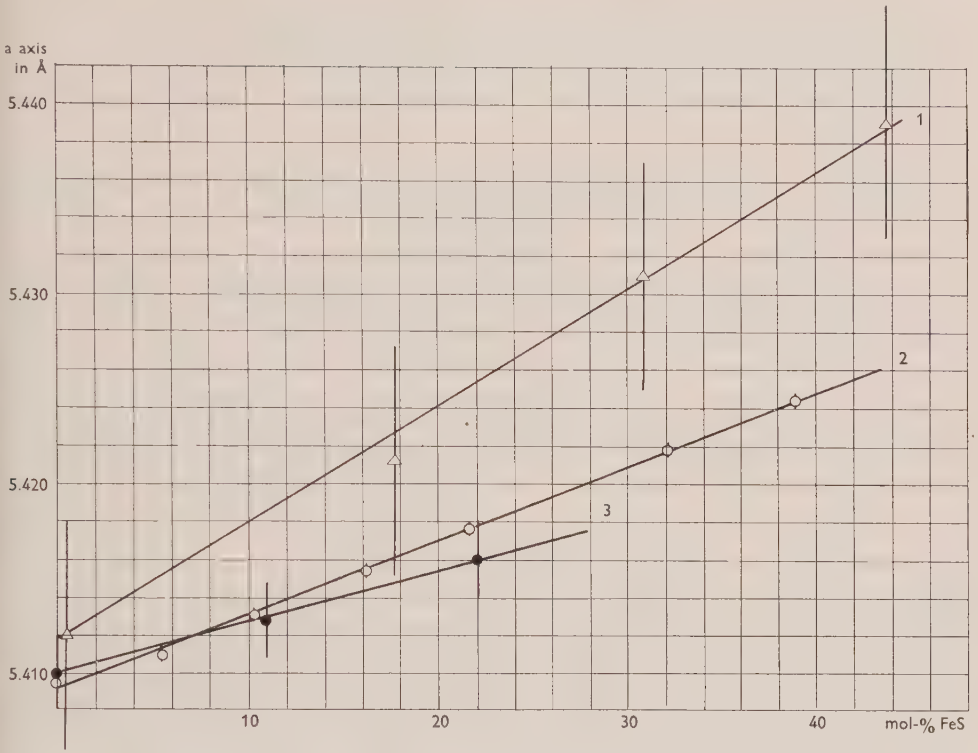

Fig. 1. Graph illustrating the relationship between the unit cell length and the FeS content of sphalerite. Determinations of Chudoba and Mackowsky (1), of Kullerud (2), and of Henriques (3).

partially be that the minerals used by Chudoba and Mackowsky were rich in "trace elements", which increased the unit cell lengths. Another explanation of why the unit cell lengths do not agree may be that the minerals (synthetic and natural) have not the same "thermal history". Abelson (1955) has reported on investigations made by J. R. Smith and H. Yoder on synthetic and natural plagioclase where it has been found that the unit cells are not equally large in spite of identical chemical composition. The reason for this is considered to be that the minerals have not been formed under identical temperature conditions. Unit cell length determinations in five natural specimens of sphalerite[1] carried out by the author show however that these do not deviate from Kullerud's (corrected) determinations. In the case of the differences between the sphalerite values obtained by Braekken and Chudoba and Mackowsky, and those obtained by Kullerud and the author, it seems more likely that these are due to the difficulty in making accurate unit cell length determinations with the equipment employed by the former.

A short compilation of the unit cell length of sphalerite according to Chudoba and Mackowsky, Kullerud (the corrected values) and the author (Table 1) follows below. Calculated and determined densities of sphalerite have been included in the same table. Kullerud has determined the density according to Biltz's (1922) pycnometer method, while the author has availed himself of the suspension method. In Fig. 1 the unit cell length (a_0) has been entered against the FeS content of the sphalerite. The chemical composition of the specimens of sphalerite examined by the author is presented in Table 2.

---

[1] The material is derived from a determination of the Vickers hardness of sphalerite.

The X-ray determinations

A short compilation of the X-ray determinations of sphalerite made by Chudoba–Mackowsky, Kullerud and the author follows below. Chudoba–Mackowsky's determinations were made with a Debye–Sherrer camera with a diameter of 57.3 mm. The thickness of the sample was 0.400 + 0.006 mm. The exposures were made in Cu radiation (Cu $K\alpha$ 1.537 and Cu $K\alpha_2$ 1.541). NaCl was used as internal standard. The unit cell length of sphalerite was determined from the (434) lines. The film measurements were made with an accuracy of 0.01–0.02 mm. Kullerud's determinations were also carried out with a Debye–Sherrer camera with a diameter of 114.6 mm. The insertion of the film was made by Straumanis' method. The thickness of the sample was 0.30 ± 0.05 mm. The exposures were made in Fe radiation Fe $K\alpha$ 1.9373 Å, Fe $K\alpha_1$ 1.93597 Å and Fe $K\alpha_2$ 1.93991 Å. NaCl was used as internal standard with a (corrected) value for a_0 of 5.62869 kX units. The unit cell length of sphalerite was calculated from the (333) and (422) lines. The film measurements were carried out with an accuracy of 0.05 mm. The present determinations were performed with a Guinier camera with a diameter of 78.9 mm. The exposures were made in Cu radiation (Cu $K\alpha$ 1.5418 Å). KCl was used as internal standard with a calculated unit cell of 6.2930 Å. The unit cell length for sphalerite was determined from the lines (211), (220), (221), (310), (311) and (321). The film measurements were made with an accuracy of 0.02 mm. The vertical lines in the diagram show the limit of error in the a_0 values.

The author wishes to express his thanks to Professor F. E. Wickman, Riksmuseet, for his critical examination of the manuscript, and to Mr. L. Jansson, who calculated the size of the unit cell.

REFERENCES

Abelson, P. H. (1955), Annual Report of the Director of the Geophysical Laboratory. 1954–1955, No. 1248. Carnegie Inst. of Washington.

van Bergen, H. (1941), Präzisionsmessungen von Gitterkonstanten mit einer Kompensationsmethode. II. Ann. Phys. *39*, 553–572.

Biltz, W. (1922), Dichtemessungen an Aluminiumshalogeniden. Quecksilber als Pyknometerflüssigkeit. Z. anorg. Chem. *121*, 257–265.

Braekken, H. (1934), Leerstellen im Kristallgitter eisenhaltiger Zinkblenden. Norsk. Ak., Forh., *7*, 119–120.

Chudoba, K. F. and Mackowsky, M. T. (1939), Über die Isomorphie von Eisen und Zink in der Zinkblende. Zbl. Min., Abt A, 12–21.

Kullerud, G. 1953), The FeS–ZnS system a geological thermometer. Norsk Geol. Tidskr., *32*, 61–147.

Wyckoff, R. W. G. (1948), Crystal Structures, Vol. I. New York.

Tryckt den 7 februari 1957

Uppsala 1957. Almqvist & Wiksells Boktryckeri AB

ARKIV FÖR MINERALOGI OCH GEOLOGI Band 2 nr 14

Communicated 28 November 1956 by PERCY QUENSEL and FRANS E. WICKMAN

Swedish pyrophyllite deposits and the optical properties of pyrophyllite

By ÅKE HENRIQUES

SUMMARY

A short account of Swedish pyrophyllite deposits is presented. New optical data together with a new chemical analysis of pyrophyllite are given.

Introduction

During the last few years pyrophyllite ($Al_2Si_4O_{10}(OH)_2$) has gained a gradually increasing importance in industry (Mudd series, 1949, and Johnstone, 1954). Figures illustrating the production of pyrophyllite are practically non-existent. This is due to the fact that in all available statistics the mineral is listed together with closely related minerals, mainly talc. It is, however, possible to mention a few production figures. Thus in 1950, 265,901 long tons were mined in Japan and in the United States, 104,286 long tons (Johnstone, 1954). Pyrophyllite has not been mined in Sweden.

Swedish pyrophyllite deposits

The Swedish occurrences of pyrophyllite are for the most part connected with Precambrian kyanite-bearing quartzites, particularly those of the Västanå area and Hållsjöberget. In the Västanå area in the parish of Näsum, county of Kristianstad, the mineral occurs mainly in the form of smallish vugs and fissure-fillings in a primary sedimentary iron ore (haematite ore) interbedded in the quartzite.

Pyrophyllite is found only sporadically *in situ* since the mine was closed during the 19th century (the mineral is, however, to be found in the dumps). According to older references (Blomstrand, 1866 and 1868) the fissures have a maximum width of about 10 cm.

At Hållsjöberget in the parish of Ny, county of Värmland, the mineral occurs again in the form of small vugs and fissure-fillings in a number of mica-schist intercalations in the quartzite. The mica schist, the thickness of which never exceeds three metres, is made up mainly of muscovite and quartz. The muscovite has at least been partly formed by the replacement of kyanite; small remnants of kyanite are therefore frequently observed in the mica schist. Apart from the above-mentioned mineral the mica schist infrequently contains several minerals that occur commonly in the quartzite, particularly rutile, ilmenite as well as various phosphatic minerals. Tourm-

Table 1. The physical properties of pyrophyllite.

Crystal system	Monoclinic*
Cleavage	Denoted by {001}
Colour	Silver-white Colourless in thin sections
Indices of refraction	$\alpha = 1.556 \mp 0.002$ $\beta = 1.589 \mp 0.002$ $\gamma = 1.601 \mp 0.002$
Optic angle	$62^{\circ}\ (-) \mp 1^{\circ}$
Optical orientation	$X \wedge a = +88^{\circ}.5 \mp 0^{\circ}.5$ $Y \wedge a = 1^{\circ}.5 \mp 0^{\circ}.5$ $Z \parallel b$ Optic plane (010)

* Pyrophyllite belongs to the monoclinic system as shown by Gruner (1934), Hendricks (1938), and others. This is emphasized here because a German textbook still refers pyrophyllite to the orthorhombic system in which it used to be placed.

aline has also been noted. Amongst other pyrophyllite localities in Sweden may be mentioned Bliaberget in the parish of Ransäter, county of Värmland, and Norrö in the parish of Utö, county of Stockholm. The first-named deposit is situated in a kyanite-poor quartzite of the same type as that at Hållsjöberget (Weibull, 1898), while the second occurrence is in a pegmatite (Erdmann, 1905). The paragenetic relationships suggest that the pyrophyllite in these deposits has been formed hydrothermally.

The deposits are all of too small a size to permit mining of the pyrophyllite. Thus, at Hållsjöberget the content of pyrophyllite only exceptionally exceeds one per cent of the mica schist. The content at Bliaberget is even lower. The deposit in the Västanå area also seems to lack any economic importance.

The optical and chemical properties of pyrophyllite

In connection with the present study of the Swedish pyrophyllite occurrences the identity of the mineral was established by means of powder diagrams and by optical determinations. As a result of the optical measurements it has become apparent that the optical properties attributed to the mineral do not entirely agree with those observed during the present investigation. Besides a small correction in the optical orientation of the mineral ($X \wedge a$ was determined as $88^{\circ}.5 \pm 0^{\circ}.5$ and $Y \wedge a$ as $1^{\circ}.5 \pm 0^{\circ}.5$; earlier values are 90° and 0° respectively) the optic angle was found to be $62^{\circ} \pm 1^{\circ}$ as opposed to the values 53°–60° given in modern optical literature. Perusal of older optical literature indicates, however, that the value of 62° was accepted by Lévy and Lacroix as long ago as 1888; also Weibull (1898) gave an optic angle of the same order of magnitude. The values of from 53° to 60° arise from determinations on the axial angle of pyrophyllite from Indian Gulch, Mariposa County, California (Larsen, 1921). The latter determinations were obtained by "measuring the distance between the hyperbolas on a section cut nearly normal to the acute bisectrix ... with a probable error of only a few degrees". The method utilisteted probably explains to a certain extent the deviations between Larsen's values on the one hand and Lévy and Lacroix', Weibull's and the present values on the other.

Table 2. Chemical analysis of pyrophyllite.

	1	2	3
SiO_2	66.70	64.88	1.0797 } *3.80*
TiO_2		0.02	0.0003
Al_2O_3	28.30	28.64	0.2809 } *1.00*
Fe_2O_3		0.48	0.0030
MnO		0.02	0.0003
CaO		0.03	0.0005
MgO		0.08	0.0020
Na_2O		0.03	0.0005
K_2O		0.04	0.0004
H_2O^-		0.09	0.0050
H_2O^+	5.00	5.47	0.3036 } *1.07*
	100 %	99.78 %	

1) Pyrophyllite, theoretical composition.
2) Pyrophyllite, Västanå 1956, analyst A. Aaremäe.
3) Molecular proportions.

An account of the optical properties of newly analyzed pyrophyllite from the Västanå area is given in Table 1. However, the optical properties of other investigated samples of pyrophyllite (8 in number) do not differ from this (only within the limits of experimental error). The optical determinations were carried out with a universal stage with the exception of the refractive indices, which were ascertained by the immersion method. In all cases sodium light was used.

In the determination of the optical orientation of the mineral the following method was used. Lamellae of pyrophyllite parallel with (001) were prised out of crystal bundles optically orientated in the same way, after which the lamellae, 12 in number, were mounted in Canada balsam on the slides in four directions, each forming 90° with the other. In the determination of the direction for X from the 12 lamellae the angular errors due to the instrument or to the fact that the lamellae are not orientated in parallel with the slides can readily be reduced in importance.

Kiefer (1950) discovered two pyrophyllite modifications which he termed pyrophyllite α and pyrophyllite β. He has been able to differentiate the two modifications by determining their temperature dehydration which differs somewhat in the two cases. Since, however, Kiefer's results do not agree with those obtained from a series of investigations (Vestergren, 1925; Noll, 1936; Thilo and Schünemann 1937) and, moreover, since the existence of the two modifications has not been proved in any other fashion (e.g. by X-ray), it seems to the author that the existence of two pyrophyllite modifications with possibly different optical properties is by no means established.

In Table 2 an analysis of pyrophyllite from Västanå is presented. From this, as also from analyses in the literature, it seems clear that the chemical composition of the mineral, if one excludes the effect of probable impurities in the material analyzed, must be constant. Only a small amount of the Al^{3+} seems to be replaceable by Fe^{3+}. In the same way hydroxyl ions can be replaced by fluorine. The similar optical properties observed would thus appear to be due to the almost constant chemical composition that characterizes pyrophyllite.

Thanks are due to Prof. F. E. Wickman for his critical perusal of the manuscript.

REFERENCES

BLOMSTRAND, C. W. (1866), Om nya mineralier från Skåne. Ak. Stockholm, Handl. Öfv. 369–378.
—— (1868), Om Westanå Mineralier. Ak. Stockholm, Handl. Öfv. 197–212.
ERDMANN, E. (1905), En ny svensk fyndplats för mineralet Pyrophyllit. Geol. För. Förh., *27*, 412–413.
GRUNER, J. W. (1934), The crystal structures of talc and pyrophyllite. Zs. Kr., Abt. A, *88*, 412–419.
HENDRICKS, S. B. (1938), On the crystal structure of talc and pyrophyllite. Zs. Kr., Abt A, *99*, 264–274.
JOHNSTONE, J. S. (1954), Minerals for the Chemical and Allied Industries. London.
KIEFER, CH. (1950), Note sur les minéraux phylliteux et leurs altérations. C. R. *230*, 977–978.
LARSEN, E. S. (1921), The microscopic determination of the nonopaque minerals. Geol. sur. Am., Bull., *679*, 1–294.
LÉVY, M. and LACROIX, A. (1888), Les minéraux des roches. Paris.
NOLL, W. (1936), Mineralbildung im System Al_2O_3–SiO_2–H_2O. Jb. Min., Beil.-Bd., *70*, 65–115.
SEELEY, W. MUDD Series (1949), Industrial Minerals and Rocks. New York.
THILO, E. and SCHÜNEMANN H. (1937), Über das Verhalten des Pyrophyllites $Al_2(Si_4O_{10})(OH)_2$ beim Erhitzen und die Existenz eines "wasserfreien Pyrophyllits" $Al_2(Si_4O_{10})O$. Zs anorg. Chem. *230*, 321–335.
VESTERBERG, K. A. (1925), Om kaolin och dess termiska förändringar. Ark. Kemi., *9*, N:o 14, 1–26.
WEIBULL, M. (1898), En ny svensk fyndort för mineralet Pyrophyllit. Geol. För. Förh., *20*, 57–62.

Tryckt den 7 februari 1957

Uppsala 1957. Almqvist & Wiksells Boktryckeri AB

ARKIV FÖR MINERALOGI OCH GEOLOGI Band 2 nr 15

Communicated 24 October 1956 by PER GEIJER and FRANS E. WICKMAN

The Vickers hardness of zinc blende

By ÅKE HENRIQUES

With 3 figures in the text

Abstract

A Durimet micro-hardness measurer equipped with a Vickers diamond has been found suitable for the determination of the hardness of zinc blende (Zn, Fe)S. The hardness of the mineral has been found to be a definite function of both the chemical composition and the crystallographic orientation.

Introduction

In metallography micro-hardness determinations are of considerable importance, above all in establishing the mechanical properties of metals. In mineralogy, however, micro-hardness determinations have been employed to only a minor degree, despite the fact that such measurements can be carried out on most minerals. The few micro-hardness determinations that have been carried out in the past have usually been made with varying types of apparatus and varying measurement standards thus often making it impossible to compare the results obtained. The crystallographic orientation and chemical composition of the mineral have as a rule not been given, although these factors are often of considerable importance for the hardness of the mineral.

The most common method in present use for carrying out micro-hardness determinations on ore minerals is the indentation method. According to this a weighted point is allowed to make a permanent impression on the mineral. The hardness is then calculated from the size of the load and the lengths of the diagonals of the indentation (see below). The various micro-hardness instruments differ from each other mainly in the shape of the body making the indentation. In the investigations here described the hardness of zinc blende, one of the most important reference minerals in ore microscopy, has been studied with the aid of a Durimet Small-Hardness Tester (Leitz construction) equipped with a Vickers diamond.

Micro-hardness tester

The micro-hardness tester (Durimet Small-Hardness Tester) is in principle designed like a normal microscope, having objective and ocular. The objectives (2 in number), as well as the Vickers diamond, are mounted on a changer which can be rotated around a vertical axis. Thus change of objectives and the Vickers diamond can be carried out quickly. When a suitable area of the sample for hardness measurement is observed in the instrument, the objective is replaced by the Vickers diamond. After the indentation has been made the objective is again brought back. The travel of the loaded Vickers diamond on to the specimen is regulated by means of an oil brake. The lengths of the indentation diagonals, a measure of the hardness, is determined by means of a graduated measuring ocular, which permits readings down to 0.1 μ. The standard instrument is equipped with a revolving graduated holder which is mounted on the objective stage. The specimen can be locked in the holder by means of screws. A more detailed description is to be found in a pamphlet published by Leitz (1954).

Vickers hardness

The Vickers hardness is determined by the lengths of the diagonals of the indentations and the magnitude of the load according to the following formula:

$$\mathrm{HV} = \frac{1854.4 \times P}{d^2},$$

where HV is the Vickers hardness in kg/mm^2, P the load in g, and d the length of the diagonal of the indentation in μ ($1\ \mu = 0.001$ mm).

Measurement technique

In the determination of the Vickers hardness the following technique has been worked out. The polished specimens (see below) are dried in a drying oven for a period of 36 to 48 hours (temp. 50°C). The specimens are then placed in the graduated, revolving holder designed for the instrument. To check the horizontal position of the specimen, the latter, together with the holder, is moved by means of the two micrometer screws on the objective stage of the instrument. If the sample has been correctly mounted the focus of the field of vision should not alter. Before mounting the specimen in the micro-hardness tester the instrument is checked by making a number of indentations on a specially provided standard block having a known Vickers hardness. With help of the oil brake the travel of the diamond on to the test surface is set to within ∓ 1 second. Thereafter the diamond is allowed to rest on the test surface for 45 seconds. After a maximum of 20 indentations the instrument is again checked as above. Since no diagnostic divergencies from the normal values could be established when the investigations were carried out, no corrections of the values obtained were required. In all cases the indentations were made with the same Vickers diamond and with the same load, viz. 100 g. The lengths of the two diagonals of the indentations were read by means of the instrument, 10 times for each diagonal (see also below). The average value as well as the errors for these determinations were calculated (see below). If cracks were found to develop more profusely than usual or the lengths of the diagonals differed by more than 0.5 μ the measurements were discarded and are thus not included in the tables. Incidentally only a few indentations have been discarded for these reasons. The instrument was mounted on a firm base so placed that it was not subjected to more than feeble vibrations and in a room with an approximately constant temperature (18°C).

Preliminary treatment of the material

In only two cases was it possible to employ the zinc blende without preliminary treatment. One specimen consisted of a well-developed rhombdodecahedral surface (Sonora (110)), the other consisted of a flat cleavage surface (Picos de Europa (110)). The remaining specimens were treated in the following manner. The specimens were first ground on a rotating cast-iron disk with "Carborundum 500" (grain size 500 mesh), after which they were ground by hand on a flat plate of mirror glass with "Alundum" (grain size 600 mesh). The polishing was done on a rotating, cloth-covered brass disk. The preliminary polishing was carried out with chromium oxide (grain size 800 mesh). The fine polishing was finally carried out with "Tonerde 2". Great importance has been attached to the hand-polishing. Small crystals were imbedded in lacquer or plastic whereby a sufficiently large surface was obtained for grinding and polishing.

The material investigated

The specimens of zinc blende which were the object of the micro-hardness investigations were obtained from collections belonging to the Geological Survey of Sweden (S.G.U.). Further material has been obtained from the Swedish Museum of Natural History, Department of Mineralogy (R.M.) and the Royal Institute of Technology (K.T.H.). The specimens obtained from R.M. and S.G.U. have previously been subjected to detailed investigations of the distribution of elements in Swedish zinc blende. This investigation was carried out by Gabrielson (1945) in the geochemical laboratory of S.G.U. The determinations were made with a quartz spectrograph of the Zeiss Q 24 type.

The material from the K.T.H. has been chemically analysed by A. Parwel (Fe) and spectrochemically analysed by V. Muld (Cd, Ca, In etc.). The analyses are given in Table 2.

Table 1. List of the material investigated.

1. Franklin, New Jersey, U.S.A. Glass-clear, very faintly yellow crystal. (K.T.H.)
2. Picos de Europa, Santander, Spain. Yellow-brown transparent crystals. (K.T.H.)
3. Chivera, Cananea, Sonora, Mexico. Feebly olive green transparent crystal. (K.T.H.)
4. Nygårdsbrottet, Tunhems s:n, Sweden. Pale yellow crystals. (S.G.U.)
5. Rockswiese, Harz, Germany, Chestnut-brown crystals. (K.T.H.)
6. Nordmarks gruva, Nordmarks s:n, Sweden. Dark-brown crystals. (R.M.)
7. Billingen, Sweden. Pale brown zinc blende. (S.G.U.)
8. Bjuv, Övre flötsen, Sweden. Black zinc blende. (S.G.U.)
9. Visby, Sweden. Black zinc blende crystals. (R.M.)
10. Tabergsfältet, Nordmarks s:n, Sweden. (R.M.)
11. Åmmebergsfältet, Godegårdsgruvan, Sweden. Brown coarsely crystalline zinc blende. (S.G.U.)
12. Skuleboda fältspatsbrott, Ryrs s:n, Sweden. Brown zinc blende. (R.M.)
13. Sala gruva, Sweden. Compact coarsely crystalline, black zinc blende.
14. S:a Fältet, Dannemora, Sweden. Compact black zinc blende. (R.M.)
15. Bersbo, Åtvidabergsfältet, Sweden. Coarsely crystalline zinc blende. (R.M.)
16. Ryllshytte gruvor, Garpenbergs s:n, Sweden. Black coarsely crystalline zinc blende. (S.G.U.)
17. Vrå marmorbrott, Hölö s:n, Södermanland, Sweden. Dark zinc blende. (R.M.)
18. Stollbergsgruvan, V. Silvberg, Norrbärke s:n, Sweden. Coarsely crystalline black zinc blende. (S.G.U.)
19. Storfallsgruvan, Grangärde s:n, Sweden. Black coarse zinc blende. (R.M.)
20. Pänninge kalkbrott, Torsåkers s:n, Sweden. Black zinc blende. (R.M.)
21. Dammbergsgruvan, V. Silvberg, Norrbärke s:n, Sweden. Black zinc blende. (S.G.U.)

Table

Analysis No.	% Zn	% Cd	% Ga	% In	% Ge	% Mn	% Fe	% Co	%
1		0.05	0.003	0.003	0.001	0.009	0.005	0.001	—
2		0.1	0.003	0.003	0.001	0.005	0.077	0.001	—
3		0.25	0.003	0.003	0.001	0.005	0.197	0.001	—
4	66	0.65	0.01	—	—	0.003	0.31	—	0.0
5		0.2	0.004	0.003	0.005	0.01	2.35	0.001	—
6		0.04	0.003	0.01	0.001	0.4	6.08	0.001	—
7	65	0.24	0.008	—	—	0.005	0.39	—	—
8	65	0.20	0.05	—	—	0.02	1.0	—	—
9	65	0.09	0.02	—	—	0.003	1.3	—	—
10	65	0.11	—	0.07	0.001	0.06	1.4	0.001	—
11	58	0.11	0.0004	0.003	—	0.04	4.6	0.003	0.0
12	58	0.16	0.001	< 0.003	—	0.45	6.0	0.01	< 0.0
13		0.27	—	—	—	0.53	9.9	0.03	—
14	52	0.10	0.002	—	0.01	0.17	10.3	—	—
15	54	0.12	0.0008	0.003	—	0.30	10.8	0.03	—
16	53	0.16	0.0007	< 0.003	—	0.18	11.6	0.01	—
17	53	0.10	—	—	—	0.18	12.2	0.001	—
18	52	0.25	—	0.013	—	0.45	12.6	—	—
19	49	0.12	—	0.003	—	1.43	12.9	0.001	0.0
20	46	0.13	0.004	—	—	0.19	17.3	0.03	0.0
21	44	0.08	—	0.003	—	0.73	19.5	—	—

Orientation of the crystal surfaces

It was soon apparent that the Vickers hardness of zinc blende varied with the crystallographic orientation. It was therefore necessary to determine this relationship accurately. The crystal surfaces of the zinc blende were determined, using a reflection goniometer. When the crystals did not have surfaces suitable for this investigation such have been developed mechanically. For measuring the new surfaces a contact goniometer has been mainly used. In other cases a check determination of the unpolished surfaces was carried out with the help of the reflection goniometer. In these repeated measurements a small, flat cover slip was attached to the finely polished surfaces thus supplying the corresponding surface reflections. By this means the tedious process of polishing for each check determination was avoided. Angular errors larger than 1° have not been permitted. In the above-mentioned manner existing or mechanically developed surfaces were determined or reaffirmed. For each chosen surface a definite direction was marked off on the specimen. Using this direction the orientation of the Vickers diamond (the direction of the diagonals) was varied by turning the graduated specimen holder through the required number of degrees around its horizontal axis. The following directions were used for the various surfaces. For surface (100) zone axis [001], for surface (110) zone axis [001], and finally for surface (111) direction $[\bar{1}\bar{1}2]$. For remaining surfaces of the type $\{100\}$, $\{110\}$, $\{111\}$ the corresponding zone axes were employed. As the specimen is rotated completely (360°) the Vickers diamond will successively occupy new positions. Because of crystal symmetry and the equisized diagonals of the Vickers diamond the crystal will, however, occupy several identical positions during such a rotation. It is thus found that for cube surfaces identical positions are occupied eight times hemical analyses.

Cu	% Ag	% Sn	% Pb	% Mg	% Al	% Si	As	Hg
—	0.0003	0.002	0.003	0.1	0.1	—		
—	0.0003	0.001	0.003	0.1	0.1	—		
—	0.0003	0.001	0.003	0.1	0.1	—		
—	—	—	—	0.1	tr	0.1		
—	0.0005	0.001	0.003	0.1	0.1	0.3		
—	0.0003	0.001	0.003	0.1	0.1	0.05		
tr	—	—	0.05	0.1	0.1	0.5		
0.1	tr	—	—	0.5	—	tr		+*
—	—	—	—	0.5	—	0.1		
0.1	—	—	—	0.1	—	< 0.1		
tr	—	—	0.003	1	1	1		
1	—	—	0.2	tr	0.15	0.1		
—	0.003	0.01	0.002	—	—	—		
1.5	0.003	—	0.002	1	0.3	0.3		
1	0.003	—	—	tr	—	< 0.1		
1	—	—	—	0.1	0.1	0.1	++*	
tr	tr	—	—	< 0.1	—	0.1		
0.1	tr	—	tr	tr	—	< 0.1		
1	—	—	—	0.3	—	2		
1.5	0.002	—	—	0.1	0.1	2		
—	—	—	—	0.1	0.1	0.3		

* + = Weak line; + + = moderately strong line.

when the crystal is turned through 360°. Corresponding figures are for the rhombdodecahedron 8, and for the tetrahedron 6. For the three above-mentioned forms the following theoretical limiting values are obtained for a crystal rotation without its occupying identical positions:

cube	$\{001\}$	0°–45°
rhombdodecahedron . . .	$\{011\}$	0°–45°
tetrahedron	$\{111\}$	0°–60°

It should be mentioned that for a great part of the material no crystallographic orientations were carried out.

The Vickers hardness of zinc blende

The systematic investigation of the Vickers hardness of zinc blende (Table 3 and Fig. 1) has given the following result. The Vickers hardness is (1) a logarithmic function of the iron content of the mineral, (2) strongly dependent on the orientation of the investigated section, (3) independent of the orientation of the Vickers diamond (i.e. the position of the diagonals at indentation). Furthermore, the investigation has shown that the deformation of the Vickers indentations varies with the crystallographic direction. In Fig. 1. the Vickers hardness of zinc blende has been plotted along the vertical axis and the iron content along the horizontal axis (logarithmic scale). Each point on the diagram corresponds to the average of all hardness determinations made on the same crystal with the same crystallographic orientation.

Table 3.

No. and locality	Orientation		Number of observ.	Hardness			Average error of means	Fractures
	surface (hkl)	direction hkl v°		Min.	Max.	Mv.		
1 *Franklin*	(100)	[001] 0°	12	126	129	127	1	
same surface	(100)	[001] 15°	8	122	125	124	1	x
,, ,,	(100)	[001] 30°	12	124	128	126	1	(x)
,, ,,	(100)	[001] 45°	10	128	133	130	1	(x)
,, ,,	(100)	var.	42	122	133	127	1	
1 *Franklin*	(110)	[001] 0°	12	146	154	150	2	
same surface	(110)	[001] 30°	11	154	158	156	1	
,, ,,	(110)	[001] 45°	10	150	157	153	2	
,, ,,	(110)	var.	33	146	158	153	1	
1 *Franklin*	(111)	$[\bar{1}\bar{1}2]$ 0°	10	153	159	157		
same surface	(111)	$[\bar{1}\bar{1}2]$ 30°	10	156	163	159	2	
,, ,,	(111)	$[\bar{1}\bar{1}2]$ 60°	10	154	159	157	1	
,, ,,	(111)	var.	30	153	163	157	1	
2 *Picos d. E.*	(100)	[001] 0°	14	142	145	143	1	(x)
same surface	(100)	[001] 15°	10	140	149	143	2	(x)
,, ,,	(100)	[001] 30°	12	147	151	149	1	(x)
,, ,,	(100)	[001] 45°	10	144	150	147	1	(x)
,, ,,	(100)	var.	46	140	151	145	1	
2 *Picos d. E.*	$(\bar{1}00)$	[001] 30°	16	145	151	149	1	(x)
Picos d. E.	(100) & $(\bar{1}00)$	var.	62	140	151	146	1	
Picos d. E.	(110)	[001] 0°	10	159	162	161	1	
same surface	(110)	[001] 15°	10	159	163	162	1	
,, ,,	(110)	[001] 30°	10	163	169	166	2	
,, ,,	(110)	[001] 45°	8	164	170	166	1	
,, ,,	(110)	var.	38	159	170	164	1	
2 *Picos d. E.*[1]	$(\bar{1}\bar{1}0)$	var.	10	161	162	161	1	
2 *Picos d. E.*	(110) & $(\bar{1}\bar{1}0)$	var.	48	159	170	163	1	
3 *Sonora*	(100)	[001] 15°	12	143	151	148	2	
same surface	(100)	[001] 30°	12	145	153	150	2	
,, ,,	(100)	[001] 45°	12	143	154	149	2	
,, ,,	(100)	var.	36	143	154	149	1	
3 *Sonora*	(010)	[001] 0°	11	143	152	148	2	
same surface	(010)	[001] 30°	11	146	155	151	2	
,, ,,	(010)	[001] 45°	12	149	156	153	1	
,, ,,	(010)	var.	34	143	156	151	1	
3 *Sonora*	(100) & (010)	var.	70	143	156	150	1	
3 *Sonora*[2]	(110)	[001] 0°	4	167	171	169		
same surface	(110)	[001] 10°	4	167	169	168		
,, ,,	(110)	[001] 15°	4	167	170	169		
,, ,,	(110)	[001] 20°	4	168	172	170		
,, ,,	(110)	[001] 25°	4	167	170	169		
,, ,,	(110)	[001] 30°	4	168	171	169		
,, ,,	(110)	[001] 35°	4	169	172	171		
,, ,,	(110)	[001] 40°	4	166	177	170		
,, ,,	(110)	[001] 45°	4	167	172	170		
,, ,,	(110)	var.	36	166	177	169	1	

---

[1] Crystal surface. [2] Cleavage surface.

Table 3 (*continued*)

No. and locality	Orientation		Number of observ.	Hardness			Average error of means	Fractures
	surface (hkl)	direction hkl v°		Min.	Max.	Mv.		
3 *Sonora*	(1$\bar{1}$0)	[001] 0°	32	161	178	170	2	
same surface	(1$\bar{1}$0)	[001] 30°	31	164	179	170	1	
,, ,,	(1$\bar{1}$0)	[001] 45°	31	167	179	171	1	
,, ,,	(1$\bar{1}$0)	var.	94	161	179	170	1	
3 *Sonora*	(110)							
	& (1$\bar{1}$0)	var.	130	161	179	170	1	
3 *Sonora*	(111)	[$\bar{1}\bar{1}$2] 0°	12	172	176	174	1	
same surface	(111)	[$\bar{1}\bar{1}$2] 30°	12	169	179	175	2	
,, ,,	(111)	[$\bar{1}\bar{1}$2] 60°	12	172	178	175	1	
,, ,,	(111)	var.	36	169	179	174	1	
3 *Sonora*	($\bar{1}\bar{1}$1)	[112] 0°	11	173	177	175	1	
same surface	($\bar{1}\bar{1}$1)	[112] 30°	12	172	177	175	1	
,, ,,	($\bar{1}\bar{1}$1)	[112] 60°	11	171	177	174	1	
,, ,,	($\bar{1}\bar{1}$1)	var.	34	169	179	175	1	
3 *Sonora*	(111)							
	& ($\bar{1}\bar{1}$1)	var.	70	169	179	175	1	
4 *Nygårds-*	(001)	var.	21	158	164	161	1	(x)
brottet	(111)	var.	32	182	190	188	1	(x)
5 *Harz*	(110)	[001] 0°	13	194	195	194	1	(x)
same surface	(110)	[001] 30°	14	193	196	194	1	(x)
,, ,,	(110)	[001] 45°	13	191	195	193	1	(x)
,, ,,	(110)	var.	40	191	196	194	1	
6 *Nordmark*	(001)	[010] 0°	12	178	180	179	1	(x)
same surface	(001)	[010] 30°	12	178	182	180	1	(x)
,, ,,	(001)	[010] 45°	12	178	183	180	1	(x)
,, ,,	(001)	var.	36	178	183	180	1	
6 *Nordmark*	(100)	[001] 0°	12	177	181	179	1	
same surface	(100)	[001] 15°	12	178	180	179	1	
,, ,,	(100)	[001] 45°	12	178	180	179	1	
,, ,,	(100)	var.	36	177	181	179	1	
6 *Nordmark*	(100)							
	& (100)	var.	72	177	183	179	1	
6 *Nordmark*	(110)	[001] 0°	9	199	203	201	1	
same surface	(110)	[001] 15°	12	199	203	202	1	
,, ,,	(110)	[001] 45°	10	194	205	200	2	
,, ,,	(110)	var.	31	194	205	201	1	
6 *Nordmark*	(1$\bar{1}$0)	[001] 0°	12	195	203	199	1	
same surface	(1$\bar{1}$0)	[001] 30°	12	201	206	203	1	
,, ,,	(1$\bar{1}$0)	[001] 45°	12	197	203	199	1	
,, ,,	(1$\bar{1}$0)	var.	36	195	206	201	1	
6 *Nordmark*	(110)							
	& (1$\bar{1}$0)	var.	67	194	206	200	1	
Nordmark	(111)	[$\bar{1}\bar{1}$2] 0°	12	201	203	202	1	
same surface	(111)	[$\bar{1}\bar{1}$2] 30°	12	202	203	202	1	
,, ,,	(111)	[$\bar{1}\bar{1}$2] 60°	12	201	205	203	1	
,, ,,	(111)	var.	36	201	205	203	1	
6 *Nordmark*	($\bar{1}\bar{1}$1)	[112] 0°	12	197	203	202	1	
same surface	($\bar{1}\bar{1}$1)	[112] 30°	12	199	203	202	1	
,, ,,	($\bar{1}\bar{1}$1)	[112] 60°	12	199	203	202	1	
,, ,,	($\bar{1}\bar{1}$1)	var.	36	197	203	202	1	
6 *Nordmark*	(111)							
	& ($\bar{1}\bar{1}$1)	var.	72	197	205	203	1	

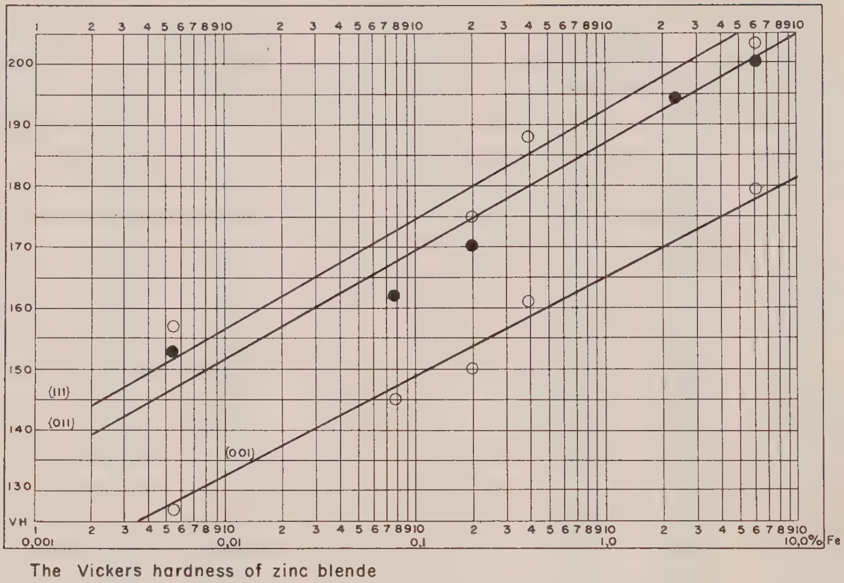

Fig. 1. The Vickers hardness of zinc blende. Black dots refer to {011}.

From the three graphs corresponding to {001}, {011}, {111} it is apparent that the hardness of the zinc blende is a logarithmic function of the iron content:

$$\mathrm{HV} = A + B \log C,$$

where HV = the Vickers hardness, A and B constants, and C the Fe content of the zinc blende in weight-%.

The Vickers hardness for the three surfaces examined can be expressed by the equations (see Fig. 1):

$$\begin{aligned}\mathrm{HV}_{\{001\}} &= 165 + 16 \log C,\\ \mathrm{HV}_{\{011\}} &= 187 + 18 \log C,\\ \mathrm{HV}_{\{111\}} &= 193 + 19 \log C.\end{aligned}$$

A further conclusion that can be drawn from Fig. 1 is that slight deviations from the ideal curves occur. These deviations, amounting at the most to appr. 6 HV, show that the hardness of zinc blende is also determined by factors other than the iron content. It should be possible to see differences in the chemical or structural nature of the crystal from these divergencies. Apart from iron, small quantities of other elements occur in zinc blende (Table 2). The correlation coefficients (not included here) have been calculated for the various elements and the hardness deviations of the zinc blende deduced from the ideal curves. It has not, however, been possible to prove any correlation between these two factors. The variations from the graphs should hence be attributed to variations in the structure of the various crystals. In connexion with the preparation of the sample, surface changes as well as stresses of various kinds may have developed which would cause changes in the Vickers

Table 4.

FeS content in zinc blende weight-%	a_0 in Å
0	5.398_5
10	5.401_8
20	5.406_6
30	5.410_9

hardness. Since, however, the preparation of the samples was carried out under standardized conditions the explanation of the deviations should probably be sought in the structure of the crystals prior to preparation. Previous hardness determinations have also shown that crystallographic structural faults, the so-called mosaic structure (i.e. the fact that the crystals are built up of ideally formed blocks, which fit together so that they form small angles with each other), have been the cause of considerable deviations from normal hardness (see for example Stranski, 1949). Apart from mosaic structure, other structural faults and stresses, submicroscopic fractures, etc. may bring about changes in the Vickers hardness of the mineral.

As mentioned above the Vickers hardness of zinc blende increases with increasing iron content. Very low contents of iron have the power of greatly increasing the hardness. An increase in the iron content of from 0.01 % to 0.1 % is accompanied by an increase in the Vickers hardness for the $\{001\}$ forms from 133 HV to 149 HV or 12 %. The reason for the increased hardness lies in lattice changes. It can be established directly that the increased hardness of the zinc blende has no connexion with changes in the density of the packing of the lattice. This is clearly apparent from Kullerud's (1953) determinations of the length of the edges of the zinc blende unit cell with varying iron content (Table 4).

At the present stage it does not appear possible to explain why the hardness of zinc blende increases with increasing iron content. But it does not appear impossible that some sort of analogy may exist to the increasing hardness of iron caused by small additions of Ni, Mn etc., which give rise to a somewhat distorted crystal lattice due to substitution in the mixed crystal.

From Fig. 1 it is apparent that the greatest and least Vickers hardnesses for zinc blende with the same iron content, has been observed for the tetrahedron and cube surfaces respectively, while the hardness of the rhombdodecahedron is somewhat less than that of the surfaces of the tetrahedron. This hardness anisotropy is, in spite of the isometric structure of zinc blende, completely accountable with reference to those factors that primarily determine the relative hardness of crystalline substances. Winkler (1950) has, *inter alia*, summarized these factors. The hardness of an ideal crystal is thus a function of size, charge and valency and of the density of the packing of the atoms or ions in the lattice. On account of the geometrical arrangement in the lattice of zinc blende the density of the packing will also vary with the orientation of the section. It is well known that the structure of zinc blende, $F\bar{4}3m$ with $Z = 4$ and the coordinates 000, $0\frac{1}{2}\frac{1}{2}$, $\frac{1}{2}0\frac{1}{2}$, $\frac{1}{2}\frac{1}{2}0$ for Zn together with the coordinates $\frac{1}{4}\frac{1}{4}\frac{1}{4}$, $\frac{1}{4}\frac{3}{4}\frac{3}{4}$, $\frac{3}{4}\frac{1}{4}\frac{3}{4}$, $\frac{3}{4}\frac{3}{4}\frac{1}{4}$ for S, is of the same type as that of the diamond with the one difference that 2C is replaced by Zn + S. The hardness anisotropy that has been observed for diamond should therefore have some analogy in zinc blende. For many years it has been known that the various surfaces of diamonds have varying polishing hardnesses. Thus the octahedral surface has the greatest hardness. Winkler (1950), using the number of C–C bonds which bind the atoms for each unit surface for the surfaces (100), (110) and (111), has obtained a measurement of the relative polishing hardness for the surfaces. Surface (100) is bound with 4 bonds, surface (110) with $4\sqrt{2}$ and surface (111) with $4\sqrt{3}$ bonds per unit surface of magnitude a^2. The relationship between the forces binding the atoms in the various surfaces is thus: (100):(110):(111) $= 1:\sqrt{2}:\sqrt{3} = 1:1.41:1.73$. It is also apparent, as mentioned above, that the octahedral surfaces have the greatest polishing hardness while the cube surfaces have the least. If this reasoning be applied to zinc blende (where it should be emphasized that the Zn–S bonds are not completely identical with the homopolar bonds of the diamond), the following results are obtained: (100):(110):(111) = $1:1.13 \pm 0.01:1.17 \pm 0.01$. That these values deviate somewhat from those of Winkler (1950) is probably due to the fact that the loosening and attrition of the parts of the lattice that occur during polishing are not entirely comparable with the particularly complicated course of events that occur when a Vickers diamond penetrates a crystal. In the investigation of the Vickers hardness of aluminium crystals Schulz and Haneman (1941) found that this is altered if the diagonals of the indenting body are permitted to take different positions (on the same surface). The material consisted of 8 crystals and the diamond was turned 15° for each new indentation; in this way 6 impressions were made as well as a check impression on every crystal. The difference between the least and the greatest Vickers hardnesses amounted to 7 %. The authors found that 2.5 % was due to the spread while 4.5 % was due to various positions of the pyramid at indentation. In the case of the Vickers hardness of zinc blende no such hardness anisotropy having any connexion with the position of the diagonals of the indenting body was discovered. This seems remarkable with reference to the deformations which the indentations suffered. (See below.)

Statistical examination of the hardness determinations

To investigate whether there are differences between the means of the lengths of the two diagonals an analysis of variance with multiple classification has been used. The estimation of the average errors of the means has been carried out for each diagonal by simple analysis of variance. The procedure has been described by Hald (1948).

The difference in length between the diagonals is sometimes significant. In some surveys, for example, one diagonal was found to be a little longer than the other. In other series, however, the opposite condition prevailed in spite of the fact that the impressions were carried out on the same surface and with the same orientation. The cause of these divergencies must be sought in irregularities in the material and not in the crystal structure as such. From the analysis of variance it is further seen that the spread of the impressions is definitely the greatest cause of variations, whilst the errors in measurement are of a considerably smaller magnitude. Thus the surveys have shown that whereas 75–90 % of the total spread is caused by differences in the hardness of the mineral, 10–25 % can be attributed to the measuring technique.

The number of measurings of the diagonals (10 in this case) could now with the present accuracy of measuring be carried out with only 3 for each diagonal. Table 5 shows an example of how the average errors of the mean only slightly diminish

Table 5.

Number of measurements	μ	Average error of means expressed in HV
1	0.110	1
2	0.106	1
3	0.104	1
5	0.103	1
10	0.102	1
20	0.102	1
	0.101	1

Table 6.

Number of measurements	μ	Average error of means (σ_0) expressed in HV
1	0.403	4
2	0.285	3
3	0.233	2
5	0.180	2
10	0.128	1
15	0.104	1
20	0.090	1
25	0.081	1
50	0.057	1
100	0.040	1
200	0.029	1

with an increasing number of measurements (impressions = 15 $\sigma_s = 0.39$ and $\sigma_m = 0.17$).

The margin of error is reduced considerably by increasing the number of impressions. Table 6 shows how the error decreases with an increased number of impressions when 3 measurements are made on each diagonal.

Deformation of the Vickers indentations

The elasticity of the crystals is apparent from the fact that the indentation is somewhat compressed when the loaded Vickers diamond is raised from the crystal. The elasticity may be measured in several ways (see e.g. Grodzinski, 1954). A deformation of the Vickers indentation has been found to be caused by slip along glide planes. Schulz and Haneman (1941) found that Vickers indentations on crystals of antimony are deformed by slip along the planes $\{01\bar{1}2\}$. Also depressions made in zinc blende are deformed; this is particularly applicable to the surfaces of cubes. Fig. 2 illustrates how the indentation on the cube surface (001) is deformed by the four sides being pressed inwards when the diagonals of the indenting body was orientated parallel with [110] and $[\bar{1}\bar{1}0]$. If, however, the diagonals are parallel with [100] and [010] the sides of the indentation bulge outwards instead. The slip move-

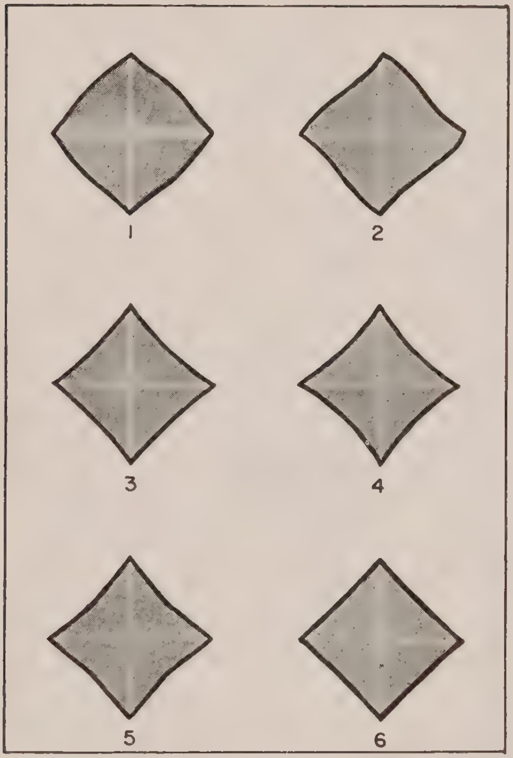

Fig. 2. The form of indentations on:

	Surface (hkl)	Direction [hkl]	v°
1	(100)	[001]	0°
2	(100)	[001]	15°
3	(100)	[001]	30°
4	(100)	[001]	45°
5	(111)	[$\bar{1}\bar{1}2$]	0°
6	(111)	[$\bar{1}\bar{1}2$]	60°

ments which were occasioned have thus taken place along the surfaces {011}. With reference to the nature of the deformation one might expect that the lengths of the diagonals would not be the same in the both cases. Since, however, this is not the case it is apparent that the deformations not only compressed the indentation but that movements also occurred in the opposite direction. The square symmetry of the deformations further indicates that the cube surface is normal to an axis of four-fold symmetry.

Hardness determinations made on unorientated sections

Hardness determinations were also made on zinc blende without orientating the section. The indentation was carried out in the same fashion as before (same preparation of the specimen and method of measurement). The indentations were concentrated towards the central parts of the grains and were made at sufficient distances from each other to prevent mutual interference. Not more than three indentations were made on each grain. Nevertheless in some cases the indentations were unreliable owing to the small thickness of the grain or to interference from neighbouring grains. Fig. 3 indicates that a definite spread in the Vickers hardness of the grains usually occurs because of variable crystallographic orientation. In some cases considerably less spread may be observed. This can probably be accounted for by assuming that the zinc blende grains are structurally arranged in these ores.

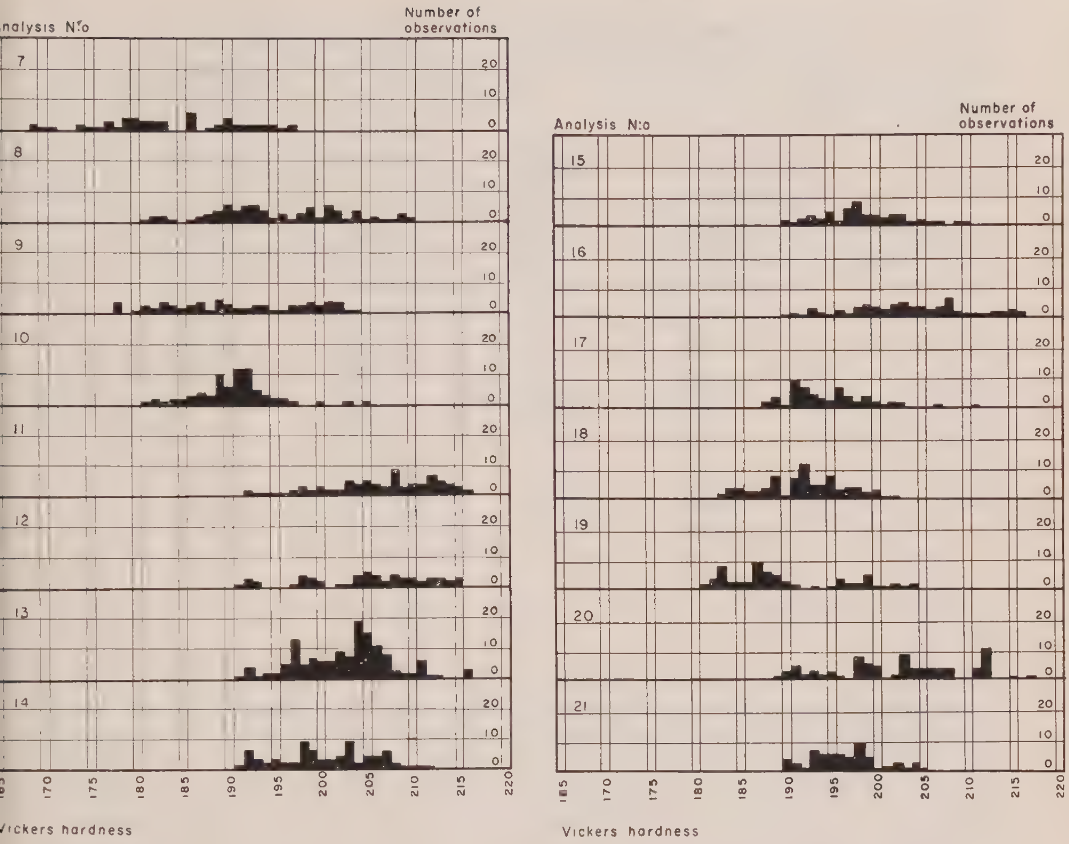

Fig. 3. Diagram illustrating the hardness variations due to variable crystallographic orientation.

Earlier determinations of micro-hardness

Micro-hardness measurements have been previously made on zinc blende with both Vickers and Knoop indenters (Table 7). Chemical analyses have in no cases been supplied and only in one instance was the crystallographic orientation given (Winchell, 1945).

Table 7.

	Hardness (Vickers or Knoop)			Type of indenter
	Min.	Max.	Mv.	
Siebel (1943)	158	178	171	Vickers
,, ,, ...	158	186	173	,,
Winchell (1945): (011) . . .	175	180	177	Knoop
Robertson & Meter (1951) . .	151	294	209	,,

Vickers hardness compared with Mohs scale of hardness

Several attempts to correlate Mohs scale of hardness and Vickers hardness have been made (Table 8).

Table 8.

Mohs scale of hardness	Krushchov 1947	Onitsch[1] 1948	Dmitriev 1949	Taylor[2] 1949
1	2.4	29	10–11	47
2	36	73	39–90	60
3	109	206	145–165	105 136 145
4	189	220	175–260	175 200
5	536	588	550–690	659
6	795	880	780–850	714
7	1 120	1 142	1 200–1 460	1 103 1 260
8	1 427	1 220	1 800–2 000	1 648
9	2 060	2 040	2 050–2 200	2 085
10	10 060			

[1] Average values.

[2] Hardness determined on 2 or 3 different surfaces are indicated by 2 or 3 values respectively.

The hardness of zinc blende, according to Mohs scale of hardness, is 3.5–4. The Vickers hardness, according to the investigation here presented, shows extreme values ranging from 117 HV {001}, iron content 0.001 % to 212 HV {111}, iron content 10 %. Even if the Vickers hardness and the hardness according to Mohs scale are not comparable fundamentally, good agreement exists nevertheless between the Vickers hardness of zinc blende on the one hand and the values calculated by Krushchov and others for Mohs scale in the range (3–4).

ACKNOWLEDGEMENTS

The author wishes to convey his thanks to Prof. F. E. Wickman, for his critical reading of the manuscript, to Dr. O. Gabrielson for the analysed specimens, to Mr. R. Cederlöv for statistical collaboration, to Mrs. I. Jansson and Mr. B. Honeth who constructed the diagrams. For financial support I am indebted to *Jernkontorsfonden för bergsvetenskaplig forskning.*

REFERENCES

DMITRIEV, S. D. (1949), The microhardness tester PMT-2, its use for mineral investigation. Zapiski Vseoyuz Mineral. Obshghestra *78*, 241–252.

GABRIELSON, O. (1945), Studier över elementfördelningen i zinkbländen från svenska fyndorter. Sveriges Geol. Undersökning, Ser C, N:o 468, 1–52.

GRODZINSKI, P. (1954), Micro-indention hardness. Metallurgia *50*, 125–131.

HALD, A. (1948), Statistiske metoder. København.

KRUSCHOV, M. M. (1947), Choice of basic method for determining hardness of materials. Zavodsk. labor. *9*.

KULLERUD, G. (1953), The FeS–ZnS system a geological thermometer. Norsk Geol. Tidsskr. *32*, 61–147.

ROBERTSON, F., and METER, W. J. (1951), The Kenton microhardness tester, a quantitative tool in opaque mineral indentication. Econ. Geol. *46*, 541–550.

ONITSCH, E. M. (1948), Über die Mikrohärte der Metalle und Mineralien. Berg.- u. hüttenmänn. Jb. *93*, 7–12.

SCHULZ, F., and HANEMAN, H. (1941), Die Bestimmung der Mikrohärte von Metallen. Zeitschrift für Metallkunde *33*, 124–134.

SIEBEL, J. (1943), Über die Anwendbarkeit der Mikrohärteprüfung als diagnostisches Hilfsmittel in der Erzmikroskopie. Metall & Erz *40*, 169–174.

STRANSKI, I. N., ref. CORRENS, C. W. (1949), Einführung in die Mineralogie, 95.

TABOR, D. (1951), The Hardness of Metals. Oxford.

TAYLOR, E. V. (1949), Correlation of Mohs scale of the hardness with the Vickers hardness numbers. Am. Min. *28*, 718–721.

TERTSCH, H. (1949), Die Festigkeiterscheinungen der Kristalle. Wien.

—— (1951), Erfahrungen bei Mikrohärte-Bestimmungen an Kristallen. Jb. Min. Monatsh. *4*, 73–87.

WINCHELL, H. (1945), The Knoop microhardness tester as mineralogical tool. Am. Min. *30*, 582–595.

WINKLER, H. G. F. (1950), Struktur und Eigenschaften der Kristalle. Berlin–Göttingen–Heidelberg.

Tryckt den 26 februari 1957

Uppsala 1957. Almqvist & Wiksells Boktryckeri AB

INNEHÅLL

Sid.

9. BROTZEN, F., Stratigraphical studies on the Triassic vertebrate fossils from Wadi Raman, Israel 191–217
10. MUTVEI, H., On the relations of the principal muscles to the shell in *Nautilus* and some fossil nautiloids. With a taxonomic appendix 219–254
11. HENRIQUES, Å., Optical and physical properties of knebelite 255–269
12. HENRIQUES, Å., The alkali content of kyanite 271–274
13. HENRIQUES, Å., Cell dimensions of sphalerite 275–278
14. HENRIQUES, Å., Swedish pyrophyllite deposits and the optical properties of pyrophyllite 279–282
15. HENRIQUES, Å., The Vickers hardness of zinc blende 283–297

Arkiv för Mineralogi och Geologi utgives i tvångsfritt utkommande häften. Sex dylika bilda ett band. — Pris för detta häfte Kr. 32:—.

Arkiv för Mineralogi och Geologi appears at irregular intervals. Six numbers will form one volume. — The price of this number Sw. Crs. 32:—.

Utgivet den 15 april 1957.

Uppsala 1957. Almqvist & Wiksells Boktryckeri AB